Using Kaposi's sarcoma-associated herpesvirus to elucidate the role of cellular microRNAs in endothelial biology.

Gemma Elizabeth Margaret Bridge BA (Hons)

University College London

Submitted for the degree of Doctor of Philosophy

2013

Declaration

I, Gemma Elizabeth Margaret Bridge, confirm that the work presented in this thesis is my own. Where information has been derived from other sources, I confirm that this has been indicated in the thesis.

Signed:

Date:

Acknowledgements

First and foremost I would like to thank my PhD supervisor Chris Boshoff for allowing me to follow this project into fascinating new areas and for the many opportunities for career development that he has provided. I would also like to thank the rest of the CRUK viral oncology group for their assistance throughout the course of my PhD. In particular, I would like to thank Vicky Emuss for her patience, support and guidance during the start of my PhD. Special thanks must also go to Dimitris Lagos, Fiona Gratrix, Juanma Funes, Leonid Nikitenko, Emanuela Cuomo and Ohad Yogev for experimental advice, scientific chats, and more importantly, plain old camaraderie. I'd also like to thank Adrian Harris and Esther Bridges for invaluable advice on endothelial assays and most importantly, Rui Monteiro and Roger Patient, without whom, none of the zebrafish experiments would have been possible.

Thank you to my amazing friends and family for listening to my complaints and for making me smile.

Finally, I cannot begin to explain how much I appreciate the limitless love and support that Tom has given me over the last few years. Thank you for pushing me to continue.

Dedication

I would like to dedicate this work to my parents, Philip and Anne. Thank you for everything.

Abstract

Kaposi's sarcoma-associated herpesvirus (KSHV) is an oncogenic γ-herpesvirus that is the etiologic agent of Kaposi sarcoma (KS). KS is an angioproliferative neoplasm composed of cells of endothelial origin. For the work described in this thesis, KSHV infection of endothelial cells was used as a tractable model to study the role of microRNAs (miRNAs) in endothelial cell biology. Previous work in the laboratory had identified miRNAs which are either upregulated or downregulated upon KSHV infection of lymphatic endothelial cells (LEC). Target prediction analysis of these miRNAs and cross-comparison of predicted targets with expression levels of pro- and anti-angiogenic genes following KSHV infection, revealed the predicted targeting of Delta-like 4 (*DLL4*) by the miR-30 family. DLL4 is significantly upregulated in KSHV-infected lymphatic endothelial cells (KLEC) whereas the miR-30 family is significantly downregulated.

DLL4 is a membrane-bound ligand belonging to the Notch signalling family that plays a fundamental role in vascular development and angiogenesis. Targeting of *DLL4* by miR-30b and miR-30c was confirmed by examining mRNA and protein expression following transfection of endothelial cells with miR-30 mimics and inhibitors or infection with miR-30-expressing lentiviruses. The exact target site within the *DLL4* 3'UTR was identified using a luciferase reporter assay and site-directed mutagenesis.

Overexpression of miR-30b in endothelial cells led to increased vessel number and length in an *in vitro* model of sprouting angiogenesis. Microinjection of miR-30 into zebrafish embryos resulted in suppression of *dll4* and subsequent excessive sprouting of intersegmental vessels and reduction in dorsal aorta diameter. Use of a target protector against the miR-30 site within the *dll4* 3'UTR upregulated *dll4* and synergised with Vegfa signalling knockdown to inhibit angiogenesis. Furthermore, restoration of miR-30b or miR-30c expression during KSHV infection attenuated viral induction of DLL4. Overall, the work presented in this thesis demonstrates that the miR-30 family targets *DLL4* to regulate angiogenesis.

Table of Contents

List of Figures

List of Tables

Abbreviations

3’UTR	3 prime untranslated region
ac-pre-miRNA	AGO2-cleaved precursor miRNA
ACTG	AIDS Clinical Trials Group
ACTG2	actin, gamma 2, smooth muscle, enteric
ACV	anterior cardinal vein
AGO	Argonaute
AGO1	argonaute 1
AGO2	argonaute 2
AIDS	Acquired Immunodeficiency Syndrome
AIDS-KS	AIDS-associated KS
AKT	v-akt murine thymoma viral oncogene homolog
ALK1	activated receptor-like kinase 1
ANGPT1	angiopoietin 1
ANGPT2	angiopoietin 2
APS	ammonium persulphate
ATM	Ataxia-telangiectasia mutated
BCL6	B-cell lymphoma 6
BEC	blood endothelial cell
bHLH	basic-helix-loop-helix
β-ME	β-mercaptoethanol
BMP	bone morphogenetic protein
BRCA	breast invasive carcinoma
BSA	bovine serum albumin
CAF1	chromatin assembly factor 1
c/c	copies per cell
CCND1	cyclin D1
CCND2	cycline D2
CCNE2	cycline E2
CDC42	cell division cycle 42
CDK4	cyclin-dependent kinase 4
CDKN1A	cyclin-dependent kinase inhibitor 1A
CDKN1B	cyclin-dependent kinase inhibitor 1B
cDNA	complimentary DNA

CIP	calf-intestinal alkaline phosphatase
CMV	cytomegalovirus
CNS	central nervous system
COAD	colon adenocarcinoma
CREB	cAMP response element-binding protein
CSF2	colony stimulating factor 2
CTGF	connective tissue growth factor
C_T	threshold cycle
CXCR4	chemokine receptor 4
DA	dorsal aorta
DAB2	disabled homolog 2
DC	Duct of Cuvier
Dcp1	decapping enzyme 1
ddH_2O	double distilled water
DGCR8	DiGeorge syndrome critical region gene 8
DIG	digoxigenin
DLAV	dorsal longitudinal anastomotic vessel
dlc	deltaC
dld	deltaD
DLL1	delta-like 1
DLL3	delta-like 3
DLL4/dll4	delta-like 4
DMEM	Dulbecco’s Modified Eagle Medium
DMSO	dimethyl sulphoxide
dNTP	deoxyribonucleotide triphosphate
dsRBP	double-stranded RNA-binding protein
EBV	Epstein-Barr virus
EDTA	ethylene diamino tetraacetic acid
EFNA3	ephrin-A3
EFNB2	ephrin B2
EGF	epidermal growth factor
EHT	endothelial haematopoietic transition
EF4A2	eukaryotic translation initiation factor 4A2
EIF4E	eukaryotic translation initiation factor 4E
EIF4F	eukaryotic translation initiation factor 4F

EIF6	eukaryotic translation initiation factor 6
EL	embryo length
EMT	epithelial-to-mesenchymal transition
ENG	endoglin
EPH	ephrin
EPHA2	EPH receptor A2
EPHB2	EPH receptor B2
EPHB4	EPH receptor B4
ER	endoplastic reticulum
ERK	extracellular-signal-regulated kinase
ETS	E-twenty six
EZH2	enhancer of zeste homolog 2
FACS	fluorescence-activated cell sorting
FAK	focal adhesion kinase
FBS	foetal bovine serum
FGF2	fibroblast growth factor 2
FGFR2	fibroblast growth factor receptor 2
fli1a	friend leukemia integration 1a
FLT1	fms-related tyrosine kinase 1
FLT4	fms-related tyrosine kinase 4
FN1	fibronectin
FOS	FBJ murine osteosarcoma viral oncogene homolog
FUS	fused in sarcoma
GAPDH	glyceraldehyde 3-phosphate dehydrogenase
GAX	growth arrest-specific homeobox
GBM	glioblastoma multiforme
G/C	guanine/cytosine
GEM	gene expression microarray
GFP	green fluorescent protein
GLCE	glucuronic acid epimerase
GO	Gene Ontology
G:U	guanine:uridine
HBP1	HMG-box transcription factor 1
HCMV	human cytomegalovirus
HER1	hairy-related 1

HER2	hairy-related 2
HER3	hairy-related 3
HER4	hairy-related 4
HES	Hairy/Enhancer of Split
HEY	Hairy/Enhancer of split related
HEY2	hairy/enhancer-of-split related with YRPW motif 2
HF	human fibroblasts
HF1	immortalised human fibroblasts
HGS	hepatocyte growth factor-regulated tyrosine kinase substrate
HHV8	human herpesvirus 8
HIF1A	hypoxia inducible factor 1 alpha subunit
HIV	human immunodeficiency virus
HMEC	human dermal microvascular endothelial cells
HOXA5	homeobox A5
hpf	hours post-fertilisation
HRP	horse-radish peroxidase
HSC	haematopoietic stem cell
HSV-1	herpes simplex virus-1
hTERT	catalytic subunit of human telomerase
HUVEC	human umbilical vein endothelial cells
HVS	herpesvirus saimiri
IFNG	interferon gamma
IGF1	insulin-like growth factor 1
IL-1	interleukin-1
IL-6	interleukin-6
ITGB3	integrin beta 3
ITGB8	integrin beta 8
ISV(s)	intersegmental vessel(s)
JAG1	jagged 1
JAG2	jagged 2
JAK1	Janus kinase 1
JUN	jun proto-oncogene
KDR	kinase insert domain receptor
kdrl	kinase insert domain receptor like

KDS	potassium dodecyl sulphate
KIT	v-kit Hardy-Zuckerman 4 feline sarcoma viral oncogene homolog
KLEC	KSHV-infected LEC
KLF2	Kruppel-like factor 2
KS	Kaposi sarcoma
KSHV	Kaposi sarcoma-associated herpesvirus
KSRP	KH-type splicing regulatory protein
LANA	latent nuclear antigen 1
LAR II	Luciferase Assay Reagent II
LB	Luria-Bertani
LEC	lymphatic endothelial cells
LEF1	lymphoid enhancer-binding factor 1
Lhx1	LIM homeobox 1
LiCl	lithium chloride
LIN28	lin-28 homolog
LMO	LIM-only
LPS	lipopolysaccharide
LUAD	lung adenocarcinoma
LYVE1	lymphatic vessel endothelial hyaluronan receptor 1
MAB	maleic acid buffer
MAF	v-maf avian musculoaponeurotic fibrosarcoma oncogene homolog
MAML1	mastermind-like 1
MAPK	mitogen-activated protein kinase
MAP2K3	mitogen-activated protein kinase kinase 3
MBT	midblastula transition
MCD	multicentric Castleman’s disease
MCS	multiple cloning site
Mib	mind bomb
miRISC	miRNA-induced silencing complex
miRNA(s)	microRNA(s)
MMP1	matrix metallopeptidase 1
MMP14	matrix metallopeptidase 14
MMPs	matrix metalloproteases

MO(s)	morpholino(s)
MS-222	tricaine mesylate
MYBL2	v-myb myeloblastosis viral oncogene homolog-like 2
NAA15	N(alpha)-acetyltransferase 15
NARG1	NMDA receptor-regulated protein 1
NF-κB	nuclear factor of kappa light polypeptide gene enhancer in B-cells
NIC	non-injected control
NICD	Notch intracellular domain
NR2F2	nuclear receptor subfamily 2 group F member 2
NRARP	Notch-regulated ankyrin repeat protein
NRAS	neuroblastoma RAS viral (v-ras) oncogene homolog
NRP1	neuropilin 1
NRP2	neuropilin 2
NRPs	neuropilins
NTC	non-targeting control
NUMB	numb homolog
nt	nucleotide
ORF(s)	open reading frame(s)
OV	ovarian serous cystadenocarcinoma
p53	cellular tumour antigen p53
PABP1	poly-A binding protein 1
PBS	phosphate buffered saline
PBST	PBS + 0.1% Tween^{20}
PCR	polymerase chain reaction
PCV	posterior cardinal vein
PDGF	platelet-derived growth factor
PDGFB	platelet-derived growth factor B
PDGFRB	platelet-derived growth factor receptor-β
PDPN	podoplanin
PECAM1	platelet/endothelial cell adhesion molecule 1
PEL	primary effusion lymphoma
PES	phenazine ethosulfate
PFA	paraformaldehyde
PFU	1-phenyl 2-thiourea

p.i.	post-infection
PI3K	phosphatidylinositol 3-kinase
PIK3R1	phosphoinositide-3-kinase regulatory subunit 1
PIK3R2	phosphoinositide-3-kinase regulatory subunit polypeptide 2
PIP_3	phosphatidylinositol-3,4,5-trisphosphate
PLB	Passive Lysis Buffer
PLCG1	phospholipase c gamma 1
PLXND1	plexin D1
POFUT1	protein O-fucosyltransferase 1
POGLUT1	protein O-glucosyltransferase 1
pre-miRNA	precursor miRNA
pri-miRNA	primary miRNA
PROX1	prospero homeobox 1
PTEN	phosphatase and tensin homolog
qPCR	quantitative PCR
qRT-PCR	quantitative reverse transcriptase PCR
RASA1	RAS p21 protein activator (GTPase activating protein) 1
RB1	retinoblastoma 1
RBP	RNA-binding protein
RBPJ	recombination signal binding protein for Ig kappa J region
RCC	renal clear cell carcinoma
READ	rectum adenocarcinoma
RHOA	ras homolog family member A
RLU	relative light units
RNU6-1	RNA, U6 small nuclear 1
ROBO1	roundabout axon guidance receptor homolog 1
ROBO4	roundabout axon guidance receptor homolog 4
ROCK	Rho-associated protein kinase
RT	room temperature
RTA	replication and transcription activator
RUNX1	runt-related transcription factor 1
RUNX2	runt-related transcription factor 2
S1PR	sphingosine-1-phosphate receptor
SAs	segmental arteries
SCF	stem cell factor

SD	standard deviation
SDS	sodium dodecyl sulphate
SDS-PAGE	SDS-polyacrylamide gel electrophoresis
SELE	selectin E
SEM	standard error of the mean
SEMA3A	semaphorin 3a
SEMA5A	semaphorin 5a
SEMA6A	semaphorin 6a
SILAC	stable isotope labelling with amino acids in cell culture
SMAD1	SMAD family member 1
SNAI1	snail family zinc finger 1
SNORA66	small nucleolar RNA, H/ACA box 66
SOX2	SRY (sex determining region Y)-box 2
SPRED1	sprouty-related EVH1 domain containing 1
SPRY2	sprouty homolog 2
SSC	standard saline citrate
SUFU	suppressor of fused homolog
SV(s)	segmental vein(s)
TACE	tumour necrosis factor (TNF)-α-converting enzyme
TAE	Tris-acetate EDTA
tal1	T-cell acute lymphocytic leukemia 1
TARBP2	TAR (HIV-1) RNA binding protein 2
Tat	trans-activator of transcription
TBS	tris buffered saline
TBST	tris buffered saline plus 0.01% (v/v) Tween20
TEK	TEK tyrosine kinase, endothelial
TEMED	tetramethylethylenediamine
TGF-β	transforming growth factor β
TGFBR2	TGF-β receptor 2
THBS1	thrombospondin 1
TIMP1	tissue inhibitor of metalloproteinase 1
TIMPs	tissue inhibitors of metalloproteinases
TM	melting temperature
TNF	tumour necrosis factor
TPA	12-O-tetradecanoyl phorbol-13-acetate

TUBA	tubulin alpha
TUBG	tubulin gamma
TUT4	TUTase4
UNC5B	unc-5 homolog B
vCCL1	viral chemokine (C-C motif) ligand 1
vCCL2	viral chemokine (C-C motif) ligand 2
vCCL3	viral chemokine (C-C motif) ligand 3
vCyclin	viral cyclin
VEGFA	vascular endothelial growth factor A
VEGFC	vascular endothelial growth factor C
VEGFR2	vascular endothelial growth factor receptor 2
VEGFR3	vascular endothelial growth factor receptor 3
vFLIP	viral FLICE-inhibitory protein
vGPCR	viral G-protein coupled receptor
VHL	von Hippel-Lindau tumor suppressor, E3 ubiquitin protein
vIL-6	viral interleukin-6
VSV-G	Vesicular stomatitis virus-G
v/v	volume/volume
wnt5b	wingless-type MMTV integration site family member 5b
WT	wildtype
w/v	weight/volume
XPO5	exportin 5
YSL	yolk syncytial layer

Publications

Some of the work described in this thesis is published in the following paper:

Bridge,G., Monteiro,R., Henderson,S., Emuss,V., Lagos,D., Georgopoulou,D., Patient,R., and Boshoff,C. (2012). The microRNA-30 family targets DLL4 to modulate endothelial cell behavior during angiogenesis. Blood *120*, 5063-72.

Chapter 1. Introduction

1.1 Kaposi sarcoma-associated herpesvirus

Kaposi sarcoma (KS) was first described by Moritz Kaposi in 1872, when he published the case histories of five elderly men suffering from “idiopathic multiple pigmented” sarcomas of the skin (Kaposi, 1972). The aetiological agent of KS was determined in 1994 using PCR-based Representational Difference Analysis, which identified two unique DNA sequences in Acquired Immunodeficiency Syndrome (AIDS)-associated KS (AIDS-KS) that were absent in adjacent skin (Chang et al., 1994). This novel herpesvirus was termed Kaposi sarcoma-associated herpesvirus (KSHV) and is also known as human herpesvirus 8 (HHV8). It is a γ-herpesvirus with a double-stranded DNA genome that encodes over 80 open reading frames (ORFs), flanked by multiple GC-rich terminal repeats, giving it a total size of approximately 170kb (Dourmishev et al., 2003). Sixty-seven of the ORFs have homologues in herpesvirus saimiri (HVS) and a number of KSHV genes are homologous to cellular host genes (Longnecker and Neipel, 2007).

1.1.1 Kaposi sarcoma

KS initially presents as multifocal skin lesions, which are red to the naked eye due to an extensive vascular component (Ganem, 2010). Aggressive forms of the disease also involve lesions in the oral cavity, lymph nodes and visceral organs (Mesri et al., 2010). These vascular tumours consist of abnormal, slit-like blood vessels, an inflammatory infiltrate and sheets of proliferating spindle cells (the tumour cell) (Mesri et al., 2010).

1.1.1.1 Stages of disease development

Classically, KS has been considered to progress through three clinical stages: patch, plaque and nodular. Patch lesions are flat dermal lesions containing inflammatory cells, elongated, spindle-shaped cells and many new blood vessels (Ganem, 2010). Progression to the plaque stage is denoted by a harder lesion in which fluid has accumulated and erythrocyte extravasation has

occurred (Ganem, 2010). It is the extravasation of erythrocytes and their subsequent degeneration that gives the lesions their colouration. As the spindle cells continue to proliferate, a raised lesion develops in which the network of slit-like blood vessels has further extended (Ganem, 2010). This is the final nodular stage. The stages of KS described would suggest that this disease progresses in a clear linear fashion. However, not all the lesions within the same patient will develop at the same rate. Additionally, whilst patch and plaque lesions may be widely disseminated throughout the body, the patient may present with more localised nodular lesions. Therefore, the AIDS Clinical Trials Group (ACTG) tumour classification has now been adopted as a more accurate measure of disease progression (Krown et al., 1997; Mesri et al., 2010).

1.1.1.2 Clinical manifestations

There are four discrete forms of KS: classic, endemic, iatrogenic and AIDS-KS (Mesri et al., 2010). Classic KS occurs predominantly in elderly men of Southern European, Middle-Eastern or Jewish origin, and is a rare, indolent disease that often affects the skin of the lower extremities (Dourmishev et al., 2003). The endemic form of KS is more aggressive than classic KS, involving the lymphatic and/or visceral organs of both children and adults; cases have been reported for many decades in some equatorial regions of Africa (Bhagwat, 1980; Dourmishev et al., 2003; Oettle, 1962; Slavin, 1970). Iatrogenic (post-transplant) KS develops in transplant patients who have received immunosuppressive therapy (Siegel et al., 1969). AIDS-KS is associated with human immunodeficiency virus (HIV)-infected individuals and is the most aggressive and prevalent form of the disease; it affects the oral cavity, gastrointestinal tract and visceral organs, as well as the skin. It was in fact an epidemic of KS in young, homosexual American men which was the first indicator of the AIDS pandemic (Centers for Disease Control, 1981; Gottlieb et al., 1981). HIV-1 infection exponentially increases the risk of developing KS, due to its associated immunosuppressive environment (Boshoff and Weiss, 2002). The direct action of the HIV-1 trans-activator of transcription (Tat) protein has also been implicated in KS development (Vogel et al., 1988).

1.1.1.3 Cellular origin

The exact cellular origin of KS has yet to be defined. The most common cell type in nodular lesions is the spindle cell, which expresses both endothelial (PECAM1, CD34, Factor VIII) and lymphatic (VEGFR3, LYVE1, PDPN) markers (Beckstead et al., 1985; Dupin et al., 1999; Jussila et al., 1998). However, some spindle cells also express markers of macrophages (CD68), dendritic cells (Factor XIII) and smooth muscle cells (ACTG2). Additionally, KSHV infection of lymphatic endothelial cells (LEC) promotes reprogramming towards a blood endothelial cell (BEC) expression profile and the opposite scenario has also been observed in BEC (Hong et al., 2004; Wang et al., 2004). Viral-induced reprogramming in LEC has been partially attributed to silencing of the transcription factor v-maf avian musculoaponeurotic fibrosarcoma oncogene homolog (MAF) by the KSHV-encoded miRNAs (Hansen et al., 2010). MAF is expressed in LEC but not BEC and maintains LEC identity by repressing the expression of BEC-specific genes (Hansen et al., 2010). One current hypothesis is that KSHV infects circulating endothelial precursor cells and drives them towards a lymphatic lineage (Mesri et al., 2010). This theory is supported by the fact that circulating vascular progenitors display KS spindle cell markers (Beckstead et al., 1985; Jussila et al., 1998). It would also help to explain the multifocal presentation of advanced KS.

1.1.1.4 Tumour microenvironment

Angiogenesis, proliferating spindle cells and a prominent immune infiltrate are the characteristic hallmarks of KS lesions. All three processes are continually active and necessary for KS progression. The inflammatory cell infiltrate appears before spindle cell formation, highlighting the importance of this component to KS pathogenesis (Ensoli and Stürzl, 1998). The immune infiltrate is largely comprised of $CD8^+$ T cells and monocyte-macrophages. Dendritic cells, $CD4^+$ T cells and B cells are also present, although not in such abundance (Ensoli and Stürzl, 1998). Consequently, KS lesions are typified by high levels of inflammatory cytokines secreted by immune cells, including interferon gamma (IFNG), tumour necrosis factor (TNF), interleukin-1 (IL-1), interleukin-6 (IL-6) and colony stimulating factor 2 (CSF2). This cytokine profile influences endothelial cell activation and induces the production of angiogenic

factors, leading to blood vessel formation and further recruitment of T cells and monocytes. KSHV-infected spindle cells also secrete pro-angiogenic (ANG2, VEGFA, TGF-β) and pro-inflammatory factors (IL-1, IL-6, CSF2). This augments the cytokine profile and has a direct mitogenic effect on infected endothelial cells (Ensoli et al., 1989). The virus also contributes to the pro-inflammatory and pro-angiogenic environment by encoding its own array of cytokines such as viral interleukin 6 (vIL-6) and viral chemokines (vCCL1-3) (Boshoff et al., 1997). KS tumourigenesis is driven by this combination of inflammatory cells, angiogenic factors and cytokines, hence it can be defined as a paracrine neoplasia (Mesri et al., 2010).

1.1.2 Lymphoproliferative disorders

KSHV is also the aetiological agent of two lymphoproliferative disorders, multicentric Castleman's disease (MCD) and primary effusion lymphoma (PEL) (Cesarman et al., 1995).

PEL is an aggressive non-Hodgkin's B cell clonal lymphoma that lacks a distinct tumour mass and presents as malignant effusions in the pericardial, pleural or peritoneal cavities (Jenner and Boshoff, 2002). PEL is characterised as a post-germinal centre B cell lymphoma, however PEL cells often lack B cell specific markers (Boshoff et al., 1998; Cesarman et al., 1995; Jenner et al., 2003). The majority of patients with PEL are co-infected with HIV and/or Epstein-Barr Virus (EBV) (Cesarman et al., 1995; Jenner et al., 2003). Cell lines established from PEL samples are commonly used for experimental investigation because they maintain the KSHV genome at high copy numbers.

MCD is a polyclonal tumour that arises from naïve B cells. Only a small population of the tumour cells are KSHV-positive in KSHV-linked MCD. These attract uninfected B cells to the tumour site, possibly through the action of both viral and human IL6 and other cytokines (Dupin et al., 2000). Only 50% of MCD cases in HIV-negative patients are KSHV-positive; however, nearly all cases of MCD in HIV-positive patients are KSHV-positive (Moore and Chang, 2003; Soulier et al., 1995). EBV co-infection does not occur in MCD tumours (Du et al., 2001).

1.1.3 Viral life cycle

1.1.3.1 Virus entry

KSHV has been shown to have a broad tropism, both *in vivo* and *in vitro*. KSHV is able to bind to cells via the glycoproteins that coat the virion: K8.1, gB, gH and gL. K8.1 and gB connect with heparan sulphate, which is ubiquitously displayed on the membrane of many human cells (Boshoff, 2012). gB may also directly interact with integrins to induce intracellular signalling (Boshoff, 2012). It has recently been shown that a heterodimer of gH and gL binds to EPH receptor A2 (EPHA2) on epithelial and endothelial cells, which triggers intracellular signal transduction pathways including focal adhesion kinase (FAK) activation (Hahn et al., 2012). This creates a permissive environment for KSHV entry into the cell, thereby triggering endocytosis of the viral particle (Boshoff, 2012). Once inside the cell, viral capsids are released by fusion of the viral envelope with the endosomal membrane. The capsids then move to the perinuclear region and the viral genome enters the nucleus via nuclear pores (Boshoff, 2012). Once in the nucleus, KSHV can undergo two modes of infection: lytic replication, culminating in the production of new virions, or latent infection resulting in persistent host cell infection.

1.1.3.2 Latent infection

The establishment of latency enables KSHV to maintain long term infection in quiescent or proliferating cells by ensuring viral genome replication and avoiding initiation of the anti-viral response. Most new KSHV infections result in the latent programme and both KS and PEL tumour cells are latently infected (Bechtel et al., 2003; Cesarman et al., 1995; Zhong et al., 1996). During latency the viral genome is maintained as a circularised extrachromosomal episome (Renne et al., 1996). To ensure that KSHV infection persists, the episome is copied by the cellular machinery during DNA replication and is attached to host chromatin during mitosis. There is a restrictive pattern of gene expression during latent infection which minimises the number of antigens available for presentation and recognition by the host immune response. The KSHV latent genes are latent nuclear antigen 1 (*LANA*; *ORF73*), viral cyclin (*vCyclin*; *ORF72*), viral FLICE-inhibitory protein (*vFLIP*; *ORF 71*), *Kaposin* (*K12)* and

several viral miRNAs (Dittmer et al., 1998; Dittmer, 2003; Zhong et al., 1996). The persistent expression of these latent genes is concomitant with progression to malignant KS.

1.1.3.3 Lytic infection

Reactivation of latent KSHV can occur sporadically, leading to lytic replication. Within KS lesions the vast majority of cells are latently infected including the spindle cells, which arise from latently infected endothelial cells after the establishment of the initial inflammatory lesion. However, there is a small lytic population of cells producing new virions, which enables propagation of the virus and recruitment of new cells to the lesion (Jenner and Boshoff, 2002). Lytic infection is induced by expression of replication and transcription activator (RTA). Subsequently, lytic immediate-early, delayed-early and late genes are expressed sequentially, viral DNA is amplified, and the infected cell is lysed, allowing the release of virions (Longnecker and Neipel, 2007). A number of factors have been shown to trigger the switch from latent to lytic infection, but the most potent and widely used chemical inducer is 12-O-tetradecanoyl phorbol-13-acetate (TPA) (Renne et al., 1996).

1.1.4 Angiogenic gene expression in KLEC

The transcriptional signature of KSHV-infected LEC (KLEC) has previously been described by obtaining gene expression microarray (GEM) profiles from six pairs of LEC and KLEC using an Affymetrix hg-u133+2 GeneChip (Lagos et al., 2007). When these data was compared to a list of 239 genes that are associated with angiogenesis it was found that 33% are significantly altered upon KSHV infection of LEC (Figure 1.1.) (Vart et al., 2007). Among the upregulated genes are many known pro-angiogenic factors. These include the transcription factor hypoxia inducible factor 1 alpha subunit (*HIF1A*), which activates the transcipriton of other pro-angiogenic genes in response to hypoxia, and matrix metallopeptidase 1 (*MMP1*), which enables endothelial cell migration by degrading the extracellular matrix (Figure 1.1).

Figure 1.1. KSHV infection regulates an array of angiogenic factors. Heat map of 79 angiogenesis genes which are significantly changed between LEC and KLEC samples ($q < 0.001$). Each gene is represented by a single probe. Genes were ordered by amount of fold change between conditions with the uppermost gene displaying the highest positive differential expression and the lowermost gene displaying the highest negative differential expression. (Figure adapted from Supplementary Figure 3 of Vart *et al*., 2007.)

1.2 Angiogenesis

Angiogenesis is strictly defined as the growth of new blood vessels from pre-established ones and occurs in response to pro-angiogenic stimuli (Risau et al., 1988). These stimuli occur during development and in response to hypoxia during growth, wound healing and pathological conditions. For sprouting angiogenesis to occur, endothelial cells must undergo several stages of morphological change. These transformations are summarised below, however for further detail regarding the role of Notch signalling in this process, see Section 1.4.5.

1.2.1 Initiation of sprouting

Upon stimulation by pro-angiogenic factors, predominantly by vascular endothelial growth factor A (VEGFA), endothelial cells must emerge from a pre-existing vessel. During quiescence this is prevented by the existence of a basement membrane, shared by both mural and endothelial cells, which forms a covering around the vessel (Eble and Niland, 2009). Therefore, at the onset of sprouting, matrix metalloproteases (MMPs) are released to degrade the basement membrane. This also serves to release pro-angiogenic growth factors that are contained within the extracellular matrix (Potente et al., 2011). In parallel, release of angiopoietin 2 (ANGPT2) by endothelial cells stimulates the detachment of mural cells (Augustin et al., 2009).

Nascent sprouts are led by endothelial tip cells (see Section 1.3.5.2) that generate long, dynamic filopodia upon VEGFA stimulation (Gerhardt et al., 2003; Ruhrberg et al., 2002), most probably as a result of cell division cycle 42 (CDC42) activation (De Smet et al., 2009). These filopodia are coated in receptors that enable the tip cells to respond to directional cues, thereby leading the sprout to the required location (Potente et al., 2011). One such receptor is vascular endothelial growth factor receptor 2 (VEGFR2), which binds VEGFA, enabling the tip cell to follow the pro-angiogenic signal. Other guidance receptors which are known to be expressed on endothelial cells are unc-5 homolog B (UNC5B), roundabout axon guidance receptor homolog 4 (ROBO4), plexin D1 (PLXND1), various neuropilins (NRPs) and several ephrin (EPH) family members (Potente et al., 2011).

1.2.2 Sprout elongation and lumen formation

The endothelial cells which make up the body of the growing sprout are known as stalk cells (see Section 1.4.5.2). These cells proliferate in response to VEGFA and display fewer filopodia than the leading tip cells (Gerhardt et al., 2003). As the sprout extends, adherens junctions containing VE-cadherin form between neighbouring stalk cells to ensure the integrity of the sprout (Potente et al., 2011). It is the stalk cells that form the lumen of the new vessel; however, the mechanism of lumen formation varies depending on the situation in which angiogenesis is occurring (Iruela-Arispe and Davis, 2009; Zeeb et al., 2010). Cell hollowing has been observed extensively *in vitro* and during the formation of the zebrafish intersomitic vessels, although this is now contested (See Section 1.3.2.3) (Blum et al., 2008; Kamei et al., 2006). Intracellular vacuoles form in the stalk cells and then coalesce with vacuoles in the neighbouring cells to create a continuous lumenal space. A second mechanism, cord hollowing, has been reported in axial vessels (Iruela-Arispe and Davis, 2009). For cord hollowing to occur, apical-basal polarity must first be established in the stalk cells. Subsequently, the apical (lumenal) membrane delivers a repulsive signal by displaying charged glycoproteins and hence begins to open the lumen. Expansion of the lumen requires morphological changes in the stalk cells and the rearrangement of cell-cell junctions. VEGFA drives the necessary endothelial cell changes by increasing Rho-associated protein kinase (ROCK) activity (Strilić et al., 2009).

1.2.3 Vessel stabilisation and maturation

When the tip cell from one sprout comes into contact with a tip cell from another sprout, vessel fusion can occur, known as anastomosis (Blum et al., 2008). This can be facilitated by macrophages, possibly through cell-to-cell communication (Fantin et al., 2010). Adherens junctions then form between the tip cells to stabilise the initial connection and allow blood to flow through the now continuous lumen. Aided by the action of tissue inhibitors of metalloproteinases (TIMPs), extracellular matrix proteins are laid down by the endothelial cells in order to establish a basement membrane which will stabilise the new vessel (Potente et al., 2011). However, the vessel is not fully mature until mural cell interactions have been established. Once blood flow has commenced through

the nascent vessel, tissue oxygenation is achieved and consequently pro-angiogenic signals are turned off, namely by a reduction in VEGFA production.

The mural cells of immature vessels and capillaries are pericytes, whereas larger arteries and veins are covered by a layer of vascular smooth muscle cells (Gaengel et al., 2009). Transforming growth factor β (TGF-β) signalling is required to stimulate mural cell induction, differentiation, proliferation and migration. Accordingly, loss of function of TGF-β receptor 2 (*Tgfbr2*), activated receptor-like kinase 1 (*Alk1*) or endoglin (*Eng*) in mice causes impaired mural cell development and hence vessel instability (Pardali et al., 2010). However, it is the platelet-derived growth factor (PDGF) signalling pathway that controls mural cell recruitment to blood vessels (Gaengel et al., 2009). Platelet-derived growth factor B (PDGFB) is released by endothelial cells and binds to PDGF receptor-β (PDGFRB) on mural cells which stimulates their migration and proliferation. Consequently, inactivation of *Pdgfb* or *Pdgfrb* in mice leads to vascular dysfunction due to pericyte deficiency (Gaengel et al., 2009). Sphingosine-1-phosphate receptor (S1PR) signalling is also required for mural cell recruitment and to strengthen the endothelial cell-pericyte connections by inducing N-cadherin trafficking (Gaengel et al., 2009). The mural cells themselves release angiopoietin 1 (ANGPT1) which binds to TEK tyrosine kinase, endothelial (TEK) on endothelial cells to tighten endothelial cell junctions and promote pericyte adhesion (Augustin et al., 2009).

1.2.4 Vascular remodelling

Once blood flow has been initiated, the resulting haemodynamic forces cause remodelling of the newly established vascular network (Lucitti et al., 2007). When shear forces are exerted on the endothelium, Kruppel-like factor 2 (KLF2) is upregulated in endothelial cells. KLF2 is a mechano-sensitive transcription factor which promotes endothelial cell quiescence, by downregulating VEGFR2, and ensures that the newly formed vessel remains open (Potente et al., 2011). If the vessel is poorly perfused, KLF2 expression is not stimulated and the endothelial cells undergo apoptosis leading to vessel regression (Potente et al., 2011). In zebrafish aortic endothelial cells, the miRNA miR-126 has been shown to act downstream of Klf2a to regulate vascular remodelling (Nicoli et al., 2010).

Other vascular alterations which can occur include intussusceptive growth, to split new vessels, and an element of additional sprouting (Phng and Gerhardt, 2009).

1.3 Zebrafish development

The zebrafish, *Danio rerio*, is a small tropical freshwater fish that is commonly used to investigate factors regulating angiogenesis and tumour development, in addition to its established role in genetics, developmental biology and neuroscience. Working with zebrafish embryos does not have the time constraints of some other models as zebrafish breed easily, produce many offspring per laying and have a very short generation time. The embryos have generally hatched by 72 hours post-fertilisation (hpf) and embryonic development is considered complete by the fifth day.

The zebrafish is an attractive *in vivo* model because fertilisation of their eggs occurs externally, therefore live embryos can be easily accessed for manipulations, such as the injection of mRNA or morpholinos (MOs). Small molecules can also be added directly to the water that holds the fish as they will diffuse into the embryo. Once the embryos have been treated, they can be monitored through all developmental stages under a microscope and individual embryos can be harvested and used for further study, such as *in situ* hybridisations. The availability of transgenic zebrafish embryos with fluorescent blood vessels has greatly aided the study of angiogenesis throughout development (Lawson and Weinstein, 2002). Vascular morphogenesis within zebrafish embryos can be easily visualised due to their optical transparency. Pigmentation of the embryos, which begins at 25 hpf, can be inhibited so that microscopic examination of the vasculature can be continued throughout development.

1.3.1 General embryonic development

Embryonic development in the zebrafish is a rapid process, especially when compared to other vertebrates. Embryogenesis takes approximately 2-3 days, the larvae hatch around the third day of development and by day 5 the vast

majority of cell types have differentiated and the organs have all begun functioning. Embryogenesis can be divided into seven periods: the zygote, cleavage, blastula, gastrula, segmentation, pharyngula and hatching (Kimmel et al., 1995). Within each period are defined developmental stages which are detailed in Table 2.7.

Between 0 and 0.75 hpf the newly fertilised egg completes the first zygotic cell division and then enters the cleavage period where cell divisions 2 to 7 occur synchronously at approximately 15 minute intervals (Kimmel et al., 1995). At ~2.25 hpf the embryo enters the blastula period, during which midblastula transition (MBT) occurs, the yolk syncytial layer (YSL) is formed and epiboly begins (Kimmel et al., 1995). During the MBT cell cycles are lengthened and start to occur asynchronously (Kane and Kimmel, 1993). The MBT also denotes the start of zygotic gene transcription (Kane and Kimmel, 1993). Prior to this point, the zygotic chromatin is condensed, hypoacetylated and hypermethylated whilst the embryo relies upon maternal mRNA for translation (Kimmel et al., 1995; Meehan et al., 2005). Epiboly is the process by which the YSL and the blastoderm thin out and spread across the yolk cell until it is completely encompassed.

The gastrula period, which occurs between 5.25 and 10 hpf, is marked by the morphogenetic movements of involution, convergence and extension that generate the epiblast, hypoblast and the embryonic axis. The epiblast evolves into the ectoderm but also contains cells capable of generating the mesoderm and endoderm. The cells of the hypoblast contribute to the formation of the embryonic endoderm, from which derive the respiratory and digestive tracts. It is also during the gastrula period that epiboly is completed (Kimmel et al., 1995). During segmentation the somites, pharyngeal arch primordia and the neuromeres develop. It is also during this period that organogenesis begins and involuntary tail movements are first observed (Kimmel et al., 1995).

The pharyngula period (24-48 hpf) is the point when the final morphology of the zebrafish really becomes apparent as the body axis of the embryo, which was curved around the yolk sac, straightens. Blood circulation commences during the segmentation period, pigmentation is observed and the fins begin to

develop (Kimmel et al., 1995). Hatching occurs from 48 hpf onwards, although not all embryos of the same clutch will hatch together. The larvae that emerge then inflate their swim bladders and by 72 hpf they actively respond to external stimuli and display food-seeking behaviour (Kimmel et al., 1995).

1.3.2 Development of the vasculature

During the developmental programme of vertebrates, the cardiovascular system is one of the first organs to evolve. This is because the development and growth of all other organs depends upon a functioning circulatory network. The establishment of this network occurs through two distinct morphogenetic processes: vasculogenesis and angiogenesis (Poole and Coffin, 1989; Risau et al., 1988). Vasculogenesis occurs when angioblasts aggregate to form a vascular cord which is then lumenised. Angiogenesis is the sprouting of new capillaries from pre-existing blood vessels (Poole and Coffin, 1989; Risau et al., 1988). These processes are clearly demonstrated in the vascular morphogenesis of zebrafish embryos.

1.3.2.1 Origin of endothelial cells

The ventrolateral mesoderm is the source of angioblasts, precursors of the endothelial cell lineage (Kimmel et al., 1995; Stainier et al., 1995). Haematopoeitic cells also arise from the ventrolateral mesoderm and specification of these two major cell types is highly conserved across a range of vertebrate species, including zebrafish. It is controlled by transcription factors belonging to the E-twenty six (ETS), GATA and (LIM-only) LMO families (De Val et al., 2008; Detrich et al., 1995; Liu and Patient, 2008; Thompson et al., 1998). These transcription factors are initially expressed in the anterior and posterior lateral mesoderm at the beginning of somitogenesis. They denote the haemangioblasts, the multipotent precursor cells that can differentiate into both haematopoietic and endothelial cells. During somitogenesis the two cell populations are differentiated by changes in gene expression. For example, those that will become haematopoietic cells express *T-cell acute lymphocytic leukemia 1* (*tal1*) but not *kinase insert domain receptor like* (*kdrl*) and vice versa for the angioblast progenitors (Gering et al., 1998). By 12-14 hpf, genetic

markers of angioblasts, such as *friend leukemia integration 1a* (*fli1a*), can be visualised in two lateral stripes along the body of the embryo (Roman et al., 2002).

1.3.2.2 Vasculogenesis: dorsal aorta and cardinal vein formation

From 14 hpf onwards, angioblasts migrate in two waves towards the midline of the embryo, following guidance cues generated by the endoderm (Fig. 1.2A, i) (Jin et al., 2005; Lawson and Weinstein, 2002). Once at the midline the angioblasts aggregate to form a vascular cord between the mesoderm and the hypochord (Fig. 1.2A, i) (Eriksson and Löfberg, 2000). There are two theories regarding the subsequent formation of the dorsal aorta (DA) and posterior cardinal vein (PCV). It has been proposed that the first wave of angioblasts form the DA and the second wave of angioblasts form the PCV (Jin et al., 2005). However, following expression of arterial and venous markers, ventral sprouting of angioblasts from the vascular cord has been observed to generate the PCV (Herbert et al., 2009). Therefore, it is now generally thought that the angioblasts from both migratory waves coalesce to form a single vascular primordium, from which both the DA and the PCV originate (Fig. 1.2A, ii) (Herbert et al., 2009).

At ~17 hpf the angioblasts of the vascular primordium begin to express either arterial or venous markers (Fig. 1.2A, ii). Vegfa signalling through Kdrl and subsequent Notch pathway activation induces arterial differentiation in a subset of angioblasts (also discussed in Section 1.4.5.1) (Lawson et al., 2001; Lawson et al., 2002; Lawson et al., 2003; Zhong et al., 2001). Vegfa signalling is stimulated in the ventral somites due to Sonic hedgehog signals from the notochord (Lawson et al., 2002). Venous differentiation however, does not require Vegfa signalling (Covassin et al., 2006; Lawson et al., 2003).

The arterially-defined angioblasts express *ephrin B2* (*efnb2*) whilst the venous precursors express eph receptor B4a (*ephb4*) (Herbert et al., 2009; Jin et al., 2005). The differential expression of these markers in arteries and veins is well established and it now appears that repulsive Ephb4-Efnb2 signalling results in ventral migration of the *ephb4*-expressing angioblasts (Fig. 1.2A, ii) (Herbert et al., 2009; Lawson et al., 2001).

Figure 1.2. Development of the zebrafish vasculature. (A) Schematic cross sections of the zebrafish trunk during dorsal aorta (DA) and posterior cardinal vein (PCV) formation. (i) Migration of angioblasts (purple) to the midline. en: endoderm; h: hypochord; s: somites; nc: notochord; nt: neural tube. (ii) Arterio-venous differentiation to generate venous (blue) and arterial (red) angioblasts followed by ventral sprouting of venous angioblasts. (iii) Lumen formation of the DA occurs by cord hollowing whereas venous angioblasts aggregate around red blood cells (brown) to form a tube. (iv) By 30 hpf both the DA and the PCV are fully formed and can carry blood flow. Endothelial cell junctions are indicated in green. (B) Diagrammatic representation of intersegmental vessel (ISV) formation. Two neighbouring sprouts are depicted as representative examples. The leading tip cells are indicated in green and purple. Lumenal spaces are shown in yellow. SA: segmental artery; SV: segmental vein; DLAV: dorsal longitudinal anastomotic vessel. Diagrams adapted from (Ellertsdóttir et al., 2010).

These coalesce around blood cells (Fig. 1.2A, iii) and by 30 hpf blood flow is established in the PCV (Fig. 1.2, iv) (Herbert et al., 2009). Lumen formation in the DA begins prior to lumenisation of the PCV at ~21 hpf and occurs through the process of cord hollowing (Herbert et al., 2009; Jin et al., 2005), as described in Section 1.2.2. Endothelial cell junctions form between the cells of the DA and apical-basal polarisation occurs (Fig. 1.2A, iii) (Jin et al., 2005). By 24 hpf the DA is fully lumenised (Fig. 1.2A, iii) and blood flow commences between 28 and 30 hpf (Fig. 1.2A, iv).

1.3.2.3 Angiogenesis: intersegmental vessel formation

The intersegmental vessels (ISVs) of the zebrafish embryo link the DA and the PCV with the dorsal longitudinal anastomotic vessel (DLAV) and are formed by two waves of angiogenic sprouting, from the DA and PCV respectively (Isogai et al., 2003; Yaniv et al., 2006). At ~22 hpf the primary wave of sprouting begins from the DA when one or two endothelial cells move out of the DA (Fig. 1.2B, i) (Blum et al., 2008; Isogai et al., 2003). This requires functional Vegfa signalling through Kdrl and kinase insert domain receptor (Kdr) and downstream phospholipase c gamma 1 (Plcg1) activity (Bahary et al., 2007; Covassin et al., 2009; Habeck et al., 2002). The growing sprout consists of 3-4 endothelial cells, one tip cell and two or three stalk cells which migrate dorsally until they reach the level of the dorsal neural tube (Fig. 1.2B, ii) (Blum et al., 2008; Isogai et al., 2003). Having reached this point, the tip cells of the nascent sprouts connect with their anterior and posterior neighbours to form the basic scaffold of the ISV and DLAV (Fig. 1.2B, iii). Due to endothelial cell proliferation and further cell rearrangements, each ISV and connecting T-junction is finally composed of 4-6 endothelial cells which overlap in a staggered fashion to form a multicellular tube with an extracellular lumen (Fig. 1.2B, iv and Fig. 1.3) (Blum et al., 2008). This mode of lumenisation has only been recently accepted, as it was previously thought that ISV lumens were formed by cell hollowing (see Section 1.2.2) (Kamei et al., 2006).

The second wave of sprouting starts at 32 hpf when endothelial cells of the PCV begin migrating dorsally (Fig 1.2B, iii) (Isogai et al., 2003; Yaniv et al., 2006). Some of these sprouts connect to a pre-existing ISV (Fig. 1.2B, iv) whilst the

remainder proceed up to the level of the horizontal myoseptum where they form the parachordal lymphangioblasts that later give rise to the lymphatic network (Hogan et al., 2009a; Isogai et al., 2003). Blood flow commences at ~48 hpf and at this point two types of ISVs are clearly visible: segmental arteries (SAs), which connect the DA to the DLAV, and segmental veins (SVs), formed by the merging of the secondary sprouts with the primary vessels to connect the PCV to the DLAV (Fig. 1.2B, v; Fig. 1.3).

1.3.2.4 VEGFR signalling

In humans and other placental mammals there are three paralogous genes which make up the VEGF receptor family: fms-related tyrosine kinase 1 (*FLT1;VEGFR1*), *KDR* (*VEGFR2*) and fms-related tyrosine kinase 4 (*FLT4:VEGFR3*). Zebrafish possess orthologues of all three receptors: *flt1*, *kdr* and *flt4*. However, along with other teleosts and some higher vertebrates such as chickens, they also encode a fourth VEGF receptor gene: *kdrl* (Bussmann et al., 2008). Both *kdr* and *kdrl* are functional orthologues of *KDR* and the Kdrl protein acts synergistically with Kdr to mediate Vegfa signalling (Bahary et al., 2007).

Figure 1.3. The arrangement of endothelial cells comprising the zebrafish intersegmental vessels. The intersegmental vessels (ISVs) are multicellular tubes consisting of 4-5 cells per vessel (each shown in a different colour). These cells are arranged so that they overlap in a staggered fashion in both the ISV and the dorsal longitudinal anastomotic vessel (DLAV). Extensive intercellular junctions maintain the integrity of the vessel. Diagram from (Blum et al., 2008).

1.4 Notch signalling

The Notch pathway is an intercellular signalling pathway that transduces signals between adjacent cells through the interaction of ligands on the surface of the "signal generating" cell and membrane-associated receptors on the "signal receiving" cell (Fig 1.4). The concept of the *Notch* gene was first identified in *Drosophila* almost 100 years ago due to the existence of a mutant strain which displayed wing "notches" (Morgan, 1917). *Notch* was originally classified as a neurogenic gene because *Notch* mutants were shown to develop an excessive number of neurons (Lehmann et al., 1983; Poulson, 1945). It was not until *Notch* homologues in *C. elegans* were discovered and characterised (*lin-12* and *glp-1*), that the role of Notch in the control of cell fate was revealed (Roehl et al., 1996; Yochem et al., 1988). It is this key function that regulates pattern formation during embryonic development and is why the Notch pathway is conserved throughout the animal kingdom (Lai, 2004).

1.4.1 Notch receptors and ligands

In mammals there are five canonical Notch ligands: delta-like 1 (DLL1), delta-like 3 (DLL3), delta-like 4 (DLL4), jagged 1 (JAG1) and jagged 2 (JAG2). These can bind to one of four Notch receptors: NOTCH1, NOTCH2, NOTCH3 and NOTCH4. Both ligands and receptors are single-pass transmembrane proteins. The extracellular domains of these proteins contain arrays of epidermal growth factor (EGF) repeats through which ligand-receptor contact occurs (Rebay et al., 1991).

1.4.2 Notch signal transduction

Ligand-receptor binding triggers proteolytic cleavage of the Notch receptor to release the Notch intracellular domain (NICD) (Fig. 1.4). Cleavage occurs do to the action of two proteases. The metalloproteinase tumour necrosis factor(TNF)-α-converting enzyme (TACE) cleaves the Notch receptor within the juxtamembrane region (Fig 1.4). This occurs because ligand binding induces conformational changes that allow access to the cleavage site (Brou et al., 2000). Subsequently, the receptor is cleaved within the transmembrane domain by γ-secretase (Fig 1.4) (De Strooper et al., 1999). The NICD then translocates

to the nucleus where it directly interacts with the transcription factor CSL, also known in mammals as recombination signal binding protein for Ig kappa J region (RBPJ) (Fig 1.4) (Jarriault et al., 1995). When not bound to NCID, CSL acts as a transcriptional repressor by interacting with a corepressor complex containing a histone deacetylase (Kao et al., 1998). The corepressor complex is displaced by NCID which instead recruits mastermind-like 1 (MAML1), and a histone acetyltransferase such as p300 (Fig 1.4). This converts CSL into a transcriptional activator and leads to the transcription of Notch target genes belonging to the Hairy/Enhancer of Split (HES) and HES-related (HEY) families (Fig 1.4) (Davis and Turner, 2001; Nakagawa et al., 2000). HES and HEY proteins are basic-helix-loop-helix (bHLH) proteins that act as transcriptional repressors to regulate a diverse range of developmental processes (Fischer and Gessler, 2007). Notch target gene specificity is determined by CSL binding to a cis-element with the consensus GTGGGAA, although variants of this consensus, including CTGAGAA, also bind CSL with high affinity (Lam and Bresnick, 1998).

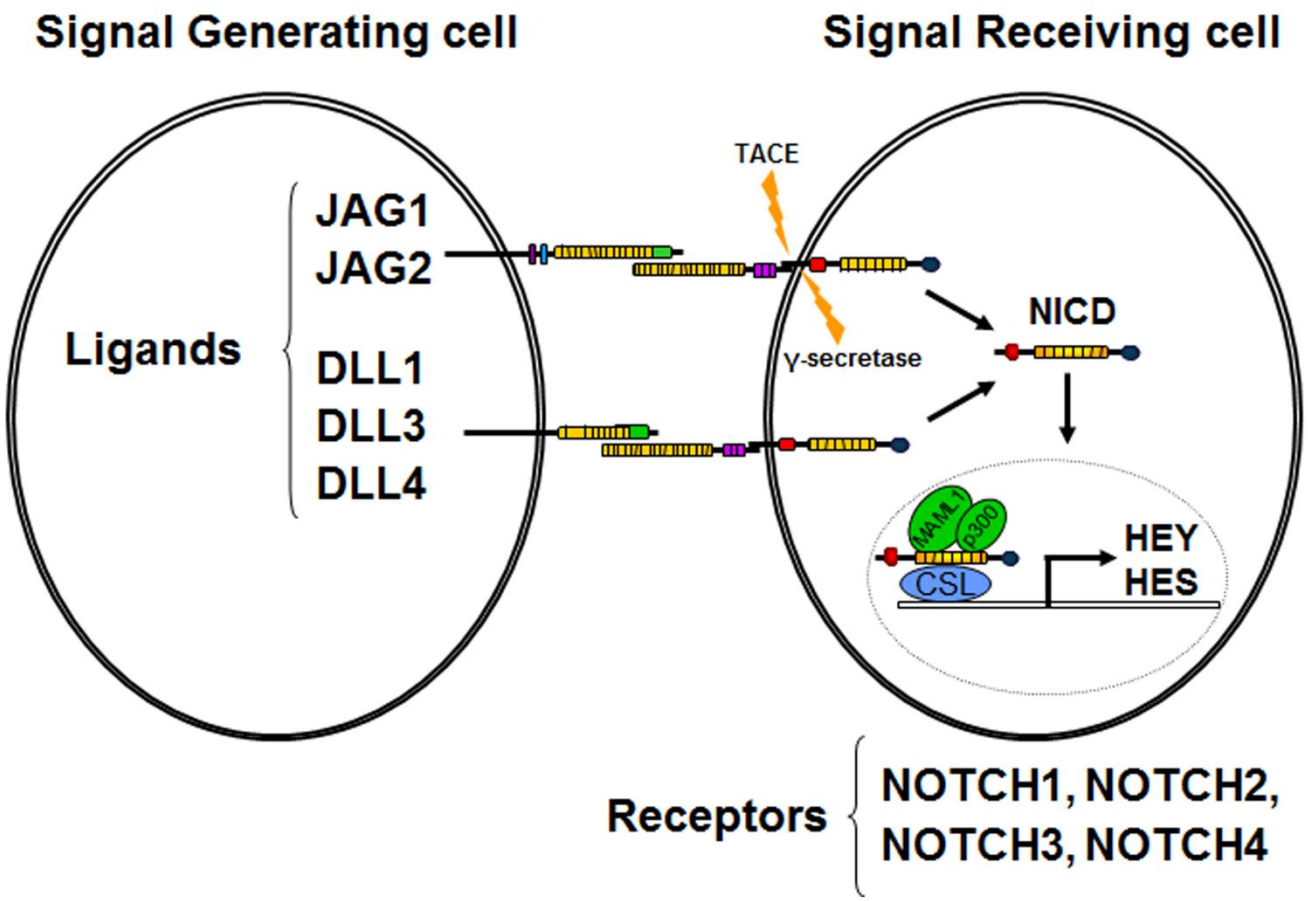

Figure 1.4. The Notch Signalling Pathway. Diagrammatic representation of Notch signal transduction between a signal generating cell and a signal receiving cell. Ligands of the Serrate (JAG1 and JAG2) or Delta (DLL1, DLL3 and DLL4) families on the signal generating cell bind to Notch receptors (NOTCH1-4) on the signal receiving cell. This triggers proteolytic cleavage of the Notch receptor by tumour necrosis factor (TNF)-α-converting enzyme (TACE) and γ-secretase to release the Notch intracellular domain (NICD). The NICD translocates to the nucleus where it binds to the transcription factor CSL and recruits coactivators such as mastermind-like (MAML1) and the histone acetyltransferase p300. This causes the transcription of Notch target genes such as those of the Hairy/Enhancer of Split (HES) and HES-related (HEY) families.

1.4.3 Regulation of the Notch pathway

1.4.3.1 Expression patterns

Notch receptor expression is spatially and temporally restricted in order to ensure that Notch signalling occurs at the proper time and in the correct cell type during development and in the adult organism. The expression patterns of NOTCH1 and NOTCH2 are the broadest and display some overlap. NOTCH1 is found in the majority of tissues, including brain, liver, heart, lung, kidney, intestine, bone marrow, skeletal muscle, spinal cord, eye and thymus (Swiatek et al., 1994). NOTCH2 expression is more restricted, being found in the brain, liver, kidney and stomach (McCright et al., 2001). NOTCH3 and NOTCH4 are the most cell-type specific Notch receptors. NOTCH3 has been detected in vascular smooth muscle, the central nervous system and in certain haematopoietic cells whilst NOTCH4 is endothelial cell specific (Joutel et al., 2000; Lardelli et al., 1994; Uyttendaele et al., 1996). These diverse expression patterns are reflected in the wide range of biological functions that have been assigned to the various Notch receptors (Wu and Bresnick, 2007). Tight transcriptional control of Notch receptor expression is required to maintain these expression patterns. The transcription factors SRY-box 2 (SOX2), FBJ murine osteosarcoma viral oncogene homolog (FOS) and jun proto-oncogene (JUN) have all been identified as downstream effectors of Notch regulation (Wu and Bresnick, 2007).

1.4.3.2 Post-transcriptional regulation

Although the differential expression patterns of Notch receptors and ligands are a key element of Notch pathway regulation, they are not sufficient to explain the differences in signalling activity which have been observed (Kopan and Ilagan, 2009). For instance, two cells that express the same panel of receptors and ligands may have varying levels of Notch signalling in response to the same stimuli. An additional level of regulation is provided in the form of post-transcriptional modifications.

The EGF repeats of Notch receptors are subject to two forms of O-glycosylation, addition of O-glucose and O-fructose (Kopan and Ilagan, 2009).

Once a Notch receptor has been translated in the endoplastic reticulum (ER), protein O-fucosyltransferase 1 (POFUT1) is able to add fructose to the EGF repeats. POFUT1 function is essential for Notch signalling in mammals; however, it is actually the ER chaperone function of POFUT1 that is required for optimal protein folding (Kopan and Ilagan, 2009). O-fructose additions can be extended further by Fringe glycosyltransferases. It is these modifications which affect ligand-receptor binding; Serrate ligands (JAG1 and JAG2) have a higher affinity for fucosylated Notch whereas Delta ligands (DLL1-4) preferentially bind to Fringe-modified receptors (Xu et al., 2007). It is also possible that O-glycosylation by protein O-glucosyltransferase 1 (POGLUT1) may contribute to receptor activation (Kopan and Ilagan, 2009). Although the exact contributions of fucosylation, glycosylation and Fringe modifications have yet to be determined and appear to differ greatly between species, these adjustments are undoubtedly involved in modifying the strength of receptor-ligand binding and hence act to modulate overall signal strength (Kopan and Ilagan, 2009).

Mono-ubiquitination of the NICD by a variety of E3 ubiquitin ligases induces endocytosis and subsequent degradation of the Notch receptors (Kandachar and Roegiers, 2012). This controls the level of Notch receptor presentation at the cell surface and hence limits receptor-ligand binding. Notch ligands are also subject to ubiquitin-induced endocytosis; however, this process appears to generate a more effective ligand and it is required for Notch activation. The mechanism behind this occurrence is not yet fully defined but two models have been proposed. The Notch ligand may be modified upon internalisation in such a way that it then becomes capable of inducing functional Notch signals (Kandachar and Roegiers, 2012). Alternatively, when ligand that is bound to a Notch receptor is endocytosed, the TACE cleavage site on the Notch receptor may be revealed due to transendocytosis of the Notch receptor extracellular domain (Itoh et al., 2003).

1.4.4 Role in development

Notch signalling has been shown to function during the development of a wide range of tissues and organs. These include the circulatory and nervous systems, muscles, the kidney, the pancreas and in keratinocytes (Wu and

Bresnick, 2007). The importance of Notch signalling during development has been demonstrated by the targeted deletion of individual Notch receptors. Loss of either *Notch1* or *Notch2* in mice is embryonically lethal. *Notch1* is require for efficacious somitogenesis, angiogenesis and neurogenesis whereas *Notch2* deletion causes kidney, heart and neural defects (Conlon et al., 1995; Hamada et al., 1999; Krebs et al., 2000; McCright et al., 2001; Swiatek et al., 1994). Neither *Notch3* nor *Notch4* deletion is lethal to mouse embryos; however, *Notch1/Notch4* double mutants die due to impaired vascular development (Domenga et al., 2004; Krebs et al., 2000). Interestingly, DLL4, which signals through both NOTCH1 and NOTCH4, displays haploinsufficient lethality due to the development of extensive arterial defects (Krebs et al., 2004).

1.4.5 Role in angiogenesis

Many members of the Notch pathway and related signalling components are expressed in endothelial cells: receptors NOTCH1 and NOTCH4 (Favre et al., 2003; Villa et al., 2001); ligands DLL1, DLL4, JAG1 and JAG2 (Claxton and Fruttiger, 2004; Favre et al., 2003; Mailhos et al., 2001; Villa et al., 2001); target genes HEY1, HEY2 and NOTCH-regulated ankyrin repeat protein (NRARP) (Fischer and Gessler, 2007; Krebs et al., 2001); the transcriptional factors RBPJ and MAML1 (Dou et al., 2008; Liu et al., 2006); the negative regulator numb homolog (NUMB) (Favre et al., 2003). Extensive functional studies in both mice and zebrafish have revealed that Notch signalling is required at all stages of the vertebrate angiogenic programme.

1.4.5.1 Arterio-venous differentiation

During development of the cardiovascular system, angioblasts, the endothelial cell precursors, are directed towards either an arterial or venous fate by a tightly regulated cell specification pathway. VEGFA signalling is sensed by angioblasts through VEGFR2 and those cells that receive a sufficiently strong signal are driven towards an arterial fate by the combined action PLCG1, mitogen-activated protein kinase (MAPK), Wnt and Notch signalling (Corada et al., 2010; Hong et al., 2006; Lawson et al., 2001; Lawson et al., 2002; Lawson et al., 2003; Wythe et al., 2013; Zhong et al., 2001). EFNB2, both a marker and a

driver of arterial differentiation, is in fact a direct transcriptional target of the Notch pathway (Grego-Bessa et al., 2007; Herbert et al., 2009). Targeted deletion or knockdown of various Notch signalling components results in the loss of correct arterial and venous specification and severe vascular abnormalities. When the expression of *notch3*, *rbpja* and *hey2* were reduced in zebrafish embryos, artery formation was disturbed, *efnb2* expression was impaired and there was an increase in expression of the venous marker *ephb4* (Lawson et al., 2001; Siekmann and Lawson, 2007; Zhong et al., 2001). Additionally, endothelial cell specification defects are observed in *mindbomb* mutants (Lawson et al., 2001). Mind bomb (Mib) is a RING ubiquitin ligase which is required for efficient Notch activation by Delta ligands (Itoh et al., 2003).

In the mouse, Dll1, Dll4, Notch1, Notch4, Rbpj, Hey1 and Hey2 are all required for successful arterio-venous differentiation (Carlson et al., 2005; Duarte et al., 2004; Fischer et al., 2004; Gale et al., 2004; Kim et al., 2008; Krebs et al., 2004; Limbourg et al., 2007; Trindade et al., 2008). Venous differentiation does not require Vegfa signalling and venous identity has long been considered the default position in the absence of Notch signalling (Covassin et al., 2006; Lawson et al., 2001; Lawson et al., 2003). However, there does appear to be some element of active Notch inhibition in venous endothelial cells. It was found that the transcription factor nuclear receptor subfamily 2 group F member 2 (Nr2f2) is only expressed in venous endothelial cells and that deletion of Nr2f2 in endothelial cells allowed them to acquired arterial characteristics (You et al., 2005). These characteristics included an upregulation of the Notch signalling components Notch1, Jag1 and Hey1. It appears that Nr2f2 acts to suppress Notch signalling by downregulating the VEGF receptor *neuropilin 1* (*Nrp1*) (You et al., 2005).

1.4.5.2 Tip cell specification

DLL4/Notch signalling has been implicated in tip cell specification in 3D endothelial cell cultures, zebrafish ISV development, the mouse retina and in tumour angiogenesis (Hellström et al., 2007; Leslie et al., 2007; Lobov et al., 2007; Noguera-Troise et al., 2006; Ridgway et al., 2006; Sainson et al., 2005;

Siekmann and Lawson, 2007; Suchting et al., 2007). DLL4 expression is highest in murine tip cells whereas the greatest Notch signalling activity has been observed in the stalk cells of nascent sprouts (Claxton and Fruttiger, 2004; Hellström et al., 2007). However, it should be noted that this does not directly translate to zebrafish as *dll4* and the tip cell marker *flt4* are expressed in both tip and stalk cells (Hogan et al., 2009b; Leslie et al., 2007; Siekmann and Lawson, 2007).

When Notch signalling was suppressed in mice by a γ-secretase inhibitor, genetic deletion of one *Dll4* allele or endothelial-specific deletion of *Notch1*, increased angiogenic sprouting and branching was observed (Hellström et al., 2007; Suchting et al., 2007; Tammela et al., 2008). This was attributed to an expansion in the number of tip cells. This conclusion was made because there was an increase in the expression of genes that are highly expressed in tip cells such as *Kdr*, *Flt4*, *Unc5b* and *Pdgfb* and also extensive filopodia formation (Hellstrom et al., 2007; Suchting et al., 2007; Tammela et al., 2008). Conversely, Notch signalling activation using exogenous Jag1 peptide reduced tip cell formation and filopodia extension in the mouse retina (Hellström et al., 2007). Similar observations have been made in the zebrafish embryo. In this system γ-secretase inhibition, *dll4* MO injections and genetic deletion of *dll4* all caused excessive sprouting and branching of the ISVs (Leslie et al., 2007; Siekmann and Lawson, 2007). These phenotypes were shown to be due to a loss of *notch1b* signalling via *rbpja*, as when these two genes were knocked down, hyperbranching was also observed (Leslie et al., 2007; Siekmann and Lawson, 2007). In fact, *rbpja*-deficient *Tg(fli1a:EGFP)* cells that were transplanted into wildtype zebrafish embryos showed an increased propensity to occupy the tip cell position in the developing ISVs (Siekmann and Lawson, 2007).

Overall it appears that tip cell fate is the default programme in the absence of Notch signalling, whereas active Notch signalling is needed to promote stalk cell specification (Hellström et al., 2007). When endothelial cells are activated by VEGFA they compete for tip cell position via DLL4/Notch signalling. This appears to be a dynamic process, where tip and stalk cell specification is not finalised (Jakobsson et al., 2010). It is likely that it is the cell that produces the

most DLL4 that remains a tip cell by suppressing tip cell specification in neighbouring cells. Exactly how this suppression occurs has yet to be completely defined but a general model has been proposed. VEGF is known to induce *DLL4* expression through KDR (Liu et al., 2003; Lobov et al., 2007; Suchting et al., 2007). So if one endothelial cell receives greater VEGF stimulation, it will express more DLL4 and activate Notch signalling in neighbouring cells. Notch activation downregulates expression of *KDR*, *FLT4* and the VEGF co-receptor *NRP1* and upregulates expression of the VEGFA decoy receptor *FLT1* (Harrington et al., 2008; Henderson et al., 2001; Hogan et al., 2009b; Li et al., 2006; Suchting et al., 2007; Trindade et al., 2008; Williams et al., 2006). This acts to reduce the responsiveness of the neighbouring cells to any further VEGFA or vascular endothelial growth factor C (VEGFC) stimulation, thereby reinforcing the direction of Notch signalling. Computational modelling of this scenario has suggested that it could result in alternating tip and stalk cells when applied to a row of endothelial cells in the presence of a VEGF gradient (Bentley et al., 2008). By preventing excessive tip-cell formation, DLL4 maintains the optimal ratio between tip and stalk cells required for the correct branching patterns in both the murine retina (Hellström et al., 2007; Lobov et al., 2007) and the intersegmental vessels of zebrafish embryos (Leslie et al., 2007; Siekmann and Lawson, 2007).

1.4.5.3 Endothelial cell motility

Several studies have demonstrated that Notch signalling via DLL4 acts to limit endothelial cell migration (Biyashev et al., 2011; Leslie et al., 2007; Siekmann and Lawson, 2007; Trindade et al., 2008). When Dll4/Notch signalling was inhibited by either *dll4* knockdown or γ-secretase inhibition in zebrafish embryos, endothelial cells displayed increased filopodial activity and migrated into ectopic locations (Leslie et al., 2007). These phenotypes were observed at a time point (54 hpf) at which the endothelial cells of the DLAV and ISVs are normally quiescent (Leslie et al., 2007). Similarly, knockdown of *rbpja* increased the number of cells that migrated into both the ISVs and the DLAV, while transplanted *Tg(fli1a:EGFP)* cells expressing activated Notch were restricted to the DA and the base of the ISVs (Siekmann and Lawson, 2007). More recently, a hyper-migratory phenotype has been reported in *dll4* morphants which leads

to individual endothelial cells breaking away from sprouting ISVs (Biyashev et al., 2011). The control of endothelial cell migration by DLL4 is not a function which is restricted to zebrafish. Overexpression of *Dll4* in mouse embryos resulted in reduced migration of endothelial cells into the ISVs (Trindade et al., 2008). Equally, overexpression of DLL4 in human umbilical vein endothelial cells (HUVEC) significantly reduced their migratory behaviour, even in response to exogenous VEGF (Trindade et al., 2008).

Although DLL4-induced Notch signalling has been established as a molecular brake on inappropriate endothelial cell migration, the mechanism through which this occurs has not been elucidated. One possibility is that the Notch pathway acts via suppression of NRP1 expression. NRP1 is a semaphorin and VEGF co-receptor which is significantly downregulated by Notch signalling *in vitro* (Harrington et al., 2008; Williams et al., 2006). Both the Semaphorin and VEGF binding activities of NRP1 have been blocked using monoclonal antibodies and in HUVEC this prevented cell migration in a transwell *in vitro* assay (Pan et al., 2007). The pro-migratory activity of NRP1 was suggested to stem from the C-terminal domain, which has been shown to promote HUVEC migration via phosphatidylinositol 3-kinase (PI3K), v-akt murine thymoma viral oncogene homolog (AKT) and ras homolog family member A (RHOA) (Wang et al., 2003). However, the cytoplasmic domain of NRP1 is not required for murine angiogenesis but is necessary for normal arterio-venous patterning in the retina and for both developmental and adult arteriogenesis (Fantin et al., 2011; Lanahan et al., 2013). *Nrp1* knockout has been shown to inhibit endothelial cell migration and is required for normal angiogenesis in the central nervous system (CNS) (Gerhardt et al., 2004; Jones et al., 2008). Recent work by Fantin and colleagues has demonstrated that NRP1 promotes tip cell function, as *Nrp1*-positive endothelial cells preferentially adopted the tip cell position over *Nrp1*-negative endothelial cells in chimeric vessel sprouts (Fantin et al., 2013). NRP1 may also be required for successful substrate switching by tip cell filopodia, as in the absence of NRP1, sprouts failed to change direction at key points in the developing hindbrain (Gerhardt et al., 2004).

1.4.5.4 Endothelial cell proliferation

During sprouting angiogenesis, endothelial cell proliferation is required in order for the new vessel to growth in length, and if necessary, in diameter. This is another element of endothelial angiogenic behaviour which Notch signalling controls in order to prevent excessive or inappropriate sprouting. Inhibition of Notch signalling in various *in vivo* models causes increased endothelial cell proliferation (Dou et al., 2008; Hellström et al., 2007; Leslie et al., 2007; Lobov et al., 2007; Noguera-Troise et al., 2006; Ridgway et al., 2006; Siekmann and Lawson, 2007; Suchting et al., 2007). Conversely, Notch pathway activation, both *in vitro* and in mice, reduced the rate of endothelial cell propagation (Harrington et al., 2008; Liu et al., 2006; Noseda et al., 2004; Trindade et al., 2008).

In zebrafish, Dll4 signalling via Notch1b is required to prevent endothelial cell proliferation once ISV sprouting is complete (Leslie et al., 2007). At an earlier point in development, *rbpja* or *dll4* knockdown caused an increase in the number of ISV endothelial cells, due to a combination of increased proliferation and migration (Siekmann and Lawson, 2007). Enhanced endothelial cell proliferation has also been observed in both embryonic and adult mice upon Notch inhibition (Dou et al., 2008; Hellström et al., 2007; Lobov et al., 2007; Suchting et al., 2007). For example, deletion of a single *Dll4* allele or inhibition of Dll4/Notch signalling by intraocular injection of blocking antibodies promoted endothelial cell division in the developing mouse retina (Lobov et al., 2007). When *DLL4* signalling is blocked in murine tumour models it causes an increase in tumour vascularity which can be partly attributed to an increase in endothelial cell proliferation (Noguera-Troise et al., 2006; Ridgway et al., 2006).

Liu and colleagues identified the MAPK and PI3K pathways as the intermediaries that suppress endothelial cell proliferation in response to Notch stimulation (Liu et al., 2006). Both signalling pathways were repressed in endothelial cells following NOTCH1 activation; this required MAML1 expression and could be recapitulated by HES1 overexpression (Liu et al., 2006). Furthermore, the expression of cyclin-dependent kinase inhibitor 1A (*CDKN1A*) is increased by NOTCH1 and NOTCH4 but inhibited upon endothelial deletion of *Rbpj* (Dou et al., 2008; Noseda et al., 2004). When Notch signalling was

activated, upregulation of CDKN1A caused a reduction in the nuclear translocation of cyclin D1 (CCND1) and cyclin-dependent kinase 4 (CDK4). This resulted in cell cycle arrest due to a lack of CCND1/CDK4-mediated retinoblastoma 1 (RB1) phosphorylation (Dou et al., 2008; Noseda et al., 2004).

1.4.5.5 Endothelial cell adhesion and vessel stability

Maturation of nascent blood vessels requires the deposition of extracellular matrix proteins by endothelial cells in order to form a basement membrane. Endothelial cells overexpressing DLL4 display increased transcription of fibronectin (*FN1*) and various collagen and laminin genes (see Table 5.1) (Harrington et al., 2008; Trindade et al., 2008). These findings correlate with the observation that $Dll4^{-/-}$ embryos have an irregular basement membrane around the DA with which not all endothelial cells are in contact (Benedito et al., 2008).

Integrins are transmembrane receptors that mediate adhesion by attaching cells to each other or the extracellular matrix. Microarray analysis of HUVECs transduced with empty vector and DLL4-encoding retroviruses has shown that integrin beta 3 (*ITGB3*) mRNA is down-regulated in DLL4-expressing HUVECs (Harrington et al., 2008). However, a CSL-independent pathway has been identified that positively regulates the activation of β1-integrins upon Notch signalling (Hodkinson et al., 2007). In this pathway the NICD does not translocate to the nucleus but instead activates the GTPase R-Ras to increase integrin binding affinity and hence integrin-mediated adhesion (Hodkinson et al., 2007). Exogenous NICD was also able to reverse the suppressive effect of H-Ras/Raf on integrin activity and NOTCH1/DLL4 signalling activated α5β1 integrins in a R-Ras-dependent manner to increase FN1 binding in myeloid cells (Hodkinson et al., 2007). It is not yet known if this pathway is relevant in endothelial cells; however, expression of constitutively active *NOTCH4* in human dermal microvascular endothelial cells (HMEC) increases β1-integrin-mediated adhesion to collagen which could occur via the R-Ras mechanism (Leong et al., 2002).

Another key molecule involved in the stabilisation of new blood vessels is the Notch target NRARP. This gene is upregulated upon Notch activation and acts

as a negative regulator of Notch signalling by promoting the degradation of NICD (Krebs et al., 2001; Lamar et al., 2001; Pirot et al., 2004). However, NRARP also stabilises the β-catenin cofactor, lymphoid enhancer-binding factor 1 (LEF1), to promote Wnt signalling (Ishitani et al., 2005; Phng et al., 2009). It is the combined regulation of both Notch and Wnt signalling that enables NRARP to stabilise nascent blood vessels during ISV formation and retinal angiogenesis (Phng et al., 2009). *Nrarp* knockout mice and *nrarp* zebrafish morphants both displayed ectopic vessel regression due to a reduction in endothelial stalk cell proliferation, endothelial cell retraction and abnormal junctional rearrangements (Phng et al., 2009). A certain level of Notch signalling is clearly required to maintain quiescence in established blood vessels as loss of *Rbpj* in the endothelial cells of adult mice caused spontaneous angiogenesis in multiple tissues (Dou et al., 2008). However, during stabilisation of vessels endothelial proliferation is still required and NRARP appears to modulate both Notch and Wnt signalling to allow this to occur (Phng et al., 2009).

1.4.5.6 Pathological angiogenesis

DLL4 has been found to be upregulated in tumours of the colon, bladder and breast and in renal clear cell carcinoma (Jubb et al., 2009; Jubb et al., 2010; Patel et al., 2005; Patel et al., 2006), where is acts to prevent excessive angiogenesis and stabilise existing vessels (Patel et al., 2006). This has proven relevant to the development of new cancer therapeutics. Several studies have demonstrated that blocking DLL4 in murine tumour models, using neutralising antibodies, inhibits tumour growth by promoting non-productive, deregulated angiogenesis (Haller et al., 2010; Hoey et al., 2009; Li et al., 2007; Noguera-Troise et al., 2006; Oishi et al., 2010; Ridgway et al., 2006). Although tumour vascularity was increased upon DLL4 blockade, the resulting vessels were poorly perfused and tumour growth was inhibited due to hypoxic conditions (Noguera-Troise et al., 2006).

The increased vascularity observed in tumours following DLL4 signalling blockade is a result of the crucial role that DLL4 plays in regulating the ratio of tip cells to stalk cells. Expression of DLL4 by the tip cells of new sprouts stimulates Notch signalling in the adjacent cells, thereby maintaining stalk cell

identity and restricting tip cell specification (Hellström et al., 2007). When DLL4 signalling or expression is inhibited, tip cell specification is not controlled, leading to excessive sprouting from existing vessels. Enhanced sprouting upon DLL4 inhibition in tumours also concurs with earlier work which demonstrated that DLL4 promotes the switch between the proliferative phase of angiogenesis to the maturation and stabilisation phase (Benedito et al., 2008; Harrington et al., 2008; Phng et al., 2009).

DLL4 blockade can also inhibit tumour growth by causing a reduction in cancer stem cell frequency (Fischer et al., 2011; Hoey et al., 2009). These discoveries have subsequently led to a Phase I clinical trial of a DLL4 blocking antibody. However, chronic blockade of DLL4 using antibody therapy may not be a viable treatment option because this leads to the pathological activation of endothelial cells, disruption of normal organ homeostasis and induces vascular tumours in mice and rats (Yan et al., 2010). More recently it has been suggested that combined targeting of DLL4 and EPHB4 may overcome this safety issue as this treatment combination displayed cumulative efficacy and did not result in the liver vascular lesions reported by Yan and colleagues (Djokovic et al., 2010).

Manipulation of DLL4/NOTCH signalling may also be a possible treatment option in other angiogenic pathologies. For example, Dll4 blockade in a model of ischaemic retinopathy enhanced the angiogenic sprouting required for the regrowth of retinal vessels but suppressed pathological neovascularisation (Lobov et al., 2007).

1.5 microRNAs

MicroRNAs (miRNAs) are a class of highly conserved, small, non-coding RNAs that negatively regulate gene expression by binding to cellular mRNA transcripts. The current release of the miRBase database (miRBase 19, August 2012) contains over 20,000 miRNA gene loci across 193 species which amounts to 25,000 mature miRNA sequences (Kozomara and Griffiths-Jones, 2011). To date over 2000 human miRNAs have been identified which are predicted to control the activity of at least 50% of all protein-coding genes (Krol

and Loedige, 2010). Thus miRNAs constitute one of the most abundant classes of gene-regulatory molecules in animals.

1.5.1 Discovery and classification

The first miRNA, lin-4, was described in *C. elegans* in 1993 by Lee and colleagues (Lee et al., 1993). Whilst characterising loss of function mutations that caused developmental timing defects, the authors showed that the *lin-4* gene gave rise to a 22 nucleotide (nt) RNA molecule, rather than encoding for a protein (Lee et al., 1993). The 3 prime untranslated region (3'UTR) of the protein coding gene *lin-14* was found to contain antisense sites complimentary for lin-4 (Lee et al., 1993; Wightman et al., 1993). These sites enabled lin-4 to reduce *lin-14* protein output without affecting mRNA levels (Wightman et al., 1993). These findings provided the first model of post-transcriptional gene regulation by an endogenous small RNA and led to the creation of a new term for this class of small RNAs: miRNAs. A second temporally regulated small RNA, let-7, was also described in *C. elegans* and shown to target the 3'UTR of *lin-41* (Reinhart et al., 2000; Slack et al., 2000). Detection of let-7 RNAs in a wide range of animal species, including *Drosophila*, revealed that miRNAs were not specific to *C. elegans*, but a widely distributed class of regulatory molecules (Pasquinelli et al., 2000). This was confirmed when an additional 60 *C. elegans* miRNAs and 20 *Drosophila* miRNAs were identified by small RNA cloning (Lagos-Quintana et al., 2001; Lau et al., 2001; Lee and Ambros, 2001). The first human miRNAs were also characterised in 2001 (Lagos-Quintana et al., 2001) and since then miRNAs have been found throughout the animal kingdom as well as in plants, algae, slime moulds and viruses (miRBase 19, August 2012).

Since their first discovery as regulators of developmental timing, miRNAs have been implicated in a hugely diverse range of cellular processes, including angiogenesis, immunity and the stress response (Baltimore et al., 2008; Leung and Sharp, 2010; Wang and Olson, 2009). It is therefore not surprising that many miRNAs have been found to be dysregulated in various pathological conditions such as cancer and heart disease (Bauersachs and Thum, 2011; Croce, 2009). Several studies support the theory that miRNAs act as rheostats by fine-tuning protein expression (Baek et al., 2008; Selbach et al., 2008).

However, this belies the crucial role they fulfil in cellular function. This is evident during development, where loss of miRNA biogenesis is embryonically lethal (Bernstein et al., 2003). More recent work has suggested that miRNAs can behave as both fine-tuners and switches, depending on where target mRNA levels lie in relation to a pre-defined threshold (Mukherji et al., 2011).

1.5.2 Biogenesis

The majority of miRNA genes are located either in intergenic regions or in an anti-sense orientation to annotated genes (Lagos-Quintana et al., 2001; Lau et al., 2001; Lee and Ambros, 2001). Although some miRNAs are individually produced from separate transcription units, the majority of miRNA genes are arranged in clusters and transcribed polycistronically (Lee et al., 2002). RNA polymerase II is the predominant enzyme responsible for miRNA transcription in animals (Lee et al., 2004). The primary transcript, termed the primary miRNA (pri-miRNA), can range from hundreds to thousands of nucleotides in length and is capped and polyadenylated (Cai et al., 2004). Each pri-miRNA contains one or more hairpin structures that are composed of a stem and a terminal loop (Fig.1.5). These hairpins are recognised and cleaved by DROSHA, an RNase III enzyme, to form hairpin-shaped precursor miRNAs (pre-miRNAs) of ~60-70nt (Fig. 1.5) (Lee et al., 2003).

DROSHA acts as part of a Microprocessor complex and the other core component is DiGeorge syndrome critical region gene 8 (DGCR8), a double-stranded RNA binding protein (dsRBP) (Gregory et al., 2004). DGCR8 binds to the junction between the single-stranded and double-stranded region of the pri-miRNA stem and directs DROSHA to cleave ~11bp away from this junction (Han et al., 2006). The Microprocessor complex also contains a variety of cofactors which may function to promote the fidelity, specificity and/or activity of DROSHA (Gregory et al., 2004). Whilst most pre-miRNAs are generated by this canonical pathway, some are produced by splicing and debranching of short hairpin introns, known as mirtrons (Fig.1.5) (Okamura et al., 2007; Ruby et al., 2007).

Fig. 1.5. MicroRNA biogenesis in mammalian cells. MicroRNAs (miRNAs) are processed from RNA polymerase II (RNAPII)-specific transcripts of independent genes or from introns of protein-coding genes. In the canonical pathway, primary miRNAs (pri-miRNAs) are cleaved by Drosha, with the assistance of DGCR8, to generate the ~70nt precursor miRNA (pre-miRNA) hairpin. However, some pre-miRNAs bypass this step as they are produced from very short introns (mirtrons) by splicing and debranching of precursor mRNA transcripts. The pre-miRNA is exported from the nucleus by Exportin 5 and then processed further by Dicer, with the assistance of the dsRBP TRBP, to generate a ~20bp mature miRNA duplex (miRNA/miRNA*). In mammals argonaute 2 (AGO2) can cleave the 3' arm of the pre-miRNA to form a processing intermediate called AGO2-cleaved pre-miRNA (ac-pre-miRNA). One strand of the mature miRNA duplex (the guide strand) is preferentially incorporated into the miRNA-induced silencing complex (miRISC). Diagram adapted from Krol and Loedige, 2010.

The pre-miRNA generated by DROSHA cleavage has a characteristic 2 nt 3' overhang. Exportin-5 (XPO5) recognises this overhang and transports the pre-miRNA into the cytoplasm via a Ran-GTP-dependent mechanism (Fig 1.5) (Yi et al., 2003). Upon entering the cytoplasm the pre-miRNA is cleaved by a second RNase III enzyme, DICER1 (Bernstein et al., 2001). This forms a miRNA duplex of approximately 22bp, known as the mature miRNA, which is loaded onto an Argonaute (AGO) protein, such as argonaute 2 (AGO2) (Fig. 1.5) (Kim et al., 2009). DICER is assisted in this process by another dsRBP, TAR RNA binding protein 2 (TARBP2), also known as TRBP. This dsRBP is not required for pre-miRNA cleavage but recruits DICER to AGO2 and is required for the formation of the miRNA-induced silencing complex (miRISC) (Chendrimada et al., 2005; Haase et al., 2005; Lee et al., 2006). Some pre-miRNAs are cleaved on the 3' arm by AGO2, before being passed on for further DICER processing (Diederichs and Haber, 2007). This forms an additional processing intermediate called AGO2-cleaved precursor miRNA (ac-pre-miRNA) (Fig 1.5).

After AGO-loading, one strand of the mature miRNA duplex is degraded (the passenger strand or miRNA*), whilst the strand with the least stable 5' end (the guide strand) is preferentially incorporated into miRISC (Khvorova et al., 2003). However, passenger strands can also be loaded into miRISC to function as miRNAs (Ghildiyal et al., 2010). The guide strand directs miRISC to the 3'UTRs of target mRNAs, leading to their subsequent silencing (Kim et al., 2009).

1.5.3 Target recognition

The majority of miRNA target sites are found within the 3'UTR of target mRNAs, which is explained by the inhibition of miRISC association by active translation (Gu et al., 2009). The main basis for miRNA target recognition is conserved Watson and Crick base pairing between the miRNA seed region (nucleotides 2-7) and the target site (Brennecke et al., 2005; Krek, 2005; Lewis et al., 2003; Lewis et al., 2005). This explains why the 5' portion of the miRNA is the most conserved region across metazoan miRNAs (Lewis et al., 2005; Lim et al., 2005). Target recognition is impaired if there are any mismatches or G:U base pairings between the seed region and the target site, whilst an adenosine at

position 1 of the target site has been shown to increase efficacy, although it does not necessarily have to be paired with the miRNA (Lewis et al., 2005). An optimal target site contains the seed match, augmented by both the additional adenosine at position 1 and base pairing to nucleotide 8 of the miRNA (Brennecke et al., 2005; Krek, 2005; Lewis et al., 2003; Lewis et al., 2005). Although complementarity outside the seed region is not essential, base pairing at nucleotides 13-16 of the miRNA can improve target identification and 3' complementarity has been shown to compensate for single-nucleotide bulges or mismatches within the seed (Brennecke et al., 2005; Friedman et al., 2009).

Several additional factors besides complementarity have been shown to affect target recognition. Target sites located at either end of a 3'UTR are known to be more effective than those in the middle, although the first 15nt downstream of the stop codon is inhospitable for targeting (Grimson et al., 2007). The nucleotides surrounding functional sites have been found to be enriched in adenosine or uracil, when compared to non-functional sites (Grimson et al., 2007). Finally, target sites which are surrounded by secondary RNA structures are less favourable because they cannot be easily accessed by miRISC (Kertesz et al., 2007).

Figure 1.6. Suggested mechanisms of miRNA-mediated silencing. (Top) mRNAs which are not subject to repression recruit initiation factors (eIF6, eIF4F and PABP1) and ribosomal subunits (60S and 40S) to form circularised structures that enhance translation. (Upper left) miRISC can inhibit translation initiation at the cap recognition stage by competing for cap binding. (Lower left) Translation initiation can also be prevented by miRISC at the 60S recruitment stage. (Bottom) miRISC binding can induced deadenylation of the mRNA by CCR4, CAF1 and NOT. This prevents circularisation of the mRNA. (Lower right) Inhibition of translation elongation can occur due to miRISC promoting the drop-off of ribosomes. (Upper right) Deadenylation of the mRNA and decapping by Dcp1 leads to mRNA degradation. eIF6: eukaryotic translation initiation factor 6; eIF4F: eukaryotic translation initiation factor 4F; PABP1: poly-A binding protein 1; CAF1: chromatin assembly factor 1; Dcp1: decapping enzyme 1. Diagram from Carthew and Sontheimer, 2009.

1.5.4 Mechanisms of silencing

The mediator of miRNA-induced silencing, miRISC, is composed of the miRNA guide strand, an AGO protein, GW182 and various subsidiary proteins involved in regulation and assembly (Carthew and Sontheimer, 2009). GW182 has been found to be both necessary and sufficient for AGO/miRNA directed silencing; therefore, miRNA-bound AGO in association with GW182 are considered the minimum requirements for a functioning miRISC (Ding and Groszhans, 2009; Eulalio et al., 2008; Jakymiw et al., 2005; Liu et al., 2005). Much debate still abounds in the literature regarding the predominant method of miRNA-mediated silencing and to what extent these methods may co-exist. If there is complete complementarity between the entire miRNA and the target, mRNA degradation has been observed and attributed to the RNase H activity of AGO (only AGO2 in mammals) (Hutvágner and Zamore, 2002; Liu et al., 2004). This was considered the dominant mechanism in plants (Jones-Rhoades et al., 2006). Where complete complementarity is lacking, silencing was said to occur via inhibition of translation. It is now thought that the default mechanism in both plants and animals is translational repression, although exactly how this occurs and whether it involves mRNA destabilisation has not been defined (Carthew and Sontheimer, 2009).

Inhibition of translation initiation is commonly given as the mechanism underlying translational repression. Three models for this have dominated until recently: competition between miRISC and eukaryotic translation initiation factor 4E (eIF4E) for binding to the mRNA 5' cap structure; deadenylation of the mRNA tail to prevent mRNA circularisation; recruitment of eukaryotic translation initiation factor 6 (eIF46) by miRISC to block the association between the 60S ribosomal subunit and the 40S pre-initiation complex (Fig. 1.6) (Carthew and Sontheimer, 2009). Now, eukaryotic translation initiation factor 4A2 (eIF4A2) has been highlighted as the key factor through which miRISC blocks translation (Meijer et al., 2013). Additionally, miRISC may also prevent translation elongation by promoting premature disassociation of ribosomes from the mRNA transcript (Fig. 1.6) (Carthew and Sontheimer, 2009).

Whilst some targets can be repressed without detectable changes in mRNA levels, those which are translationally repressed by more than a third also display clear mRNA destabilisation and it has been argued that this is the predominant cause of reduced protein output (Baek et al., 2008; Guo et al., 2010). The increase in mRNA degradation caused by some miRNAs has been attributed to deadenylation, decapping and exonucleolytic digestion (Behm-Ansmant et al., 2006; Giraldez et al., 2006; Wu et al., 2006). It has not yet been definitively determined whether increased mRNA degradation occurs independently of or as a consequence of translational inhibition; however recent findings point towards the latter scenario (Carthew and Sontheimer, 2009; Meijer et al., 2013).

1.5.5 Role in angiogenesis

Disruption of DICER and DROSHA has been shown to impair both embryonic and postnatal angiogenesis and reduce angiogenic behaviour in HUVEC *in vitro* (Kuehbacher et al., 2007; Suarez et al., 2007; Suarez et al., 2008; Yang et al., 2005). These findings suggest that miRNAs play a key role in regulating endothelial cell behaviour and are crucial for successful angiogenesis. Defined as “angiomiRs”, many different miRNAs have now been identified as regulators of angiogenesis (Table 1.1) (Wang and Olson, 2009). These include both pro- and anti-angiogenic miRNAs. For example, miR-126 is required for vascular development in both zebrafish and mouse embryos (Fish et al., 2008; Wang et al., 2008). Reduced or ablated miR-126 expression resulted in haemorrhaging and embryonic lethality due to a loss of vascular integrity, phenotypes which resemble the defects seen following VEGF signalling inhibition (Fish et al., 2008; Wang et al., 2008). It was determined that the functional targets of miR-126 in these systems are the negative regulators of VEGF, sprouty-related EVH1 domain containing 1 (*SPRED1*) and phosphoinositide-3-kinase regulatory subunit polypeptide 2 (*PIK3R2*) (Fish et al., 2008; Wang et al., 2008). Additionally, it has been shown that miR-126 is upregulated by the transcription factor Klf2 in response to shear stress (Nicoli et al., 2010). The subsequent downregulation of *spred1* results in activation of Vegf signalling which is required for aortic arch remodelling during zebrafish development (Nicoli et al., 2010).

miRNA	Angiogenic function	Relevant gene targets	References
let-7	Promotes endothelial cell proliferation and motility. Hypoxia induced.	*TIMP1 and AGO1*	(Chen et al., 2013; Otsuka et al., 2008)
miR-1 and miR-206	Negatively regulate angiogenesis during zebrafish development.	*vegfaa*	(Stahlhut et al., 2012)
miR-10	Promotes VEGFR2 signalling during zebrafish development.	*flt1*	(Hassel et al., 2012)
miR-106/107	Promotes angiogenesis by releasing VEGF from AGO1-mediate suppression. Hypoxia induced.	*AGO1*	(Chen et al., 2013)
miR-15a	Overexpression in tumour cells inhibits angiogenesis.	*VEGFA*	(Sun et al., 2013)
miR-15b	Hypoxia regulated miRNA.	*VEGFA*	(Hua et al., 2006)
miR-16	Overexpression in tumour cells inhibits angiogenesis. Hypoxia regulated miRNA.	*VEGFA*	(Hua et al., 2006; Sun et al., 2013)
miR-17~92 cluster	Contradictory pro- and anti-angiogenic reports. miR-20a and miR-20b regulated by hypoxia.	*CTGF; THBS1*; *TIMP1*; *ITG5A*; *JAK1*; *MAP2K3*; *KDR*	(Bonauer et al., 2009; Dews et al., 2006; Doebele et al., 2010; Otsuka et al., 2008; Pin et al., 2012; Suarez et al., 2008; Yin et al., 2013)
miR-125b & miR-199a	Overexpression inhits tumour-induced angiogenesis.	*HER2* and *HER3*	(He et al., 2013)
miR-126	Required for vascular integrity and angiogenesis *in vivo*.	*SPRED1* and *PIK3R2*	(Fish et al., 2008; Kuhnert et al., 2008; Nicoli et al., 2010; Wang et al., 2008)
miR-130a	Antagonises the anti-angiogenic activity of GAX and HOXA5.	*GAX* and *HOXA5*	(Chen and Gorski, 2008)
miR-132	Induces pathological neovascularisation .	*RASA1*	(Anand et al., 2010)
miR-145	Inhibits tumour angiogenesis.	*NRAS* and *VEGFA*	(Zou et al., 2012)
miR-155	Promotes tumour angiogenesis	*VHL*	(Kong et al., 2013)
miR-210	Enhances angiogenesis and survival response to hypoxia *in vitro*.	*EFNA3*	(Fasanaro et al., 2008; Pulkkinen et al., 2008)
miR-218	Essential for normal vascularisation of the retina.	*ROBO1, ROBO2 and GLCE*	(Small et al., 2010)
miR-2188	Overexpression disrupts ISV development in zebrafish embryos.	*nrp2a*	(Soares et al., 2012)
miR-221/222	Impair SCF-induced angiogenesis *in vitro* but required for tip cell proliferation and migration *in vivo*.	*KIT*	(Nicoli et al., 2012; Poliseno et al., 2006)
miR-27a/b	Promotes angiogenesis during zebrafish development but inhibits tumour angiogenesis.	*sema5a, spry2, dll4* and *VEGFC*	(Biyashev et al., 2011; Urbich et al., 2012; Ye et al., 2013)
miR-29a	Regulates the angiogenic properties of HUVEC	*HBP1* and *PTEN*	(Wang et al., 2013a; Yang et al., 2013)
miR-296	Required for tumour angiogenesis.	*HGS*	(Würdinger et al., 2008)
miR-320	Inhibition improves angiogenesis in diabetic endothelial cells.	*IGF1*	(Wang et al., 2013b)
miR-378	Promotes tumour angiogenesis.	*SUFU and FUS*	(Lee et al., 2007)
miR-503	Inhibits tumour angiogenesis	*FGF2* and *VEGFA*	(Zhou et al., 2013)
miR-93	Promotes angiogenesis.	*ITGB8*	(Fang et al., 2011)

Table 1.1. miRNAs that have been shown to modulate the angiogenic response. Gene targets have been given using the nomenclature of the species in which they were identified.

Conversely, miR-1 and miR-206 have been identified as anti-angiogenic miRNAs as they inhibit *vegfaa* during zebrafish development to negatively regulate angiogenesis in muscle (Stahlhut et al., 2012). For some miRNAs the data is more confusing. The miRNA family members miR-221 and miR-222 were originally identified as negative regulators of angiogenesis *in vitro* because they target *KIT*, thereby inhibiting the angiogenic activity of stem cell factor (SCF) and preventing HUVEC tube formation (Poliseno et al., 2006). However, it has recently been shown that knockdown of miR-221 but not miR-222 reduces tip cell migration and proliferation during ISV development in zebrafish embryos, an exact phenocopy of *flt4* knockdown (Nicoli et al., 2012). It was demonstrated that miR-221 promotes tip cell behaviour by targeting *cyclin dependent kinase inhibitor 1b* (*cdkn1b*), and *phosphoinositide-3-kinase regulatory subunit 1* (*pik3r1*), which control endothelial proliferation and migration respectively. Alongside those miRNAs which have been shown to regulate physiological angiogenesis, many miRNAs have been identified as mediators of pathological angiogenesis (Anand et al., 2010; Fang et al., 2011; He et al., 2013; Lee et al., 2007; Sun et al., 2013; Ye et al., 2013; Zhou et al., 2013; Zou et al., 2012).

1.5.6 MicroRNA expression in KLEC

Many studies have revealed important roles for miRNAs in regulating endothelial cell function, especially during angiogenesis (Anand et al., 2010; Biyashev et al., 2011; Bonauer et al., 2009; Chen and Gorski, 2008; Fang et al., 2011; Fasanaro et al., 2008; Fish et al., 2008; Lee et al., 2007; Poliseno et al., 2006; Suarez et al., 2008; Urbich et al., 2012; Wang et al., 2008), however the full extent of miRNA involvement in vascular biology has yet to be determined. KSHV infection of endothelial cells, including LEC, is a tractable model to study endothelial cell biology (Mesri et al., 2010; Wang et al., 2004).

The miRNA signature of KLEC was previously described by this laboratory (Lagos et al., 2010) and the GEM data from this study has been used to establish lists of miRNAs which are upregulated or downregulated upon KSHV infection of LEC (Tables 1.2 and 1.3). This work has already revealed that several miRNAs which enhance KSHV gene expression are upregulated within

the first 6h post-infection (p.i.). These include miR-132, which is induced by cAMP response element-binding protein (CREB) and promotes KSHV replication by inhibiting the expression of interferon-stimulated genes (Lagos et al., 2010). It is known that KSHV infection of LEC alters the expression of many pro- and anti-angiogenic factors (Vart et al., 2007). The miRNA GEM data of KLEC provides a valuable resource which may allow miRNAs to be identified that directly regulate these angiogenic factors.

1.5.7 Role in zebrafish development

To date, 247 mature miRNAs have been identified in zebrafish (miRBase v19, Aug 2012). Expression of these miRNAs begins in the zebrafish embryo at 4 hpf and displays variable temporal and spatial patterns (Chen et al., 2005; Wienholds et al., 2005). Zebrafish defective in miRNA processing due to *dicer1* knockout arrest during the larval stage, indicating that correct miRNA expression is critical for the developmental programme (Wienholds et al., 2003). A certain level of miRNA processing is actually maintained in *dicer1* knockout embryos due to residual Dicer from the maternal gamete (Wienholds et al., 2003). When this pool of Dicer was eliminated, embryonic defects were evident at a much earlier stage of development (Giraldez et al., 2005). Zebrafish miRNAs are now known to be involved in a diverse range of developmental processes including clearance of maternal mRNAs, germ cell migration, cardiac patterning, erythropoiesis and angiogenesis (Dore et al., 2008; Giraldez et al., 2006; Morton et al., 2008; Staton et al., 2011; Urbich et al., 2012).

MicroRNA	LEC #1	LEC #2	LEC #3	LEC #4	KLEC #1	KLEC #2	KLEC #3	KLEC #4	Av LEC	Av KLEC	Fold Δ
hsa-miR-193a	2.680585	1.348849	2.132635	1.219923	4.859499	4.645699	4.986489	4.307769	1.85	4.70	7.232
hsa-miR-132	1.826182	1.722629	3.400029	2.246356	4.986564	5.145566	5.221302	4.696019	2.30	5.01	6.559
hsa-miR-31	3.05232	2.425748	2.541032	3.051801	5.106421	4.744857	5.39024	5.181373	2.77	5.11	5.056
hsa-miR-338	1.084668	1.028672	0.769259	1.691475	3.762336	2.467751	3.866759	2.619417	1.14	3.18	4.100
hsa-miR-210	2.951988	2.294344	3.007216	2.361736	4.488102	4.257033	4.711666	4.087814	2.65	4.39	3.323
hsa-miR-95	-0.47737	0.521868	0.634429	0.423345	2.148923	0.994032	2.826692	1.712227	0.28	1.92	3.127
hsa-miR-7	1.064877	0.714747	2.659138	0.239624	2.783792	2.663663	3.45435	2.260789	1.17	2.79	3.076
hsa-miR-503	0.843835	0.305265	1.301496	0.890123	2.913552	1.293139	3.28055	2.168257	0.84	2.41	2.987
hsa-miR-487b	2.918355	1.536502	3.630647	1.877718	3.954395	3.398166	4.47727	3.853369	2.49	3.92	2.694
hsa-miR-455	-0.15252	-0.76701	1.079673	0.092445	1.360908	0.241524	1.708958	1.740183	0.06	1.26	2.297
hsa-miR-155	4.511507	4.246431	4.980054	4.2406	5.645527	5.615625	5.751856	5.64262	4.49	5.66	2.249
hsa-miR-582	2.625819	2.51956	2.94155	2.922895	4.051159	3.120076	4.29004	4.003197	2.75	3.87	2.164
hsa-miR-432	1.07585	0.887918	1.069105	1.247066	2.66177	1.762803	2.831428	1.334421	1.07	2.15	2.111
hsa-miR-663	4.279541	3.716615	3.917612	4.328053	5.424328	4.86849	5.44294	4.804473	4.06	5.14	2.106
hsa-miR-495	1.119139	0.598585	2.475687	1.377378	3.133842	1.909225	3.703947	0.786906	1.39	2.38	1.987
hsa-miR-557	1.114524	-0.1702	1.55363	-0.83023	1.263937	1.458058	1.089999	1.507333	0.42	1.33	1.883
hsa-miR-329	0.213809	0.209639	0.701756	0.70124	0.756478	0.63174	1.871883	2.055166	0.46	1.33	1.830
hsa-miR-501	2.256172	1.45594	1.236825	1.490307	3.385179	2.413441	2.88236	1.009389	1.61	2.42	1.757
hsa-miR-365	5.212407	5.252085	5.766608	5.452514	6.235574	6.267207	6.379127	6.043093	5.42	6.23	1.754
hsa-miR-629	1.952087	0.760611	1.140278	1.398318	2.721102	1.756193	2.604975	1.316302	1.31	2.10	1.725
hsa-miR-148a	0.981573	0.69433	1.731296	2.50495	2.107042	1.570001	3.108787	2.257229	1.48	2.26	1.720
hsa-miR-136	0.549913	0.624604	0.951379	1.146028	2.181421	0.684636	2.130751	1.324116	0.82	1.58	1.696
hsa-miR-140	3.705566	2.889446	3.405749	3.494798	4.416159	3.67074	4.531536	3.794439	3.37	4.10	1.658
hsa-miR-212	-0.24741	-0.28662	0.565864	0.491734	0.552387	0.182662	1.53361	0.941824	0.13	0.80	1.593
hsa-miR-126	11.79386	12.28393	12.62988	12.43303	12.97338	12.93326	13.10441	12.77123	12.29	12.95	1.581
hsa-miR126*	8.503008	8.862253	9.34826	9.164389	9.749109	9.55634	9.778365	9.40407	8.97	9.62	1.572
hsa-let-7i	8.261037	8.46942	8.945643	8.797333	9.298967	9.246797	9.441158	9.07973	8.62	9.27	1.567
hsa-miR-191	4.511201	3.530955	4.415651	4.449697	4.363172	4.996688	5.428358	4.706812	4.23	4.87	1.566
hsa-miR-454-3p	2.638055	3.67882	3.769802	1.958927	3.888756	3.658129	3.945975	3.11072	3.01	3.65	1.558
hsa-miR-154	0.96864	0.203599	1.264911	1.026298	2.010604	0.563313	2.118836	1.290996	0.87	1.50	1.548
hsa-miR-146b	-0.12688	-0.18904	0.149139	0.009727	-0.05114	0.004417	1.321537	1.077401	-0.04	0.59	1.545
hsa-miR-197	3.387481	2.977609	2.904873	2.558075	3.939771	3.213227	4.146544	2.990909	2.96	3.57	1.532
hsa-miR-532	2.284251	1.5454	2.146553	1.970761	2.813261	1.899087	3.751636	1.939672	1.99	2.60	1.531
hsa-miR-584	4.387312	4.405568	4.316232	4.113335	4.928368	4.834093	5.272319	4.565755	4.31	4.90	1.510
hsa-miR-26a	4.227413	3.662418	3.794291	3.76195	4.457494	4.395531	4.704057	4.25933	3.86	4.45	1.508
hsa-miR-424	5.227224	5.298026	6.117461	5.822627	6.159354	6.100451	6.415259	6.148446	5.62	6.21	1.505
hsa-miR-98	5.009131	4.808316	5.96523	5.365574	5.9372	5.77703	6.067952	5.719232	5.29	5.88	1.503
hsa-miR-602	0.935123	0.481353	1.921405	0.290319	2.180026	0.863426	1.9827	0.943806	0.91	1.49	1.500

Table 1.2. miRNAs upregulated by 1.5 fold or greater 72 h post-KSHV infection of LEC. Raw data with normalisation applied were obtained from Dr Dimitrios Lagos (Lagos *et al*., 2010). Orange shading: scatter plots of PITA score against TargetScan 4.2 score were generated for these miRNAs. All other miRNAs lacked a PITA prediction when the target prediction analysis was conducted.

MicroRNA	LEC #1	LEC #2	LEC #3	LEC #4	KLEC #1	KLEC #2	KLEC #3	KLEC #4	Av LEC	Av KLEC	Fold Δ
hsa-miR-99a	7.75816	8.19896	8.255226	8.333136	5.904055	5.91338	6.169641	5.987195	8.14	5.99	0.226
hsa-miR-100	7.117643	7.354377	7.668636	7.654211	5.648484	5.447821	5.856828	4.915421	7.45	5.47	0.253
hsa-miR-125b	8.369381	8.73544	8.940254	8.90634	6.897136	6.898805	6.989951	6.868966	8.74	6.91	0.282
hsa-miR-30b	5.752814	6.040285	6.277433	6.403999	5.020121	4.041641	4.798868	3.698623	6.12	4.39	0.302
hsa-miR-204	5.169028	5.270195	5.910926	5.449812	4.075009	3.563922	4.426569	2.893307	5.45	3.74	0.306
hsa-miR-370	7.755948	7.689458	7.452195	7.978741	6.392429	6.209713	6.257599	5.946771	7.72	6.20	0.349
hsa-miR-513	9.629476	9.339348	9.220378	9.884403	8.075828	7.980795	8.052207	7.949746	9.52	8.01	0.353
hsa-miR-494	9.738636	9.73343	9.534111	10.05253	8.462424	8.291642	8.302319	8.218959	9.76	8.32	0.367
hsa-miR-662	1.936784	1.117238	0.83947	2.334613	-0.11655	0.607197	0.23713	-0.12217	1.56	0.15	0.377
hsa-miR-194	0.726481	1.852902	1.196585	1.946435	-0.05184	-0.44083	1.248264	-0.03137	1.43	0.18	0.421
hsa-miR-801	4.608255	4.382871	4.324151	4.286356	3.565071	2.628404	4.032369	2.510842	4.40	3.18	0.430
hsa-miR-30d	7.30378	7.606504	7.614802	7.784246	6.477977	6.312494	6.491982	6.309793	7.58	6.40	0.442
hsa-miR-452	4.622719	4.552408	4.704417	4.348523	3.820566	3.076603	3.96439	2.684721	4.56	3.39	0.444
hsa-miR-630	6.08186	5.880151	5.676642	6.027922	4.885628	4.520204	4.993346	4.658047	5.92	4.76	0.450
hsa-miR-30a	8.711069	9.089672	9.098668	9.252089	8.006361	7.853047	8.041136	7.739246	9.04	7.91	0.458
hsa-miR-361	5.515045	5.992441	6.13191	5.963497	4.995938	4.662561	4.980153	4.654313	5.90	4.82	0.474
hsa-miR-30a*	4.266807	3.932265	4.182892	4.381878	3.290315	2.316618	4.139584	2.854637	4.19	3.15	0.486
hsa-miR-221	8.128872	8.255769	8.476395	8.602289	7.348709	7.266235	7.575209	7.247093	8.37	7.36	0.498
hsa-miR-30c	5.999949	5.952153	6.237855	6.224468	5.304869	5.059418	5.321078	4.748576	6.10	5.11	0.502

Table 1.3. miRNAs downregulated by 50% or more 72 h post-KSHV infection of LEC. Raw data with normalisation applied were obtained from Dr Dimitrios Lagos and was generated for his paper (Lagos *et al*., 2010).

1.6 Thesis aims

The angiogenic characteristics of KS and the targeting of endothelial cells by KSHV mean that changes in endothelial cells following infection may provide further insight into signalling networks that are important for endothelial regulation and function. Previous identification of the cellular miRNA expression signature following KSHV infection has provided an invaluable tool with which to begin investigating novel regulatory pathways in endothelial cells (Lagos et al., 2010). It was hypothesised that KSHV infection of endothelial cells leads to alterations in the expression of miRNAs that are involved in the regulation of endothelial cell function, particularly angiogenesis. The aim of this thesis was to identify such miRNAs, determine their relevant target/s and to explore the functional consequences of this targeting, both *in vitro* and *in vivo*. The specific aims of each chapter are detailed below.

Aims of Chapter 3

- To identify miRNAs which target genes implicated in angiogenesis.
- To select a target and it's predicted regulatory miRNA for further investigation.

Aims of Chapter 4

- To determine whether the selected target from Chapter 3 is a genuine target of the miRNA predicted to regulate its expression. If this is confirmed, secondary aims would be:
    - To identify the specific target site(s) through which the miRNA regulates the expression of its target.
    - To investigate the relevance of the miRNA/target regulatory axis on endothelial cell biology *in vitro*.

Aims of Chapter 5

If a functioning miRNA/target pair is identified through *in vitro* studies in Chapter 4, the aims of this chapter would be:

- To confirm targeting in a suitable *in vivo* model.

- To ascertain whether overexpression and/or inhibition of the miRNA has an effect on endothelial cell behaviour *in vivo*. If a phenotype is characterised, a secondary aim would be:
    - To investigate whether this phenotype is due to mis-regulation of the target mRNA of interest or can be attributed to another target.

Chapter 2. Materials and Methods

2.1 Cell Culture

All cells were cultured using a CB 53 incubator (Binder) at 37°C with 5% CO_2 in a humid environment.

2.1.1 Lymphatic endothelial cells

Lymphatic endothelial cells (LEC) of human dermal origin were purchased from Promocell. These cells were confirmed as LEC using qRT-PCR analysis and staining for lymphatic-specific markers including podoplanin (PDPN), lymphatic vessel endothelial hyaluronan receptor 1 (LYVE1) and prospero homeobox 1 (PROX1). LEC were purchased at passage 0 then expanded and used for experiments between passages 2 to 8. LEC were cultured on T75 flasks (TPP, MIDSCI) in 10 ml of Endothelial Cell Growth Medium MV (Promocell) which was supplemented with 10 ng/ml of VEGFC (R&D Systems) and changed every 48 h.

LEC were split 1:3 or 1:4 when a confluency of 70-80% was reached (approximately 1.5-2x10^6 cells per T75 flask). The cells were washed with phosphate buffered saline (PBS) (Sigma-Aldrich) and then incubated for 3 to 4 min at 37°C with 5 ml of 0.01% trypsin-EDTA, which was made by diluting 0.05% trypsin-EDTA (Gibco, Life Technologies) 1:5 with PBS. Once the majority of cells had detached from the flask the trypsin-EDTA was quenched by the addition of an equal volume of LEC media. Cells were collected and then pelleted by centrifugation for 5 min at 1200 rpm. LEC were resuspended in LEC media and then seeded at a density of ~5x10^5 cells per T75 flask.

2.1.2 Human umbilical vein endothelial cells

HUVEC were purchased from Promocell at passage 0 then expanded and used for experiments between passages 2 to 8. HUVEC were cultured on T75 flasks in 10 ml of Endothelial Cell Growth Medium MV2 which was changed every 48 h. HUVEC were split 1:4 using the same method as described for LEC (see 2.1.1).

2.1.3 Immortalised human fibroblasts

Human fibroblasts (HF) were previously immortalised using a retrovirus to introduce the catalytic subunit of human telomerase (hTERT) (Funes et al., 2007). These immortalised human fibroblasts (HF1) were cultured on T75 flasks in 10 ml of Dulbecco's Modified Eagle Medium (DMEM) (Gibco, Life Technologies) containing 10% Foetal Bovine Serum (FBS) (Sigma-Aldrich).

HF1 were split 1:10 every 2 to 3 days when a confluency of 80-90% was reached. The cells were washed with PBS and then incubated for 5-10min at 37°C with 5 ml of 0.05% trypsin-EDTA. Once the cells had detached from the flask the trypsin-EDTA was quenched by the addition of an equal volume of DMEM. Cells were collected and then pelleted by centrifugation for 5 min at 1200 rpm. HF1 were resuspended in DMEM media and then seeded in T75 flasks at a density of ~$1x10^6$ per T75 flask.

HF1 conditioned endothelial media was obtained by incubating cells for 48 h with Endothelial Cell Growth Medium MV2 and then passing the media through a 0.2 µm filter (Nalgene,Thermo Scientific) to remove any cell debris. The filtered supernatant was immediately used for the 3-D *in vitro* sprouting assay as described in 2.7.2.

2.1.4 BCBL-1 cells

BCBL-1 cells are a PEL derived cell line which are EBV-negative but are latently infected with a green fluorescent protein (GFP)-expressing KSHV, which also confers resistance to G418 (Geneticin) (Vieira et al., 2001). BCBL-1 cells were grown in suspension in RPMI 1640 medium (Gibco, Life Technologies) containing 10% FBS and supplemented with 400 ng/ml of Geneticin (Gibco, Life Technologies). Cells were standardly grown in T75 flasks in 25ml of media at densities in the range of 2.5-$6x10^5$ cells/ml. Cells were split 1:5 every 2 to 3 days by adding 5 ml of the suspension culture to 20 ml of fresh media.

2.1.5 293T cells

293T cells were cultured on T75 flasks in 10 ml of DMEM containing 10% FBS. Cells were split 1:10 every 2 to 3 days when a confluency of 80-90% was reached using the same method as described for HF1 cells (see Section 2.1.3).

2.1.6 Freezing and thawing cells

The following procedure was used to cryogenically store all cell types used. Live cell pellets were resuspended in FBS containing 10% dimethyl sulphoxide (DMSO). The cell suspension was aliquoted into cryovials, which were insulated in polystyrene containers and placed at -80°C for 48 h before being transferred into liquid nitrogen for long term storage.

Frozen cells were recovered by placing a frozen cryovial into a 37°C water bath until thawed. For LEC and HUVEC, the thawed cell suspension was placed into a T75 flask containing 10 ml of the appropriate media (pre-warmed). After 5 h the media was removed and 10 ml of fresh media was added. For all other cells, the thawed cell suspension was added to 10 ml of the appropriate pre-warmed media and then spun at 1200rpm for 5min. The supernatant was removed and the cell pellet was resuspended in the appropriate media and placed into a T75 flask or 10 cm dish.

2.2 Transfection, virus production and infection

2.2.1 DNA transfection of 293T cells

Cells were seeded the day before transfection, with the density of the seeding varying according to the experiment, as specified in the text. DNA transfection of 293T cells was performed using FuGENE (Roche) according to the manufacturer's instructions. FuGENE is a nonliposomal transfection reagent comprised of a mixture of lipids and other components, which facilitates DNA uptake by eukaryotic cells. Prior to transfection, the media was removed from all wells or plates to be transfected and cells were washed twice with pre-warmed Opti-MEM Reduced Serum Medium (Gibco, Life Technologies). An overlay of 400 µl, 800 µl or 8 ml was then added to a 12-well, 6-well or 10 cm

plate respectively. For every 1 µg of DNA to be transfected, 3 µl of FUGENE was prepared and this ratio was maintained, regardless of the number of cells being transfected. The DNA to be transfected was suspended in double distilled water (ddH_2O), and made up to 12.5 µl, 25 µl or 50 µl with Opti-MEM in a 1.5 ml Eppendorf tube, depending on whether the transfection mixture was for a 12-well, 6-well or 10 cm plate. In a separate 1.5 ml Eppendorf tube, FuGENE was added dropwise to Opti-MEM to give a final volume of 12.5 µl, 25 µl or 50 µl. The FuGENE/Opti-MEM mix was incubated at room temperature (RT) for 5 min before being added to the DNA mix to give a final volume of 25 µl, 50 µl or 100 µl. The FuGENE/DNA mix was incubated for 20-30 min at RT. 25 µl, 50 µl or 100 µl was then added dropwise to a 12-well, 6-well or 10 cm plate respectively. Mastermixes of DNA and/or FuGENE were prepared when more than one well or plate was to be transfected. The transfection media was removed 5 h after DNA addition and 1 ml, 2 ml or 10 ml of the appropriate fresh cell culture media was added. Cells were harvested 24, 48 or 72 h post-transfection.

2.2.2 Lentivirus production and infection of LEC and HUVEC

Vesicular stomatitis virus-G (VSV-G) envelope-pseudotyped lentivirus virions were produced by co-transfecting 1.5 µg of pMD.G plasmid (containing the VSV-G envelope gene) with 2 µg of lentiviral construct (pSIN-MCS or pCSGW) and 1.5 µg of the packaging plasmid p8.91 into a 10 cm plate of ~70% confluent 293T cells using the FuGENE protocol described in Section 2.2.1. Five hours post-transfection, the Opti-MEM media was removed and 10 ml of fresh 293T media was added. Virus containing supernatants were harvested 48-60 h post-transfection, passed through a 0.45 µM filter, aliquoted and then stored at -80°C. Some lentiviral constructs always led to the production of lentiviral preparations with low infectivity. In these situations the virus containing supernatant was concentrated 10x by spinning for 5 h at 48,000 x g and 4°C using a Beckman JA-25.50 rotor in an Avanti J-26 XPI Centrifuge. After centrifugation the supernatant was poured off and the virus containing pellet was resuspended in LEC, HUVEC or 293T media at a ratio of 1 ml of media to one 10 cm plate of 293T cells. The supernatant was then aliquoted and stored at -80°C.

Standard lentiviral infections were performed by incubating $1x10^5$ LEC or HUVEC, suspended in 0.5 ml of the appropriate media, with the required volume of lentivirus. The virus was removed either 5 h or 16 h p.i., once the cells had adhered to the plate, and 1 ml of fresh media was added per well of a 6-well plate. Cells were harvested 72 h p.i. for genomic DNA, total RNA or protein extraction. Infectivity of lentiviral preparations was assessed by quantifying the level of lentiviral packaging signal using quantitative PCR (qPCR) (see Section 2.3.10). Expression of the lentiviral constructs was determined by quantifying the level of the gene of interest cloned into the lentiviral backbone using quantitative reverse transcriptase-PCR (qRT-PCR) (see Section 2.3.13).

For lentiviral infections of LEC that would subsequently be infected with KSHV, $7x10^4$ cells were suspended in 0.5 ml of LEC media and incubated with 0.85 ml of pSIN_MCS, pSIN_30b or pSIN_30c. The virus was removed 5 h p.i. and replaced with 1 ml of LEC media. KSHV infection was performed 48 h after lentiviral infection.

2.2.3 KSHV production and infection of LEC

KSHV was produced from BCBL-1 cells which were latently infected with recombinant GFP-expressing KSHV (Vieira et al., 2001). For KSHV production, BCBL-1 cells were expanded to ~2.5 L which yielded ~11 ml of concentrated virus. Geneticin was omitted from the media during the expansion of the BCBL-1 cultures. Expansion was conducted by transferring 25 ml of a confluent BCBL-1 culture to a T150 flask (TPP, MIDSCI) containing 100 ml of BCBL-1 media (minus Geneticin). After 72 h ~375 ml of BCBL-1 media was added to the culture until a volume of 500 ml was obtained and then this was split into two T150 flasks, each containing 250 ml. After 48 h the cultures was split into five T150 flasks (100 ml in each) and ~400 ml of BCBL-1 media was added to each flask to obtain a total volume of ~2.5 L with a cell density of $5\text{-}6x10^5$ cells/ml. Lytic replication of KSHV was induced by the addition of TPA (Sigma Aldrich) at a final concentration of 20 ng/ml. KSHV was harvested 3 to 4 days after the induction of lytic replication. The ~2.5 L culture was first centrifuged at 400 x g and 4°C for 15 min using a Beckman JLA-10.500 rotor in an Avanti J-26 XPI

Centrifuge (Beckman Coulter), which pelleted the majority of the cells and cell debris. The supernatant containing the virus was then poured into clean centrifuge tubes and spun at 12,500 x g and 4°C for 3 h. The supernatant was then poured off and neutralised using Virkon (Antec International) whilst the virus-containing pellets were resuspended in 12 ml of LEC media. The LEC media containing KSHV was then spun at 2000 rpm and 4°C for 10 min in an Eppendorf desktop centrifuge and the supernatant was passed through a 0.45 µm filter to remove all traces of cell debris before being aliquoted and stored at -80°C. LEC media from the same batch that was used to resuspend the virus was also frozen at the same time to be used for uninfected cells.

293T cells were used to test the infectivity of each batch of KSHV. $2.5x10^4$ 293T cells were seeded in one well of a 12-well plate (TPP, MIDSCI) in 1 ml of 293T media. After 24 h the 293T media was removed, 500 µl of KSHV preparation was added to the well and the plate was spun at 2500 rpm for 30 min in an Eppendorf desktop centrifuge. 500 µl of 293T media was then added to the well and the cells were left for 24 h before changing the media for 1 ml of fresh 293T media. 72 h p.i., cells were visualised on an Axiovert 100 microscope (Zeiss) using an AxioCam (Zeiss). Provided more than 50% of 293T cells were GFP positive, KSHV preparations were then used to infect LEC.

For standard KSHV infections of LEC, $1x10^5$ cells were seeded per well of a 6-well plate in 1 ml of LEC media. 24 h later, the LEC media was removed, 1 ml of KSHV preparation or thawed LEC media was added to the well and the plate was spun at 2500 rpm for 30 min in an Eppendorf desktop centrifuge. After 24 h the media was replaced with 1 ml of fresh LEC media per well. The media was replaced again 48 h p.i. and cells were harvested for total RNA extraction 72 h p.i. Infectivity was assessed both visually, using an Axiovert 100 fluorescent microscope (Zeiss), and by flow cytometry using a CyAn ADP High-Performance Flow Cytometer (Beckman Coulter).

For KSHV infections of pSIN_MCS, pSIN_30b and pSIN_30c transduced LEC, 1 ml of KSHV preparation was added to cells 48 h after infection with the appropriate lentivirus. The plates were then spun at 2000 rpm for 10 min in an Eppendorf desktop centrifuge. After 24 h the media was replaced with 1 ml of

fresh LEC media per well. Cells were harvested for total RNA and protein extraction 48 h post-KSHV infection and 96 h after lentiviral infection.

2.2.4 Transfection of LEC, HUVEC, or 293T cells with miRNA mimics, miRNA inhibitors or siRNA

The following synthetic small RNAs were used for these transfections: miRIDIAN microRNA Mimics (Dharmacon, ThermoScientific), miRIDIAN microRNA Hairpin Inhibitors (Dharmacon, ThermoScientific) and ON-TARGET*plu*s siRNA Reagents (Dharmacon, ThermoScientific). The lyophilised small RNAs were resuspended in 1x siRNA buffer, made up with 5x siRNA buffer (Dharmacon, ThermoScientific) and sterile H_2O (Gibco, Life Technologies), to give a working concentration of 10 µM for the mimics and inhibitors and 20 µM for the siRNAs.

For LEC and HUVEC, cells were seeded at a density of $2.5x10^4$ cells per well of a 12-well plate or $5x10^4$ cells per well of a 6-well plate. For 283T, cells were seeded at a density of $5x10^4$ cells per well of a 12-well plate. 16 h later the media was removed and cells were washed twice with pre-warmed Opti-MEM before an overlay of Opti-MEM was added to each well: 400 µl for a 12-well plate, 800 µl for a 6-well plate. Transfections were performed using Oligofectamine Transfection Reagent (Invitrogen, Life Technologies) according to the manufacturer's instructions. For every 0.1 nmoles of small RNA to be transfected, 5 µl of Oligofectamine was prepared. This ratio was maintained, regardless of the number of cells being transfected. The required amount of small RNA was made up to 87.5 µl (12-well plate) or 175 µl (6-well plate) with Opti-MEM in a 1.5 ml Eppendorf tube. In a separate 1.5 ml Eppendorf tube, the required volume of Oligofectamine was added dropwise to Opti-MEM to give a total volume of 12.5 µl (12-well plate) or 25 µl (6-well plate). The Oligofectamine/Opti-MEM mix was incubated for 10 min at RT before being added to the diluted small RNA to give a final volume of 100 µl (12-well plate) or 200 µl (6-well plate). The Oligofectamine/small RNA mix was incubated at RT for 20 min and then added dropwise to one well of a 12-well or 6-well plate containing the Opti-MEM overlay. Mastermixes of small RNA and/or Oligofectamine were prepared when more than one well was to be transfected.

0.75 ml (12-well plate) or 1.5 ml (6-well plate) of the appropriate media was added to each well 4 h post-transfection to neutralize the transfection reagent. The transfection media was completely removed 24 h post-transfection and the cells were washed with sterile PBS before fresh media was added.

LEC and HUVEC were harvested 48 h post-transfection with mimics and/or inhibitors for total RNA and protein extraction. 293T cells were transfected with luciferase reporter plasmids 48 h post-transfection with mimics (see Sections 2.2.1 and 2.6). LEC and HUVEC were harvested at 48 h and 72 h post-transfection with siRNA for total RNA and protein extraction. LEC and HUVEC were collected 48 h post-transfection with siRNA to set-up the Matrigel tube formation assay (see Section 2.7.1). HUVEC were collected 24 h post-transfection with mimics or inhibitors to set-up the Matrigel 3D sprouting assay (see Section 2.7.2).

2.3 Molecular biology techniques

2.3.1 PCR cloning strategy

hsa-miR-30b, hsa-miR-30c-1 and the *dll4* 3'UTR were cloned using the following polymerase chain reaction (PCR) cloning strategy. Primers were designed against the 5' and 3' ends of the required DNA fragment. All primers were designed to end on at least one guanine or cytosine to increase binding affinity. Primers were designed so that each set of forward and reverse primers had a similar melting temperature (TM) and a guanine/cytosine (GC) content of around 50%. NCBI Blast was used to check that the primers were only specific to the DNA sequence of interest. These primers contained different restriction enzyme digestion sites at their 5' ends, along with some "junk" DNA to aid restriction enzyme digestion. Two different restriction enzymes were used in the cloning process, this aided cloning of the fragment in the correct orientation and minimised vector re-ligation. The restriction enzymes to be used were selected based on three criteria. Firstly, two restriction enzymes were chosen that would allow insertion of the DNA fragment into the chosen vector at the correct location. When cloning the hsa-miR-30b or hsa-miR-30c-1 into pSIN_MCS, a variety of restriction enzymes were available due to the presence of the multiple

cloning site (MCS), immediately downstream of the internal promoter. The MCS is a collection of restriction enzyme sites which was inserted into a defined region of the vector during vector design in order to facilitate cloning. The pSIN_MCS vector is based on the pCSGW vector (Godfrey et al., 2005). To create the pSIN_MCS vector, the GFP ORF from the pCSGW vector was removed with *Bam*HI and *Not*I and the MCS was inserted (Vart et al., 2007). When cloning the *dll4* 3'UTR into pCSGW, there was a more limited choice of restriction enzymes as the 3'UTR needed to be inserted directly downstream of the *GFP* ORF. Once two restriction enzymes were selected, the second criterion was that the DNA to be cloned could not contain restriction sites for either of the proposed enzymes. To check this, the DNA sequence to be cloned was obtained from the NCBI GenBank depository of sequenced DNA. This sequence was entered into pDRAW32 (www.acaclone.com) and examined in order to identify all restriction enzyme sites present within the sequence. If either of the two selected restriction enzymes had restriction sites within the DNA sequence, that particular enzyme could not be used and the vector was re-examined for an alternative enzyme. The third criterion was only considered if there was more than one option with regards to restriction enzyme combinations. In this situation, two enzymes were chosen which had the same or very similar digestion conditions (i.e. buffer), in order to increase the efficiency of co-digestion. The primers used are shown in Table 2.1.

PCR was performed with 0.25 µl of 100 µM forward and reverse primers, 10 µl of 5x HotStar HiFidelity PCR Buffer (Qiagen) or 5 µl of 10x PCR Buffer (Qiagen), 1 µl of HotStar HiFidelity DNA Polymerase (2.5 units) (Qiagen) or 0.25 µl of HotStarTaq DNA Polymerase (1 unit) (Qiagen) and 100 ng or 500 ng of template DNA made up to a final volume of 50 µl with ddH_2O. When using HotStarTaq DNA Polymerase 1 µl of 10mM deoxyribonucleotide triphosphate (dNTP) mix (Invitrogen) was also required as these were not included in the buffer. For some reactions 10 µl of Q-Solution and/or 1 µl of $MgSO_4$ were also included in an attempt to optimise the PCR conditions. The PCR conditions used were those specified by the manufacturer's instructions. Typically, the polymerase was activated by incubating the reaction mixture at 95°C for 2-15 min and was followed by 35-40 cycles of 94°C for 1 min, 55°C for 1 min and 72°C for 1 min. During these steps double stranded DNA is denatured, the

primers anneal and PCR product is synthesised by DNA polymerase mediated extension from the primers. The final step was a 10 min hold at 72°C which ensured full elongation of any remaining single stranded DNA. The cycle number, primer annealing temperature and the length of the extension step were varied to optimise the PCR program for the particular combination of primers and PCR target. The extension time was dependent on the length of the product, with 1min being allowed for every 1 kb of DNA. The initial primer annealing temperature was set at 4°C lower than the TM of the primer with the lowest TM. If no product was produced, the annealing temperature was lowered by 1-2°C at a time. If non-specific products were synthesised, the annealing temperature was increased. On some occasions temperature gradient PCR was used as a quick method of determining the optimum primer annealing temperature. With gradient PCR the annealing temperature was increased by specified increments from right to left across the PCR block. Gel electrophoresis was then performed with all samples and the annealing temperature which yielded the most amount of specific product was used for subsequent PCRs, if required.

Target	Vector	Construct	Template	Restriction enzymes	Forward primer	Reverse primer	PCR conditions
hsa-miR-30b	pSIN_MCS	pSIN_30b	HF1 genomic DNA	*Bam*HI / *Not*I	CGCGGATCCAGCCTGGGC AATATAGTGAGAC	ATAAGAATGCGGCCGCACT ACTCCTACTGCAACCATGC	35 cycles of: 94°C for 1 min 52-61°C gradient for 1 min 72°C for 1 min
hsa-miR-30c-1	pSIN_MCS	pSIN_30c	HF1 genomic DNA	*Bam*HI / *Not*I	CGCGGATCCAGTTGGAGGC AATCCACAGG	ATAAGAATGCGGCCGCGAA AGCTCTGTGGTCACTGAGG	35 cycles of: 94°C for 1 min 52-61°C gradient for 1 min 72°C for 1 min
dll4 3'UTR	pCSGW	pCSGW_dll4-3'UTR	Whole Zebrafish embryo cDNA from 48 hpf	*Not*I / *Sbf*I	ATAAGAATGCGGCCGCATT ACAGGCTGATGTCTATGAG GAG	AAATATCCTGCAGGAAACA ATCCAAGAAGACCCTGGG	35 cycles of: 94°C for 1 min 50.6-60°C gradient for 1 min 72°C for 1 min

Table 2.1. PCR cloning details. The pCSGW and pSIN-MCS vectors were generated by Richard Jenner and Richard Vart Godfery et al., 2005; Vart et al., 2007). Red: junk DNA; green: restriction enzyme site; blue: primer sequence which is complimentary to target sequence. All primers are shown 5' to 3'.

2.3.2 Restriction enzyme digestion

Restriction enzyme digestion was performed on PCR amplified products and plasmid DNA prior to ligation. Restriction enzyme digestion was also used to confirm the presence of a cloned insert within a plasmid. All restriction enzyme digests were performed for 1-2 h at 37°C, except for digestions with *Not*I which required overnight digestion at 37°C. Most restriction enzyme digests were double-digests where both restriction enzymes were added at the same time. For each restriction enzyme digest, 5-10 units of each enzyme was used in a total volume of 20-25 µl containing the appropriate amount of 10x restriction enzyme buffer. The appropriate buffer was selected by consulting the enzyme buffer compatibility charts provided by Promega and New England Biolabs and determining which buffer would obtain the maximum activity for the two enzymes. If the two enzymes were not compatible then two single digests were performed with the DNA being cleaned in between using the QIAquick Gel Extraction Kit (see Section 2.3.4). For some restriction enzymes the appropriate amount of 100x bovine serum albumin (BSA) (New England Biolabs) was also added to the reaction mixture. Approximately 1 µg of DNA was used per restriction enzyme digest. If required, the restriction enzymes were heat inactivated at the end of the restriction digestion by incubating the reaction mixture at 65°C for 20 min.

Following restriction enzyme digestion, plasmids required for ligation were treated with calf-intestinal alkaline phosphatase (CIP) (New England Biolabs) in order to remove the 5’ phosphate groups. This helped to prevent re-circularisation and re-ligation of the linearized plasmid because DNA fragments that lack the 5' phosphoryl termini cannot self-ligate. The plasmid DNA was incubated with 1 µl of CIP at 37°C for 1 h before undergoing agarose gel purification (see Sections 2.3.3 and 2.3.4).

2.3.3 Agarose gel electrophoresis

Gel electrophoresis was used to visualise DNA and/or to purify DNA. To resolve DNA fragments of >200 bp, 1% agarose gels were used. These were produced by heating 1% weight/volume (w/v) agarose powder (Sigma-Aldrich) in 1x TAE

buffer (Tris-acetate 0.4 M, ethylene diamino tetraacetic acid (EDTA) 0.01 M). To resolve DNA fragments of <200 bp, 2-4% agarose gels were used. DNA was visualised through the addition of either 0.5 µg/ml of ethidium bromide (Sigma-Aldrich) or 1 µl/ml of GelRed Nucleic Acid Stain (Biotium). Before loading, the DNA was mixed with DNA Loading Dye (Fermentas) to enable an estimation of DNA running speed. The loading dye contained Xylene Cyanol FF and Bromophenol blue which ran at 4160 bp and 370 bp respectively. Agarose gels were electrophoresed at 100 V in TAE buffer. The G:Box gel documentation system (Syngene) was used to visualise DNA bands. DNA ladders (Fermentas, ThermoScientific) of the appropriate size range were run alongside experimental samples to allow the size of DNA fragments to be estimated.

2.3.4 Agarose gel extraction

If the DNA fragments run on an agarose gel were going to be used for subsequent ligation or sequencing (PCR products or digested plasmids), agarose gel extraction was performed using the QIAquick Gel Extraction Kit (Qiagen). Gel pieces containing the required DNA band were excised with the help of a UVI tec BTX-20-M UV gel box and then weighed in a 1.5 ml Eppendorf. QG buffer was added to the gel pieces: 300 µl for every 100 mg of gel. The gel was dissolved in the QG buffer by incubating the Eppendorf tube at 50°C for 10 min, vortexing occasionally. Once all the gel was in solution isopropanol was added: 100 µl for every 100 mg of gel. The sample was then loaded onto a QIAquick spin column and processed according to the manufacturer's instructions. The DNA was eluted from the column in 30 µl of ddH_2O.

The QIAquick Gel Extraction Kit was also used to clean PCR products following restriction digest, however these products were not submitted to agarose gel electrophoresis because digestion had very little effect on their size and therefore digested and undigested DNA could not be identified using an agarose gel. 300 µl of QG buffer was added to the digested DNA, followed by 100 µl of isopropanol. The sample was then loaded onto a QIAquick spin column and processed according to the manufacturer's instructions. The DNA was eluted from the column in 30 µl of ddH_2O.

2.3.5 Ligation

Ligation reactions were performed in a total volume of 20 µl using 400 units (1 µl) of T4 DNA ligase and 2 µl of 10x T4 DNA ligase buffer (New England Biolabs). Varying ratios of insert to plasmid DNA were used in ligation reactions, always keeping the insert at a higher concentration to the plasmid DNA to encourage ligation and prevent vector re-ligation. The ligation mixture was incubated either at RT for 1-2 h or at 16°C overnight in a MWG-Biotech Primus 96 plus thermal cycler.

2.3.6 Bacterial transformation

Plasmid DNA was amplified through chemical transformation of bacteria and subsequent expansion of bacterial cultures. For each transformation, one vial of 50 µl One Shot TOP10 Chemically Competent *E.coli* (Invitrogen, Life Technologies) was thawed on ice before the addition of 1-5 µl of ligation reaction or plasmid DNA (~100 ng). The bacteria were incubated on ice in the presence of the DNA for 30 min and then heat shocked at 42°C for 30 sec before being returned to the ice for a further 2 min. Using aseptic technique, 250 µl of pre-warmed S.O.C media (Invitrogen, Life Technologies) was added to each vial of bacteria which were incubated in a bacterial shaker at 37°C and 225 rpm for 1 h.

If the bacteria had been transformed with ligation mixture, the vial was then spun down for 30 sec at 13,000 rpm in a Heraeus Biofuge pica centrifuge (Thermo Fischer Scientific) and 100 µl of the media was removed. The bacteria were resuspended in the remaining media (200 µl) and streaked out on Luria-Bertani (LB) agar plates containing the appropriate antibiotic. LB agar plates were made by dissolving 32 g of LB Agar (Lennox L Agar) powder (Invitrogen) in a total volume of 1 L of ddH_2O. This solution was autoclaved and allowed to cool slightly before the addition of the appropriate antibiotic: 100 µg/ml of ampicillin (Sigma-Aldrich) for pCSGW and pSIN-MCS; 50 µg/ml of kanamycin (Fluka BioChemika) for pEZX-MT01. Plates were incubated overnight at 37°C. Successfully transformed bacteria contained an antibiotic resistant cassette (either ampicillin or kanamycin, depending on the plasmid), and therefore

survived antibiotic selection and grew to form visible colonies. Several colonies were then picked for subsequent expansion in 3 ml cultures of LB broth.

If the bacteria had been transformed with a pure solution of plasmid DNA, the S.O.C. media culture was added to 5 ml of pre-warmed LB broth, containing the appropriate antibiotic, and incubated in a bacterial shaker at 37°C and 225 rpm for 1 h. This feeder culture was then expanded to 100 ml with LB broth and incubated overnight in a bacterial shaker at 37°C and 225 rpm. The LB broth was prepared by dissolving 20 g of LB Broth Base (Lennox L Broth Base) (Invitrogen) in a total volume of 1 L of ddH_2O. This solution was autoclaved and allowed to cool slightly before the addition of the appropriate antibiotic: 100 µg/ml of ampicillin (Sigma-Aldrich) for pCSGW and pSIN-MCS; 50 µg/ml of kanamycin (Fluka BioChemika) for pEZX-MT01.

2.3.7 Plasmid purification

Plasmid DNA was extracted from transformed bacterial cultures and purified using either a QIAprep Spin Miniprep kit (Qiagen) or a QIAGEN Plasmid Maxi kit (Qiagen), according to the manufacturer's instructions.

Minipreps were performed on 1.5 ml of bacterial cultures, which were typically transformed with ligation reactions during the cloning process. Obtaining plasmid DNA at this stage enabled tests to be carried out to check for the presence of a particular DNA insert. To generate a miniprep culture, a single bacterial colony was picked from a LB agar plate and placed into 3 ml of LB broth containing the appropriate antibiotic. These cultures were incubated overnight in a bacterial shaker at 37°C and 225 rpm. 1.5 ml of the culture was stored at 4°C, to be used to inoculate a maxiprep culture if required. The other 1.5 ml of culture was spun at 1200 rpm for 1 min in a Heraceus Biofuge pica desktop centrifuge to pellet the bacteria. Once the supernatant had been removed, bacterial pellets could be processed immediately or stored at -20°C. To extract the plasmid DNA, the bacterial pellet was resuspended in 250 µl of Buffer P1 and lysed through an alkaline lysis method by the addition of 250 µl Buffer P2. LyseBlue (Qiagen) was included in Buffer P1 in order to ensure homogenous mixing (a blue precipitate appeared upon addition of Buffer P2).

The mixture was then neutralised through the addition of 350 µl Buffer N3, which caused the LyseBlue to turn colourless. The presence of a homogeneous solution with no traces of blue indicated that the sodium dodecyl sulphate (SDS) from the lysis buffer has been effectively precipitated. Buffer N3 also adjusts the mixture to the high-salt conditions required for effective DNA binding to the column. Cellular debris and genomic DNA were pelted by spinning at 13,000 rpm for 10 min in an Eppendorf 5810R desktop centrifuge and the resulting clear solution containing the plasmid DNA was passed through a QIA-prep silica membrane column by spinning at 13,000 rpm for 1 min in a desktop centrifuge. The DNA was absorbed onto the silica due to the presence of high salt. Wash steps were performed according to the manufacturer's protocol. Endonucleases were efficiently removed by a brief wash step with Buffer PB whilst salts were efficiently removed by a brief wash step with Buffer PE. Clean, high-quality plasmid DNA was then eluted in 50 µl of ddH_20. Each miniprep yielded approximately 10 µg of plasmid DNA.

Maxipreps were performed on 100 ml of bacterial culture from which bacteria were pelleted by spinning at 4000 rpm for 15 min at 4°C in a desktop Eppendorf centrifuge. Once the supernatant had been removed, bacterial pellets could be processed immediately or stored at -20°C. To extract the plasmid DNA, the bacterial pellet was resuspended in 10 ml Buffer P1 and lysed through a modified alkaline lysis method by the addition of 10 ml of Buffer P2. LyseBlue (Qiagen) was included in Buffer P1 in order to ensure homogenous mixing (a blue precipitate appeared upon addition of Buffer P2). After 5 min incubation at RT, the mixture was neutralised through the addition of 10 ml of chilled Buffer P3, which caused the LyseBlue to turn colourless. The presence of a homogeneous solution with no traces of blue indicated that the SDS from the lysis buffer has been effectively precipitated. The mixture was incubated on ice for 20 min to enhance precipitation of genomic DNA, proteins, cell debris, and potassium dodecyl sulphate (KDS). The mixture was centrifuged at 3,500 rpm for 30 min at 4°C to remove the precipitated material. The supernatant containing the plasmid DNA was applied to a QIAGEN-tip through a 70 µm cell strainer (BD Falcon), to catch any residual precipitate. The QIAGEN-tip was previously equilibrated by applying 10 ml of Buffer QBT. The QIAGEN-tip contained QIAGEN Anion-Exchange Resin, to which the plasmid DNA bound

under the appropriate low-salt and pH conditions. The QIAGEN-tip was washed twice with 20 ml of Buffer QC, a medium-salt wash which removed RNA, proteins, dyes and low-molecular-weight impurities. The plasmid DNA was then eluted in 15 ml of a high-salt buffer, Buffer QF, and precipitated and desalted through the addition of 10.5 ml of isopropanol (VWR). Centrifugation for 30 min at 4000 rpm and 4°C led to pelleting of the DNA, which was washed with 5 ml of 70% ethanol before a final centrifugation of 10 min at 4000 rpm and 4°C. Once the DNA pellet had been air dried, it was resuspended in 300 µl of ddH_2O. Maxipreps typically yielded 1-2 µg/µl of plasmid DNA.

Plasmid DNA concentration was quantified by measuring the absorbance at 260nm using a NanoDrop UV spectrophotometer (Thermo Scientific). All the plasmid DNA samples had a 260/280 ratio of ~1.8 indicating pure DNA. The 260/230 ratios were all in the range of 1.8-2.2, indicating a lack of co-purified contaminants.

2.3.8 Site directed mutagenesis

Site directed mutagenesis was performed using the QuikChange XL Site-Directed mutagenesis kit (Stratagene) to mutate the seed regions of miR-30b and miR-30c-1 and to mutate the miR-30 target site within the *DLL4* 3'UTR. Mutagenic primers were designed according to the protocol guidelines and are detailed in Table 2.2. Both the forward and reverse primers were designed so that they contained the desired mutation and would anneal to the opposite strands of the same DNA sequence. The primers were all within the specified size range of 25-45 nt, had a TM greater than or equal to 78°C, had a minimum GC content of 40% and terminated in one or more guanine or cytosine bases. The mutated bases to be incorporated into the target DNA, indicated in red in Table 2.2, were located in the centre of the primers with ~10-15 nt of correct sequence on either side.

The first step was to incorporate the altered bases through PCR with the mutagenic primers using *PfuTurbo* DNA polymerase, according to manufacturer's instructions. *PfuTurbo* replicated both plasmid strands with high fidelity and without displacing the mutant oligonucleotide primers. Incorporation

of the oligonucleotide primers therefore generated a mutated plasmid containing staggered nicks. PCR was performed with 125 ng of forward and reverse primers and 10 ng of the relevant vector (pSIN_30b, pSIN_30c or pEZX-MT01_DLL4-3'UTR). PCR conditions were as detailed in Table 2.2. The parental plasmids containing the wild type miRNA target site or seed region were all originally isolated from *E. coli,* which dam methylates all DNA. Therefore, all un-mutated parental DNA was removed from the mixture following the PCR reactions by treatment with DpnI endonuclease, which is specific for methylated and hemi-methylated DNA. 1 µl of DpnI (10 units) was incubated with each PCR mixture for 1 h at 37°C.

After DpnI digestion, 2 µl of each PCR reaction was used to transform XL10-Gold*** Ultracompetent Cells (Stratagene), which have the capability to repair the staggered nicks in the mutated plasmids. The ultracompetent cells were thawed on ice and then 45 µl per transformation were transferred to a pre-chilled 14 ml BD Falcon polypropylene round-bottom tube. Following the addition of 2 µl of β-mercaptoethanol (β-ME) the ultracompetent cells were incubated on ice for 10min and swirled every 2 min. Once the PCR mixture had been added the ultracompetent cells were incubated on ice for 30 min and then heat-shocked at 42°C for 30 sec followed by 2 min on ice. The transformed bacteria were plated out on agar plates containing the appropriate antibiotic for selection. Bacterial colonies were picked after 24 h and used to seed miniprep cultures. Plasmid DNA was purified from the miniprep cultures and sent for sequencing to confirm the presence of the mutated sites.

Target	Plasmid name	Forward primer	Reverse primer	PCR conditions
miR-30 site in *DLL4* 3'UTR	pEZX-MT01_DLL4-UTR	GGACCTTCCTTCTGCATTGGGG ACATTGCATCCTGGATGGG	CCCATCCAGGATGCAATGTCCC CAATGCAGAAGGAAGGTCC	95°C for 1 min Then 18 cycles of: 95°C for 55 sec 60°C for 50 sec 68°C for 8 min and 15 sec Then a final step at 68°C for 7 min
Seed region of hsa-miR-30b	pSIN_30b	CCAAGTTTCAGTTCATGTCCCCA TCCTACACTCAGCTGTAATAC	GTATTACAGCTGAGTGTAGGAT GGGGACATGAACTGAAACTTGG	95°C for 1 min Then 18 cycles of: 95°C for 55 sec 60°C for 50 sec 68°C for 10 min Then a final step at 68°C for 7 min
Seed region of hsa-miR-30c-1	pSIN_30c	CCATGCTGTAGTGTGTGTCCCC ATCCTACACTCTCAGC	GCTGAGAGTGTAGGATGGGGAC ACACACTACAGCATGG	95°C for 1 min Then 18 cycles of: 95°C for 55 sec 60°C for 50 sec 68°C for 10 min Then a final step at 68°C for 7 min

Table 2.2. Primers and PCR conditions used for site directed mutagenesis. Red: mutated bases to be incorporated into plasmid; blue: target site/seed region surrounding the mutated bases. All primers are shown 5' to 3'.

2.3.9 Genomic DNA extraction

Genomic DNA was extracted from cultured cells using the QIAmp DNA Mini Kit (Qiagen). Cells were detached with trypsin, counted, washed with PBS and pelleted by centrifugation for 1 min at 5000 rpm in a table top centrifuge. A maximum of $5x10^6$ cells were used per sample, according to the manufacturer's instructions. Cells were resuspended in 200 µl of PBS to which 20 µl of Proteinase K (Qiagen) was added. To lyse the cells, 200 µl of Buffer AL was added to the sample which was mixed by pulse-vortexing for 15 sec. Samples were incubated at 56°C for 10 min and then 200 µl of 100% ethanol was added and mixed by pulse-vortexing for 15 sec. These steps ensured that the lysate buffering conditions had been adjusted correctly to allow optimal binding of the DNA to the QIAamp membrane. The samples were then applied to a QIAmp Mini spin column which was centrifuged in a table top centrifuge at 8000 rpm for 1 min to allow DNA absorption onto the QIAamp silica membrane. The filtrate was discarded and the columns were washed with 500 µl of Buffer AW1 followed by 500 µl of Buffer AW2, both by centrifugation at 8000 rpm for 1 min. The use of two different wash buffers significantly improved the purity of the eluted DNA by ensuring complete removal of any residual contaminants without affecting DNA binding. The DNA was eluted in 70 µl of ddH_2O by centrifugation at 8000 rpm for 1 min. The DNA was then separated into three aliquots of 3 µl, 5 µl and 62 µl. The 3 µl aliquot was used to determine the concentration and purity of the DNA by measuring absorbance at 260 nm (A260) and 280 nm (A280) with a NanoDrop-1000 Spectrophotometer. All samples exhibited an A260/A280 ratio of ~1.8, indicating that the DNA was free of contaminants. The 5 µl aliquot had 45 µl of ddH2O added to it to produce the 1/10 dilution required for qPCR (see Section 2.3.10). DNA was stored at -20°C until use.

2.3.10 Quantitative polymerase chain reaction (qPCR)

Following lentiviral infection, qPCR was performed for the glyceraldehyde 3-phosphate dehydrogenase (*GAPDH*) gene and the lentiviral packaging signal, in order to determine the number of lentiviral copies per cell (c/c). Genomic DNA was extracted 72 h p.i. as described in Section 2.3.9. The GAPDH primers and probe were as previously described (Bourboulia et al., 2004). The *GAPDH*

primers and probe and their concentrations used for qPCR were as follows: forward primer 5'-GGAGTCAACGGATTTGGTCGTA-3', 0.7 µM; reverse primer 5'-GGCAACAATATCCACTTTACCAGAGT-3', 0.7 µM; TaqMan probe (Applied Biosystems, Life Technologies) 5'-FAM-CGCCTGGTCACCAGGGCTGC-TAMRA-3', 0.15 µM. The primers and probe for the lentiviral packaging signal were as previously described (Vart et al., 2007). The lentiviral packaging signal primers and probe and their concentrations used for qPCR were as follows: forward primer 5'-GCACGGCAAGAGGCGA-3', 0.3 µM; reverse primer 5'-CGCACCCATCTCTCTCCTTCTA-3', 0.3 µM; TaqMan probe 5'-FAM-CGGCGACTGGTGAGTACGCCAAAAAT-TAMRA-3', 0.15 µM. Reactions were performed using 25 µl of ABsolute QPCR ROX Mix (ABgene, ThermoScientific) and 10 µl of genomic DNA at a concentration of 50-100 ng/µl, made up to a total volume of 50 µl using ddH_2O. The qPCR conditions used were as follows: 95°C for 15 min followed by 40 cycles of 95°C for 15 sec and 60°C for 1 min. Fluorescence readings were taken at the end of the 60°C incubation. Reactions were run in MicroAmp® Optical 96-Well Reaction Plates (Applied Biosystems, Life Technologies) sealed with MicroAmp® Optical Adhesive Films (Applied Biosystems, Life Technologies) on an Eppendorf Mastercycler ep Realplex (Eppendorf). The standard used for each qPCR was a DNA mixture of linearized pSIN-MCS plasmid (Vart et al., 2007) and linearized pcDNA3.1/V5-His-TOPO-GAPDH plasmid (Bourboulia et al., 2004) at a known copy number of $1x10^8$ copies per 10 µl. This was serially diluted to give standards of $1x10^7$, $1x10^6$, $1x10^5$, $1x10^4$, $1x10^3$ and $1x10^2$ copies per 10 µl. For each sample a neat and 1/10 dilution of genomic DNA was run and both samples and standards were run in duplicate. So at least 40 µl of each neat and dilute DNA sample and each standard was required. A negative control of 10 µl ddH_2O was performed for all qPCRs for both the *GAPDH* and lentiviral packaging signal reaction mixtures. A standard curve for both *GAPDH* and the lentiviral packaging signal was used to determine how many copies of the *GAPDH* gene and the lentiviral construct was present in each sample. The number of c/c was determined by adjusting the number of lentiviral constructs present to the number of cells analysed, using *GAPDH.*

2.3.11 RNA extraction

Before any RNA work was conducted, all surfaces, Eppendorf racks and pipettes were cleaned with RNaseZAP (Ambion) to remove any traces of RNase enzymes which could contaminate samples and lead to RNA degradation. Once the RNA extraction had been completed, the amount and purity of the RNA was determined by measuring absorbance at 260 nm (A260) and 280 nm (A280) with a NanoDrop-1000 Spectrophotometer. All samples exhibited an A260/A280 ratio of ~2.0, indicating that the RNA was pure and free of contaminants. RNA was stored at -80°C until use.

2.3.11.1 miRNeasy Mini Kit (Qiagen)

Total RNA was extracted from cultured cells using the miRNeasy Mini Kit (Qiagen) according to the manufacturer's instructions. This kit enables extraction of all RNA, including the small RNA fraction (<200 bp), which is discarded by other RNA extraction kits. The small RNA fraction contains miRNAs, among other species, and therefore it was desirable to keep this RNA fraction.

A maximum of $1x10^7$ cells were processed per sample. When working with adherent cells, the media was simply removed from the cells before lysis. When working with cells grown in suspension or trypsinised cells, the cells were first pelleted by centrifugations at 1200 rpm for 5 min before the media was removed. To lyse the cells, 700 µl of QIAzol Lysis Reagent (Qiagen) was added to each sample. QIAzol Lysis Reagent is a monophasic solution of phenol and guanidine thiocyanate which is designed to facilitate lysis of cells or tissue, inhibit RNases and also to enable the removal of the majority of cellular DNA and proteins through organic extraction. Adherent cells were collected using a cell scraper whereas pelleted cells were resuspended in the QIAzol Lysis Reagent through repeated pipetting. This initial step caused complete disruption of the plasma membranes of all the cells and organelles in the sample. Homogenisation was then required to reduce the viscosity of the lysates produced by disruption. Homogenisation shears high-molecular-weight genomic DNA and other cellular components to create a homogeneous lysate. If the sample contained $<3x10^6$ cells, the lysate was homogenised by vortexing for 1

min. If the sample contained >3x10^6 cells, the lysate was passed through a QIAshredder spin column (Qiagen) by centrifugation at 13,000 rpm for 1 min in a table top centrifuge. The homogenised lysate was incubated at RT for 5 min before the addition of 140 µl of chloroform (Sigma-Aldrich). The sample was then shaken vigorously for 15 sec and incubated at RT for 2-3 min. To separate the sample into the aqueous and organic phases it was centrifuged for 15 min at 12,000 x g and 4°C. The RNA could be found in the upper aqueous phase whilst DNA partitioned to the interphase and proteins partitioned to the interphase or the lower organic phase. The upper aqueous phase was transferred to a new Eppendorf tube and mixed with 1.5 volume of 100% ethanol (typically 525 µl). This provided the appropriate binding conditions for all RNA molecules from 18nt upwards. The sample was then applied to an RNeasy Mini spin column (Qiagen) by centrifugation at 10,000 rpm for 15 sec at RT in a table top centrifuge, which allowed binding of the total RNA to the silica membrane. The column was washed with 350 µl of Buffer RWT (15sec spin at 10,000 rpm at RT) before the addition of 80 µl of DNase I incubation mix. The DNase I incubation mix was prepared using an RNase-Free DNase Set (Qiagen) by adding 10 µl of DNase I stock solution to 70 µl of Buffer RDD. After 15 min incubation at RT, the column was again washed with 350 µl of Buffer RWT. The final two washes were performed with 500 µl of Buffer RPE, the first at 10,000 rpm for 15 sec and then at 10,000 rpm for 2 min. The second longer centrifugation dried out the spin column, ensuring that no ethanol was carried over during RNA elution. A final centrifugation at 13,000 rpm from 1 min was performed without any wash buffer and with a clean collection tube. This eliminated the possibility of any carryover of Buffer RPE or other residual flow-through remains. The RNA was eluted in 30 µl of RNase-free water (Qiagen) by centrifuging at 10,000 rpm for 1 min.

2.3.11.2 TRI Reagent (Sigma-Aldrich)

RNA extraction and purification using TRI Reagent (Sigma-Aldrich) was performed when obtaining RNA from zebrafish embryos. The number of embryos from which the RNA was harvested varied between experiments but was kept consistent between samples within the same experiment. Typically ~30 embryos were collected per sample. The embryos were transferred to an

Eppendorf tube and a Pasteur pipette was used to remove as much fish water as possible. 500 µl of TRI Reagent was added to each sample and the sample was disrupted by repeatedly passing the solution through a 1 ml syringe and needle. A further 500 µl of TRI Reagent was added to prevent saturation and the sample was homogenised by vortexing for 1 min. They lysate was centrifuged at 12,000 rpm and 4°C for 10 min to remove insoluble material. The supernatant was transferred to a clean Eppendorf tube and 200 µl of chloroform was added. The sample was vortexed for 30 sec and left to incubate at RT for 5 min before centrifuging at 12,000 rpm and 4°C for 10 min. The upper aqueous phase was transferred to a clean Eppendorf tube, mixed with 500 µl of isopropanol and incubated at RT for 5 min in order to precipitate the RNA. The RNA was pelleted by centrifugation at 12,000 rpm and 4°C for 10 min and then the pellet was washed in 1 ml of 75% ethanol. A final centrifugation for 5 min at 7,500 rpm and 4°C occurred before the supernatant was removed and the RNA pellet was allowed to air-dry. The RNA was then resuspended in 40 µl of ddH_2O.

Instead of on-column DNase treatment, as in Section 2.3.11.1, 1 µl of DNase I (Fermentas, ThermoScientific) was added to the sample which was incubated at 37°C for 15 min. To inactivate the DNase, 1 µl of EDTA was added to the sample before precipitating the RNA overnight at -20°C using 5 µl of 4 M lithium chloride (LiCl) (Ambion, Life Technologies) and 150 µl of 100% ethanol. Following precipitation the sample was centrifuged at 12,000 rpm and 4°C for 30 min before being air-dried and resuspended in 30 µl of ddH_2O.

2.3.12 cDNA synthesis

Complimentary DNA (cDNA) synthesis was performed using 1-2000 ng of RNA, previously isolated by one of the methods described in Sections 2.3.11.1 or 2.3.11.2. The RNA was first incubated at 70°C for 6 min in a MWG-Biotech Primus 96 plus thermal cycler with 1 µl of 100 µM oligo(dT) and 1 µl of 10 mM dNTP mix (Invitrogen, Life Technologies), made up to a total volume of 12 µl with ddH_2O. This step denatured any RNA secondary structure. After incubation the mix was cooled on ice for 2 min to allow the oligo(dT) to anneal and then the following mixture was added: 4 µl of 5x first-Strand buffer (Invitrogen, Life

Technologies), 2 µl of 0.1M DTT (Invitrogen, Life Technologies), 1 µl of RNaseOUT™ Recombinant Ribonuclease Inhibitor (40 units) (Invitrogen, Life Technologies) and 1 µl of Superscript II Reverse Transcriptase (200 units) (Invitrogen Life Technologies). The Superscipt II Reverse Transcriptase is a modified form of the *pol* gene of Moloney Murine Leukaemia Virus (M-MLV-RT). It can be used to synthesise first-strand cDNA at higher temperatures than conventional M-MLV RT therefore it provides increased specificity, higher yields of cDNA, and more full-length product. Following gentle mixing and a brief centrifugation step the samples were incubated for 1h at 42°C in a MWG-Biotech Primus 96 plus thermal cycler and then heated to 70°C for 10 min to inactivate the reverse transcriptase. The samples were cooled to 4°C before being used or stored at -20°C until required.

cDNA synthesis for qRT-PCR quantification of mature miRNAs was performed using the TaqMan® miRNA Reverse Transcription Kit (Applied Biosystems), according to the manufacturer's instructions. RNA was extracted from cells or tissue using the miRNeasy Mini Kit (see Section 2.3.11.1). Total RNA was diluted to a concentration of 2 ng/µl and 10 ng of RNA (5 µl) was used for each 15 µl reaction. A reverse transcription master mix of the following was first prepared on ice: 4.16 µl of nuclease-free water, 1.5 µl of 10x reverse transcription buffer, 0.15 µl of 100 mM dNTPs, 0.19 µl of RNase Inhibitor (20 units/µl) and 1 µl MultiScribe™ Reverse Transcriptase (50 units/µl). 7 µl of this mastermix was added to each reaction tube on ice followed by 5 µl of RNA and finally 3 µl of miRNA specific primers from TaqMan® MicroRNA Assays (Applied Biosystems). The reaction conditions were as follows: 16°C for 30 min, 42°C for 30 min, 85°C for 5 min. Samples were then cooled to 4°C before being used directly or stored at -20°C until required.

cDNA synthesis for qRT-PCR quantification of pre-miRNAs was performed using GenoExplorer™ miRNA qRT-PCR Kit (GenoSensor Corporation) according to the manufacturer's instructions. RNA was extracted from cells or tissue using the miRNeasy Mini Kit (see Section 2.3.11.1). The first step involved linking an adaptor to the 5' end of all the pre-miRNAs and miRNAs in the sample using a ligase. The adaptor was then polyadenlyated using poly A polymerase. To complete this reaction, 100 ng of total RNA was added to 3 µl of

Poly(A) extension mix and made up to a total volume of 10 µl with DNase/RNase-free water. The sample was incubated at 37°C for 30 min in a MWG-Biotech Primus 96 plus thermal cycler and the extension reaction was stopped by 5 min incubation at 95°C before cooling the sample on ice. Each extension reaction provided enough for five cDNA synthesis reactions. A universal RT Primer was used to synthesize cDNA from the tailed miRNA population by reverse transcriptase. 2 µl of the extended RNA was added to 8 µl of the RT priming mix and incubated at 46°C for 10 min in a MWG-Biotech Primus 96 plus thermal cycler. After incubating the sample on ice for 1 min, 10 µl of 2x RT mix was added and the sample was incubated at 42°C for 1 h in a MWG-Biotech Primus 96 plus thermal cycler. The sample was then incubated at 95°C for 5 min to inactivate the reverse transcriptase before being cooled to 4°C. The sample was then either used directly or stored at -20°C until required.

2.3.13 Quantitative reverse transcriptase-polymerase chain reaction (qRT-PCR)

Quantitative RT-PCR was performed using either SYBR Green (Applied Biosystems), TaqMan® Gene Expression Assays (Applied Biosystems) or TaqMan® MicroRNA Assays (Applied Biosystems), as detailed in Table 2.3. All qRT-PCR reactions were plated out in a PCR hood within a designated PCR room and all equipment and the nuclease-free water were subjected to 900 mJ of UV radiation in a UV Stratalinker 2400 before use. The cDNA was added in a separate “clean” laboratory using dedicated pipettes. All qRT-PCR reactions for each biological repeat were performed in either duplicate or triplicate.

The primers used for qRT-PCR with SYBR Green are listed in Table 2.3. Primer optimisation was performed for all primers before use. The *GAPDH* and selectin E (*SELE*) primers were designed as previously described (Bourboulia et al., 2004; Emuss et al., 2009). The actin b1 (*actb1*) primers were designed using Primer Express software (Applied Biosystems). The primers were used at the concentrations stated in Table 2.3. All qRT-PCRs were performed using 12.5 µl of SYBR® Green PCR Master Mix (Applied Biosystems, Life Technologies), the required volumes of forward and reverse primers and 1 µl of neat or diluted cDNA, made up to a total reaction volume of 25 µl using nuclease-free water.

qRT-PCRs were performed in MicroAmp® Optical 96-Well Reaction Plates (Applied Biosystems, Life Technologies) sealed with MicroAmp® Optical Adhesive Films (Applied Biosystems, Life Technologies) on an Eppendorf Mastercycler ep Realplex (Eppendorf).The reaction conditions were as follows: 95°C for 10 min to activate the DNA polymerase, followed by 40 cycles of 95°C for 15 sec and 60°C for 1 min. Fluorescence readings were taken at the end of the 60°C incubation. For primer optimisation an additional dissociation step was added at the end of the PCR program which consisted of 95^{o}C for 15 sec, 60^{o}C for 20 sec, a 19 min 59 sec ramping step and then 95°C for 15 sec. The dissociation data was collected on the ramping step. Relative expression of the gene of interest was quantified using the comparative C_T method with either *GAPDH* or *actb1* being used as the housekeeping gene, as stated.

qRT-PCRs using a TaqMan® Gene Expression Assay were performed in a total volume of 25 µl with the following reagents: 12.5 µl of TaqMan® Universal PCR Master Mix (Applied Biosystems, Life Technologies), 1.25 µl of the required 20x TaqMan® Gene Expression Assay (containing primer and probe), 1 µl of neat or diluted cDNA and 10.25 µl of nuclease-free water. The reactions were performed and analysed as described above for SYBR Green qRT-PCRs.

Quantification of miRNA and human small nucleolar RNA expression was performed using TaqMan® MicroRNA Assays (Applied Biosystems). qRT-PCRs were performed in a total volume of 20 µl with the following reagents: 10 µl of 2x TaqMan® Universal PCR Master Mix, no AmpErase UNG (Applied Biosystems, Life Technologies), 1 µl of 20x TaqMan® MicroRNA Assay, 1.33 µl of miRNA specific cDNA and 7.67 µl of nuclease-free water. qRT-PCRs were performed in MicroAmp® Optical 96-Well Reaction Plates (Applied Biosystems, Life Technologies) sealed with MicroAmp® Optical Adhesive Films (Applied Biosystems, Life Technologies) on an Eppendorf Mastercycler ep Realplex (Eppendorf). The reaction conditions were as follows: 95°C for 10 min to activate the DNA polymerase, followed by 40 cycles of 95°C for 15 sec and 60°C for 1 min. Fluorescence readings were taken at the end of the 60°C incubation. Relative expression of the gene of interest was quantified using the comparative CT method. For human miRNA quantification, small nucleolar RNA H/ACA box 66 (*SNORA66*) was used as a housekeeping gene, although RNA

U6 small nuclear 1 (*RNU6-1*) was also tested. For zebrafish miRNA quantification, *actb1* was used as a housekeeping gene.

Gene symbol	Assay type	Forward primer	Reverse primer
GAPDH	SYBR green	GGAGTCAACGGATTT GGTCGTA – 0.3µM	GGCAACAATATCCAC TTTACCAGAGT-0.3µM
actb1		TACAGCTTCACCACC ACAGC 0.3µM	AAGGAAGGCTGGAAG AGAGC 0.3µM
SELE		CAGCCTCAAGATCAT CAGCA– 0.3µM	ACAGTCTTCTGGGTG GCAGT– 0.3µM
DLL4	TaqMan®	N/A	N/A
JAG1		N/A	N/A
dll4		N/A	N/A
hsa-miR-26a		N/A	N/A
hsa-miR-30b		N/A	N/A
hsa-miR-30c		N/A	N/A
hsa-miR-30d		N/A	N/A
hsa-miR-30e		N/A	N/A
let-7i		N/A	N/A
hsa-miR-29c*		N/A	N/A

Table 2.3. Real-time qRT-PCR assays and primers. N/A: not applicable, purchased TaqMan® assays contained primers and probe, primers shown 5' to 3', primer concentration used in qRT-PCR shown.

2.4 Protein analysis

2.4.1 Western blotting

Protein was extracted from cells using M-PER Mammalian Protein Extraction Reagent (Pierce, ThermoScientific) to which cOmplete ULTRA Tablets, Mini, EDTA-free, EASYpack Protease Inhibitor Cocktail Tablets had been added (Roche). The lysis buffer was either added to cell pellets (1-2x10^5 cells) in a 1.5 ml Eppendorf tube, or directly to cells in 1-2 wells of a 6-well plate. For ~1x10^5 cells or one well of a 6-well plate, 70 µl of lysis buffer was used. For ~2x10^5 cells or for two wells of a 6-well plate, 150 µl of lysis buffer was used. When lysing cell pellets, the lysis buffer was mixed with the cells by repeated pipetting. If the lysis buffer was to be added directly to the cells in culture, the media was first removed and the cells were washed twice with cold PBS. The plates were then placed on ice, to prevent evaporation and reduce protein degradation, and the required quantity of lysis buffer was added. Cells were dislodged from the plate using a cell scraper and collected in a 1.5 ml Eppendorf tube. All cell lysates, whether harvested from cell pellets or directly from the plate, were vortexed briefly and incubated on ice for 5min before centrifugation at 13,000

rpm for 5-30 min at 4°C in a Heraceus Biofuge fresca desktop centrifuge to pellet cell debris. The supernatant containing the protein was removed and stored at -20°C until required.

Protein concentration was measured using Pierce BCA Protein Assay Kit (ThermoScientific) according to the manufacturer's instructions. Protein standards were produced by performing seven serial dilutions of the provided albumin stock (2 µg/µl) to give standards at the following concentrations: 2 µg/µl, 1 µg/µl, 0.5 µg/µl, 0.25 µg/µl, 0.125 µg/µl, 0.0625 µg/µl, 0.03125 µg/µl and 0.015625 µg/µl. A sample of the ddH_2O used to produce these dilutions was also set aside to be kept with the standards. The standards could be kept at 4°C for two to three weeks, or at -20°C for long term storage. All standards and samples were plated out in duplicate in a 96-well flat bottomed plate (TPP, MIDSCI). 15 µl of ddH_2O was added to all the wells which would contain the samples of unknown concentration. 20 µl of each standard was added to the appropriate wells. 5 µl of each sample was added to the appropriate wells. Reagent A and Reagent B from the Pierce BCA Protein Assay Kit were then diluted at a ratio of 1:50 and 180 µl of the mixture was added to each well containing either standard or sample using a multichannel pipette. The plate was tapped gentle to agitate, covered in tin foil and incubated at 37˚C for 30 min. The plate was allowed to cool to room temperature and then the absorption at 562 nm of each well was measured using the Varioskan Flash Multimode Reader (ThermoScientific). A standard curve was plotted using the mean absorption readings for the standards. A scatter graph was plotted in Excel with protein concentration as the dependent variable on the Y-axis and absorbance as the independent variable on the X-axis. A polynomial trend line (2^{nd} order regression) was added and the equation of the line was displayed, of the format $y = ax^2 + bx + c$. The protein concentration was represented by y, therefore the equation and hence the protein concentration could be solved for each protein sample by entering the known mean absorbance value for that sample (x). Because all the protein samples had been diluted 1:4 before the assay was performed, the calculated protein concentration then had to be multiplied by 4 to obtain the protein concentration of the neat sample.

The range of protein concentrations amongst all the samples from the same experiment was examined and then the same amount of protein for each sample (5-20 µg) was made up to the same total volume using ddH_2O. The protein samples were then mixed with the same volume of 4x SDS-polyacrylamide gel electrophoresis (SDS-PAGE) sample loading buffer, the composition of which is listed below. For each polyacrylamide gel, 10 µl of Precision Plus Protein Dual Color Standards (Bio-Rad) or 10 µl of ColorPlus Prestained Protein Ladder, Broad Range (10-230 kDa) (NEB) was mixed with the same volume of 4x SDS-PAGE sample loading buffer as the samples and made up to the same total volume as the samples using ddH_2O. If there were any empty wells in the polyacrylamide gel, a suitable volume of 4x SDS-PAGE sample loading buffer was prepared with ddH_2O so that every well in the gel was loaded with the same volume of solution, each containing the same concentration of SDS-PAGE sample loading buffer. Prior to loading, protein was denatured by heating at 100°C for 5 min in a heat block (Grant). The samples were then spun down and allowed to cool.

4x SDS-PAGE sample loading buffer
250nM Tris-HCL pH 6.8 (Sigma-Aldrich)
8% (w/v) SDS (Sigma-Aldrich)
10% (v/v) Glycerol (Sigma-Aldrich)
5% (v/v) β-ME (Sigma-Aldrich)
0.05% (w/v) Bromophenol blue (Sigma-Aldrich)

Denatured protein lysates were run on 10% polyacrylamide gels which were composed of a 1.5 mm thick stacking gel and a 1.5 mm thick 10% resolving gel. The gels were made using a Mini-PROTEAN 3 comb, spacer plates, short plates, casting frame and casting stand (Bio-Rad). The resolving gel was made first, poured into the apparatus and allowed to set for 15 min. The stacking gel was then made, poured on top of the resolving gel and allowed to set for 15 min. Gels were either used immediately or stored at 4°C wrapped in damp paper towels. The composition of each gel is listed:

10% Resolving gel

4 ml ddH_2O

3.3 ml 30% (w/v) acrylamide (National Diagnostics)

2.5 ml 1.5 M Tris pH 8.8 (Severn Biotech Ltd)

0.1 ml 10% (w/v) SDS (Sigma-Aldrich)

0.1 ml 10% (w/v) ammonium persulphate (APS) (Sigma-Aldrich)

0.004 ml tetramethylethylenediamine (TEMED) (Sigma-Aldrich)

5% Stacking gel

3.4 ml ddH_2O

0.83 ml 30% (w/v) acrylamide (Sigma-Aldrich)

0.63 ml 1 M Tris pH 6.8 (Severn Biotech Ltd)

0.05 ml 10% (w/v) SDS (Sigma-Aldrich)

0.05 ml 10% (w/v) APS (Sigma-Aldrich)

0.005 ml TEMED (Sigma-Aldrich)

The lysates and protein ladder were loaded into a polyacrylamide gel and the component proteins were separated by electrophoresis at 100 V in SDS-PAGE running buffer (Flowgen Bioscience). Electrophoresis was continued until the bromophenol blue marker ran off the bottom of the gel. Protein was transferred onto Immobilon-P Transfer Membrane (Millipore) at 20 V for 45 min using a semi-dry transfer apparatus (Bio-Rad) and transfer buffer (Flowgen Bioscience). Prior to transfer the membrane was activated by soaking in methanol for 5 min, washed in ddH_2O and equilibrated in transfer buffer. All Extra ThickBlot Paper (Bio-Rad) used for the transfer was previously soaked in transfer buffer and the negative electrode of the transfer apparatus was wet with transfer buffer.

Following transfer, the membrane were blocked in blocking solution [5% (w/v) milk powder in tris buffered saline (TBS) containing 0.1% (v/v) TWEEN® 20 (Sigma-Aldrich) (TBST)] for 1 h at RT. The composition of the 10x TBS used to produce the TBST was as follows:

10x TBS

40 g NaCl (Sigma-Aldrich)

1 g KCl (Sigma-Aldrich)

15 g Tris (Sigma-Aldrich)

ddH_2O up to a total volume of 500 ml

Concentrated HCl was used to bring the pH to 8.0 before all H_2O added

After blocking, the membrane was incubated overnight on a SRT9D roller mixer (Stuart) at 4°C with the required primary antibody diluted in blocking solution. The primary antibodies used and the dilutions at which they were used are listed in Table 2.4. After primary antibody incubation the membrane was washed three times for 10 min on a SSL4 see-saw rocker (Stuart) in TBST at RT. The membrane was then incubated for 1 h at RT on a SRT9D roller mixer with the appropriate horse-radish peroxidase (HRP) conjugated secondary antibody diluted 1/5000 in blocking solution. The secondary antibodies used are listed in Table 2.5. After incubation with secondary antibody any unbound antibody was washed off with 3 x 10 min washes on a SSL4 see-saw rocker in TBST at RT. After removing excess liquid from the membrane, bound antibody was visualized using either Amersham ECL or Amersham ECL Plus Western Blotting Reagents (GEHealthcare), depending on the primary antibody, as indicated in Table 2.4. For ECL, Reagents 1 and 2 were mixed 1:1 and used to completely cover the membrane for 5min incubation at RT. For ECL Plus, Reagents A and B were mixed 40:1 and used to completely cover the membrane for a 5 min incubation at RT. Excess ECL or ECL Plus was remove from the membrane and the resulting chemiluminescence signal was detected with Amersham Hyperfilm™ ECL (GE Healthcare). After development, ECL or ECL Plus was washed off with 3 x 10 min washes on a SSL4 see-saw rocker in TBST at RT. The membrane was then incubated with Restore™ Western Blot Stripping Buffer (ThermoScientific) for 10 min at 37°C with shaking. The stripping buffer was removed with 3 x 10 min washes on a SSL4 see-saw rocker in TBST at RT. The membrane was then dried out, wrapped in clingfilm and stored at -20°C.

Protein	Raised in	Made by	Cat No.	Clone	Dilution	Reagent
DLL4	Rabbit	Cell Signaling Technology	2589	Polyclonal	1:1000	ECL Plus
GAPDH	Mouse	Advanced Immunochemical Inc.	2-RGM2	6C5	1:10000	ECL
TUBG	Mouse	Sigma-Aldrich	T6557	GTU-88	1:5000	ECL
TUBA	Mouse	Sigma-Aldrich	T5168	B-5-1-2	1:8000	ECL

Table 2.4. Primary antibodies used for Western blotting.

Raised in	Anti-	Made by	Cat No.	Lot No.	Dilution
Goat	Rabbit	Dako	P0448	00038290	1:5000
Goat	Mouse	Dako	P0447	00035941	1:5000

Table 2.5. Secondary antibodies used for Western blotting.

2.4.2 Flow cytometry for GFP expression

Flow cytometry was used to evaluate the percentage of KSHV-positive cells in a population of LEC exposed to GFP-expressing KSHV. LEC were plated out at a density of $5x10^4$ cells per well of a 6-well plate and infected with GFP-recombinant KSHV as described in Section 2.2.3. Uninfected LEC were used as a control cell population. These were the same passage as the KLEC and were cultured alongside the KLEC in media that was frozen at the same time as the KSHV supernatant.

Cells from each experimental condition were trypsinised, pelleted by centrifugation, washed in PBS, pelleted by centrifugation and resuspended in a minimum of 300 µl of PBS. The volume of PBS was varied in order to achieve a cell density within $5x10^5$–$2x10^6$ cells per ml. The cell suspension was transferred to a FACS tube (BD) and placed on ice until analysis could be performed on a CyAn ADP High-Performance Flow Cytometer (Beckman-Coulter). For analysis, gates were set first on live cells and then on GFP-positive cells.

2.4.3 Fluorescence-activated cell sorting

Fluorescence-activated cell sorting (FACS) was performed on LEC infected with GFP-recombinant KSHV in order to separate confirmed KSHV-infected cells from surrounding cells based on GFP expression. LEC were plated out at a

density of $5x10^4$ cells per well of a 6-well plate and infected with GFP-recombinant KSHV as described in Section 2.2.3. Uninfected LEC of the same passage were cultured alongside the KLEC to use as a control. LEC and KLEC were trypsinised 72 h p.i, pelleted by centrifugation and resuspended in 300 µl of PBS. The cell suspensions were transferred to FACS tubes (BD) and placed on ice until FACS could be performed using a MoFlo™ XDP High-Speed Cell Sorter (Beckman-Coulter). A gate was first set on live cells and then two gates were set on GFP-positive and GFP-negative cells which was the basis of separation when the sort was performed. The uninfected LEC were also passed through the cell sorter so that all cells had experienced the same procedure. Once FACS had been completed the cells were pelleted through centrifugation and 700 µl of Qiazol (Qiagen) was added to each tube. Total RNA was then extracted as described in Section 2.3.11.1.

2.5 Luciferase reporter assays

Luciferase assays were performed to quantify miRNA repression of the *DLL4* 3'UTR in 293T cells. The plasmids used for the luciferase assays are listed in Table 2.6.

Plasmid	Promoters	Downstream of firefly luciferase	Supplier
pEZX-MT01	firefly luciferase - SV40 enhancer *Renilla* luciferase – CMV promoter	polyA signal	GeneCopoeia
pEZX_DLL4-3'UTR	firefly luciferase - SV40 enhancer *Renilla* luciferase – CMV promoter	*DLL4* 3'UTR and polyA signal	GeneCopoeia
pEZX_DLL4-3'UTR-mut	firefly luciferase - SV40 enhancer *Renilla* luciferase – CMV promoter	*DLL4* 3'UTR containing mutated miR-30 target site and polyA signal	GeneCopoeia but altered by site-directed mutagenesis

Table 2.6. Plasmids used for luciferase reporter assays.

To investigate miRNA activity, 293T cells were seeded at a density of $5x10^4$ cells per well of a 12-well plate. 16 h later the cells were transfected with non-targeting control (NTC) mimic, miR-30b mimic, miR-30c mimic or a combination of miR-30b and miR-30c, at a total concentration of 100nM, as detailed in

Section 2.2.4. 48 h post-mimic transfection each well of cells was transfected with 100ng of reporter plasmid (pEZX-MT01, pEZX_DLL4-3'UTR or pEZX_DLL4-3'UTR_mut), as detailed in Section 2.2.1. The pEZX-MT01 and pEZX_DLL4-3'UTR plasmids were purchased from GeneCopoeia. The pEZX_DLL4-3'UTR_mut plasmid was created by site-directed mutagenesis of the pEZX_DLL4-3'UTR plasmid, as detailed in Section 2.3.8.

Cells were harvested 24 h post-transfection with the reporter plasmids. Cells were washed with PBS and lysed in 250 µl of 1x Passive Lysis Buffer (PLB) which was formed by diluting 5x PLB (Promega) in ddH_2O. The PLB was added to each well of the 12-well plate and then the plate was shaken on a SSL4 see-saw rocker at 50 rpm for 15 min at RT. The samples were pipetted up and down to lyse any remaining cells and then either stored at -20°C in a 1.5 ml Eppendorf tubes or placed on ice before analysis. To pellet any insoluble elements the samples were spun at for 30sec at 13,000 rpm and 4°C in a Heraceus Biofuge Fresca desktop centrifuge. According to the manufacturer's instructions, this is not necessary for use with the Dual-Luciferase Reporter Assay System (Promega). However, it is necessary if the protein concentration of the samples is to be subsequently determined or if the samples may be used for Western blotting, therefore this step was always performed. The Fluoroskan Ascent FL luminometer and fluorometer (Thermo Scientific) was first prepared by washing the dispensers with 2 ml of ddH_2O, 2 ml of 70% ethanol and then another 2 ml of ddH_2O. It was then primed with 0.8 ml of Luciferase Assay Reagent II (LAR II) (Promega) and Stop & Glo® Reagent (Promega). LARII was prepared by resuspending 1 vial of lyophilised Luciferase Assay Substrate (Promega) with 10ml of Luciferase Assay Buffer II (Promega) and could be stored like this at -80°C. Stop & Glo® Reagent was prepared by adding 1 volume of 50x Stop & Glo® Substrate to 50 volumes of Stop & Glo® Buffer. 10 µl of each sample was assayed in triplicate in a 96-well white Sterilin* Microtiter Plates (Thermo Scientific). The Fluoroskan Ascent FL dispensed 50 µl of LAR II into the designated wells of the 96-well plate and then after a 2 sec pre-measurement delay, recorded the luminescent signal over the course of 10 sec. Luminescence was recorded as relative light units (RLU). This luminescent signal was generated by the activity of the firefly (*Photinus pyralis*) luciferase. Subsequently, 50 µl of Stop & Glo® Reagent was then dispensed into each well

to simultaneously quench the firefly luciferase reaction and provide a substrate for the Renilla (*Renilla reniformis* or sea pansy) luciferase. Again, after a 2 sec pre-measurement delay, the luminescent signal was recorded over the course of 10 sec. The Fluoroskan Ascent FL was then thoroughly cleaned by washing the dispensers with 2 ml of ddH_2O, 2 ml of 70% ethanol and then another 2 ml of ddH_2O.

Before examining the results, firefly luciferase RLU was normalised to *Renilla* luciferase RLU to control for variations in cell number, transfection efficiencies and pipetting errors between samples.

2.6 Functional *in vitro* assays

2.6.1 Matrigel tube formation assay

BD Matrigel™ Basement Membrane Matrix Growth Factor Reduced (BD Biosystems) was thawed overnight at 4°C, aliquoted into appropriate volumes and stored at -20°C. The day before setting up the tube formation assay, the required amount of Matrigel was thawed overnight at 4°C. Throughout the preparation of the plate the Matrigel was kept on ice. 80 µl of Matrigel was added to the appropriate number of wells of a pre-chilled 96-well flat bottomed plate (TPP, MIDSCI) using pre-chilled pipette tips. The pipette was not fully ejected to avoid the creation of bubbles and the plate was kept flat at all times. The plate was then incubated at 37°C for 30 min to allow the Matrigel to set.

LEC and HUVEC were trypsinised as detailed in Section 2.1.1 and resuspended in the appropriate media. For some experiments, cells were transfected with NTC or DLL4 siRNA 48 h prior to the tube formation assay. On these occasions LEC and HUVEC were plated out at a density of $5x10^4$ cells per well of a 6-well plate and transfected at a concentration of 100 nM, as detailed in Section 2.2.4. When optimising the tube formation assay, LEC and HUVEC were resuspended at a density of 5,000, 7,500 and 10,000 cells per 100 µl of media. For subsequent tube formation assays, LEC were resuspended at a density of 7,000, 10,000 and 12,500 cells per 100 µl of media whereas HUVEC were resuspended at a density of 2,500, 5,000 and 7,500 cells per 100

µl of media. For each cell density and cell treatment, 100 µl of cells was added per well of the 96-well plate containing Matrigel in triplicate. The plate was returned to the CB 53 incubator (Binder) at standard cell culture conditions for 24 h. The cells were photographed at various time points on an Axiovert 100 microscope (Zeiss) using an AxioCam (Zeiss) and the images were acquired using AxioVision software (Zeiss).

2.6.2 Spheroid-based in vitro angiogenesis assay

HUVEC were trypsinised, as detailed in Section 2.1.1, and resuspended in HUVEC media at a density of $2.5x10^4$ cells per ml. The HUVEC media contained 20 µl of sterile 0.25% w/v methylcellulose (Sigma-Aldrich) per 2 ml. For some experiments, HUVEC were transfected with miRNA mimics or inhibitors 24 h prior to the 3D sprouting assay. On these occasions HUVEC were plated out at a density of $5x10^4$ cells per well of a 6-well plate and transfected at a concentration of 100 nM, as detailed in Section 2.2.4. For each treatment condition, 2 ml of cells were plated out in Nunc® 60-well MicroWell® MiniTrays (Sigma-Aldrich) with 20 µl of cells (500 cells) added to each well. This would lead to the formation of 100 spheroids per condition. The mini-trays were then inverted and placed in a CB 53 incubator (Binder) at standard cell cultures conditions for 24 h.

BD Matrigel™ Basement Membrane Matrix (BD Biosystems) was thawed overnight at 4°C, aliquoted into appropriate volumes and stored at -20°C. The day before setting up the 3D sprouting assay, the required amount of Matrigel was thawed overnight at 4°C. Throughout the preparation of the plate the Matrigel was kept on ice. The mini-trays were examined to check for spheroid formation and then the spheroids from each experimental condition were collected using a p1000 pipette tip and very gently pipetted into a 15 ml falcon tube (BD Biosciences). The spheroids were centrifuged at 1000 rpm for 1 min in an Eppendorf table-top centrifuge and the majority of the media was removed (leaving ~10-50 µl of media above the spheroids). The falcon tubes were placed on ice and the spheroids from each experimental condition were gently resuspended in 200 µl of Matrigel using pre-chilled pipette tips. Each Matrigel sample was added to one well of a 12-well flat bottomed plate (TPP, MIDSCI)

using pre-chilled pipette tips. The Matrigel formed a blob in the centre of the well and was prevented from spreading across the well as this was found to be detrimental to the assay as it encouraged the spheroids to cluster around the edges of the plate. The plate was then incubated at 37°C for 15 min to allow the Matrigel to set. 1 ml of conditioned HUVEC media was then added to each well of the 12-well plate. The HUVEC media had been conditioned by 48 h incubation with HF1 cells, as detailed in Section 2.1.3. The plate was then placed in a CB 53 incubator (Binder) at standard cell culture conditions for up to 5 days. The spheroids were photographed using an Axiovert 100 microscope (Zeiss) using an AxioCam (Zeiss) and the images were acquired using AxioVision software (Zeiss). To calculate the average sprouts per spheroid, sprouts were counted using Adobe Photoshop CS4. Only 60 spheroids were analysed per condition due to disruption and loss of spheroids during collection and resuspension. Average sprout length was measured using the segmented lines tool in Image J (NIH). Five sprouts were measured per spheroid (n=20).

2.7 *In vivo* angiogenesis studies using *Danio rerio* (zebrafish) embryos and larvae

2.7.1 Culture of zebrafish embryos and larvae

Zebrafish embryos were obtained by natural spawning of adult zebrafish. The transgenic lines *Tg*(*kdrl:EGFP*) (Beis et al., 2005) and *Tg*(*fli1a:EGFP*) (Lawson and Weinstein, 2002) lines were used to monitor blood vessel development. Embryos were raised and maintained at 28.5°C in system water and staged as described in Section 11 (Development Staging Series) of Chapter 3 of The Zebrafish Book: A guide for the laboratory use of zebrafish *Danio* (*Brachydanio*) *rerio* (Westerfield, 2000). The various developmental stages are detailed in table 2.7.

2.7.2 Microinjection of zebrafish embryos

Antisense morpholinos (MOs) (GeneTools), miRIDIAN microRNA mimics (Dharmacon, Thermo Scientific) and pCSGW_dll4-3'UTR reporter plasmid were injected into 1- to 4- cell stage embryos using a Picospritzer III microinjector

(Parker). The MOs used in this work are listed in Table 2.8. *dll4*-TP^{miR-30} was designed so that the 3' end binds to the miR-30 target site within the *dll4* 3'UTR whilst the 5' region binds to the downstream flanking sequence, as described (Choi et al., 2007). *dll4*-TP^{control} was designed so that it binds to another unrelated region of the *dll4* 3'UTR (596-620 nt), which is not predicted to contain any other miRNA binding sites, as described (Choi et al., 2007). Lyophilised MOs and miRNA mimics were resuspended in sterile ddH_2O to give a stock solution of 50 µg/µl and 10 µg/µl respectively. 10 µl working solutions of MOs and miRNA mimics were prepared by added 1 µl of 0.5% Phenol Red (Sigma-Aldrich) to the required volume of stock solution and ddH_2O. For most experiments 1 nl of MO or miRNA mimic was injected per embryo because this is volume is ~1/10 of the total cell volume. Therefore if 5 ng of MO was to be injected per embryo, a working solution of 5µg/µl (5 ng/nl) was produced. Injection volumes of up to 2 nl could be tolerated and were used to inject a large quantity of MO or for co-injections. Phenol red is a non-toxic dye which enabled visualisation of the injection solution to aid needle loading and so that successful injections could be confirmed. Stock and working solutions were stored at -20°C and were heated to 65°C once thawed in order to eliminate secondary structures and duplexes.

Egg laying was controlled by regulating the light/dark intervals of the fish. The night before laying was to be initiated, two stacked plastic boxes were placed in the bottom of the relevant tank. The top box contained marbles on a fine wire mesh; the bottom box was empty. Normally the fish would eat their own eggs after laying as they are a rich source of protein and this behaviour reduces the energy loss experienced in egg production and breeding behaviour by cycling the protein within the tank. When the plastic boxes were placed in the tank the eggs fell between the marbles, through the wire mesh and into the bottom box, thereby escaping predation. Fish would lay shortly after the lights were turned on and the plastic boxes were then removed. The newly fertilised eggs were collected with a net, washed in system water and placed in petri dishes containing system water and methylene blue (Sigma-Aldrich). The methylene blue killed any fungi that would otherwise harm the embryos.

Glass microinjection needles were first broken using tweezers and then back-loaded with 3µl of the appropriate working solution. The needles often had to be flicked in order to move the fluid down to the tip. The loaded needle was then secured to the microinjector. In order to calibrate the microinjector, injections were first performed into a petri dish containing oil and the resulting bubble of injection solution was measured using a Nikon SMZ1500 Stereo Microscope and an eye-piece containing a graticule ruler. At 11.25x magnification, a bubble of 1nl has a diameter of ~14.2 graticule units. Therefore the length of the gas pulse controlling the microinjection was altered until a bubble of this diameter was achieved. Generally the gas pulse was between 20 and 35 msec long. Once the needle had been calibrated, the embryos were transferred into an empty petri dish containing a glass slide and most of the water was removed. The embryos were then lined up against the edge of the glass slide. The needle was pushed through the chorion of each embryo and the required volume of injection solution was injected inside. The embryos were then collected, placed in a petri dish containing system water plus methylene blue and incubated at 28.5°C.

Period	Stage	Hours post-fertilisation (hpf)	Developmental landmarks
Zygote (0-0.75 hpf)	1-cell	0	Cytoplasm streams toward animal pole to form blastodisc
Cleavage (0.75-2.2 hpf)	2-cell	0.75	Partial cleavage
	4-cell	1	2 X 2 array of blastomeres
	8-cell	1.25	2 X 4 array of blastomeres
	16-cell	1.5	4 X 4 array of blastomeres
	32-cell	1.75	4 X 8 array of blastomeres
	64-cell	2	3 regular tiers of blastomeres
Blastula (2.25-5.25 hpf)	128-cell	2.25	5 blastomere tiers; cleavage planes irregular
	256-cell	2.5	7 blastomere tiers
	512-cell	2.75	9 blastomere tiers; yolk syncytial layer (YSL) forms
	1k-cell	3	11 blastomere tiers; single row of YSL nuclei; asynchronous cell cycle
	High	3.33	Greater than 11 blastomere tiers; blastodisc flattening begins; YSL nuclei in two rows
	Oblong	3.66	Blastodisc flattening; multiple rows of YSL nuclei
	Sphere	4	Spherical shape; flat border between blastodisc and yolk
	Dome	4.33	Yolk cell bulging toward animal pole as epiboly begins
	30%-epiboly	4.66	Blastoderm an inverted cup of uniform thickness
Gastrula (5.25-10 hpf)	50%-epiboly	5.25	Blastoderm remains of uniform thickness
	Germ-ring	5.66	Germ ring visible from animal pole; 50%-epiboly
	Shield	6	Embryonic shield visible from animal pole; 50%-epiboly
	75%-epiboly	8	Dorsal side distinctly thicker; epiblast, hypoblast, evacuation zone visible
	90%-epiboly	9	Axis and neural plate; brain and notochord rudiments
	Bud	10	Tail bud prominent; early polster; 100%-epiboly
Segmentation (10-24 hpf)	1-4 somites	10.33	First somite furrow
	5-9 somites	11.66	Polster prominent; optic vesicle, Kupffer's vesicle, neural kee
	10-13 somites	14	Pronephros forms
	14-19 somites	16	EL (embryo length) = 0.9 mm; otic placode, brain neuromeres
	20-25 somites	19	EL = 1.4 mm; lens, otic vesicle, hindbrain neuromeres
	26+ somites	22	EL = 1.6 mm; blood islands, otoliths, midbrain-hindbrain boundary
Pharyngula (24-48 hpf)	Prim-5	24	EL = 1.9 mm; early pigmentation, heartbeat
	Prim-15	30	EL = 2.5 mm; early touch reflex, retina pigmented
	Prim-25	36	EL = 2.7 mm; early motility, tail pigmentation
	High-pec	42	EL = 2.9 mm; rudiments of pectoral fins
Hatching (48-72 hpf)	Long-pec	48	EL = 3.1 mm; elongated pectoral fin buds
	Pec-fin	60	EL = 3.3 mm; pectoral fin blades
Larval	Protruding-mouth	72	3.5 mm total body length

Table 2.7. Zebrafish Developmental Staging Series. Adapted from www.zfin.org/zf_info/zfbook/stages/index.html. Percentage-epiboly indicates the fraction of the yolk cell that the blastoderm covers. Somites are undifferentiated mesodermal components of early trunk or tail segments or metameres which are derived from paraxial mesoderm.

Morpholino (MO)	Sequence (5' to 3')	Targets	Injected per embryo (ng)	Reference
MO1-*dll4*	GTTCGAGCTTACCGG CCACCCAAAG	Splice blocking	5 and 6	(Siekmann and Lawson, 2007)
MO4-*dll4*	TGATCTCTGATTGCT TACGTTCTTC	Exon 4/intron 4 splice-donor site	6 and 8	(Hogan et al., 2009b)
dll4-TP^{miR-30}	TGTAAACAATCCAGA AAAAAAGATT	miR-30 target site within *dll4* 3'UTR	5 and 10	N/A
dll4-TP^{control}	ATAGCACTCTATTTAA CTCTTTTAA	Random site within *dll4* 3'UTR which does not contain any miRNA target sites	5 and 10	N/A
MO2-*kdr*	TATGCTCTATTAGAT GCCTGTTTAA	5'UTR of *kdr*	4.5	(Bahary et al., 2007)
MO2-*kdrl*	CCGAATGATACTCCG TATGTCACTT		4.5	(Bahary et al., 2007)

Table 2.8. Morpholinos used for *in vivo* angiogenesis studies in zebrafish embryos. *dll4*-TP^{miR-30} and *dll4*-TP^{control} were designed in-house as described (Choi et al., 2007).

2.7.3 Zebrafish whole mount in situ hybridisation

Before whole mount *in situ* hybridisation could be performed, zebrafish embryos had to be fixed. Embryos up to 15 somites could be fixed in their chorions however older embryos were dechorionated before fixing. This was to aid examination of the older embryos, as if they were fixed in their chorions they would have been fixed curled up rather than straighten out. Dechorionation was performed manually using two pairs of tweezers under a Nikon E1500 dissecting scope. The chorion was pinched with one pair of tweezers and pulled apart with the other pair, taking care not to puncture the yolk sac or damage the tail of the embryo.

All embryos of the same stage and experimental condition were collected and transferred to a 1.5 ml Eppendorf tube using a Pasteur pipette (Sterilin). The majority of the water was removed from the tube, leaving ~50 µl. The embryos were then covered with 4% paraformaldehyde (PFA) in PBS and incubated at 4°C overnight to allow fixation to occur. The PFA was made by adding 10 ml of 16% PFA (Sigma-Aldrich) to 4ml of sterile 10x PBS (Sigma-Aldrich) and 26 ml of ddH_2O. The PFA was then removed using a Pasteur pipette and the embryos were washed three times for 5 min with PBS + 0.1% Tween® 20 (Sigma-Aldrich) (PBST). Enough PBST was added to each tube to completely cover the embryos (0.5-1 ml). At this stage, embryos of 15 somites or younger could be dechorionated, also using tweezers. The fixed embryos were then dehydrated

by two 5min washes with 50% ethanol/50% PBST and two 5 min washes with 100% ethanol. For each wash 0.5-1 ml of solution was added to each Eppendorf tube in order to completely cover the embryos. The last ethanol wash was removed with a Pasteur pipette and 0.5 ml of fresh ethanol was added to each Eppendorf tube before the embryos were stored at -20°C. A minimum of overnight storage at -20°C was required before the *in situ* hybridisation could be performed, however longer -20°C storage was found to improve the quality of the staining.

On day one of the *in situ* hybridisation procedure the embryos were first rehydrated by two 5 min washes with 50% ethanol/50% PBST and four 5 min washes with 100% PBST. For each wash 0.5-1 ml of solution was added to each Eppendorf tube in order to completely cover the embryos. Embryos older than 24 hpf were then treated with Proteinase K (Sigma-Aldrich) for 3-20 min, depending on stage and potency of enzyme, which varies from batch to batch. A 20 mg/ml stock solution of Proteinase K was thawed on ice and then added to PBST to produce a 10 µg/ml working solution. This was used to completely cover the relevant embryos for the required time period. Removal of the Proteinase K was begun 30 sec prior to the end of the required time period so that all Proteinase K had been removed within the required time. If embryos were incubated in Proteinase K for too long damage and disintegration could occur. Any residual Proteinase K was removed by two washes in PBST. The embryos were then re-fixed by incubation with 4% PFA in PBST for 20 min at RT. The PFA was removed with a Pasteur pipette and two quick washes with PBST were performed before five 5 min washes with PBST to remove any residual PFA. The embryos from each experimental condition and/or time point were then split into several different Eppendorf tubes, one per probe. This was done over a light box so that the embryos could be easily visualised.

Hybe solution was removed from storage at -20°C and warmed up slightly on ice to reduce pipetting errors. The recipe for the Hybe solution is shown below. The embryos were then washed with 50% Hybe solution/50% PBST for 5 min before being prehybridised in 200 µl of 100% Hybe solution for 1 h at 65°C. A heat block was used for this incubation step and it was turned on its side so that the embryos were spread out along each Eppendorf tube. To generate the

probes, a PCR fragment spanning ~1 kb was used as a template. This had been amplified from 24 hpf embryo cDNA. Digoxigenin (DIG)-labelled antisense RNA probes were transcribed from linearized templates using T3, T7 or Sp6 RNA polymerases (Roche). The probes were thawed on ice and then 1:200 dilutions were made up using Hybe solution. The diluted probe was heated to 65°C for 15 min to destroy any secondary structures. The 100% Hybe solution was then removed from the embryos and 200 µl of diluted probe was added to each Eppendorf tube. The embryos were then incubated overnight at 65°C on a heat block which was turned on its side.

Hybe Solution - pH 6.0

Formamide (Sigma-Aldrich)	25 ml
20x Standard saline citrate (SSC) (Sigma-Aldrich)	12.5 ml
tRNA (50 mg/ml) (Sigma-Aldrich)	0.5 ml
Heparin (100 mg/ml) (Sigma-Aldrich)	25 µl
Citric acid (1 M) (Sigma-Aldrich)	460 µl
Tween® 20 (Sigma-Aldrich)	250 µl
ddH_2O	11.5 ml

On day two of the *in situ* hybridisation procedure the diluted probe was removed from the embryos and stored in Eppendorf tubes at -20°C as it could be reused twice. The embryos were then returned to the heat block and pre-warmed 100% Hybe minus solution was added to each Eppendorf tube, enough to cover the embryos. Hybe minus solution is Hybe solution lacking the heparin and tRNA. Hybe minus solution was added to the bottom of a 24- or 48-well *in situ* hybridisation plate (Intavis Bioanalytical Instruments AG) and the plate was placed on a light box. Embryos labelled with each probe and from each experimental condition or time point were then added to separate wells of the plate using a Pasteur pipette. The plate was then placed in the Biolane™ HTI *in situ* hybridisation machine (Intavis Bioanalytical Instruments AG) and connected to the dispensing and extraction tubes. The *in situ* hybridisation protocol was then started, which is detailed in Table 2.9. All the solutions had to be made up in advance from stock solutions and incubated at the required temperature so that they were already equilibrated before entering the *in situ* hybridisation machine. The recipes for 10x maleic acid buffer (MAB) and MAB block are

shown below. Before each step, whilst the machine was pumping out the previous wash from the plate, the bottles of solution had to be switched to provide the machine with the correct solution for the next wash or incubation.

10x Maleic acid buffer (MAB)

0.1 M Maleic Acid (Sigma-Aldrich)

0.15 M NaCl (Sigma-Aldrich)

Adjust pH to 7.5 using NaOH (Sigma-Aldrich)

MAB block

Blocking reagent (Boehringer Mannheim, Roche) 0.8 g

1x MAB up to 40 ml

Heat to ~80° until granules disappear

Step/Solution	Volume of solution (ml)	Time per wash (min)	Washes	Total length of step (min)	Temp (°C)
Pump out					
75% Hybe minus / 25% 2x SSC	50	10	1	10	65
50% Hybe minus / 50% 2x SSC	50	10	1	10	65
25% Hybe minus / 75% 2x SSC	50	10	1	10	65
100% 2x SSC	50	10	1	10	65
100% 0.2x SSC	200	15	4	60	65
25% MABT / 75% 0.2x SSC	50	10	1	10	21
50% MABT / 50% 0.2x SSC	50	10	1	10	21
75% MABT / 25% 0.2x SSC	50	10	1	10	21
100% MABT	50	10	1	10	21
MAB block	40	60	1	60	21
Anti-DIG antibody	40*	600	1	600	4
100% MABT	400	15	8	120	21
Hold (does not pump out)					

Table 2.9. Incubations and washes performed by *in situ* hybridisation machine. Volume of solution indicates the total volume of solution required for that step in the procedure for a 24-well plate. Volumes are doubled for a 48-well plate. Standard saline citrate (SSC); Maleic acid buffer (MAB); 1x MAB plus 0.1% Tween® 20 (MABT); 1x MAB plus Boehringer block (MAB block). *Final volume in plate was 40 ml to achieve antibody dilution of 1:5000 however the machine was provided with 10 µl of anti-DIG antibody in 10ml of MAB block and separately provided with 30 ml of MAB Block which it cools to 4°C before addition to plate.

On the third day of the *in situ* hybridisation procedure, the *in situ* hybridisation machine was provided with AP buffer (developing buffer) and the developing procedure was run on the machine (three washes of 5 min). The recipe for AP buffer is shown below.

AP buffer

24-well plate	48-well plate
1 M TrisHCl (pH9.5) (Sigma-Aldrich)	20 ml	40 ml
5 M NaCl (Sigma-Aldrich)	4 ml	8 ml
1 M $MgCl_2$ (Sigma-Aldrich)	10 ml	20 ml
Tween® 20 (Sigma-Aldrich)	1 ml	2 ml
ddH_2O	165 ml	330 ml

The embryos were then removed from the *in situ* hybridisation machine and transferred from the *in situ* hybridisation plate into a sterile 24-well flat bottomed plate (Corning) with the aid of a light box. Any remaining AP buffer was removed from each well and the embryos were covered with 0.5-1 ml of staining buffer. Staining buffer was prepared by mixing AP buffer and BM Purple (Roche) in a 1:1 ratio. The plate was wrapped in foil and placed on a Gyro rocker STR (Stuart® Scientific) for between 10 min and 24 h, depending on the probe and the strength of the signal. Embryos were frequently examined under a Nikon E1500 dissecting scope to check the extent of the staining so that it could be stopped before it reached saturation. To stop the staining reaction temporarily, the staining buffer was removed and the embryos were washed three times for 5 min in PBST plus 20 mM EDTA. To permanently stop the staining reaction, the staining buffer was removed and the embryos were washed two times for 5 min with PBST. The embryos were then re-fixed in 4% PFA for 20 min at RT or overnight. Once fixed, the embryos were washed three times for 5 min in PBST.

If the embryos were 24 hpf or older they had to be bleached before being examined or photographed as the pigment would obscure the *in situ* hybridisation staining. Bleaching solution was prepared by mixing hydrogen peroxide (H_2O_2) with 50% formamide (see below for recipes). 1 ml of bleaching solution was added to each subset of embryos and then they were incubated on the light box until the pigment was removed: ~5min for 24 hpf; 10 min for 30 hpf; 15-20 min for 48 hpf; 30-35 min for 3-5 dpf.

50% formamide		Bleaching solution	
Formamide (Sigma-Aldrich)	4 ml	ddH_2O	5.67 ml
20x SSC (Sigma-Aldrich)	2 ml	H_2O_2 (Sigma-Aldrich)	3.33 ml
1x PBS (Sigma-Aldrich)	2 ml	50% formamide	1 ml

The bleached embryos were washed three times for 5 min in PBST and then all embryos were resuspended in 50% glycerol (in PBS) for 10 min before 1 ml of fresh 50% glycerol was added to each Eppendorf tubes. Embryos were stored at 4°C until photographed but at RT for long term storage. Images of *in situ* hybridisations were taken using a Nikon 1200F camera on a Nikon E1500 dissecting scope and acquired using ACT-1 software (Nikon). Embryos were orientated with the anterior to the left and posterior to the right. 5x magnification was used to photograph the whole embryo whereas 11.25x magnification was used to photograph specific areas. Figures were generated using Adobe Photoshop CS4.

2.7.4 Imaging and quantification of live zebrafish embryos

Brightfield images of whole embryos within the chorion were taken using a Nikon 1200F camera on a Nikon E1500 dissecting scope and acquired using ACT-1 software (Nikon).

Fluorescent images of *Tg(kdrl:EGFP)* and *Tg(fli1a:EGFP)* embryos were taken using a Zeiss Axiocam on a Zeiss AxioVision SteREO Lumar V12 dissecting microscope and acquired using AxioVision v4.8 software. 1-phenyl 2-thiourea (PFU) (Sigma-Aldrich) was added to the water of *Tg(kdrl:EGFP)* or *Tg(fli1a:EGFP)* embryos at 24 hpf if they were to be used for live imaging. PTU inhibited melanogenesis by blocking all tyrosinase-dependent steps in the melanin pathway and therefore prevented pigmentation of the embryos which would obscure imaging or hinder identification of phenotypes. PTU treatment was initiated before pigmentation began because it does not remove already formed pigment. Before imaging and/or quantification, the embryos were dechorionated and placed in 3% methylcellulose (Sigma-Aldrich) within the dip of a depression slide. To stop embryos from moving during imaging and/or

quantification, a few drops of 5 g/L tricaine mesylate (MS-222) (Sigma-Aldrich) was added to the water in the petri dish to give a final concentration of 0.01-0.05%. If this was done, the embryos were transferred to a new petri dish with fresh water after imaging. MS-222 is a muscle relaxant that operates by preventing action potentials. x45 magnification was used to photograph whole embryos and x120 magnification was used to obtain detailed photographs of the DA, ISVs and other specific areas. Images were cropped and arrowheads were added using Adobe Photoshop CS4. The n numbers for all quantification experiments are displayed in Table 2.10.

Figure	Microinjection group	n number
Figure 5.9A	NIC	30/32
	0.2 ng NTC mimic	24/25
	0.5 ng NTC mimic	33/34
	0.05 ng miR-30b mimic	36/40
	0.1 ng miR-30b mimic	42/48
	0.2 ng miR-30b mimic	80/99
	0.1 ng miR-30c mimic	56/60
	0.2 ng miR-30c mimic	34/40
	0.4 ng miR-30c mimic	74/83
Figure 5.9B	NIC	24/31
	0.2 ng NTC mimic	22/23
	0.5 ng NTC mimic	35/36
	0.05 ng miR-30b mimic	37/39
	0.1 ng miR-30b mimic	41/43
	0.2 ng miR-30b mimic	34/52
	0.1 ng miR-30c mimic	47/49
	0.2 ng miR-30c mimic	26/29
	0.4 ng miR-30c mimic	46/55
Figure 5.11C	NIC	66/71
	NTC mimic	27/27
	TP alone	50/52
	miR-30b mimic	36/41
	miR-30c mimic	29/31
	NTC mimic + TP	59/63
	miR-30b mimic + TP	27/31
	miR-30c mimic + TP	47/53
Figure 5.13B	uninjected	60/60
	kdr MO	41/41
	kdrl MO	40/40
	kdrl MO + *kdr* MO	40/40
	control TP	50/50
	control TP + *kdr* MO	49/49
	miR-30 TP	35/35
	miR-30 TP + *kdr* MO	37/37

Table 2.10. List of n numbers for the microinjection groups quantified in Figures 5.9A, 5.9B and 5.11C. For each microinjection group the n value is given as counted embryos/total embryos. This reflects the fact that embryos with severe morphological defects which prevented ISV phenotyping were not counted. NIC: non-injected control; NTC: non-targeting control; MO: morpholino; TP: target protector.

2.8 Bioinformatics analysis

Processing and statistical analysis of the KLEC GEM data was performed by Stephen Henderson using the Bioconductor packages (Gentleman et al., 2004) (affy (Irizarry et al., 2003) and limma (Smyth, 2004)) for the R programming language.

2.8.1 Data mining of DLL4 and miR-30 expression from TGCA

GEM and RNAseq data for analysis of the correlation between *DLL4* and miR-30 in tumours compared to normal tissue were obtained from The Cancer Genome Atlas (www.cancergenome.nih.gov) data portal (www.tcga-data.nci.nih.gov) by Gemma Bridge and analysed by Stephen Henderson. As data for each sample were individually processed rather than normalised as a batch, and since data from different platforms and data-types were analysed, both the miRNA and gene expression data were scaled (i.e. between 0 and 1) and centred (i.e. about 0) before merging. A full list of the sample numbers, data-types and platforms are shown in Table 2.11.

Tumour type	Number of samples	mRNA data-type	mRNA expression platform	miRNA data-type	miRNA expression platform
Breast invasive carcinoma	326	GEM	AgilentG4502A	RNAseq	Illumina-GAmiRNAseq
Colon adenocarcinoma	147	GEM	AgilentG4502A	RNAseq	Illumina-GAmiRNAseq
Gioblastoma multiforme	498	GEM	AgilentG4502A	GEM	Agilent 8x15H-miRNA
Renal clear cell carcinoma	62	GEM	AgilentG4502A	RNAseq	Illumina-GAmiRNAseq
Lung adenocarcinoma	32	GEM	AgilentG4502A	RNAseq	Illumina-GAmiRNAseq
Rectum adenocarcinoma	63	GEM	AgilentG4502A	RNAseq	Illumina-GAmiRNAseq
Ovarian serous cystadenocarcinoma	462	GEM	AgilentG4502A	RNAseq	Illumina-HimiRNAseq

Table. 2.11. Sample numbers, data-types and platforms for tumours analysed for Figure 3.5. All data for both tumour and normal samples were obtained from The Cancer Genome Atlas (www.cancergenome.nih.gov) data portal (www.tcga-data.nci.nih.gov).

2.9 Statistical analysis

Standard error of the mean (SEM) was used to determine the confidence limits for all experiments which had been performed in replicate. SEM is a method used to estimate the standard deviation (SD) of a sampling distribution. SEM was calculated by dividing the SD (σ) by the square root of the number of samples (N):

$$SEM = \frac{\sigma}{\sqrt{N}}$$

SD is the square root of the variance (σ^2). The variance is a measure of how spread out a set of values is and therefore SD indicates how much variability there is about the mean and can be used as a measure of variation between sample values.

$$\sigma = \sqrt{\sigma^2} \qquad \sigma^2 = \frac{\sum (X - \mu)^2}{N}$$

(Where X is a sample value and μ is the mean of the sample values).

To determine whether the difference between two experimental conditions was significant (with the exception of the analysis of zebrafish phenotypes) *p* values were calculated using a two-sided unpaired Student's t test for samples with equal variance (homoscedastic). The difference was considered significant if $p<0.05$.

For some experiments which have only been repeated once, SD was used to evaluate the technical error of that particular experiment. Where this has occurred it has been explained in the figure legend.

To determine the statistical significance between the indicated zebrafish phenotypes in Fig. 5.13, each observation of no phenotype, moderate phenotype and severe phenotype was given the value 0, 1 and 2 respectively and then a Wilcoxon rank-sum test was performed.

Chapter 3. Evaluation of the predicted targets of miRNAs altered upon KSHV infection LEC.

3.1. Aims

The aims of this chapter were:

i. To investigate the predicted targets of miRNAs that are upregulated or downregulated upon Kaposi sarcoma-associated herpesvirus (KSHV) infection of lymphatic endothelial cells (LEC) using TargetScan 4.2 and PITA prediction algorithms.

ii. To compare any predicted targets to a list of pro- and anti-angiogenic genes and also to angiogenic factors which are known to be regulated following KSHV infection of LEC.

iii. To select a predicted miRNA/target pair of interest based on opposite changes of expression in KSHV-infected LEC (KLEC) and/or due to the importance of the target to endothelial cell biology.

iv. To confirm the upregulation or downregulation of the chosen miRNA and its predicted target in KLEC using qRT-PCR.

3.2. Target prediction of miRNAs upregulated or downregulated in KLEC

Microarray data had been previously generated in this laboratory to measure the expression of cellular miRNAs in LEC and in KLEC (Lagos et al., 2010). These data had been analysed to determine miRNA expression levels 72h post-infection (p.i.) (Lagos et al., 2010). Those miRNAs which were upregulated by 1.5-fold or greater (Table 1.2), or with at least a 50% reduction in expression (Table 1.3), were taken forward for further investigation in this work. Two target prediction algorithms, TargetScan 4.2 (Grimson et al., 2007; Lewis et al., 2003; Lewis et al., 2005) and PITA (Kertesz et al., 2007) were used to predict potential targets of these miRNAs. The two chosen target prediction algorithms are based on different criteria and hence generate varying lists of predicted targets.

TargetScan 4.2 only displays conserved target sites (Lewis et al., 2003) and only considers the 3'UTR of target mRNAs, excluding target sites within 5'UTRS, ORFs or within 15nt of the stop codon (Grimson et al., 2007). It produces a Total Context Score for each mRNA/miRNA pair which is the sum of the context scores for all the target sites specific to that particular miRNA. The context score of a specific site combines scores for the following features: type of target site, additional pairing to the 3' region of the miRNA, local AU composition and position of the target site within the 3'UTR (Grimson et al., 2007). The four types of target site, listed in order of efficacy, are 6mer, 7mer-A1, 7mer-m8 and 8mer. The 6mer is the perfect 6nt match to the miRNA seed, miRNA nucleotides 2-7 (Lewis et al., 2005). The 7mer-A1 contains the seed match augmented by an adenine at target position 1 (Lewis et al., 2005). The 7mer-m8 is the best 7mer site and contains the seed match augmented by a match to miRNA nucleotide 8 (Brennecke et al., 2005; Krek, 2005; Lewis et al., 2003; Lewis et al., 2005). The best site, an 8mer, comprises the seed match flanked by both the adenine at position 1 and the match at position 8 (Lewis et al., 2005). Additional Watson-Crick pairing at the 3' end of the miRNA, particularly nucleotides 13-16, was found to be an effective determinant, especially for 7mer-m8 sites. Therefore a score for 3' binding is calculated that is equal to the greatest number of contiguously paired bases but weighted towards pairing at nucleotides 13-16 (Grimson et al., 2007). When comparing functional and non-functional target sites, it was found that the nucleotides flanking functional sites were highly enriched for adenine and uracil, therefore a score for local AU composition is calculated with a higher score indicating greater local AU composition in the region flanking the target site (Grimson et al., 2007). Target sites located near either end of a 3'UTR were found to be more effective than those near the centre and site-conservation analysis revealed that more sites were selectively maintained near the end of 3'UTRs than in the central region. Therefore the score for target site position is based on the distance in nucleotides between the site and the nearest end of the 3'UTR (Grimson et al., 2007).

The PITA algorithm is very different in that it focuses on target site accessibility and the binding energy of miRNA-target duplexes, rather than considering target site location and sequence-based criteria. This model was based on the

finding that mutations which diminished target site accessibility significantly reduced miRNA-mediate translational repression to an extent that was comparable with mutations that disrupted sequence complementarity (Kertesz et al., 2007). Therefore the PITA algorithm calculates ΔΔG for each target site, which is the difference between the free energy gained by the binding of the miRNA to the target (ΔG_{duplex}) and the free energy lost by separating the target site nucleotides (ΔG_{open}) (Kertesz et al., 2007). To assign an overall miRNA-mRNA target score, the algorithm computes the statistical weight of all configurations in which exactly one of the sites is bound by the miRNA. For negative values of ΔΔG, the summation formula is -log ($\Sigma(e^{-\Delta\Delta G_i})$). The PITA algorithm allows you to dictate the minimum seed size you wish to consider (6mer, 7mer or 8mer), permits you to allow G:U wobble and single mismatches within the seed region and to alter the minimum seed conservation required.

Even with stringent search requirements the target prediction results returned by TargetScan and PITA were excessive, therefore initial analysis focussed on those targets that were predicted by both algorithms (Fig. A1 and A2). To increase the chance of overlap between these two algorithms the PITA target predictions were performed with the broadest search criteria. Therefore 6mer seeds were considered, G:U wobbles and single mismatches within the seed region were permitted and minimum seed conservation was used. For some miRNAs a PITA score could not be calculated and hence these miRNAs were discounted from further analysis (highlighted in white in Tables 1.2 and 1.3). Predicted targets were considered to be of potential interest if they possessed target prediction scores which fell below one or both of the threshold scores which are indicated by the dotted red lines in Figures A1 and A2. The threshold score for TargetScan was set as a Total Context Score of -0.4 as previous experience in the laboratory had indicated that this was a suitable threshold for this algorithm. The threshold score for PITA was set as an overall miRNA-mRNA target score of -10. The ΔΔG value calculated by PITA is an energetic score, therefore the lower its value, the stronger the binding between a miRNA and the given target site is expected to be. The creators of the PITA algorithm suggest that target sites with ΔΔG values below -10 are likely to be functional at endogenous miRNA expression levels. Each miRNA may only have one target

site within each target mRNA therefore an overall miRNA-mRNA target score of -10 seemed appropriate as a threshold score.

The specific aim of this project was to identify miRNAs which target genes implicated in angiogenesis, therefore a list of genes that are involved in the regulation of angiogenesis and vascular integrity was compiled (Table A1). This list was based on a list of angiogenic genes as defined by Vart *et al*., 2007. Additional genes were added to this list due to recent reports of pro- or anti-angiogenic functions, based on the Gene Ontology (GO) biological process terms. The predicted targets generated by both TargetScan and PITA were compared to this list in order to identify any targets which play a role in angiogenesis (Table A2 and A3). A target was of particular interest if it had a good PITA score (-10 or less) and/or was predicted by TargetScan, particularly if it displayed the opposite expression pattern from the miRNA in KLEC, as determined by Vart et al., 2007 (Fig. 1.1).

For example, when the predicted targets of upregulated miRNAs were examined, phosphatase and tensin homologue (*PTEN)* stood out as a strong predicted target of miR-26a due to the low PITA and TargetScan 4.2 Scores and the fact that PTEN is downregulated in KLEC (Table A2, Fig. 1.1 and 3.1A). The TargetScan 4.2 and PITA scores for *PTEN* were also much more favourable than those of any previously reported miR-26a targets: SMAD family member 1 (*SMAD1*) (Luzi et al., 2008), enhancer of zeste homolog 2 (*EZH2*) (Wong and Tellam, 2008), cyclin-E2 (*CCNE2*) (Kota et al., 2009) and cyclin-D2 (*CCND2*) (Kota et al., 2009) (Fig. 3.1B). *PTEN* is a well-documented tumour suppressor gene and therefore its expression is not restricted to endothelial cells (Keniry and Parson, 2008). However, PTEN has been shown to have an anti-angiogenic effect because it is an antagonist of the phosphatidylinositol 3-kinase (PI3K) pathway, which is the major signalling route of pro-angiogenic factors (Jiang and Liu, 2009). My target prediction strategy was validated when miR-26a targeting of PTEN was confirmed, and the miR-26a/PTEN axis implicated in gliomagenesis (Huse et al., 2009).

A

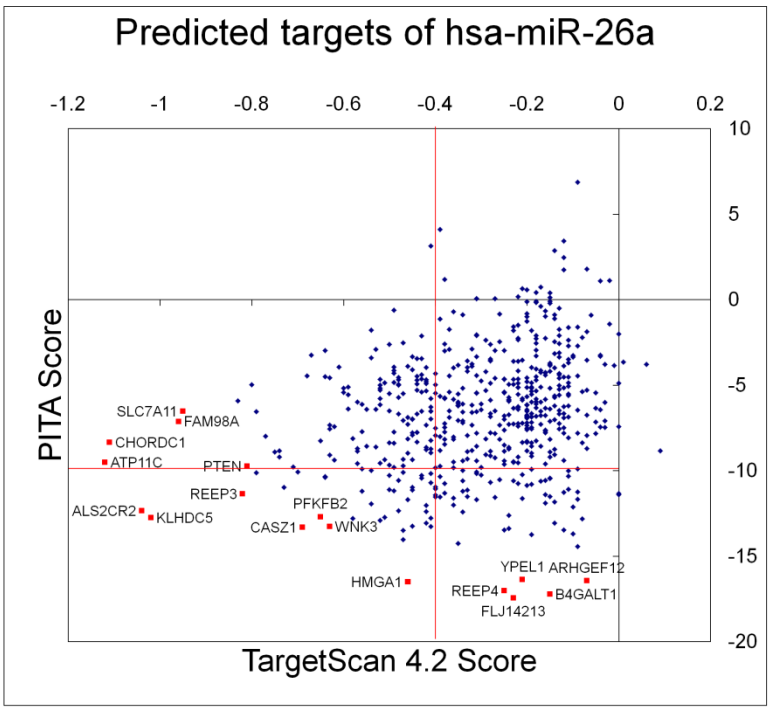

B

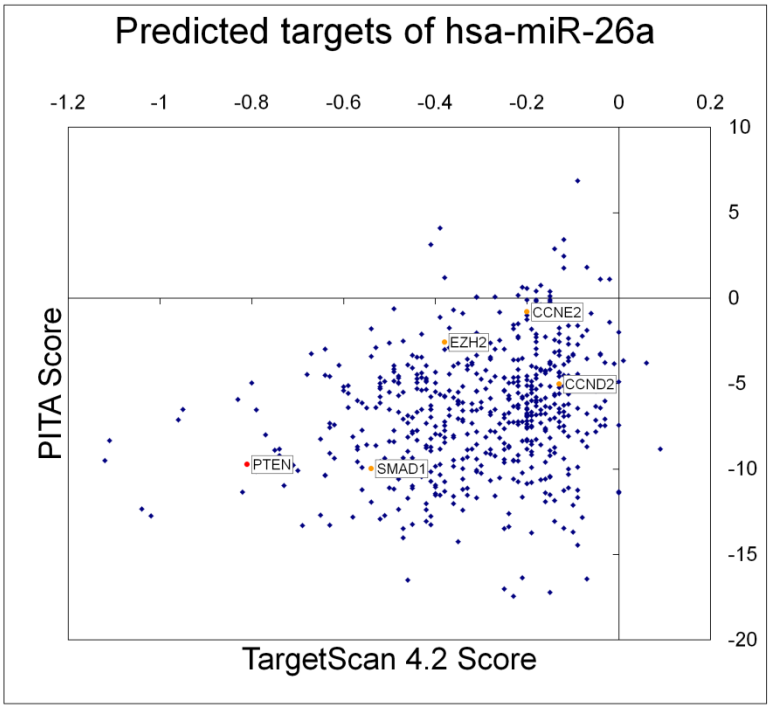

Figure 3.1. hsa-miR-26a is predicted to target PTEN. TargetScan Version 4.2 Total Context Scores plotted against PITA ddGSum scores for hsa-miR-26a. (A) Potential targets of interest are shown as red squares and have been named. The red lines indicate threshold scores; targets which fall below both these thresholds are of particular interest. Targets with either a favourable TargetScan Version 4.2 Total Context Score or a favourable PITA ddSum score have also been labelled. (B) PTEN is indicated by a red circle, genes known to be targeted by hsa-miR-26a at the time of conducting the target prediction analysis are marked with orange circles.

3.3 The miR-30 family is predicted to target *DLL4*

The target prediction analysis described in Section 3.2 revealed that hsa-miR-30a, -30b, -30c and -30d, all members of the miR-30 family, were predicted to target *DLL4*. These miR-30 family members were all downregulated by 0.5 fold or less in KLEC (Table 1.3), whilst *DLL4* is one of the most significantly upregulated genes in KLEC (Fig. 1.1) (Emuss et al., 2009). The miRNA-mRNA binding between miR-30 and *DLL4* was predicted by both PITA and TargetScan, with an almost favourable TargetScan 4.2 Total Context Score of -0.38 (Table A2). *DLL4* is not the most promising miR-30 target out of those upregulated in KLEC, especially when compared to known targets (Fig. 3.2A). However, when the reverse analysis was performed, searching for miRNAs predicted to target *DLL4*, the miR-30 family was found to be the best scoring miRNA for this 3'UTR (Fig. 3.2B).

The predicted target site within the *DLL4* 3'UTR is an 8mer which is the best possible binding site: complete complementarity with the seed region of the miRNA plus additional complementarity at position 8 and an adenine at position 1 (Fig. 3.3A). The target site is located towards the beginning of the 3'UTR at positions 59-66. This is another positive factor as target sites located near either end of the 3'UTR have been found to be the most effective (Grimson et al., 2007). All miRNAs of the miR-30 family share an identical seed, however their sequences vary outside of the seed region which was reflected in variations in predicted 3' complementary binding (Fig. 3.3A). TargetScan takes conservation into consideration when calculating the Total Context Score and the miR-30 target site is absolutely conserved within the *DLL4* 3'UTR across 24 species, suggesting an essential function for this predicted miRNA-mRNA interaction (Fig. 3.3B).

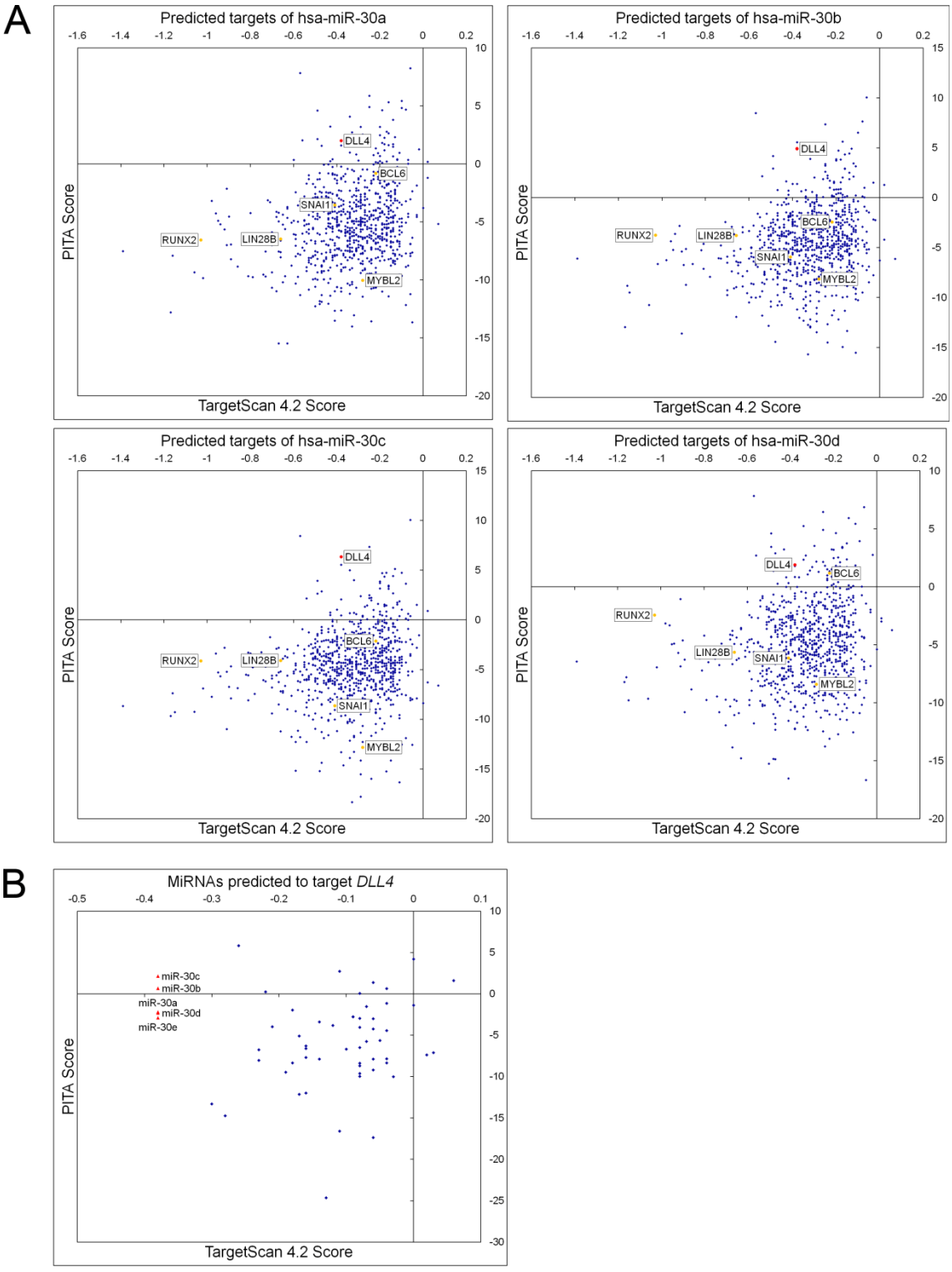

Figure 3.2. The miR-30 family is predicted to target DLL4. (A) Predicted targets of hsa-miR-30a, -30b, -30c and -30d. TargetScan Version 4.2 Total Context Scores are plotted against PITA ddGSum scores for the indicated miRNAs. *DLL4* is indicated by a red circle and label, genes known from the literature to be targeted by miR-30 members at the time of conducting the target prediction analysis are marked with orange circles and labelled. (B) MiRNAs predicted to target *DLL4*. TargetScan Version 4.2 Total Context Scores are plotted against PITA ddGSum scores. All five members of the miR-30 family are indicated by red triangles and labelled.

A

B

Homo sapiens	CUGCAUUGUUUACA
Pan troglodytes	CUGCAUUGUUUACA
Macaca mulatta	CUGCAUUGUUUACA
Mus musculus	CUGCAUUGUUUACA
Rattus norvegicus	CUGCAUUGUUUACA
Cavia porcellus	CUGCACUGUUUACA
Oryctolagus cuniculus	CUGCGUUGUUUACA
Sorex araneus	CUGCACUGUUUACA
Erinaceus europaeu	CUGCACUGUUUACA
Canis familiaris	CUGCAUUGUUUACA
Felis catus	CUGCAUUGUUUACA
Equus caballus	CUGCAUUGUUUACA
Bos taurus	CUGCAUUGUUUACA
Dasypus novemcinctus	CUGCAUUGUUUACA
Loxodonta africana	CUGCAUUGUUUACA
Echinops telfairi	UUGCGUUGUUUACA
Monodelphis domestica	CUGCAUUGUUUACA
Ornithorhychus anatinus	CUGCACUGUUUACA
Anolis carolinensis	CUACAUUGUUUACA
Gallus gallus	CUGCAUUGUUUACA
Xenopus tropicalis	CUCCGUUGUUUACA
Danio rerio	CUGGAUUGUUUACA

Figure 3.3. Graphical representation of the miR-30 target site within the *DLL4* 3'UTR. (A) Complementarity between miR-30 family members and the *DLL4* 3'UTR. Black lines indicate canonical Watson and Crick base-pairing, grey lines indicate G:U wobbles. The predicted target site within the *DLL4* 3'UTR, positions 59-66 is shown in red; miR-30 seed region is shown in green. (B) Alignment demonstrating conservation of the miR-30 target site (red) and surrounding sequence within the *DLL4* 3'UTR across 24 species. Positions 53-66 of the 3'UTR are shown.

3.4 miR-30 and *DLL4* expression inversely correlate in cancer

miRNAs are known to target Notch components during tumour development, but a function for this cross-talk in tumourigenesis is unclear (Wang et al., 2010). Downregulation of the miR-30 family is associated with enhanced tumourigenesis in anaplastic thyroid carcinoma and breast cancer (Braun et al., 2010; Yu et al., 2010). However, an association between *DLL4* and miR-30 expression has not been described. Expression data from The Cancer Genome Atlas (www.cancergenome.nih.gov) was analysed, with a specific focus on angiogenic solid tumours. A significant negative correlation between one or more miR-30 family members and *DLL4* expression was found in breast adenocarcinoma, ovarian serious cystadenocarcinoma and the highly angiogenic renal clear cell carcinoma (Fig. 3.4). Most of the other tumours analysed also displayed a negative correlation, although non-significant (Fig. 3.4). These results provided additional evidence to support the hypothesis that miR-30 targets DLL4 and suggested that this interaction could be functionally relevant during human cancer development.

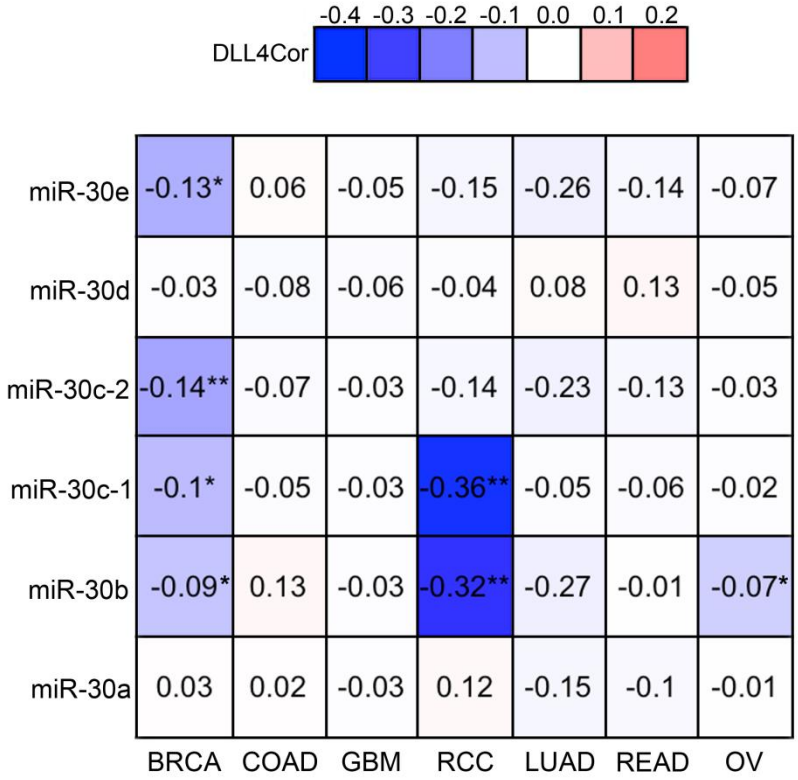

Figure 3.4. *DLL4* and miR-30 expression inversely correlate in human tumour samples. Heatmap table displaying the correlation coefficient R between expression of *DLL4* and each member of the miR-30 family in the indicated tumour types. GEM and RNAseq data was obtained from The Cancer Genome Atlas (www.cancergenome.nih.gov) data portal (tcga-data.nci.nih.gov), as described in Section 2.8.1 of Chapter 2. Due to the large difference in the number of replicates for each tumour type, the significance of R was calculated for each miR-30 vs. *DLL4* combination. The values and fill-in colour indicate the degree of negative correlation. Non-significant correlations are greyed out; significant correlations are marked with an asterisk *, $p<0.05$; **, $p<0.01$. Tumour types included are breast invasive carcinoma (BRCA), colon adenocarcinoma (COAD), glioblastoma multiforme (GBM), renal clear cell carcinoma (RCC), lung adenocarcinoma (LUAD), rectum adenocarcinoma (READ) and ovarian serous cystadenocarcinoma (OV). Data was selected and obtained by Gemma Bridge. Bioinformatic analysis and heatmap were completed by Stephen Henderson.

3.5 Confirmation of miR-30b and -30c downregulation in LEC

From expression microarray data previously generated in our laboratory (Lagos et al., 2010), it was known that miR-30a, -30b, -30c and -30d are downregulated in KLEC 72h p.i. When all the probes for members of the miR-30 family were examined individually, the probes corresponding to miR-30b and miR-30c were found to be significantly suppressed whilst downregulation in KLEC was a trend displayed by most members of the miR-30 family (Fig. 3.5A). To validate these microarray data, new KSHV infections were performed in human dermal LEC and miR-30b and miR-30c expression was quantified 72h p.i. using qRT-PCR (Fig. 3.5B). Both miR-30b and miR-30c were significantly repressed in KLEC by ~45% whereas expression of let-7i, an unrelated miRNA, was not significantly altered (Fig. 3.5B). Fluorescence-activated cell sorting (FACS) was performed on KLEC to separate infected cells from non-infected cells, based on GFP expression. The expression of miR-30b and miR-30c was examined in the two cell populations but was not found to be significantly different; therefore future analysis of KLEC was performed with the mixed cell population.

The mature miR-30c miRNA detected by the microarray can be produced from two distinct precursor hairpins (pre-miR-30c-1 and -2). This is because there are two pri-miRNA transcripts from which the pre-miRNAs are derived (Kozomara and Griffiths-Jones, 2011). These in turn are transcribed from two genomic locations: human chromosome 1 for miR-30c-1 and human chromosome 6 for miR-30c-2. Therefore, the observed downregulation of miR-30c could have been due to a reduction in just one or both sources of miR-30c. To investigate this, qRT-PCR was performed using primers and probes specific to pre-miR-30c-1 and -2. Expression of both precursor hairpins was found to be reduced in KLEC 72h p.i., although pre-miR-30c-1 was only downregulated by ~45% compared to the ~70% reduction in pre-miR-30c-2 (Fig. 3.5C).

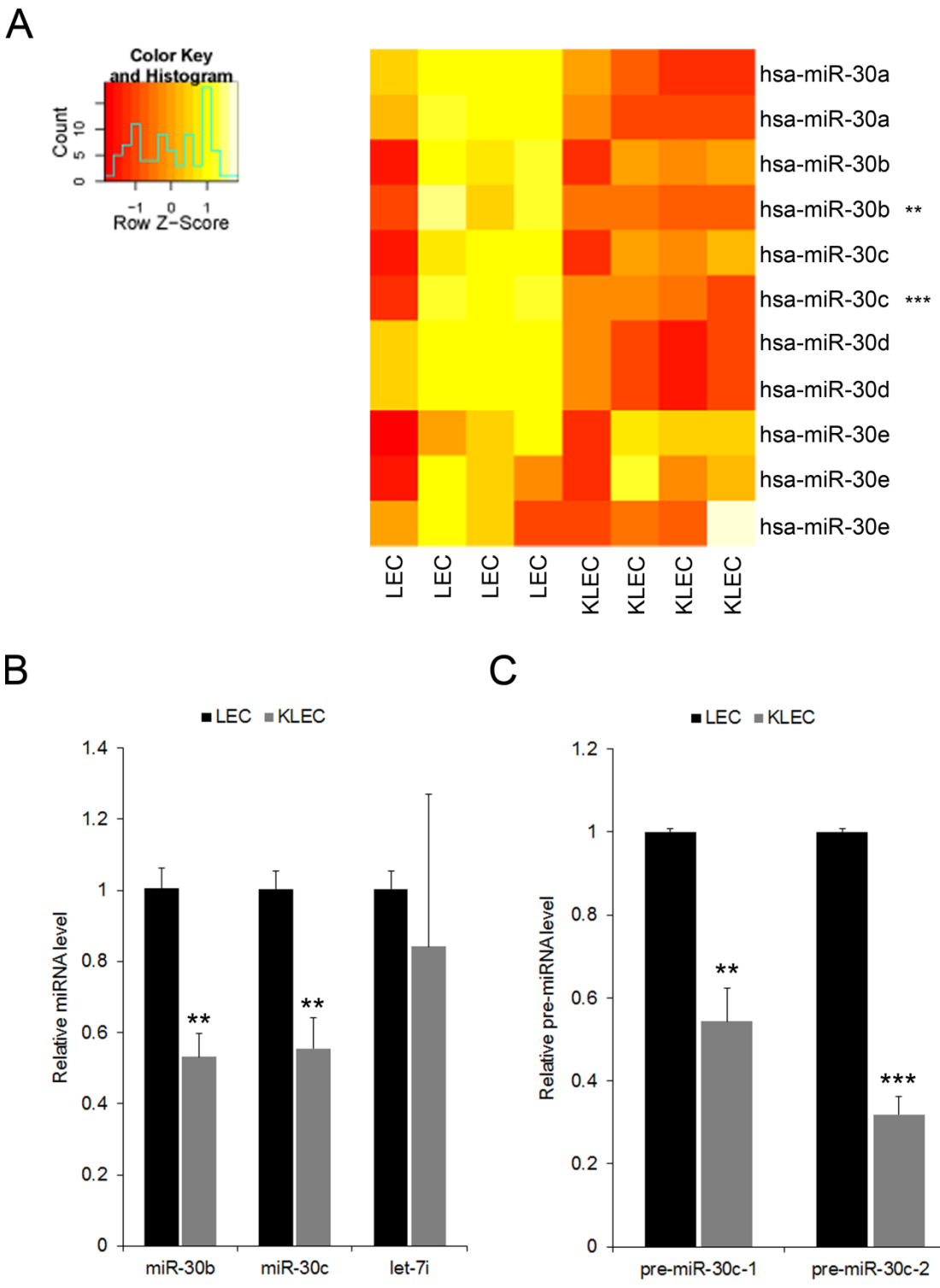

Figure 3.5. The miR-30 family is downregulated in KLEC. (A) Heatmap representing relative changes in expression of hsa-miR-30 family members in LEC 72 h post-KSHV infection. Red and yellow denote low and high expression respectively. Probes for hsa-miR-30b and hsa-miR-30c showed significant changes in expression (**, Q<0.01; ***, Q<0.001). Original GEM data from Lagos et al., 2010. Heatmap generated by Stephen Henderson. (B) Confirmation of downregulation of miR-30b and -30c in KLEC 72 h p.i., as quantified by qRT-PCR (means + SEM, n=4). Expression is relative to LEC. **, p<0.01. (C) pre-miR-30c-1 and pre-miR-30c-2 are both downregulated in KLEC 72 h p.i., as quantified by qRT-PCR (means + SEM, n=3). Expression is relative to LEC. **, p<0.01; ***, p<0.001.

3.6 Confirmation of *DLL4* upregulation in human dermal LEC

Previous work in our laboratory showing upregulation of DLL4 and JAG1 in KLEC had been performed in LEC derived from adult lymph nodes (Emuss et al., 2009), however the work described here was performed using human dermal LEC. It was therefore necessary to confirm that the alterations in Notch signalling components were also observed in this cell type. Uninfected human dermal LEC displayed the expected cobble-stone morphology of LEC (Fig. 3.6A) whereas KSHV-infected human dermal LEC developed the typical spindle-shape morphology (Fig. 3.6B). This morphological change is most likely due to cytoskeletal rearrangements induced by nuclear factor of kappa light polypeptide gene enhancer in B-cells (NF-κB) which is activated by vFLIP (Grossmann et al., 2006). The recombinant strain of KSHV used for these infections (rKSHV.152), contains the GFP gene within its genome (Vieira et al., 2001). Therefore, KSHV infection was also confirmed by GFP expression (Fig. 3.6B). Significant upregulation of *DLL4* and *JAG1* was observed in KSHV-infected human dermal LEC when compared to uninfected human dermal LEC (Fig. 3.6C). This verified that human dermal LEC were suitable for future investigations into miRNA regulation of DLL4 following KSHV infection.

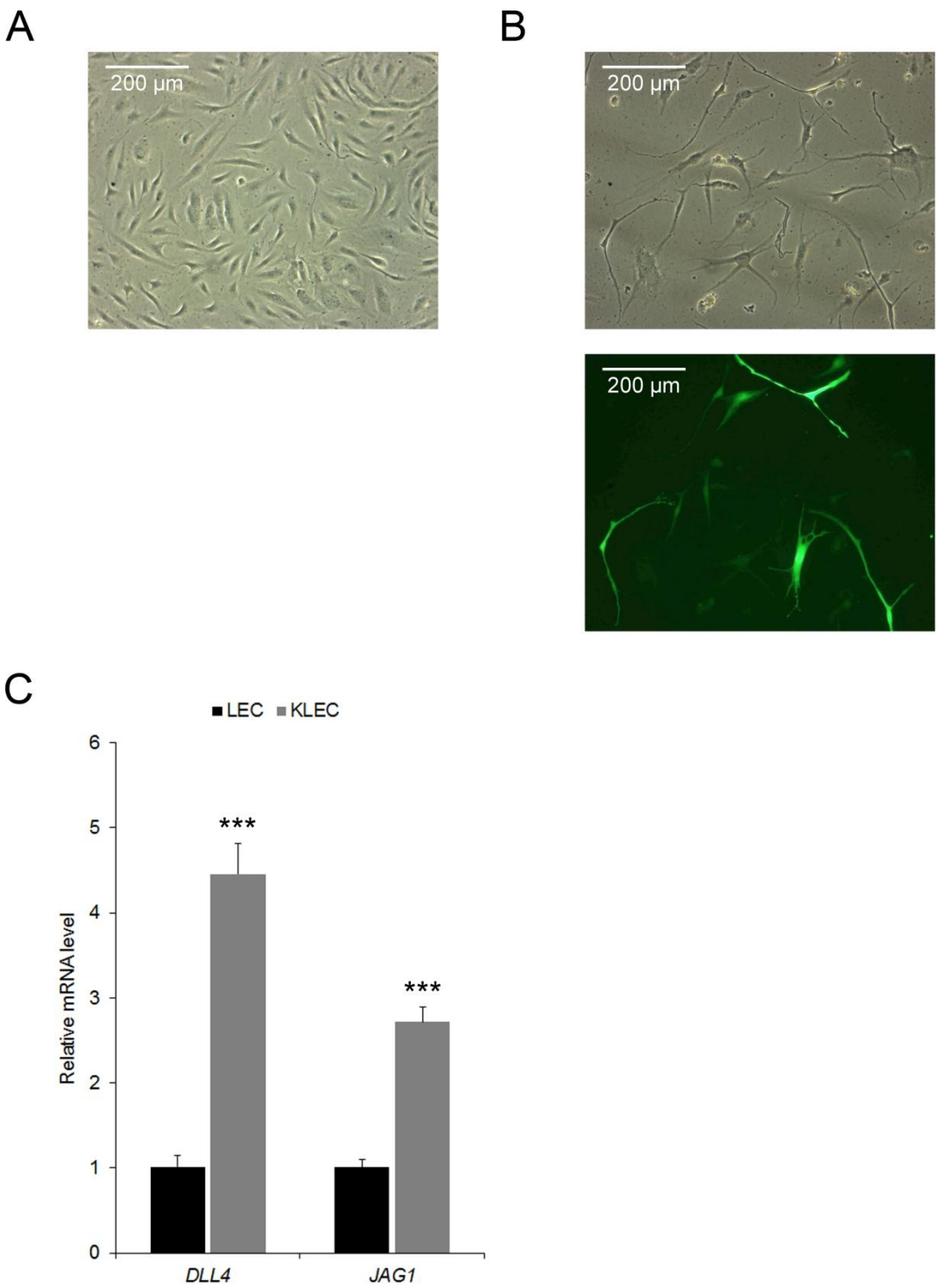

Figure 3.6. Characterisation of KSHV infection in human dermal LEC. (A) Phase contrast image of human dermal LEC taken 72 h after cells had been plated. Photograph taken at 10x magnification on an Axiovert 100 microscope (Zeiss) using an AxioCam (Zeiss). (B) Upper panel: phase contrast image of human dermal LEC 72 h post-KSHV infection. Photograph taken at 10x magnification on an Axiovert 100 microscope (Zeiss) using an AxioCam (Zeiss). Lower panel: fluorescent image of the same field of view as in the upper panel, showing GFP expression. Photograph taken at 10x magnification on an Axiovert 100 microscope (Zeiss) using an AxioCam (Zeiss). (C) Upregulation of *DLL4* and *JAG1* mRNA 72 h following KSHV infection of human dermal LEC, as quantified by qRT-PCR (means + SEM, n=3). Expression is relative to uninfected human dermal LEC. ***, $p<0.001$.

3.7 Discussion

The target prediction analyses presented here highlight the inherent difficulties of identifying functional miRNA-mRNA regulation. Depending on the particular algorithm used, and the stringency of the filters, each miRNA has hundreds to thousands of predicted targets. One method to refine a list of potential targets is to look at the overlap between the results of two or more algorithms, as adopted here. The advantages of this approach are that it reduces the targets of interest to a manageable number whilst also focusing on those that are most likely to be genuine targets.

For this study TargetScan 4.2 and PITA were used as they incorporate a range of different parameters when producing a final target prediction score (Grimson et al., 2007; Kertesz et al., 2007; Lewis et al., 2003; Lewis et al., 2005). TargetScan considers target site conservation with an emphasis on the extent of seed match, 3' complementarity and impact of target site position, whereas PITA allows the cut-off level for cross-species conservation to be reduced whilst focusing on target site accessibility. Only two prediction algorithms were selected for the cross-comparison of predicted targets as we decided that including a third algorithm would lead to excessive numbers of genuine targets being discarded. TargetScan was of particular interest because, along with PicTar, it performed best in a test of target prediction algorithms (Baek et al., 2008). miR-223 was knocked out in mouse neutrophils and changes in protein expression were examined using stable isotope labelling with amino acids in cell culture (SILAC). Perturbations in endogenous targeting were then compared to target predictions from miRBase Targets (Griffiths-Jones et al., 2008), miRanda (Betel et al., 2008; John et al., 2004), PicTar (Krek, 2005; Lall et al., 2006), PITA and TargetScan 4.2.

However, as TargetScan heavily weights perfect seed pairing, PITA is preferential for allowing identification of non-canonical sites, such as those containing G:U wobbles or with imperfect seeds (Thomas et al., 2010). Since these target analyses were completed, the task of miRNA target prediction has been further complicated by the discovery of non-canonical 3'-supplementary,

3’-complementary (Bartel, 2009) and centred miRNA target sites (Shin et al., 2010) and the suggestion that miRNAs can also ORFs (Duursma et al., 2008).

The cross-comparison between miRNAs differentially expression in KLEC with angiogenic genes which are simultaneously upregulated or downregulated revealed an extensive network of predicted interactions. However, it was notable that many miRNA upregulated in KLEC are predicted to target genes that are also upregulated and vice versa. This does not necessarily mean that these miRNAs do not regulate expression of these genes. It could imply that in this system, other viral-induced signalling pathways predominate. Yet, amongst both the targets of upregulated and downregulated groups of miRNAs, specific genes stood out due to strong predictive scores and opposing changes in expression of target and miRNA. Several genes were also predicted to be targets of multiple similarly expressed miRNAs. For example, the pro-angiogenic gene fibroblast growth factor receptor 2 (*FGFR2*) is upregulated in KLEC (Fig. 1.1) (Vart et al., 2007) and is predicted by both PITA and TargetScan to be a target of miR-494 and miR-513, both of which are downregulated in KLEC (Table 1.3). Conversely, N(alpha)-acetyltransferase 15 (*NAA15*), previously known as NMDA receptor-regulated protein 1 (*NARG1*), is downregulated in KLEC (Vart et al., 2007) and is predicted by both PITA and TargetScan to be a target of several upregulated miRNAs: miR-148a, miR-26a, miR-329, miR-503 and miR-582. *NAA15* has been reported to maintain endothelial homeostasis by preventing retinal neovascularisation and to enhance the ubiquitination of hypoxia-inducible factor 1 alpha subunit (*HIF1A*), which is upregulated in KLEC (Fig. 1.1) (Gendron et al., 2001; Gendron et al., 2006; Jeong et al., 2002). Therefore, co-ordinated upregulation of miRNAs that target *NAA15* could be responsible for the subsequent downregulation of this potent anti-angiogenic gene and hence contribute to the pro-angiogenic environment of KSHV infected endothelial cells. Further examination of the target prediction analyses could reveal other interesting targets for future investigation.

The outcome of the target prediction analyses described in Section 3.2 was to uncover the predicted targeting of *DLL4* by the miR-30 family. Further examination of this prediction revealed a potential 8mer miR-30 target site

located in a beneficial position within the *DLL4* 3'UTR. *DLL4* was of particular interest as a target gene because it is overexpressed in human tumours, often in association with markers of inflammation, hypoxia and angiogenesis (Jubb et al., 2009; Jubb et al., 2010; Patel et al., 2005; Patel et al., 2006). Blockade of DLL4 signalling suppresses experimental tumour growth by inducing non-productive, deregulated angiogenesis (Haller et al., 2010; Hoey et al., 2009; Noguera-Troise et al., 2006; Oishi et al., 2010; Ridgway et al., 2006). This discovery has subsequently led to a Phase I trial of a DLL4 blocking antibody (www.clinicaltrials.gov). However, as long term treatment of rats with such an antibody led to the development of vascular neoplasms (Yan et al., 2010), there is a potential need for more subtle mechanisms to moderately reduce DLL4 expression or signalling. Regulation of expression using exogenous miRNAs could be investigated as a potential solution.

The miR-30 family contains five members: miR-30a, miR-30b, miR-30c, miR-30d and miR-30e. Four of these family members demonstrate some level of downregulation in KLEC (miR-30a-d). This group of related miRNAs are encoded by six genes spread across three chromosomes. pre-miR-30a and pre-miR-30c-2 are transcribed individually from chromosome 6, pre-miR-30b and pre-miR-30d are clustered together as a pri-miRNA transcript on chromosome 8 and pre-miR-30c-1 and pre-miR-30e are also clustered on chromosome 1. All members of the family share the same seed sequence and there is very little variation in the remaining sequence of the mature miRNAs. Therefore, the entire family share common predicted targets. This level of redundancy suggests that this miRNA family possesses a critical function, potentially the regulation of a key mediator of angiogenesis.

The potential link between miR-30 and *DLL4* was highlighted partly because of the inverse expression of these genes in KLEC, according to microarray expression data. The Notch ligand *DLL4* is one of the most significantly upregulated genes in KLEC of lymph node origin (Emuss et al., 2009), and this was independently confirmed here in human dermal LEC. Whilst four of the miR-30 members show some level of downregulation, probes for miR-30b and miR-30c were found to be significantly downregulated in KLEC and this was confirmed in three independent infections by qRT-PCR. Additionally,

downregulation of miR-30c was shown to be due to a reduction in both pre-miR-30c-1 and pre-miR-30c-2. A putative promoter for pri-miR-30a has been identified (Fujita and Iba, 2008) and NF-κB binding has been shown to mediate lipopolysaccharide (LPS) induced upregulation of miR-30b (Zhou et al., 2009; Zhou et al., 2010). However, when the regions upstream of the various pri-miR-30 transcripts were investigated, a common transcription factor binding site could not be identified. Given the multitude of genomic locations, it is possible that the altered expression of miR-30 family members following KSHV infection is due to regulation at the level of pri-miRNA processing.

Chapter 4. miR-30b and miR-30c target *DLL4*

4.1. Aims

Having identified *DLL4* as a predicted target of the miR-30 family, the aims of this chapter were:

i. To investigate whether functional targeting of *DLL4* by miR-30 occurs *in vitro* by overexpressing miR-30 using miRNA mimics and lentiviral constructs and inhibiting endogenous miR-30 using miRNA inhibitors.
ii. If miR-30 does regulate DLL4 expression, to identify the specific target site(s) through which miR-30 acts by employing a luciferase reporter assay to examine miR-30 binding to the *DLL4* 3'UTR.
iii. To elucidate whether miR-30 targeting of DLL4 can influence endothelial cell behaviour *in vitro* using a tube formation assay.

4.2. Cloning hsa-miR-30b and hsa-miR-30c-1

To confirm the targeting of *DLL4* by miR-30b and miR-30c, these two miRNAs would need to be overexpressed *in vitro*. For short-term expression, synthetic miRNA mimics from Dharmacon (ThermoScientific) was employed. However, to obtain long-term stable expression, miR-30b and miR-30c-1 were also cloned into the pSIN-MCS vector which would allow expression using a lentiviral system, as described in Section 2.2.2. Primers were designed which were complementary to either end of a ~500-600bp region surrounding the mature hsa-miR-30b and hsa-miR-30c-1 sequences (Table 2.1). These regions were smaller than the predicted pri-miRNAs for hsa-miR-30b and hsa-miR-30c-1, but would fully encompass the pre-miRNA sequences. This method has previously been shown in our laboratory to allow effective expression and processing of human miRNAs (Hansen et al., 2010; Lagos et al., 2010).

Genomic DNA was extracted from LEC and used as a template to perform gradient PCR, as detailed in Table 2.1. The PCR samples were then run on an agarose gel using electrophoresis in order to visualise any products (Fig. 4.1A). The expected PCR product containing pre-miR-30b was 624bp and a band between 500 and 750bp was generated at all the annealing temperatures used, although more product was synthesised at annealing temperatures of 55-58°C

(Fig. 4.1A, upper panel). Some smaller, non-specific bands were also visualised at lower annealing temperatures and primer dimers appeared to have occurred at all annealing temperatures, indicating that these PCR reactions/primers were not efficient. The expected PCR product containing pre-miR-30c-1 was 564bp and a very strong band between 500 and 750bp was generated at all the annealing temperatures used, indicating very efficient PCR reactions with these primers (Fig. 4.1A, lower panel). All the DNA bands of the correct size were excised from the gels, extracted and pooled to produce a more concentrated PCR product for both miR-30b and miR-30c-1.

The PCR products and the pSIN-MCS plasmid were then digested with *BamHI* and *NotI* restriction enzymes to generate the required sticky ends before ligation overnight at 16°C using T4 DNA ligase. Ligation reactions were performed at two ratios of vector to insert; 1:8 and 2:10. Following transformation and growth on ampicillin-containing agar plates, colonies were picked and grown up overnight as mini cultures. For pre-miR-30b both the 1:8 and 2:10 ligations generated colonies whereas only the 1:8 ligation was successful for pre-miR-30c-1. DNA was extracted from half of the mini cultures and a diagnostic digest was performed with *BamHI* and *NotI* restriction enzymes. When gel electrophoresis was performed with the digested products, minipreps C-P for miR-30b and minipreps B, C and G for miR-30c-1, all displayed inserts of the expected size (Fig 4.1B). Sequencing revealed that miR-30b miniprep M and miR-30c-1 miniprep G contained the correct insert without any mutations and therefore the remainder of these cultures were used to seed maxi cultures to produce DNA maxipreps.

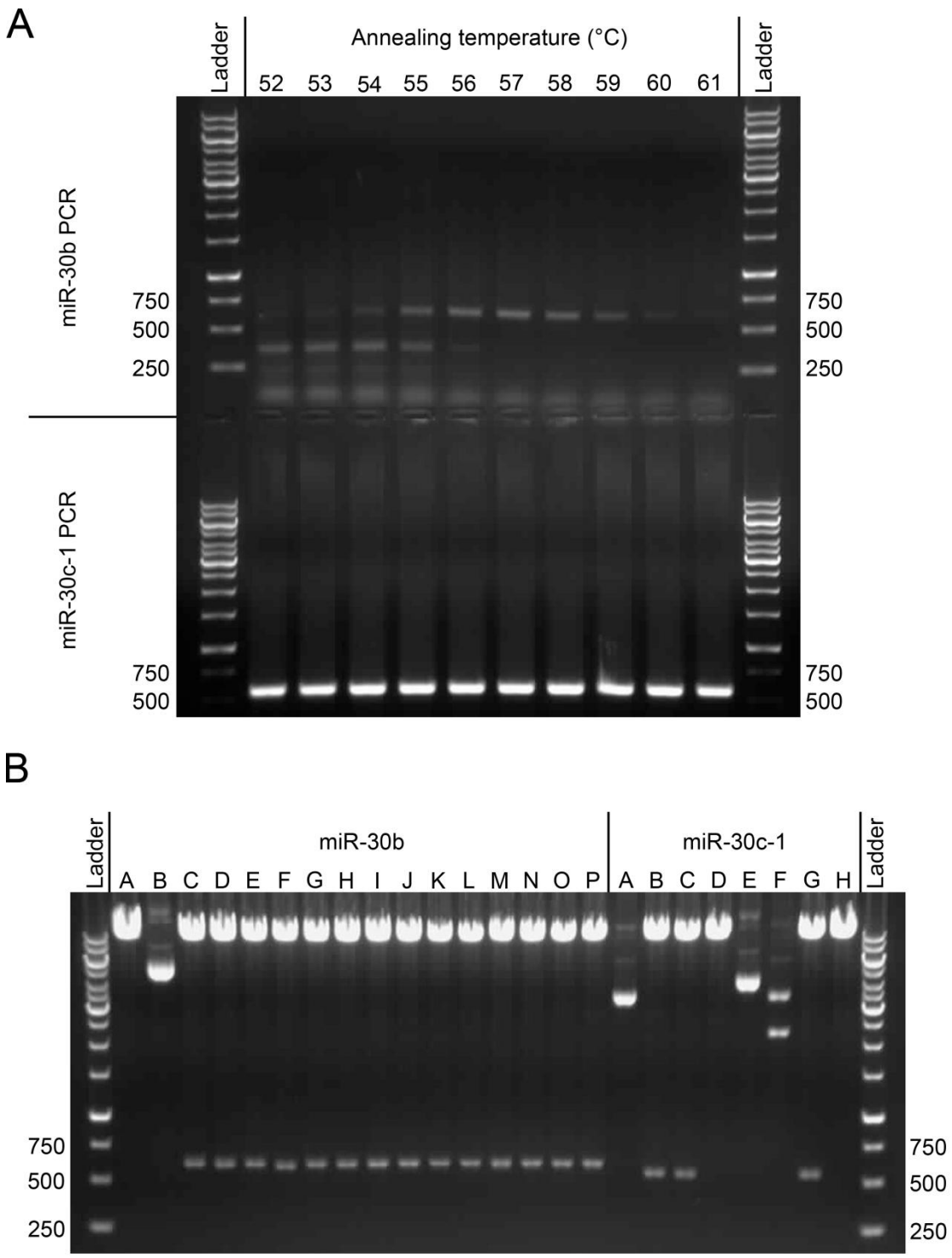

Figure 4.1. Cloning hsa-miR-30b and hsa-miR-30c-1 into a lentiviral vector. (A) Gel electrophoresis of miR-30b and miR-30c-1 PCRs. Correct bands for both products shown between 500 and 750bp. Ladder: lanes containing Generuler 1kb DNA Ladder (Fermentas). 250, 500 and 750bp bands are indicated. Images were taken using G:Box gel documentation system (Syngene) at 100ms exposure. (B) Gel electrophoresis of miR-30b and miR-30c-1 minipreps following digestion with *BamHI* and *NotI* restriction enzymes. miR-30b minipreps labelled A-H were picked from the 1:8 ligation agar plate. miR-30b minipreps labelled I-P were picked from the 2:10 ligation agar plate. Ladder: lanes containing Generuler 1kb DNA Ladder (Fermentas). 250, 500 and 750bp bands are indicated. Images were taken using G:Box gel documentation system (Syngene) at 100ms exposure.

4.3. miRNA expression from pSIN_miR-30b and pSIN_miR-30

Before using pSIN_30b and pSIN_30c to generate lentiviruses it was necessary to confirm that the cloned miRNAs were expressed from these plasmids. $1x10^5$ 293T cells were transfected with either 500ng or 1000ng of pSIN_MCS, pSIN_30b or pSIN_30c and total RNA was harvested 48 h later. Both miRNAs were found to be expressed from the relevant plasmid; however miR-30c expression was ~4x higher than miR-30b expression at both concentrations (Fig. 4.2A). It was therefore decided that the miR-30b lentivirus but not the miR-30c lentivirus would be concentrated.

Lentiviruses encoding empty vector, GFP, hsa-miR-30b and hsa-miR-30c were produced in 293T cells after transfection with the relevant pSIN vector, the packaging plasmid pCMV-8.91 and the envelope plasmid pMD.G. The infectivity of the lentiviral preparations was determined by qPCR for the lentiviral packaging signal. $1x10^5$ LEC were initially infected with 1 ml of each lentivirus and a successful infection was deemed to have occurred when the pSIN_GFP infected cells were 100% GFP-positive at 72 h p.i. (Fig. 4.2B). Both genomic DNA and total RNA were harvested at 72 h p.i. and qPCR analysis revealed that 1 ml of lentivirus yielded ~250 lentiviral copies per cell (c/c) for pSIN_30c but only 40 c/c for pSIN-30b (Fig. 4.2C). Despite the greater infectivity of pSIN_30c, the upregulation of miR-30c was only slightly higher than that of miR-30b, 19-fold compared to 12-fold (Fig. 4.2D). It was decided that matching miRNA expression between the two lentiviruses was more important than matching copy number and therefore volumes of pSIN_30c lentivirus were titrated to ascertain a volume which would also achieve 12-fold upregulation of miR-30c. This was found to be 500 µl (Fig. 4.3A). For all remaining lentiviral experiments 1 ml of concentrated pSIN_30b and 500 µl of unconcentrated pSIN_MCS and pSIN_30c were used.

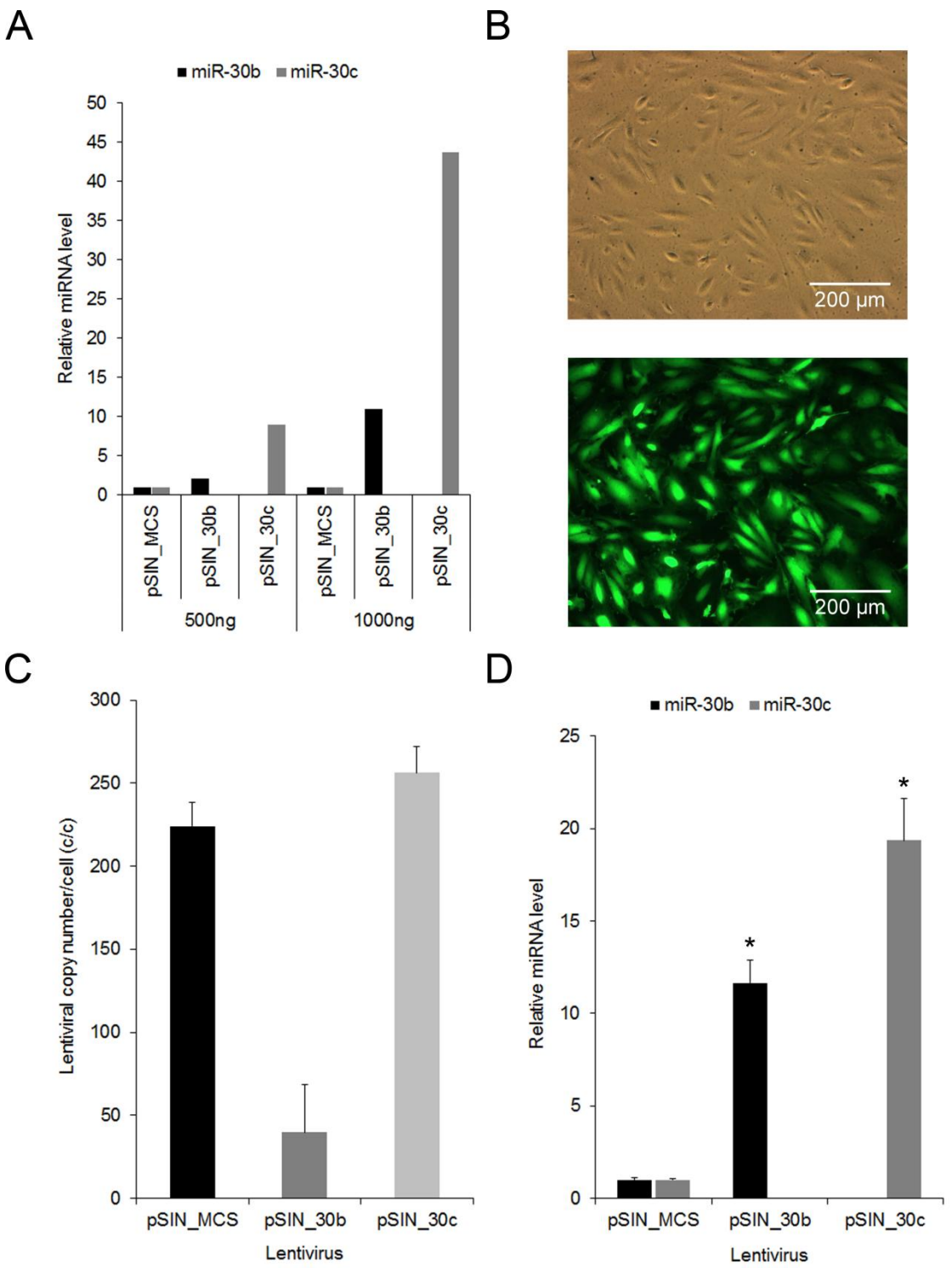

Figure 4.2. Optimising miRNA expression from pSIN_30b and pSIN_30c. (A) Expression of miR-30b and miR-30c in 293T cells 48 h following transfection with the either 500 ng or 1000 ng of the indicated plasmid, as quantified by qRT-PCR. Expression is relative to pSIN_MCS transfected cells (SEM is not shown as n=1). (B) Top panel: phase contrast image of LEC 72 h p.i. with pSIN_GFP. Bottom panel: fluorescent image of the same field of view as in the upper panel showing GFP expression. Photographs taken at 10x magnification on an Axiovert 100 microscope (Zeiss) using an AxioCam (Zeiss). (C) Lentiviral titre in LEC 72 h p.i. with 1 ml of the indicated lentivirus, as measured by qPCR (means + SEM, n=2 therefore SEM has only been included to give an approximate indication of reproducibility). (D) Overexpression of miR-30b and -30c in LEC 72 h p.i. with the relevant lentivirus, as quantified by qRT-PCR (means + SEM, n=2 therefore SEM has only been included to give an approximate indication of reproducibility). Expression is relative to pSIN_MCS infected LEC. *, $p<0.05$.

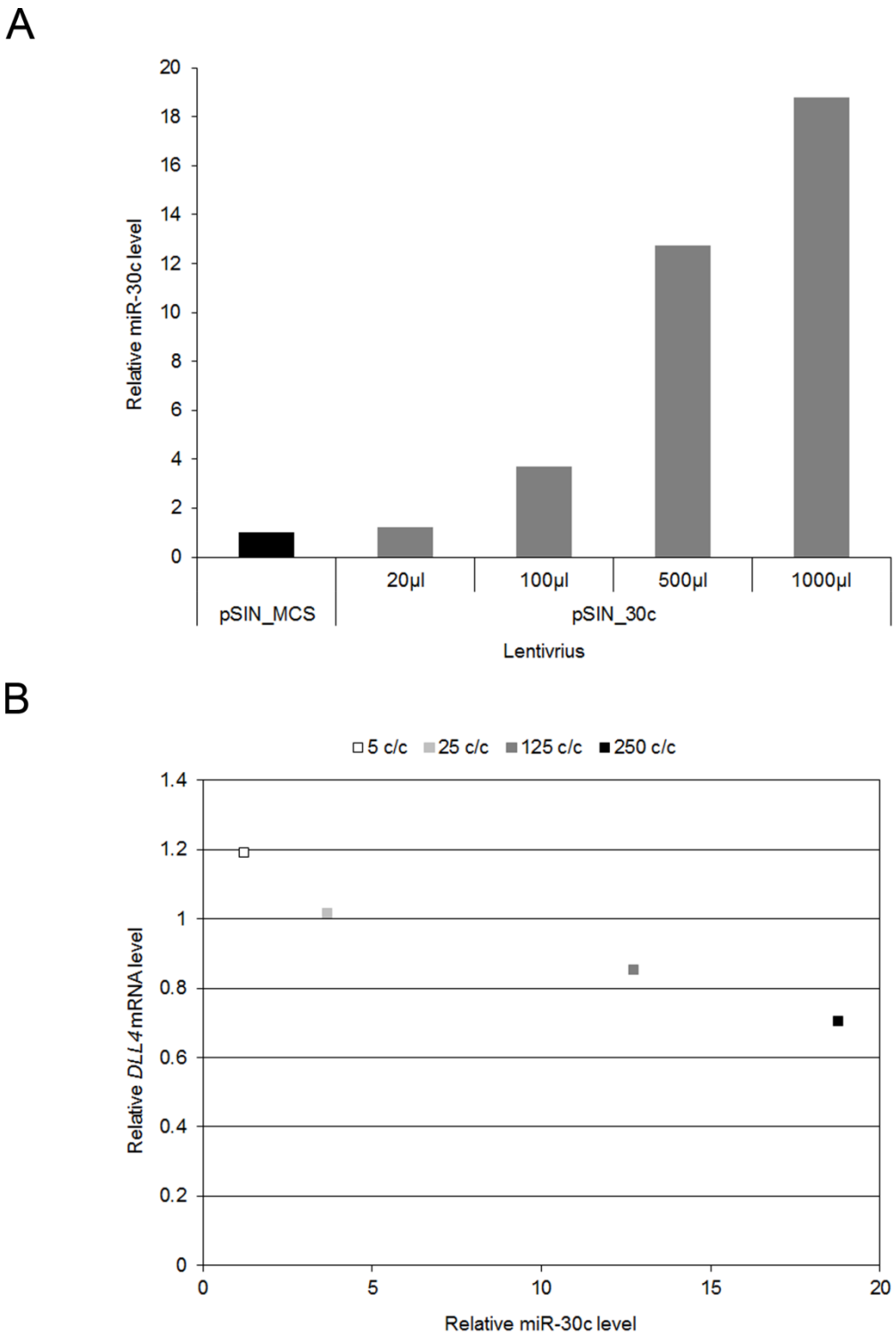

Figure 4.3 Titration of pSIN_miR-30c lentivirus in LEC. (A) miR-30c expression increases with increasing volume of pSIN_30c lentivirus, as quantified by qRT-PCR. Expression is relative to LEC infected with the equivalent volume of empty vector, pSIN_MCS (SEM is not shown as n=1). (B) Downregulation of *DLL4* mRNA and upregulation of miR-30c in LEC both correlate with lentiviral copy number, as quantified by qRT-PCR. Expression is relative to LEC infected with the equivalent copy number of empty vector, pSIN_MCS (SEM is not shown as n=1).

4.4. DLL4 is downregulated by miR-30b and miR-30c

To ascertain whether *DLL4* was a genuine target of miR-30b and -30c, these two miRNAs needed to be overexpressed in LEC. Initially Dharmacon miRIDIAN microRNA mimics (ThermoScientific) were used to achieve this goal. Oligofectamine was used for delivery of the non-targeting control (NTC), miR-30b and -30c mimics. To determine the most suitable concentration of mimic to use in LEC a titration experiment was performed and selectin E (*SELE*) and *DLL4* mRNA were quantified by qRT-PCR. A mimic concentration of 100nM was chosen because at this concentration ~40% reduction in *DLL4* expression was observed for both miR-30b and -30c whilst expression of *SELE*, an unrelated mRNA, was unchanged (Fig 4.4A). Using 200nM of mimics did not suppress *DLL4* expression further and caused significant cell death due to the required increase in transfection reagent (Fig. 4.4A).

When the mimic transfections were repeated using 100nM, DLL4 mRNA and protein levels were significantly reduced by 40-50% in LEC expressing either mimic (Fig. 4.5A and B). This effect was not seen with the miR-29c* mimic, which is a miRNA that is not predicted to target *DLL4* (Fig. 4.5A). Expression of an unrelated mRNA (*SELE*) was unchanged, suggesting that the suppression of *DLL4* mRNA does not reflect a non-specific effect of these mimics on global mRNA levels (Khan et al., 2009). The effect of the miR-30 mimics on *DLL4* mRNA expression was noted to be dose dependent as significant suppression was first observed at 20-40nM and increased as the mimic concentration was increased to 100nM (Fig. 4.4B).

Co-transfection of miR-30b and -30c, at an equivalent total concentration, did not increase *DLL4* repression, suggesting that there are no additive or synergistic effects between these miR-30 family members (Fig. 4.4B). This finding concurred with the target prediction studies, which indicated only one miR-30 target site in the *DLL4* 3'UTR (Fig. 3.3A).

A

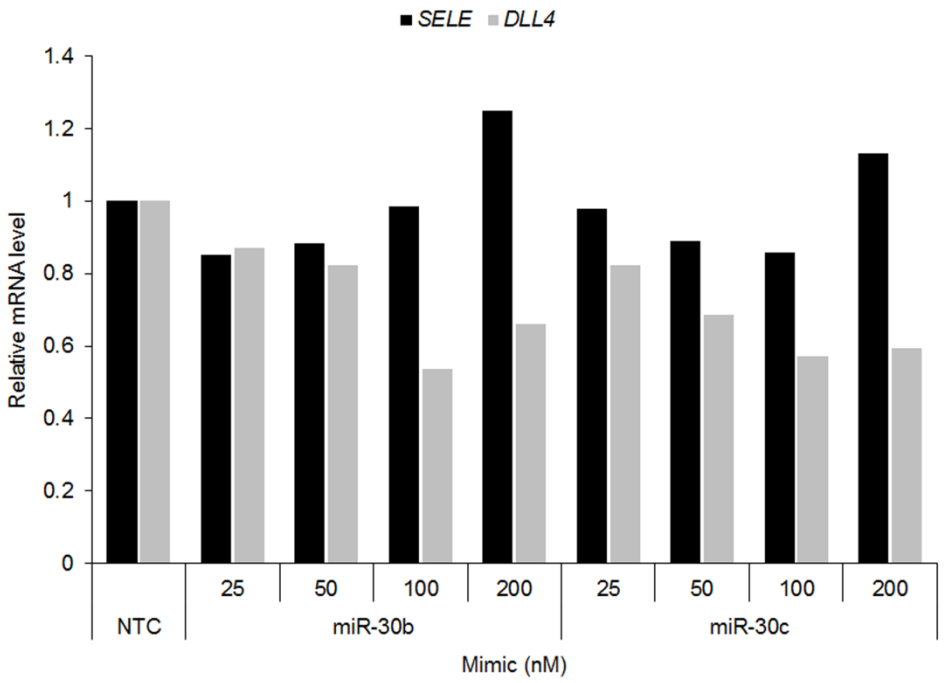

B

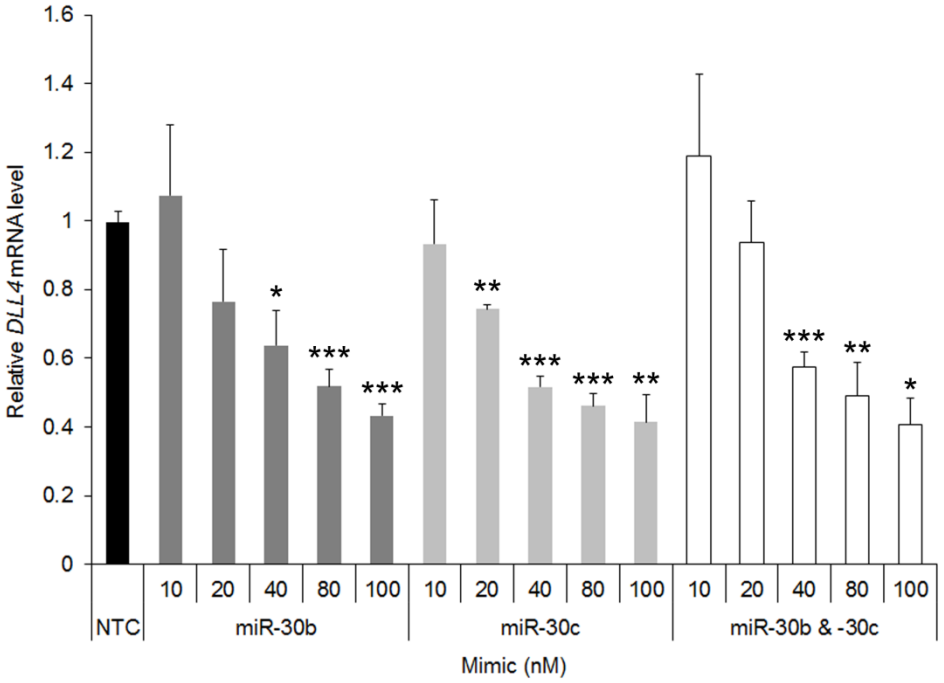

Figure 4.4. The effect of miR-30 mimic concentration on *DLL4* expression in LEC. (A) *DLL4* and *SELE* mRNA expression in LEC 48 h following transfection with the indicated concentrations of miRNA mimic (nM), as quantified by qRT-PCR. Expression is relative to LEC transfected with the equivalent concentration of NTC mimic (SEM is not shown as n=1). (B) Downregulation of *DLL4* mRNA in LEC increases with increasing concentration of transfected mimic (nM), as quantified by qRT-PCR (means + SEM, n=3). Expression is relative to LEC transfected with the equivalent concentration of NTC mimic. *, $p<0.05$; **, $p<0.01$; ***, $p<0.001$.

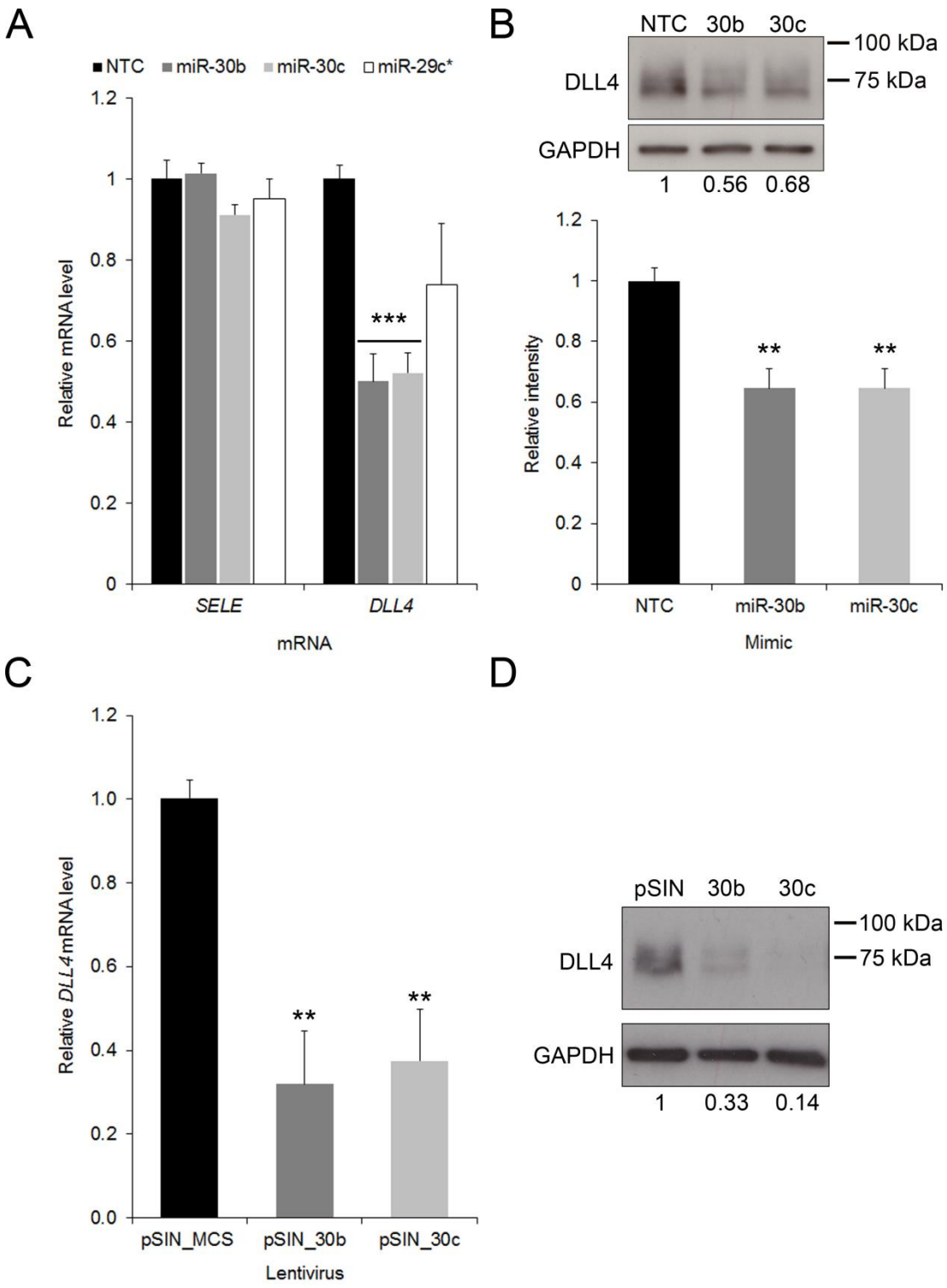

Figure 4.5. Overexpression of miR-30 causes downregulation of DLL4 in LEC. (A) *DLL4* and *SELE* mRNA expression in LEC transfected with NTC, miR-29c*, miR-30b or -30c mimics, as quantified by qRT-PCR (means + SEM, n=4). Expression is relative to NTC-transfected LEC. ***, $p<0.001$. (B) DLL4 protein expression in LEC transfected with miR-30b or -30c mimics measured by Western blotting and normalised to GAPDH expression. Upper panel: representative western blot. Values beneath blot denote intensity of antibody ECL signal relative to NTC mimic. Molecular weight markers are represented to the right. Lower panel: intensity of antibody ECL signal relative to NTC-transfected LEC (means + SEM, n=3). **, $p<0.01$. (C) *DLL4* mRNA expression in LEC infected with miR-30b or -30c expressing lentiviruses, as quantified by qRT-PCR (means + SEM, n=4). Expression is relative to empty vector, pSIN_MCS. **, $p<0.01$. (D) Representative Western blot showing DLL4 protein levels in LEC infected with miR-30b or -30c expressing lentiviruses. Values beneath blot denote intensity of antibody ECL signal relative to empty vector, pSIN. Molecular weight markers are represented to the right.

Transduction of LEC with pSIN_30b and pSIN_30c through infection with the relevant lentivirus also suppressed *DLL4* mRNA and protein (Fig. 4.5C and D). Although the observed downregulation was more variable with the lentiviruses, a greater degree of suppression was achieved, sometimes as high as 70-85% (Fig. 4.5D).

KSHV infection of endothelial cells results in transcriptional reprogramming from a LEC to a BEC phenotype and *vice versa* (Hong et al., 2004; Wang et al., 2004). Therefore, the effect of miR-30 overexpression in human umbilican vein endothelial cells (HUVEC) was then examined to determine whether the suppression of DLL4 was specific to lymphatic endothelial cells or also relevant in blood vascular endothelial cells. Transfection of HUVEC with miR-30b and -30 mimics at 100nM led to a significant reduction in *DLL4* mRNA and protein 48 h post-transfection (Fig. 4.6A and B). This effect was also dose dependent in HUVEC as *DLL4* suppression increased as the mimic concentration was increased from 100nM to 200nM (Fig. 4.7A and B). HUVEC transduced with pSIN_30b and pSIN_30c displayed a significant downregulation of DLL4 mRNA and protein when compared to pSIN_MCS or pSIN_GFP transduced cells (Fig. 4.6C and D). This effect was not seen in HUVEC overexpressing miR-132, a miRNA which is not predicted to target *DLL4* (Fig. 4.6C and D). *DLL4* mRNA suppression was also not observed in HUVEC expressing mutant miR-30b or -30c (pSIN_30b-m and pSIN_30c-m) (Fig. 4.6C). These constructs contain a mutation within the predicted miRNA seed, as described in Section 2.3.8, which should prevent miR-30 from binding to target mRNAs.

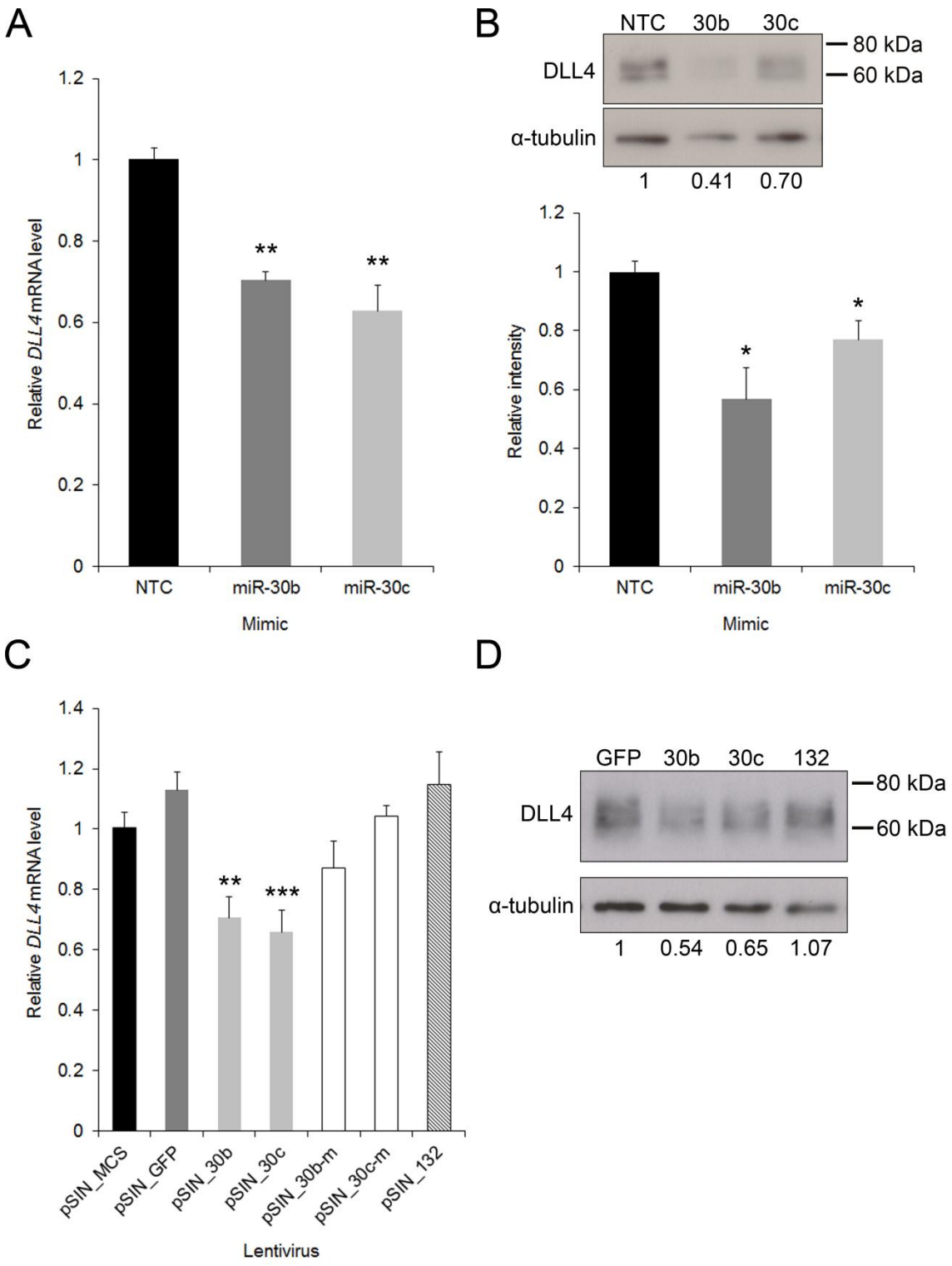

Figure 4.6. Overexpression of miR-30 causes downregulation of DLL4 in HUVEC. (A & C) *DLL4* mRNA expression in HUVEC transfected with NTC, miR-30b or -30c mimics (A) or infected with the indicated lentiviruses (C), as quantified by qRT-PCR. Means + SEM, n=4 (A) or n=6 (C). Expression is relative to NTC (A) or empty vector, pSIN_MCS (C). (B) DLL4 protein expression in HUVEC transfected with miR-30b or -30c mimics measured by Western blotting and normalised to α-tubulin expression. Upper panel: representative Western blot. Values beneath blot denote intensity of antibody ECL signal relative to NTC mimic. Molecular weight markers are represented to the right. Lower panel: intensity of antibody ECL signal relative to NTC-transfected HUVEC (means + SEM, n=3). (D) Representative Western blot showing DLL4 protein levels in HUVEC infected with GFP, miR-30b, -30c or -132 expressing lentiviruses. Values beneath blot denote intensity of antibody ECL signal relative to pSIN_GFP-infected cells. Molecular weight markers are represented to the right.*, $p<0.05$; **, $p<0.01$; ***, $p<0.001$.

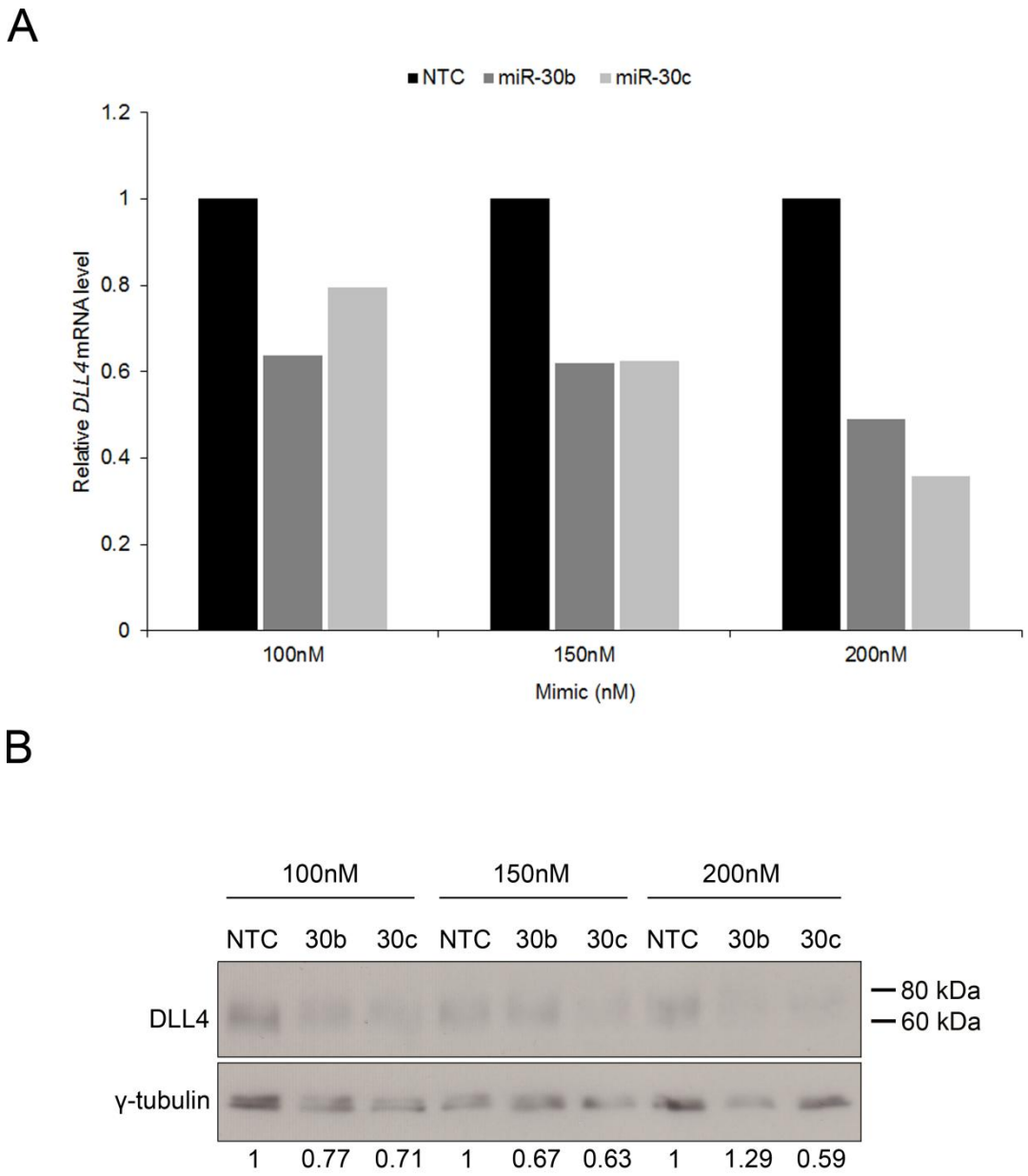

Figure 4.7. The effect of miR-30 mimic concentration on DLL4 expression in HUVEC. (A) *DLL4* mRNA expression in HUVEC transfected with NTC, miR-30b or -30c mimics at the indicated concentrations, as quantified by qRT-PCR. Expression is relative to HUVEC transfected with the equivalent concentration of NTC mimic (SEM is not shown as n=1). (B) DLL4 protein expression in HUVEC transfected with NTC, miR-30b or -30c mimics at the indicated concentrations, as measured by Western blotting. Values beneath blot denote intensity of antibody ECL signal relative to NTC mimic at the equivalent concentration. Molecular weight markers are represented to the right.

4.5. Endogenous miR-30 regulates DLL4 expression

Overexpression of miR-30b and -30 in endothelial cells, using both miRNA mimics and lentiviral infection, had proven that *DLL4* could be targeted by the miR-30 miRNA family. However, these experiments only revealed that miR-30b and -30 could suppress DLL4 expression when expressed at supra-physiological levels. To ascertain whether regulation of *DLL4* by miR-30 occurs endogenously in endothelial cells, LEC were transfected with Dharmacon miRIDIAN microRNA hairpin inhibitors (ThermoScientific) at a concentration of 100nM, again using Oligofectamine as the delivery agent.

miRNA inhibitors are synthetic RNA oligonucleotides which are complementary to a particular mature miRNA of interest. The first generation of miRNA inhibitors contained 2'-O-methyl modifications, which promoted rapid and stable hybridisation to single-strand RNA and protected the oligoribonucleotides from degradation (Hutvágner et al., 2004; Meister et al., 2004). These inhibitors were shown to successfully interact with the miRNA-RISC nucleoprotein and block target mRNA degradation (Hutvágner et al., 2004; Meister et al., 2004). The miRIDIAN hairpin inhibitors contain additional proprietary chemical modifications and secondary structural elements flanking the anti-sense miRNA sequence. These modifications have improved the ability of the inhibitors to bind to and sequester the required miRNA and allow the inhibition to be maintained for longer.

When LEC were transfected with the hairpin inhibitor against miR-30b, a slight but non-significant increase in DLL4 protein levels was observed 42 h post-transfection (Fig. 4.8A and B). When LEC were transfected with the inhibitor against miR-30c, a larger and significant increase of DLL4 protein levels was observed (Fig. 4.8A and B). This modest effect was to be expected as each inhibitor would only block the action of one member of the miR-30 family. Interestingly, when mRNA levels were quantified by qRT-PCR, an increase in *DLL4* mRNA was only observed at 72 h post-transfection (Fig 4.8C). This would suggest that miR-30b and -30 are primarily acting through translation inhibition, with mRNA degradation occurring as a secondary consequence.

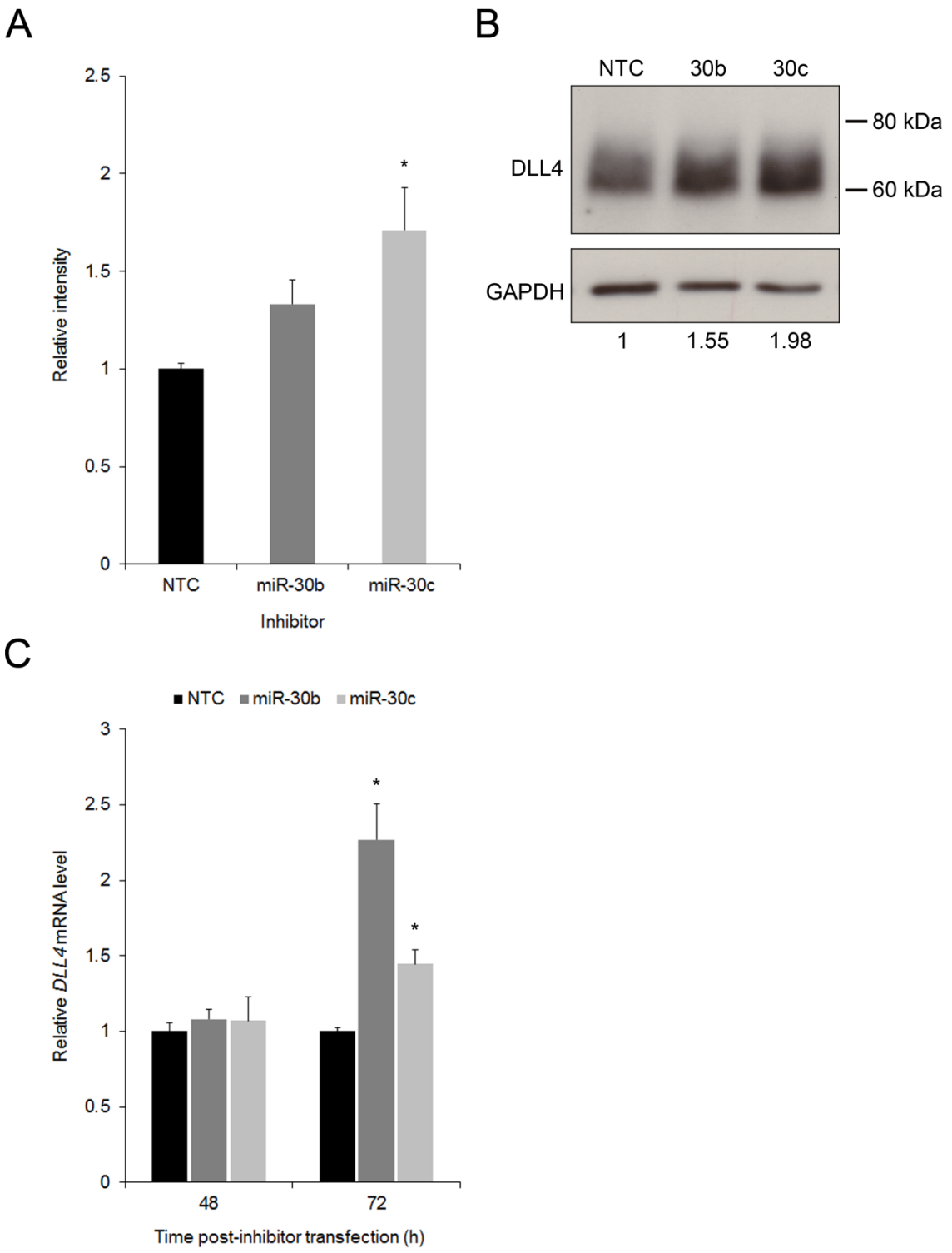

Figure 4.8. Inhibition of miR-30 causes upregulation of DLL4 in LEC. (A) DLL4 protein expression in LEC transfected with NTC, miR-30b or -30c inhibitors measured by Western blotting and normalised to GAPDH expression. Intensity of antibody ECL signal relative to NTC-transfected LEC (means + SEM, n=3). *, $p<0.05$. (B) Representative Western blot showing DLL4 protein levels in LEC transfected with NTC, miR-30b or -30c inhibitors. Values beneath blot denote intensity of antibody ECL signal relative to NTC mimic. Molecular weight markers are represented to the right. (C) *DLL4* mRNA expression in LEC transfected with NTC, miR-30b or -30c inhibitors, as quantified by qRT-PCR (means + SEM, n=2). Expression is relative to NTC transfected LEC. *, $p<0.05$.

4.6. DLL4 silencing occurs via a miR-30 target site within the 3'UTR

The loss of DLL4 suppression seen when the seed region of miR-30b and -30c were mutated had confirmed that this region of the miRNAs is required for *DLL4* targeting (Fig. 4.6C). However, this experiment did not elucidate the exact region of the *DLL4* transcript which is subject to miR-30-binding. To confirm that miR-30b and miR-30c specifically target the *DLL*4 3'UTR, a reporter plasmid was used which contained the Firefly luciferase coding sequence upstream of the *DLL4* 3'UTR (pEZX_DLL4-3'UTR), under the control of the SV40 enhancer. The plasmid also contained the *Renilla* luciferase coding sequence under the control of a separate promoter (CMV). Therefore, minor variations in transfection efficiency and cell density between samples could be controlled for by normalising firefly luciferase RLU to *Renilla* luciferase RLU. This construct was expressed in 293T cells in the presence of miR-30b- or -30c mimics and a 50% reduction in luciferase activity was observed when compared to NTC mimic-transfected cells (Fig. 4.9A). The control plasmid (pEZX-MT01) maintained luciferase activity in the presence of exogenous miR-30, suggesting the changes in activity were due to the action of miR-30 on the *DLL4* 3'UTR. To identify the exact site of miR-30 binding the predicted miR-30 target site in the *DLL4* 3'UTR was mutated (see Section 2.3.8) to prevent miRNA association (pEZX_DLL4-3'UTR-mut). Luciferase activity was significantly increased to near-baseline levels in cells transfected with the mutant plasmid (Fig. 4.9A), confirming that miR-30 silencing occurs via the predicted target site.

A

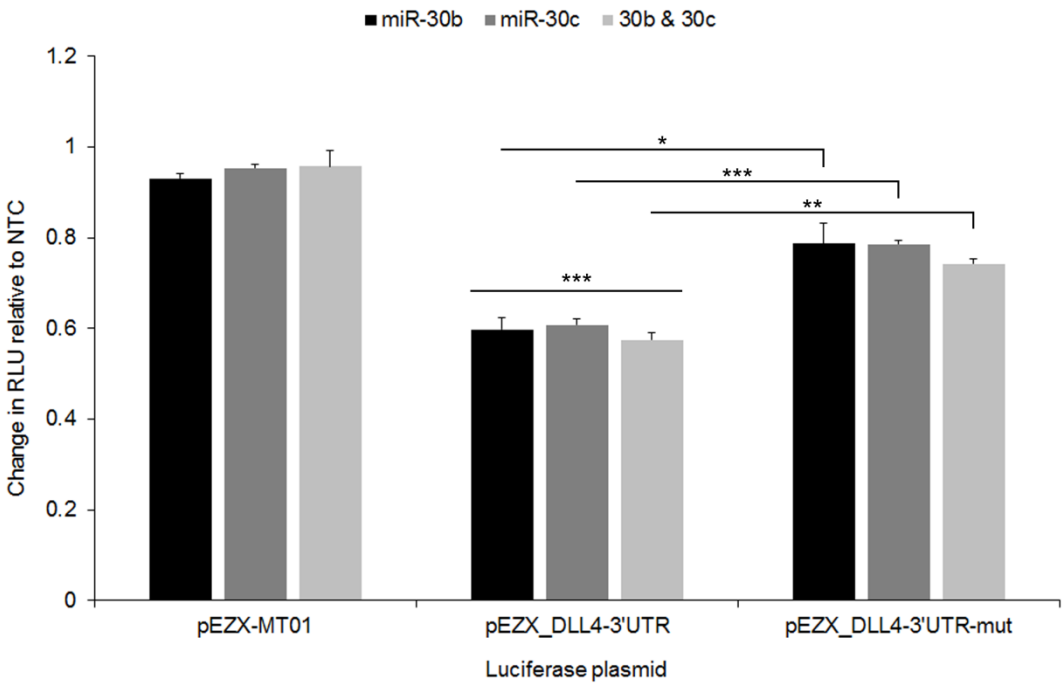

Figure 4.9. Confirmation of predicted miR-30 target site within the *DLL4* 3'UTR (A) Reporter assay indicating the response of wildtype or mutant (mut) *DLL4* 3'UTR to miR-30b and -30c mimics in 293T cells (means + SEM, n=3). Firefly expression was normalised to Renilla expression to give the relative light units (RLU), which are shown relative to NTC mimic. pEZX-MT01 is a control reporter, lacking a 3'UTR sequence but containing the Firefly and Renilla luciferase genes. Related statistically significant values are indicated by horizontal bars *, $p<0.05$; **, $p<0.01$; ***, $p<0.001$.

4.7. Overexpression of miR-30 attenuates upregulation of DLL4 in KLEC

The link between miR-30 and DLL4 was first identified in KLEC due to the downregulation of miR-30 and upregulation of DLL4 in these cells. This induction of DLL4 in KLEC is well characterised and has been attributed to the viral gene viral G-protein coupled receptor (*vGPCR*) acting through an extracellular-signal-regulated kinase (ERK)-dependent mechanism (Emuss et al., 2009). It was hypothesised that suppression of the miR-30 family in KLEC could contribute to the observed increase in *DLL4* mRNA and protein levels. To test this theory, LEC were infected with pSIN_MCS, pSIN_30b or pSIN_30c and then after 48 h half the cells were also infected with KSHV. All cells were harvested 96 h post-lentivirus infection (48 h post-KSHV infection). *DLL4* mRNA expression was increased 3-fold in pSIN_MCS infected KLEC compared to pSIN_MCS infected LEC (Fig. 4.10A), which was comparable to previously reported levels of *DLL4* induction (Emuss et al., 2009). However, this induction was attenuated to 2-fold in KLEC expressing exogenous miR-30 (Fig. 4.10A). This was also reflected at the protein level where KSHV infection induced a 5-fold increase in DLL4 that was reduced to 4-fold in pSIN_30c transduced cells (Fig. 4.10B).

Having determined that miR-30 suppression can modulate DLL4 induction in KLEC, miR-30b and -30c expression was quantified in LEC transduced with the KSHV gene *vGPCR*, to ascertain whether *vGPCR* expression results in downregulation of these two miRNAs. Expression of *vGPCR* did not influence miR-30b or miR-30c levels in LEC, either 24 h, 48 h or 72 h post-transduction (Fig. 4.11A). Therefore *vGPCR*-induced upregulation of DLL4 does not occur by way of the regulation of the miR-30 family.

It has previously been reported that miR-30b and miR-30d are upregulated in response to hypoxia (Herbert et al., 2007; Hua et al., 2006; Kulshreshtha et al., 2007). However, these findings are all based on microarrays and have not been confirmed using qRT-PCR. In addition, another family member, miR-30e, is reported to be downregulated in hypoxic conditions (Herbert et al., 2007).

A

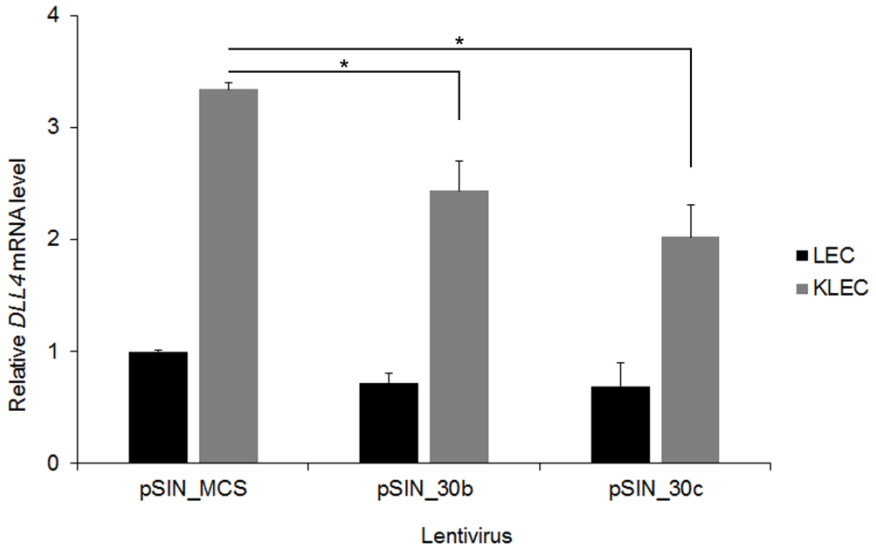

B

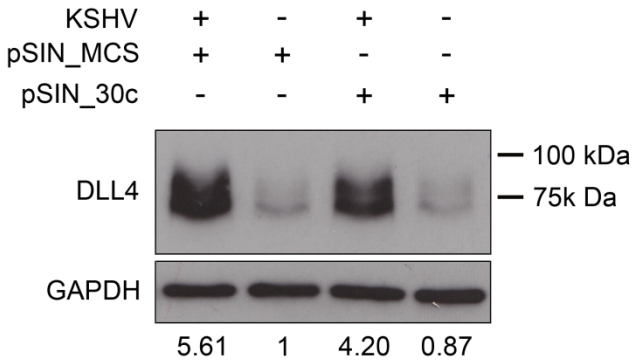

Figure 4.10. Changes in DLL4 expression upon overexpression of miR-30 in KLEC. (A) *DLL4* mRNA expression in LEC or KLEC infected with miR-30b- and miR-30c-expressing lentiviruses, as measured by qRT-PCR (means + SEM, n=3). Expression is relative to LEC infected with empty vector, pSIN_MCS. Related statistically significant values are indicated by horizontal bars (*, $p<0.05$). (B) DLL4 protein expression in LEC measured by Western blotting. Values beneath blot denote intensity of DLL4 antibody ECL Plus signal normalised to GAPDH antibody ECL signal and relative to KSHV-/pSIN_MCS+. Molecular weight markers are represented to the right. Western blotting was performed by Dimitra Georgopoulou.

A

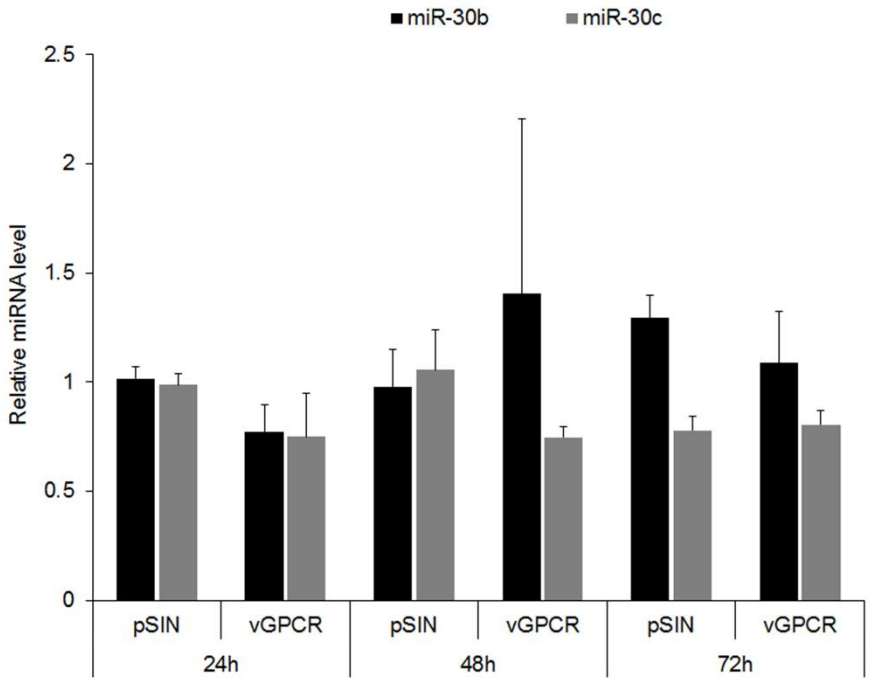

B

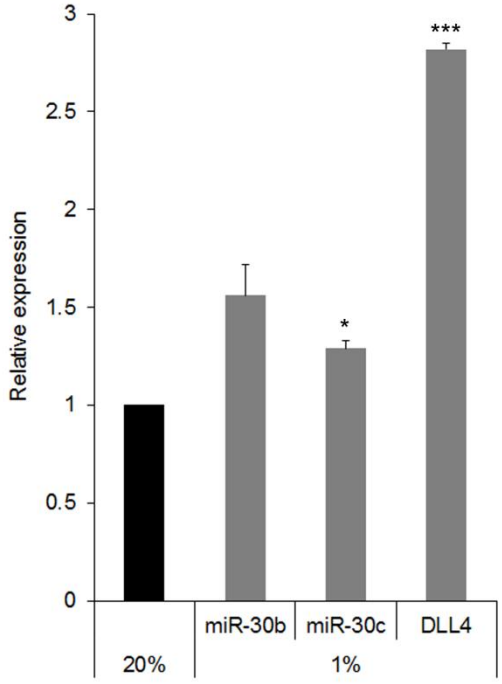

Figure 4.11. The effect of *vGPCR* expression and hypoxia on miR-30b and -30 levels. (A) miR-30b and miR-30c expression in LEC transduced with *vGPCR* at the indicated time points, as quantified by qRT-PCR (means + SEM, n=2). Expression is relative to empty vector, pSIN_MCS. (B) miR-30b, miR-30c and *DLL4* mRNA expression in LEC grown at 1% oxygen for 24 h, as quantified by qRT-PCR (means + SEM, n=2). Expression is relative to LEC grown at 20% oxygen for the same time period. (*, $p<0.05$; ***, $p<0.001$).

Given the important influence hypoxia has on angiogenesis, and to clarify whether the miR-30 family is regulated by hypoxia, miR-30b and -30c expression was quantified in hypoxic LEC. A slight increase in both miR-30b and miR-30c was observed in LEC exposed to 1% oxygen, but this increase was only significant for miR-30b (Fig. 4.11B). DLL4 is known to be upregulated by hypoxia in endothelial cells (Diez et al., 2007) and an increase of 2.5-fold was observed in LEC exposed to 1% oxygen (Fig. 4.11B). If the miR-30 family were involved in the induction of DLL4 during hypoxic conditions a reduction in miR-30b and -30c expression would be seen, which was not observed (Fig. 4.11B).

4.8. miR-30b promotes sprouting angiogenesis *in vitro*

To investigate the effect of miR-30 overexpression on endothelial cell function the Matrigel tube formation assay was first employed. Previous work had shown that overexpression of DLL4 in HUVEC using a retroviral vector impaired the ability of the cells to form the characteristic network of orderly branching cordlike structures when plated onto the surface of Matrigel (Williams et al., 2006). Compared to the HUVEC infected with GFP-expressing retrovirus, the DLL4 overexpressing HUVEC formed fewer cord-like structures and the network was often incomplete (Williams et al., 2006). I hypothesised that in the reverse scenario, when DLL4 was downregulated by exogenous miR-30, an increase in network formation would be observed.

Before embarking on the complete experiment, the assay conditions were optimised. Both HUVEC and LEC were plated on complete Matrigel in a 96-well plate at densities of 5000, 7500 and 10,000 cells per well and 24 h later the wells were photographed in order to examine network formation. Cord-like structures were observed at all three cell densities for both cell types (Fig. 4.12); however, LEC required 10,000 cells per well to obtain a complete network of branching cords, whereas network formation was evident for the HUVEC at 5000 cells per well (Fig. 4.12). 10,000 cells per well was an excessive number for the HUVEC, as at this cell density single cells began to cluster around the branch points of the network, without being incorporated into the cords (Fig. 4.12).

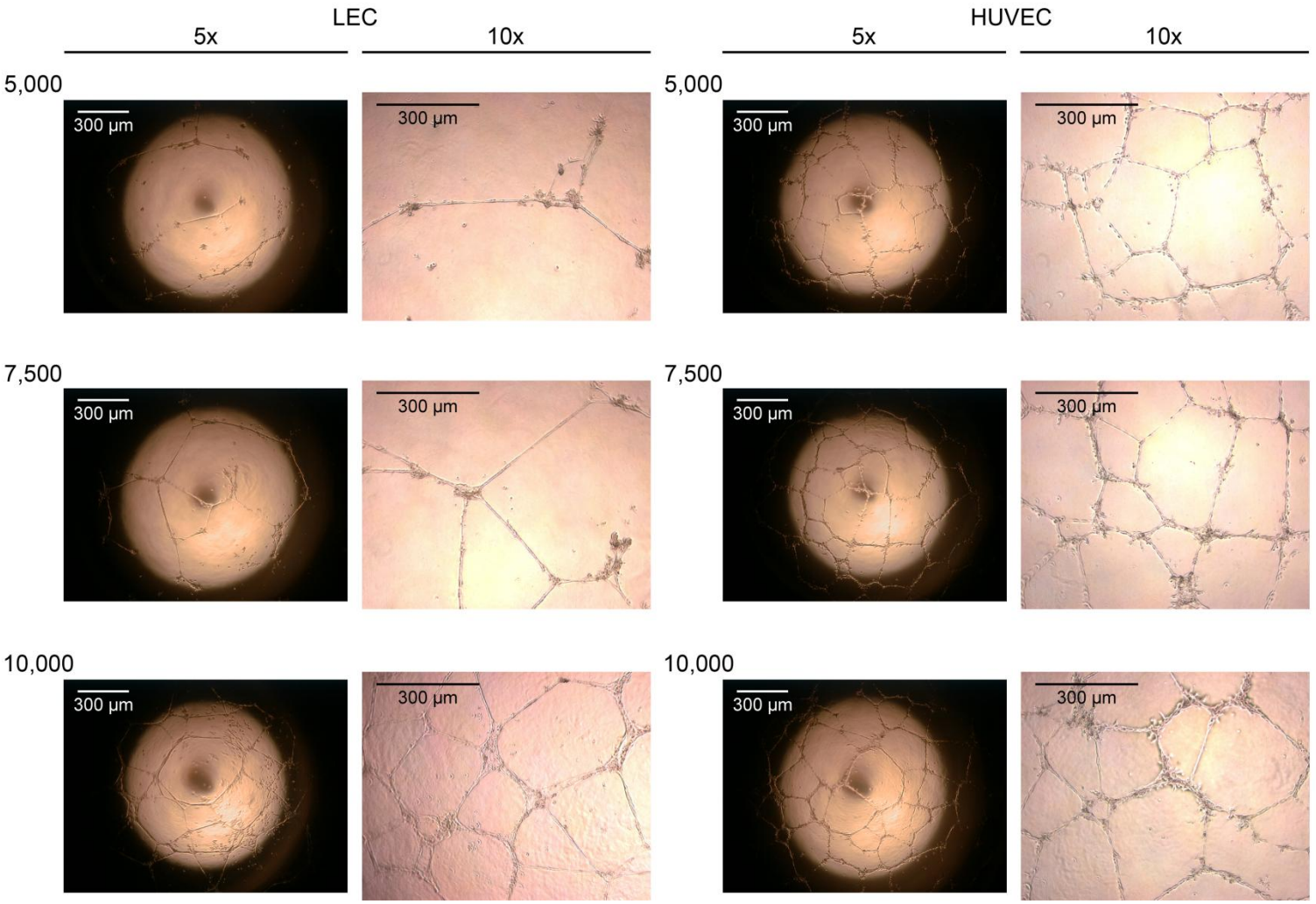

Figure 4.12. Optimising cell densities for Matrigel tube formation assay. Representative images of a tube formation assay performed with LEC and HUVEC. Photos taken at 5x and 10x magnification, 24 h after cells were plated on Matrigel. Values indicate number of cells per well of a 96-well plate.

It was therefore decided that in order to be able to properly assess the effect of any agents on network formation, the LEC would be plated out at 7500, 10,000 and 12,500 cells per well whilst the HUVEC would be plated out at 2500, 5000 and 7500 cells per well.

The aim of the Matrigel tube formation assay experiment was to assess the effect of miR-30-induced *DLL4* downregulation on endothelial cell function. A siRNA against *DLL4* was used as a positive control for DLL4 knockdown. The ON-TARGETplus siRNA for DLL4 was obtained from Dharmacon (ThermoScientific) and transfected into LEC and HUVEC at a final concentration of 100nM using Oligofectamine as the delivery reagent. This resulted in a ~70% reduction in *DLL4* mRNA in LEC 48 h post-transfection when compared to NTC-transfected cells and a ~40% reduction in HUVEC at the same time point (Fig. 4.13A). The observed downregulation of *DLL4* mRNA was concordant with a ~60% reduction in DLL4 protein levels at the same time point (Fig. 4.13B). The downregulation of DLL4 mRNA and protein was still evident at 72 h post-transfection and DLL4 protein reduction in HUVEC actually increased to 80% (Fig. 4.13A and B). This was beneficial for the purposes of the Matrigel tube formation assay, as it meant the cells could be given suitable recovery period before being plated on the Matrigel, whilst still maintaining DLL4 knockdown.

LEC and HUVEC were transfected with NTC and DLL4 siRNA at a concentration of 100nM and then trypsinised and counted 48 h post-transfection. The cells were plated on Matrigel at the cell densities determined during assay optimisation and 20 h later the wells were photographed to assess network formation (Fig. 4.14). For both LEC and HUVEC, at all three cell densities, DLL4 knockdown prevented tube formation (Fig. 4.14). It is probable that the effect of the Oligofectamine and exogenous small RNA had a negative impact on tube formation, as NTC-transfected LEC and HUVEC displayed impaired tube formation at cell densities which were previously compatible to network formation (10,000 and 5000 cells per well respectively).

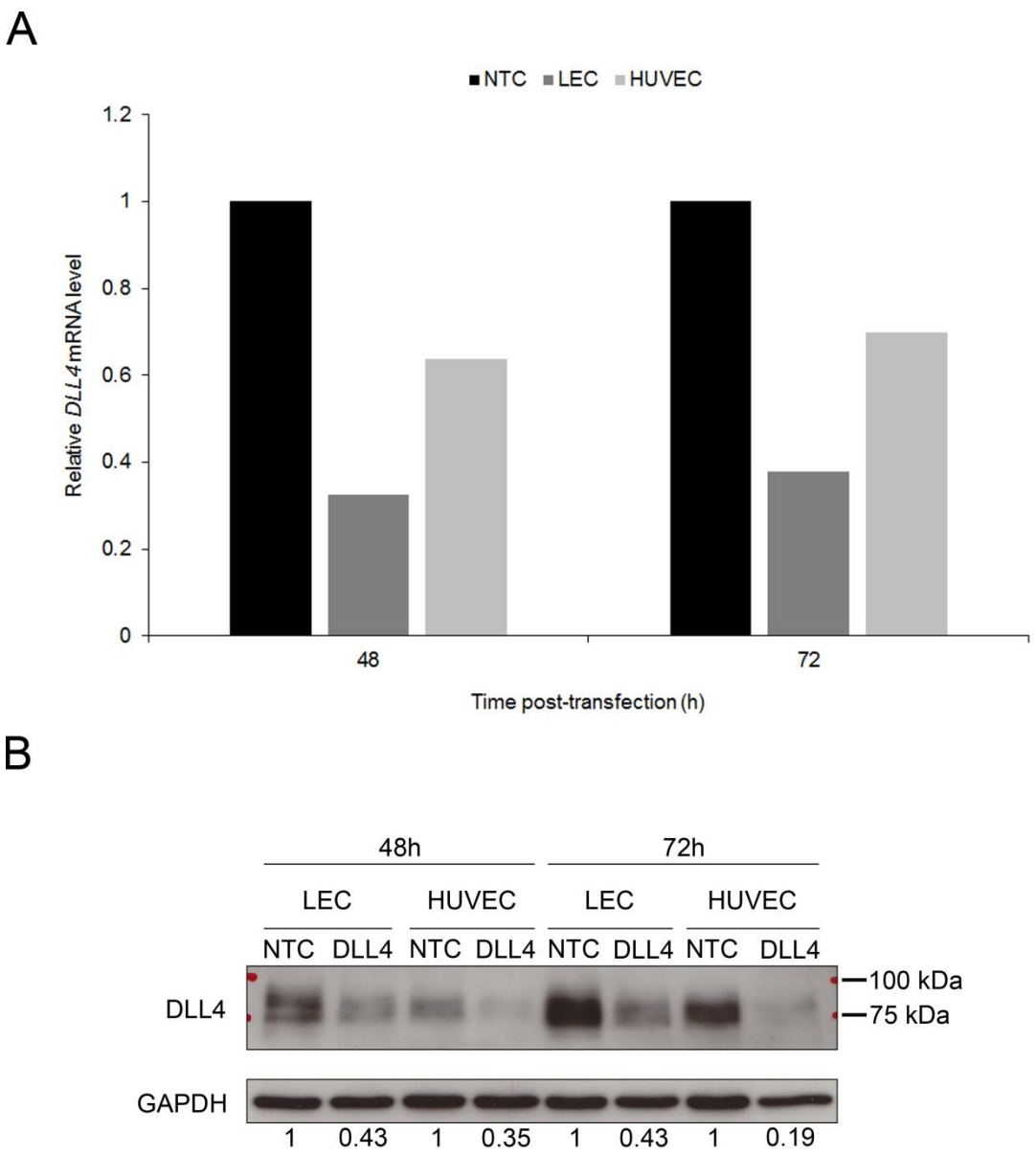

Figure 4.13. Confirmation of DLL4 knockdown using siRNA in endothelial cells. (A) Downregulation of *DLL4* mRNA in LEC and HUVEC, 48 h and 72 h following transfection with NTC and DLL4 siRNA, as quantified by qRT-PCR. Expression is relative to cells transfected with NTC mimic (SEM is not shown as n=1). (B) Downregulation of DLL4 protein in LEC and HUVEC, 48 h and 72 h following transfection with NTC and DLL4 siRNA, as quantified by Western blotting. Values beneath blot denote intensity of DLL4 antibody ECL Plus signal normalised to GAPDH antibody ECL signal and relative to NTC mimic. Molecular weight markers are shown to the right.

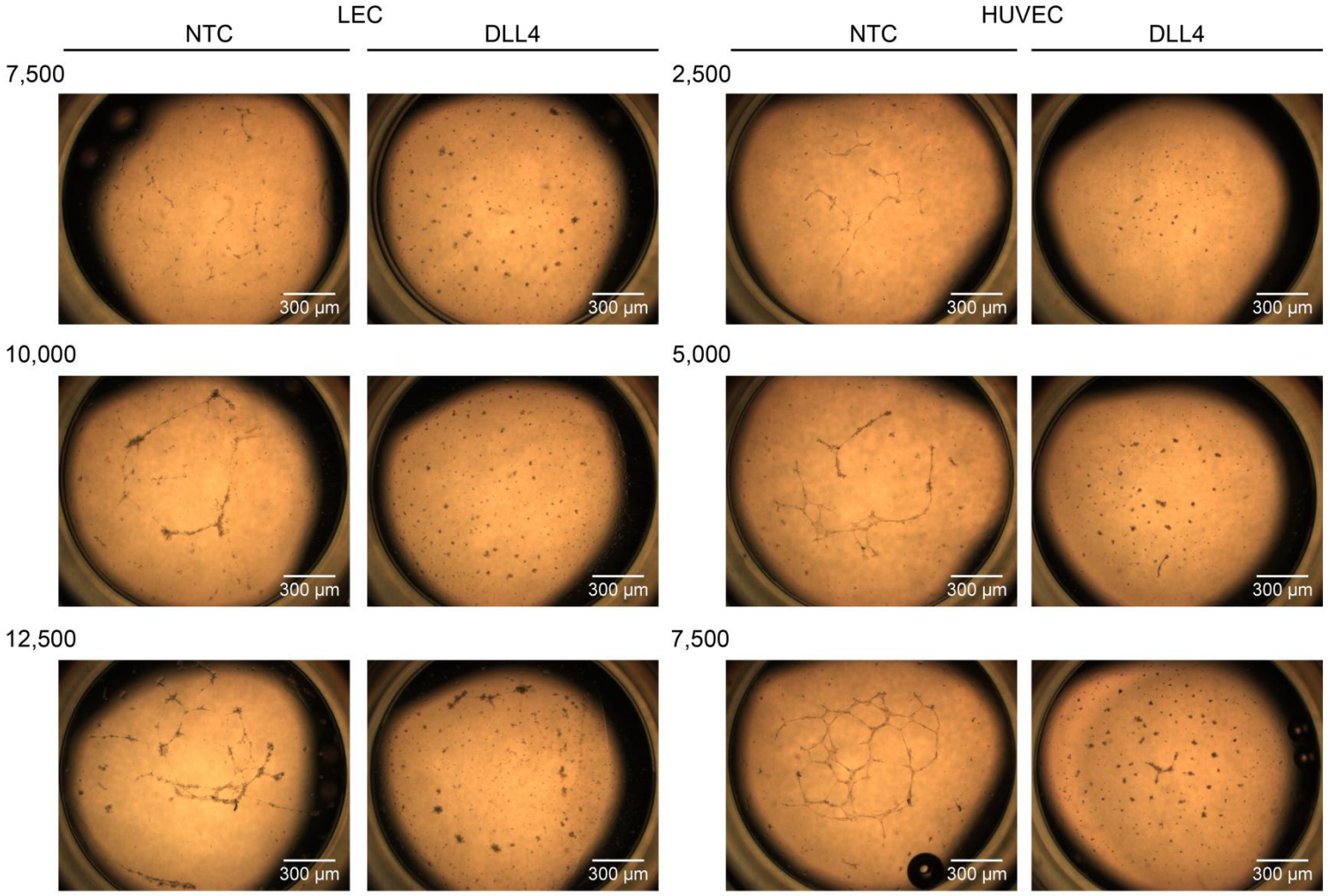

Figure 4.14. Knockdown of DLL4 inhibits tube formation in endothelial cells. Representative images of a tube formation assay performed with LEC and HUVEC 48 h post-transfection with NTC and DLL4 siRNA. Photos taken at 5x magnification, 20 h after cells were plated on Matrigel. Values indicate number of cells per well of a 96-well plate.

However, at the highest cell densities, the NTC-transfected cells displayed clear cord-like structures, whereas the siRNA-transfected cells had only managed to gather in small clusters (Fig. 4.14). From discussions with Professor Adrian Harris (University of Oxford) and further examination of the literature it was determined that, whilst overexpression of DLL4 in endothelial cells impairs tube formation (Williams et al., 2006), a decrease in the basal level of DLL4 also decreased network formation (Patel et al., 2005). These contradictory observations are due to the different roles of DLL4 at varying expression levels. When overexpressed, DLL4 inhibits the proliferative and migratory responses to VEGF-A by downregulating VEGFR2 expression (Williams et al., 2006); a downregulation of DLL4 inhibits basal endothelial cell proliferation (Patel et al., 2005).

Further discussions with Professor Adrian Harris revealed it would be better to use a spheroid-based *in vitro* angiogenesis assay to assess the effect of miR-30 on endothelial cell function. The Matrigel tube formation assay depends on endothelial cell migration, as cells migrate into cord-like structures. This is similar to the formation of the primary vessels during developmental vasculogenesis in zebrafish embryos when angioblasts migrate towards the midline of the embryo where they coalesce to form a vascular cord (Ellertsdóttir et al., 2010). The spheroid-based cellular angiogenesis assay more closely resembles sprouting angiogenesis as endothelial cells sprout from the spheroid to form vessel-like structures (Alajati et al., 2008).

HUVEC were transfected with NTC or miR-30b mimics and 24 h post-transfection they were collected and induced to form spheroids by suspension in hanging droplets for 24 h. These spheroids were then collected, embedded in Matrigel and monitored for up to 5 days. Spheroids comprised of miR-30b overexpressing HUVEC displayed an increased propensity to form sprouts, as can be seen from the representative photographs (Fig 4.15; left-hand panels) and the quantification of sprouts per spheroid (Fig. 4.15; middle panels). This phenotype was maintained for 5 days, at which point the sprouts began to regress. Furthermore, the sprouts from the miR-30b-expressing spheroids were significantly longer (Fig 4.15; right-hand panels). These studies demonstrated that miR-30 overexpression in endothelial cells increases their angiogenic

potential. *DLL4* mRNA suppression was confirmed by qRT-PCR in a small sample of miR-30-transfected HUVEC which were isolated prior to spheroid formation (data not shown).

Having optimised the spheroid-based cellular angiogenesis assay, it seemed appropriate to also investigate sprouting angiogenesis upon KSHV infection of HUVEC, which has not yet been reported (Fig. 4.16). HUVEC were infected with KSHV during spheroid formation and then the spheroids were embedded in Matrigel and monitored for 96 h. At all three time points, KSHV-infected HUVEC generated significantly more sprouts per spheroid, which were of a longer length than those from uninfected spheroids (Fig. 4.16). The difference in sprout frequency was most clearly seen at 24 h. By 96 h, the sprouts from both spheroids had started to regress, so the overall sprouts numbers were decreased (Fig. 4.16). However, the KSHV-infected HUVEC sprouts were still significantly longer (Fig. 4.16). These findings concur with previous work, in which KLEC were shown to possess an increased propensity to form capillary-like sprouts when compared with uninfected LEC, in the presence of both VEGFA or VEGFC (Cheng et al., 2011). The HUVEC used in this work were grown in media containing VEGF and 3D tubular sprouts were also observed (Fig. 4.16).

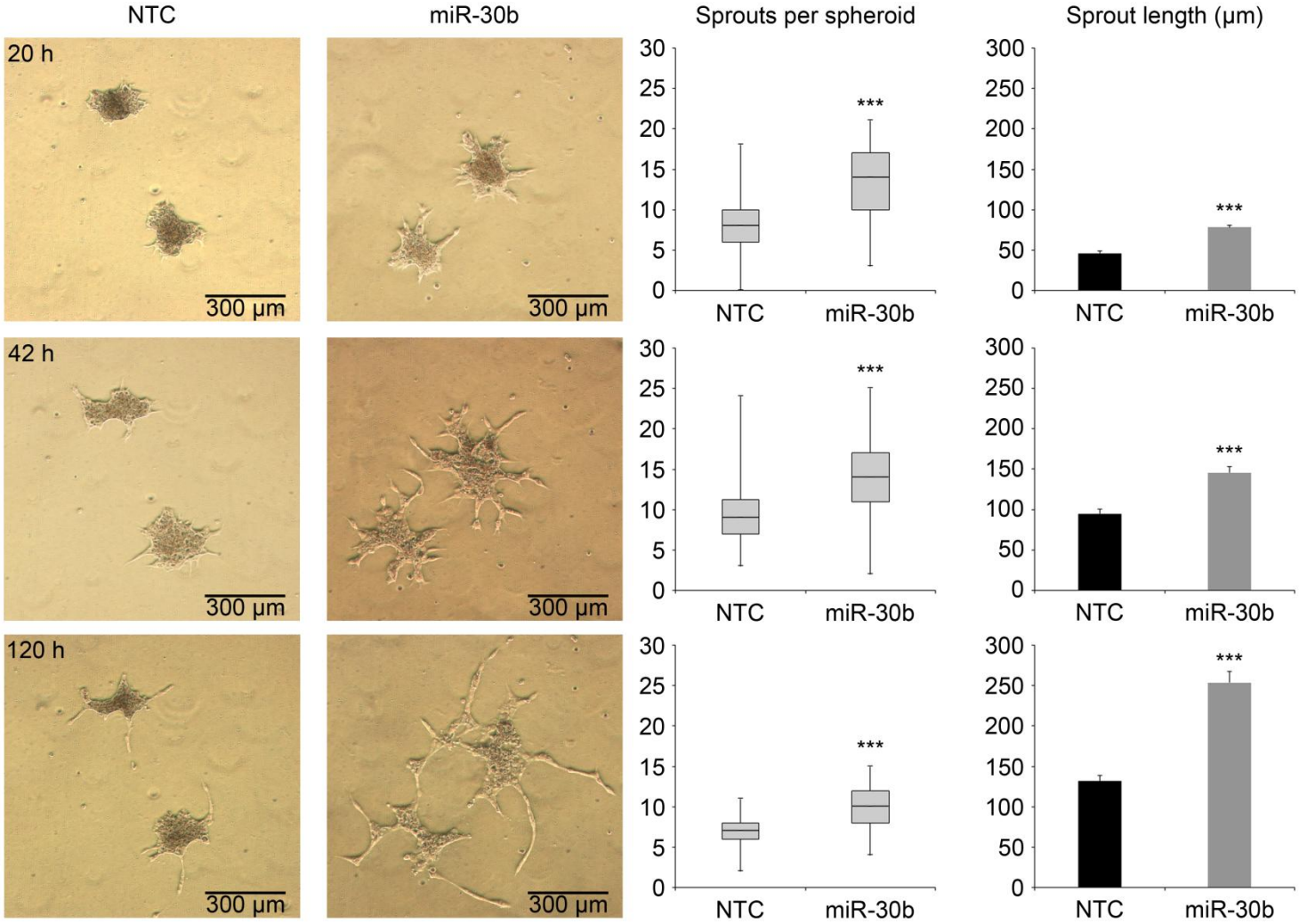

Figure 4.15. Overexpression of miR-30b promotes sprouting angiogenesis *in vitro*.
Left-hand panels: representative photographs at indicated time points of HUVEC spheroids embedded in Matrigel. HUVEC were transfected with indicated mimic before being induced to form spheroids. Middle panels: quantification of total sprouts per spheroid (y-axis) at indicated time points (n=60). Box plot indicates inter-quartile range, whiskers indicate total range, black line denotes median. Sprouts were counted using Adobe Photoshop CS2. The difference between NTC-transfected and miR-30-transfected spheroids was significant (***, $p<0.001$). Right-hand panels: quantification of average sprout length in µm (y-axis) (means + SEM, n=20). Average sprout length was measured using the segmented line tool in Image J (NIH). Five sprouts were measured per spheroid. The difference between NTC-transfected and miR-30b transfected cells was significant (***, $p<0.001$).

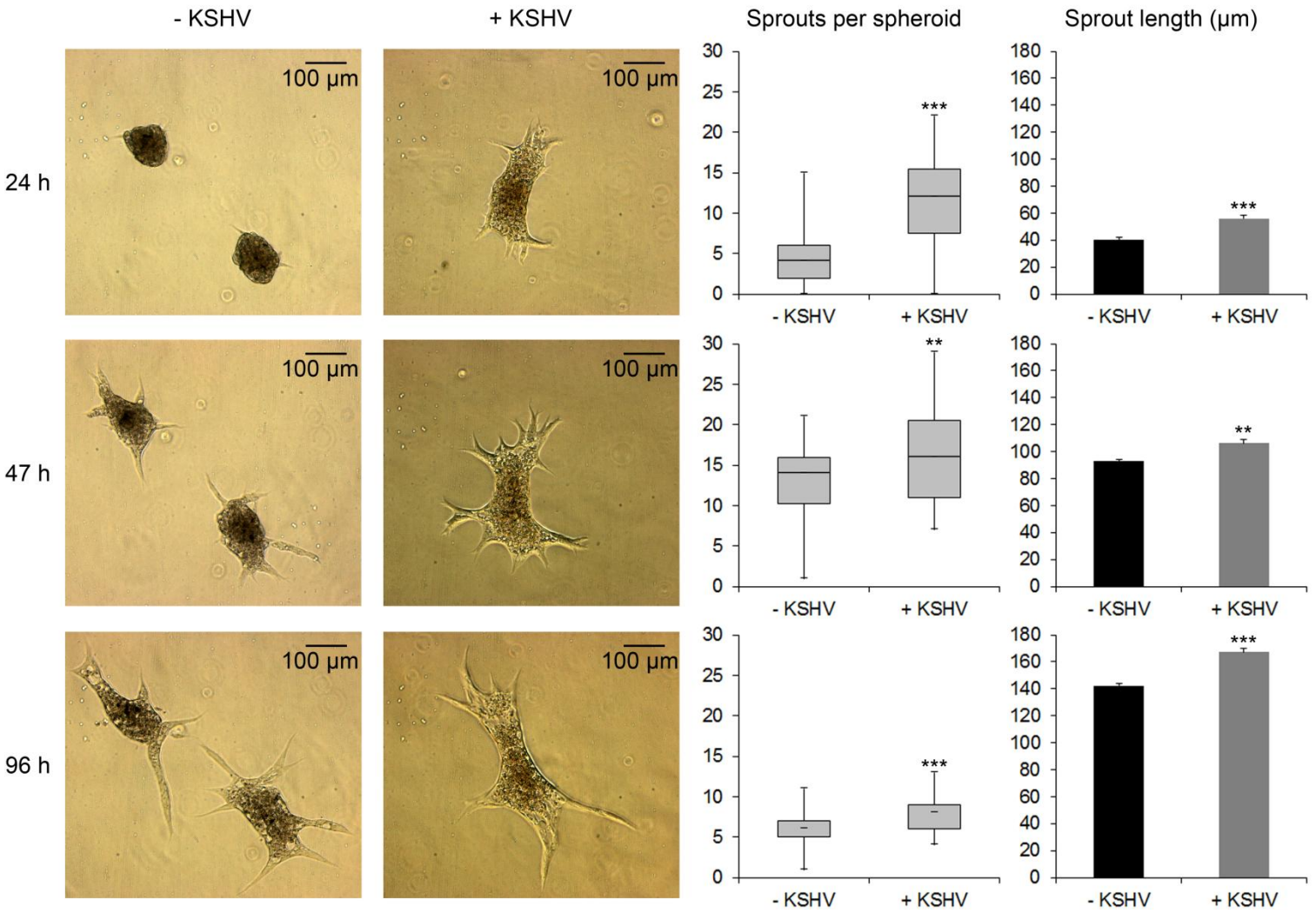

Figure 4.16. KSHV infection of HUVEC promotes sprouting angiogenesis *in vitro*. Left-hand panels: representative photographs at indicated time points of uninfected and KSHV-infected HUVEC spheroids embedded in Matrigel. HUVEC were infected with KSHV before being induced to form spheroids. Middle panels: quantification of total sprouts per spheroid (y-axis) at indicated time points (n=35-50). Box plot indicates inter-quartile range, whiskers indicate total range, black line denotes median. Sprouts were counted using Adobe Photoshop CS2. The difference between non-infected and KSHV-infected spheroids was significant (**, $p<0.01$; ***, $p<0.001$). Right-hand panels: quantification of average sprout length in µm (y-axis) (means + SEM, n=20-45). Average sprout length was measured using the segmented line tool in Image J (NIH). Five sprouts were measured per spheroid. The difference between NTC-transfected and miR-30b transfected cells was significant (**, $p<0.001$; ***, $p<0.001$).

4.9. Discussion

DLL4 mRNA was downregulated by 50 to 70% in LEC or HUVEC, when transfected with miR-30 mimics or transduced with pre-miR-30b or -30c; this led to a similar reduction in DLL4 protein levels. This level of repression is comparable to other validated miRNA targets. During development *DLL4* haploinsufficiency results in embryonic lethality (Gale et al., 2004), indicating that the developing vasculature is sensitive to minor alterations in DLL4 dosage. Therefore, a reduction in DLL4 of the magnitude described would be expected to have a significant impact on endothelial cell behaviour during development and in other biological systems.

DLL4 protein was upregulated by 1.5 to 2-fold in LEC transfected with hairpin inhibitors of miR-30b or miR-30c. This indicates that endogenous miR-30 actively regulates *DLL4* in endothelial cells, as inhibition of miR-30 family members would release *DLL4* mRNA from miR-30-directed RISC targeting, thereby preventing translation inhibition and mRNA degradation. The protein increase is fairly modest, which is expected if *DLL4* were regulated by all members of the miR-30 family, as each inhibitor should only block one family member. This theory could be tested by simultaneously transfecting inhibitors of two or more miR-30 family members and examining DLL4 protein expression. If this level of redundancy exits, it would highlight the importance of sensitive regulation of DLL4 expression.

Exogenous miR-30 suppressed luciferase activity, and hence expression, when the Firefly luciferase coding sequence was expressed upstream of the *DLL4* 3'UTR. Disruption of the predicted miR-30 target site within the *DLL4* 3'UTR using site directed mutagenesis almost abolished miR-30-directed silencing of this luciferase reporter. These data confirm that the miR-30 family is able to direct miRISC to the *DLL4* 3'UTR and instigate target suppression via binding to one particular target site. When miR-30b and -30c were co-expressed at an equivalent total concentration, luciferase activity was not suppressed further, indicating that both these family members act through the same target site(s). However, mutation of the predicted miR-30 target site did not entirely rescue the repression of luciferase activity. It is possible that a residual level of targeting

occurred through this site due to the extensive 3' complementarity exhibited by miR-30b and miR-30c. Alternatively, the miR-30 family may also act through a non-canonical target site within the *DLL4* 3'UTR. Both "seedless" and "centred" miRNA target sites have been identified (Lal et al., 2009; Shin et al., 2010). More recently, differential CLIP-seq has revealed that for one particular miRNA, miR-155, 40% of miRNA-dependent Argonaute binding occurs at sites containing at least one seed mismatch and that these non-canonical sites enable modest regulation of gene expression (Loeb et al., 2012). The *DLL4* 3'UTR does not contain a centred site for miR-30, which is defined as 11 contiguous nucleotides that pair to positions 4-14 or 5-15 of the miRNA. However, it does contain four predicted non-canonical sites: one 8mer, one 7mer and two 6mer sites, each containing one nucleotide mismatch or G:U wobble. One or several of these non-canonical sites could account for the low level of residual luciferase suppression observed following mutation of the canonical 8mer target site. This could be investigated by disrupting each of the non-canonical sites in the pEZX_*DLL4*-3'UTR-mut background using site-directed mutagenesis. If mutation of one or more of these sites completely removes luciferase suppression in the presence of exogenous miR-30, it would confirm the role of non-canonical targeting of *DLL4* by miR-30.

Overexpression of miR-30b or miR-30c attenuated KSHV-induced DLL4 upregulation *in vitro*. However, as overexpression of *vGPCR* did not downregulate miR-30b or miR-30c, the suppression of the miR-30 family in KLEC cannot be attributed to the reported viral signalling pathway which leads to DLL4 upregulation (Emuss et al., 2009). It is possible that viral induced downregulation of miR-30 is a secondary mechanism by which DLL4 is upregulated, independent of the action of *vGPCR*. To confirm this, miR-30 levels would need to be returned to baseline in KLEC, which proved technically challenging using lentiviral delivery. A small degree of miR-30 overexpression was always observed (~10 fold compared to KLEC/pSIN); hence the attenuation of DLL4 could simply reflect the ability of miR-30 to regulate DLL4, even in a system where it is upregulated.

The current literature confers contradictory information with regards to the regulation of the miR-30 family in response to hypoxia. miR-30b is reported to

be upregulated in hypoxic conditions, whereas miR-30e is downregulated (Herbert et al., 2007; Hua et al., 2006; Kulshreshtha et al., 2007). Given that all miR-30 family members share common targets, it might be expected for them to be regulated in a co-ordinated manner by hypoxia, as is seen following KSHV infection of LEC. In all studies where miR-30 expression was reported to change following hypoxia, expression was assessed by miRNA microarray, but not confirmed by qRT-PCR. Using qRT-PCR, I found that exposure of LEC to hypoxic conditions only increased miR-30b and miR-30c levels by 1.25-1.5 fold, and this minor increase was only significant for miR-30c. This suggests that hypoxic signalling does not have a major impact on miR-30 expression, and that changes in miR-30 expression do not contribute to the induction of DLL4 following hypoxia, which was previously attributed to HIF1A-mediated activation of the DLL4 promoter (Diez et al., 2007).

A putative promoter of pri-miR-30a has been identified (Fujita and Iba, 2008). Studies have also shown the promoters of pri-miRNA transcripts are usually found within 1000bp upstream of the transcription start site. Therefore the putative promoters or upstream regions of pri-miR-30a, pri-miR-30b/pri-miR-30d (clustered miRNAs), pri-miR-30c-1/pri-miR-30e (clustered miRNAs) and pri-miR-30c-2 were analysed using MAPPER to identify potential transcription factor binding sites (Marinescu et al., 2005). Whilst several transcription factor binding sites were predicted, a transcription factor binding site common to all the members of the family could not be identified. It is therefore possible that the altered expression of miR-30 family members following KSHV infection is due to regulation at the level of pri-miRNA or pre-miRNA processing, rather than transcriptional regulation.

Several different proteins have been identified that influence the processing of either one specific miRNA or a group of similarly regulated miRNAs. The most extensively studied of these is the RNA-binding protein Lin28 which regulates the production of the Let-7 family of miRNAs, particularly during development (Viswanathan and Daley, 2010). Lin28 binds to conserved nucleotides in the loop region of pri-let7 which prevents Drosha processing of the pri-miRNA (Newman et al., 2008). The miR-30 family pri-miRNAs and/or pre-miRNAs may

also contain a conserved RNA-binding protein sequence which allows collective regulation of the family.

Not all miRNA regulation by RNA-binding proteins is inhibitory: SMAD proteins bind to a conserved sequence found within ~20 pri-miRNAs to promote Drosha processing in response to transforming growth factor β (TGFβ)/bone morphogenetic protein (BMP) signalling (Davis et al., 2010). In addition to directly binding to precursor miRNAs, some proteins regulate miRNA maturation indirectly. Cellular tumour antigen p53 (p53) interacts with the Drosha processing complex to enhance the maturation of a group of "growth-suppressive" miRNAs (Suzuki et al., 2009). Ataxia-telangiectasia mutated (ATM) induces the biogenesis of approximately one-fourth of miRNAs by phosphorylating the KH-type splicing regulatory protein (KSRP), leading to enhanced interaction between KSRP and pri-miRNAs (Zhang et al., 2011). KSRP is a component of both the Drosha and Dicer complexes and binds to the terminal loop of pri-miRNAs to promote their cleavage (Trabucchi et al., 2009). Interestingly, miR-30a, miR-30c and miR-30d expression was reduced when KSRP was knocked-down in HeLa cells and these miRNAs are induced in ATM +/+ cells in response to DNA damage, but not in ATM -/- cells (Trabucchi et al., 2009; Zhang et al., 2011). However, a KSRP-based mechanism could not account for the upregulation of miR-30b in KLEC and a common regulatory pathway for all miR-30 family members has yet to be identified.

Overexpression of miR-30b in HUVEC promoted sprouting from Matrigel-embedded spheroids. The sprouts which developed from the miR-30-transfected spheroids were also of a greater length, compared to the NTC-transfected spheroids. This is consistent with the known role of DLL4 during angiogenesis. DLL4 is thought to control angiogenic sprouting, in part through the regulation of VEGF signalling and tip cell specification. Therefore, the increased sprouting observed from miR-30b expressing spheroids is most likely due to the concomitant decrease in DLL4 in these cells. To confirm this, I attempted to express a DLL4 construct lacking the 3'UTR in HUVEC using lentiviral infection. This construct would be immune to miR-30b targeting and therefore sufficient DLL4 expression would be maintained in these cells to regulate tip cell specification. However, I was not able to develop a transfection

protocol that was compatible with lentiviral infection, in order to carry out this experiment. Recently, *in vitro* target protectors have been developed that enable inhibition of miRNA interaction with a specific target. This technique would allow future investigations into the mechanism behind the increased sprouting observed in miR-30b expressing HUVEC. Inhibition of *DLL4* targeting by miR-30 would be expected to rescue the pro-angiogenic phenotype.

The spheroid assay was also used to investigate *in vitro* sprouting upon KSHV infection of HUVEC. KSHV-positive spheroids displayed significantly more sprouts, which were of a longer length than those from uninfected spheroids. These findings highlight the complex signalling milieu at work in KSHV-infected endothelial cells. Although DLL4 is upregulated upon KSHV infection, which would be expected to inhibit sprouting angiogenesis, a multitude of other pro-angiogenic factors are also upregulated and appear to increase the angiogenic potential of KSHV-infected HUVEC (Vart et al., 2007).

Chapter 5. miR-30-mediated regulation of *dll4* affects endothelial cell behaviour during zebrafish development.

5.1. Aims

The work described in Chapter 4 showed that DLL4 expression is actively suppressed by miR-30 in endothelial cells and that upregulation of miR-30 in these cells increases their angiogenic potential *in vitro*. However, regulation in the *in vitro* context does not always directly translate to the *in vivo* setting. Therefore, the aims of this final chapter were:

i. To ascertain whether active regulation of DLL4 by miR-30 occurs *in vivo.* This will be achieved by both overexpressing miR-30 in zebrafish embryos using microinjection of miRNA mimics and disrupting endogenous miR-30/*dll4* targeting using target protector morpholinos (TPs). The subsequent expression of zebrafish *dll4* will be monitored using qRT-PCR and *in situ* hybridisation.

ii. To document any changes in the expression of selected vascular markers upon both miR-30 overexpression and the inhibition of miR-30/*dll4* targeting.

iii. To characterise the effects of miR-30 overexpression and TP injection on vasculogenesis and sprouting angiogenesis by imaging vascular development in transgenic zebrafish embryos with GFP-expressing endothelial cells.

iv. If a phenotype is observed upon miR-30 overexpression, to attempt to rescue this phenotype using co-injection of the TP.

The zebrafish embryo was selected as a suitable *in vivo* model because the developing zebrafish vasculature is an established model of angiogenic processes (Ny et al., 2006). Because manipulation of miR-30 expression could potentially interfere with normal vascular development, it was of great benefit that zebrafish embryos can develop normally for several days with a perturbed or absent circulatory system. This is because they receive enough oxygen via

passive diffusion from their surroundings (Ellertsdóttir et al., 2010; Ny et al., 2006).

Given the potential applications of miR-30 in human medicine, a model system was required which did not differ entirely from the human organism. It was therefore ideal that most human genes have orthologues in zebrafish (Gates et al., 1999) and that human and zebrafish organs share many molecular, physiological and anatomical similarities (Ny et al., 2006). Importantly, both DLL4 and miR-30 homologues are known to be expressed during zebrafish development (Chen et al., 2005; Leslie et al., 2007; Wienholds et al., 2005) and *dll4* knockdown has been well characterised in zebrafish embryos (Hogan et al., 2009b; Leslie et al., 2007; Siekmann and Lawson, 2007). Targeted knockdown of *dll4* and other genes in the developing embryos is easily achieved by the injection of MOs into the embryo at the 1-4 cell stage (Nasevicius and Ekker, 2000). Morpholino injection has also been adapted to block miRNA binding to specific target mRNAs (Choi et al., 2007), which is an invaluable tool for dissecting the biological roles of particular miRNA-target interactions. Previous work had shown that miRNA mimics can be injected into zebrafish embryos and that this achieves functional targeting (Deacon et al., 2010; Zeng et al., 2009).

5.2. Characterisation of *dll4* and miR-30 expression during zebrafish development

During zebrafish development, *dll4* mRNA has been detected by RT-PCR from 8 hpf (Leslie et al., 2007). This semi-quantative analysis showed a clear increase in expression at 12 hpf and further slight increases at 18, 30, 50 and 72 hpf. To detect changes in miR-30 expression with a quantitative method, total RNA was extracted from ~30 embryos at more frequent intervals up to 48 hpf and qRT-PCR analysis was performed (Fig. 5.1A). Expression is shown relative to the 6 hpf time point.

This analysis revealed robust *dll4* induction from 12 hpf onwards (Fig 5.1A). Interestingly, there was a stepwise decrease in *dll4* expression between 18 hpf and 24 hpf. During this temporal window, angiogenic sprouts from the DA are

first initiated and progress towards the dorsal roof of the neural tube to form the ISVs (Isogai et al., 2003). Given that *dll4* is known to dampen angiogenic sprouting, a slight decrease in *dll4* expression at this point might release the endothelial cells of the DA from this negative regulation, allowing sprouting to occur.

Homologues of miR-30b and miR-30c have been detected in both the developing embryo and the adult zebrafish (Wienholds et al., 2005). When the RNA samples described above were used to perform miRNA qRT-PCR, miR-30b, -30c, -30d and 30e were found to be expressed, with an overall trend of increasing expression from 6 hpf to 48 hpf (Fig. 5.1B). During the angiogenic sprouting window (18-24 hpf), the expression of miR-30 steadily increased (Fig. 5.1B). Although this experiment was only repeated once, the decrease in *dll4* expression and increase in miR-30 expression during the period of angiogenesis was of particular interest. These temporally coincident changes in *dll4* and miR-30 could indicate a functional interaction that may contribute to the tight control of Dll4 expression during zebrafish vascular development. Decreased *dll4* expression immediately prior to and during sprouting of the ISVs could be partly due to increased miR-30-directed miRISC targeting.

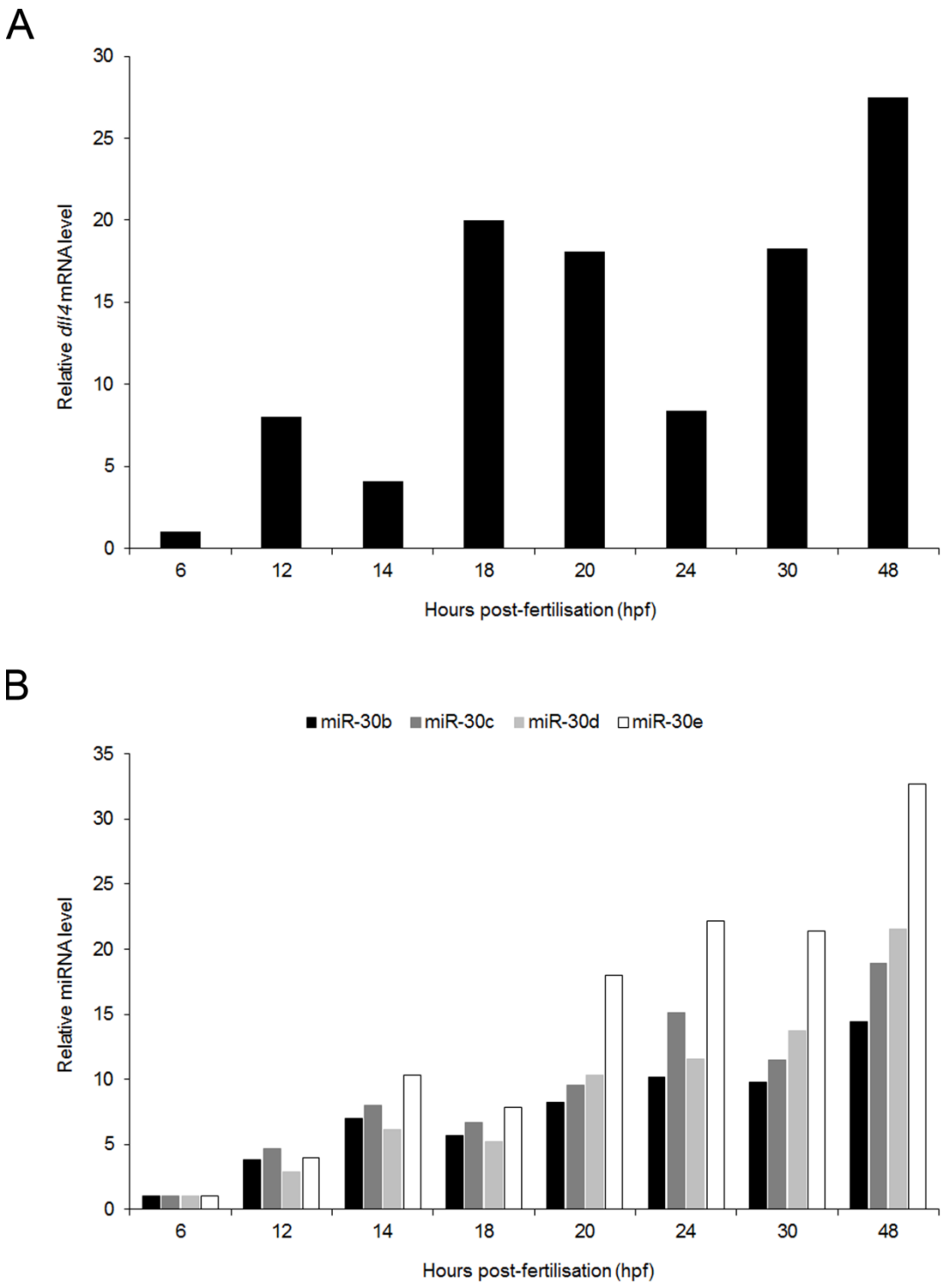

Figure 5.1. Expression of *dll4* and the miR-30 family during zebrafish development. (A) *dll4* mRNA expression in zebrafish embryos at the indicated stage of development, as measured by qRT-PCR. Expression is relative to 6 hpf. RNA was extracted from ~30 embryos for each developmental stage (SEM is not shown as n=1). (B) Expression of miR-30b, miR-30c, miR-30d and miR-30e in zebrafish embryos at the indicated stage of development, as measured by qRT-PCR. Expression is relative to 6 hpf. RNA was extracted from ~30 embryos for each developmental stage (SEM is not shown as n=1). RNA extraction was performed by Rui Monteiro. qRT-PCR was performed by Gemma Bridge.

5.3. Optimisation of miR-30 mimic microinjections

Having identified a potential functional interaction between miR-30 and *dll4* during zebrafish development, miR-30 overexpression was adopted to investigate this relationship. Examination of the literature revealed that miRNA mimics had previously been injected at 3ng per embryo for overexpression studies (Zeng et al., 2009). Therefore, microinjections of 2.5ng/embryo and 5ng/embryo were tested for NTC, miR-30b and miR-30c mimics. By 24 hpf the embryos injected with 5ng of NTC mimic displayed slightly abnormal anatomical features, including an oversized yolk sac extension. However, the embryos injected with 5ng of miR-30b or miR-30c mimic were severely abnormal with extensive necrosis and embryonic death. This quantity of mimic was therefore discounted from future studies. The embryos injected with 2.5ng of mimic were imaged at 24 hpf (Fig. 5.2). For this quick examination of anatomical features, the embryos were not dechorionated or sedated with muscle relaxant. Therefore, the tails of the wildtype (WT) and NTC-injected embryos were moving during the imaging process and hence are slightly blurry in the images (Fig 5.2). This highlights one of the first developmental abnormalities of the miR-30 injected embryos: the tails were either missing entirely (Fig. 5.2; red arrowheads), severely stunted (Fig. 5.2; black arrowheads) or short and curved (Fig. 5.2; grey arrowheads). None of the miR-30 injected embryos had mobile tails.

The only obvious abnormal feature of the NTC-injected embryos was an oversized yolk sac extension (Fig. 5.2; black arrow). The miR-30-injected embryos also displayed this feature to a greater extent but in addition these embryos were generally stunted with small heads and often exhibited necrosis in the head region (Fig 5.2; red arrow). Necrosis of the head is a common feature when MOs are injected at high concentrations. The fact that both NTC- and miR-30-injected embryos displayed large yolk sac extensions would suggest that this is a side-effect of high miRNA mimic concentrations. Indeed, qRT-PCR analysis of total RNA from embryos injected with 2.5ng of miR-30 mimic revealed that miR-30 expression was over 200 fold higher than in uninjected controls (Fig. 5.3A). However, the extensive abnormalities shown in

the miR-30-injected embryos alone would suggest that this miRNA is capable of targeting one or many factors that are crucial for normal zebrafish development.

Due to the severe abnormalities displayed upon injection of large quantities of miR-30 mimic, the amount of microinjected mimic was titrated to an amount where overall embryo morphology was normal (Fig. 5.2B) and miR-30 expression was detectable at a level that is within the physiological range for zebrafish miRNAs (Fig. 5.3A). This was 0.05ng/embryo for miR-30b and 0.1ng/embryo for miR-30c. An upregulation of 20-25 fold was considered to be compatible with normal variations in zebrafish miRNA expression, as changes of this magnitude are seen for various different miRNAs during zebrafish development (Chen et al., 2005).

Extraction of total RNA from whole embryos also allowed *dll4* levels to be quantified by qRT-PCR in embryos injected with each quantity of miRNA mimic (Fig. 5.3B). *dll4* expression titrated with levels of miR-30, displaying the expected inverse correlation (Fig. 5.3B). *dll4* mRNA was suppressed by 40-50% in embryos injected with 2.5ng of miR-30 mimic when compared to NTC; however a 20-30% suppression was still observed in the lowest mimic concentrations chosen for further studies (Fig. 5.3B). Downregulation of *dll4* expression in the DA and ISVs was confirmed by *in situ* hybridisation when the mimics were injected at 0.05ng/embryo and 0.1ng/embryo for miR-30b and miR-30c respectively (Fig. 5.3C). Ten miR-30b-injected embryos were examined by *in situ* hybridisation. Eight of these displayed repressed *dll4* expression, whilst the remaining two embryos showed wildtype *dll4* levels. Similarly, for the miR-30c-injected embryos, *dll4* levels were reduced in 11 embryos with only one embryo exhibiting normal *dll4* expression (Fig. 5.3C).

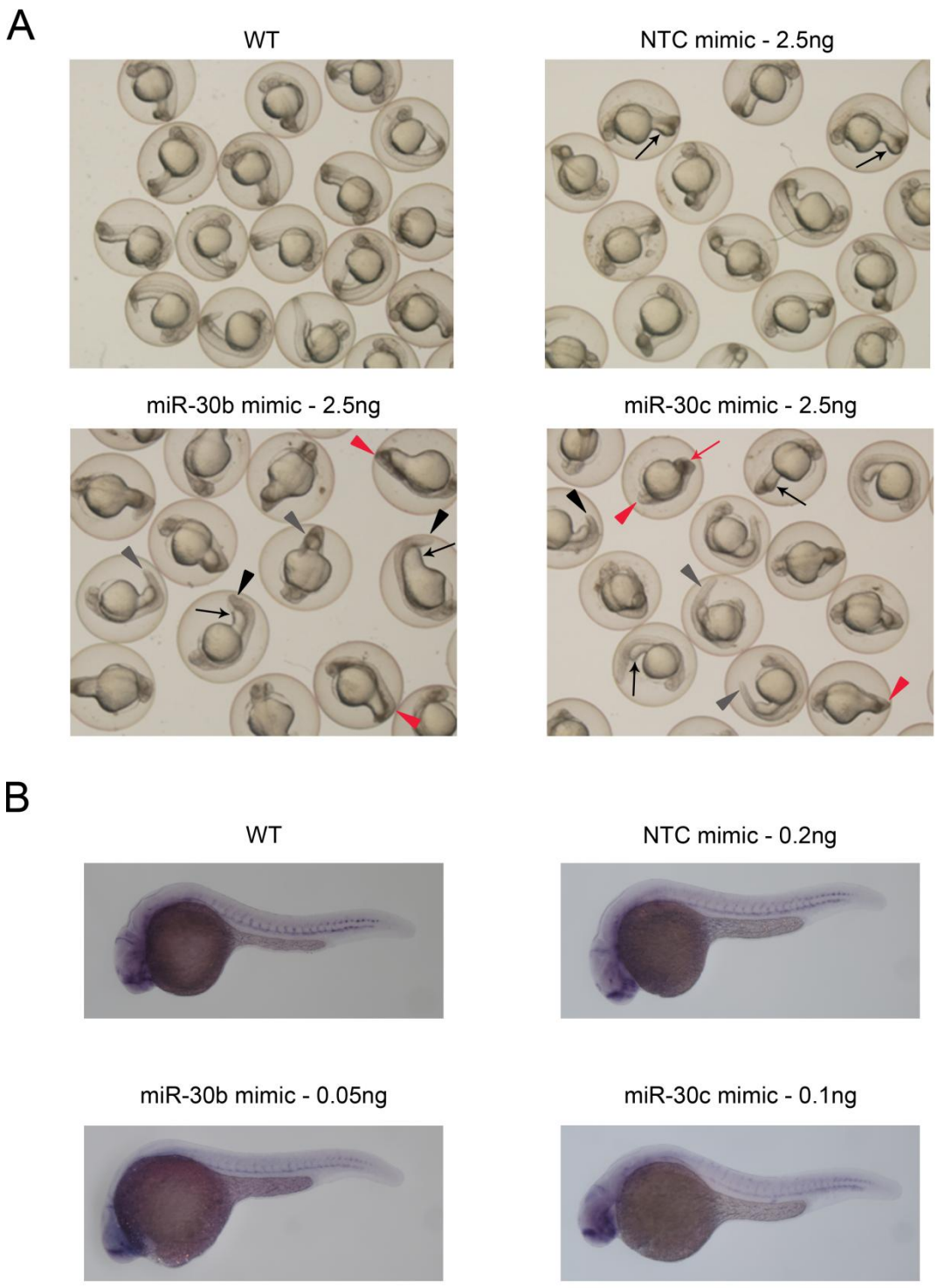

Figure 5.2. Testing miR-30 mimics in zebrafish embryos. (A) Images of wildtype (WT) zebrafish embryos or embryos injected with 2.5ng of the indicated miRNA mimic at 24 hpf. Red arrowheads indicate missing tails; black arrowheads indicate stunted tails; grey arrowheads indicate short, curved tails. Red arrows indicate head necrosis; black arrows indicate oversized yolk sac extensions. Magnification: 2.5x. (B) Representative images of a wildtype (WT) zebrafish embryo or embryos injected with the indicated quantity of miRNA mimic at 27 hpf. *In situ* hybridisations were performed on the embryos to assess *dll4* expression; however the images are shown here to examine overall embryo morphology. Microinjections were performed by Rui Monteiro and Gemma Bridge. *In situ* hybridisations were performed by Gemma Bridge. Images were taken by Gemma Bridge.

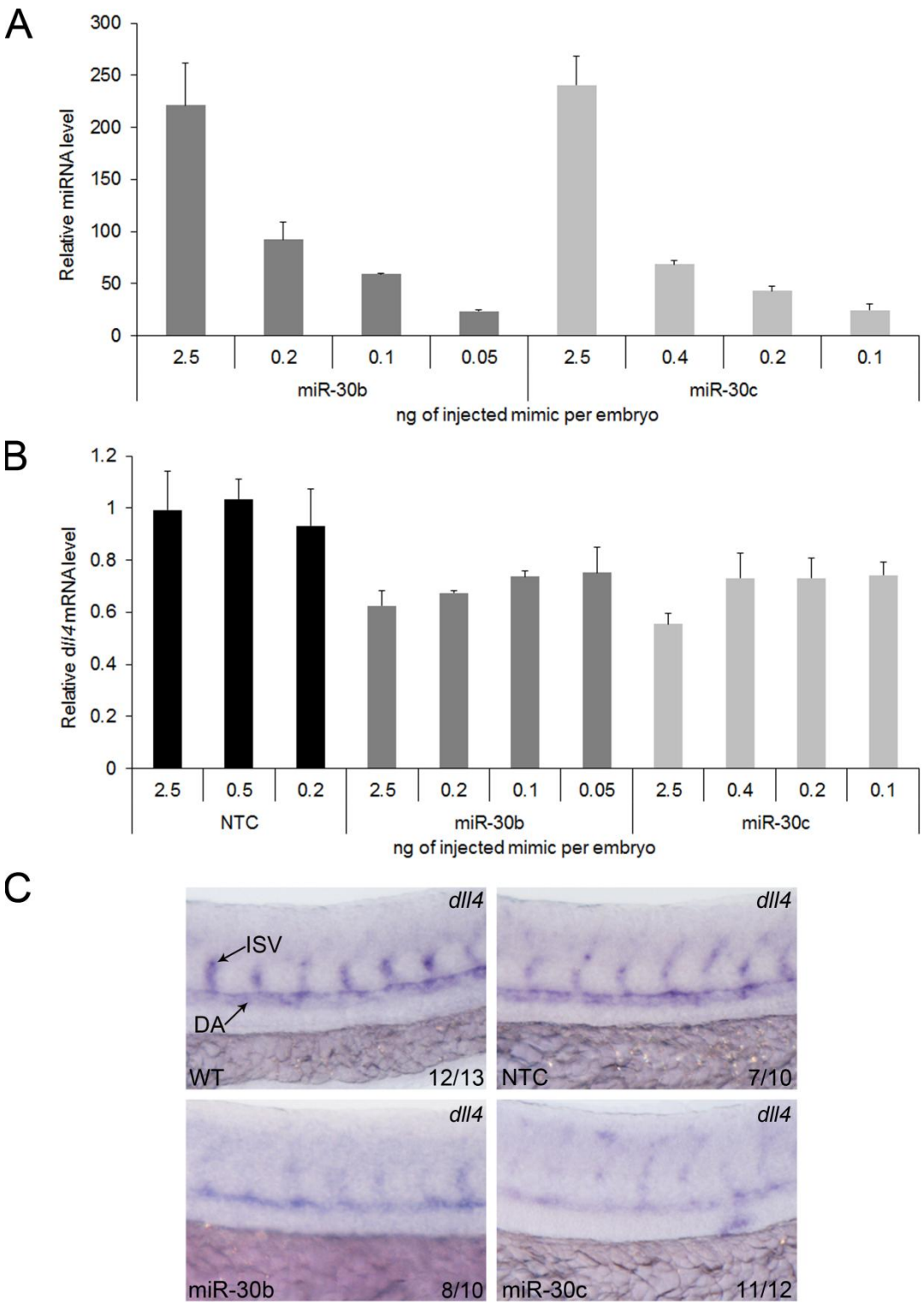

Figure 5.3. *dll4* mRNA is suppressed in zebrafish embryos following miR-30 mimic injection. (A and B) Expression of miR-30 (A) and *dll4* mRNA (B) in whole zebrafish embryos following microinjection of the indicated amount of miRNA mimics, as measured by qRT-PCR. Expression is relative to uninjected control embryos. Error bars indicate SD of qRT-PCR experiment which was performed in triplicate. n=1 but RNA was collected from 20-30 embryos per condition. (C) Representative *in situ* hybridization showing *dll4* mRNA expression in the developing vasculature of wildtype (WT) embryos and embryos injected with 0.2ng (NTC), 0.05ng (miR-30b) and 0.1ng (miR-30c) miRNA mimics. Values indicate the number of embryos with the predominant, displayed phenotype versus the total number of embryos assayed. Dorsal aorta (DA) and intersegmental vessels (ISV) are labelled. Microinjections were performed by Rui Monteiro and Gemma Bridge. RNA extraction, qRT-PCR and *in situ* hybridization were performed by Gemma Bridge. Images were taken by Rui Monteiro.

5.4. The effects of miR-30 overexpression on other vascular markers

The primary focus of this chapter of work was the effect of miR-30 regulation on *dll4* expression *in vivo* and the subsequent functional consequences with regard to ISV sprouting. However, given the severe anatomical abnormalities observed at high levels of miR-30 overexpression (Fig. 5.2), I also decided to assess the expression of other vascular markers following miR-30 overexpression by *in situ* hybridisation.

Knockdown of Dll4 was used as a positive control. To achieve Dll4 knockdown, two previously published *dll4* MOs were tested: MO1-*dll4* (Siekmann and Lawson, 2007) and MO4-*dll4* (Hogan et al., 2009b). The sequences of these MOs are given in Table 2.8. The MOs were injected into *Tg(kdrl:EGFP)* embryos at levels previously used in publication and the trunk vasculature was imaged 48 hpf (Fig. 5.4A). The genetic marker *kdrl* is only expressed in blood endothelial cells; therefore, the *kdrl* promoter specifically drives *EGFP* expression in blood endothelial cells alone, allowing easy visualisation on a fluorescent microscope. Embryos injected with either MO1-*dll4* or MO4-*dll4*, also known as *dll4* morphants (Nasevicius and Ekker, 2000), displayed ISV hyperbranching as expected (Fig. 5.4A; red arrowheads), but this phenotype was much more pronounced in the embryos injected with MO4-*dll4*. Because miR-30 acts to downregulate *dll4* but does not entirely eliminate its expression, it was not expected that miR-30 microinjection would cause extremely excessive hyperbranching. Therefore, MO1-*dll4* was chosen as a positive control for Dll4 knockdown. Misplicing of *dll4* mRNA in the embryos injected with MO1-*dll4* was confirmed by RT-PCR (Fig. 5.4B). Increased *dll4* mRNA expression was observed in *dll4* morphants (Fig. 5.5A). This was expected because the *dll4* MO blocks *dll4* mRNA splicing leading to the accumulation *dll4* mRNA (Siekmann and Lawson, 2007).

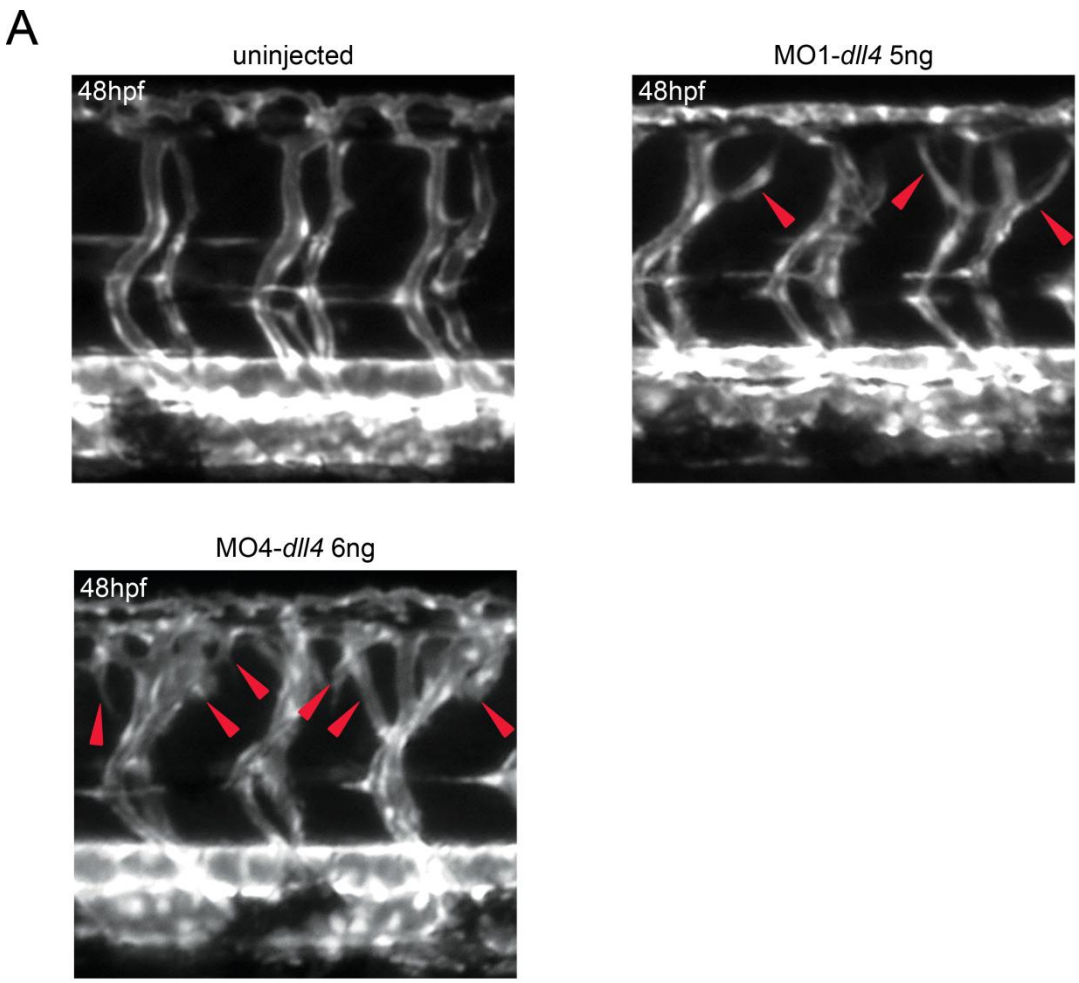

Figure 5.4. Testing *dll4* morpholinos in zebrafish embryos. (A) Trunk vasculature in uninjected *Tg(kdrl:EGFP)* embryos or embryos injected with the indicated morpholino at 48 hpf. Red arrowheads denote extra sprouts from the ISVs. Microinjections were performed by Rui Monteiro and Gemma Bridge. Fluorescent images were taken by Rui Monteiro with the assistance of Gemma Bridge. (B) RT-PCR for *dll4* and *ef1a* using RNA extracted at 24 hpf from wildtype (WT) embryos or embryos injected with the indicated morpholino type and quantity. The *dll4* primers used were as described in (Siekmann and Lawson, 2007). Microinjections were performed by Rui Monteiro and Gemma Bridge. RNA extractions were performed by Gemma Bridge. RT-PCR was performed by Rui Monteiro.

Notch signalling is known to be required for haematopoietic stem cell (HSC) emergence, for example the expression of *runt-related transcription factor 1 (runx1)* is absent in embryos treated with the Notch inhibitor DAPT or in the Notch signalling mutant *mindbomb* (Burns et al., 2005; Gering and Patient, 2005). The transcription factor *runx1* is a marker of HSCs in zebrafish (Zhang et al., 2013). It was therefore of interest whether *runx1* expression is also absent or reduced upon miR-30 overexpression, potentially due to a reduction in DLL4-mediated Notch signalling.

Through a process called endothelial haematopoietic transition (EHT), zebrafish HSCs are generated from the ventral wall of the DA (Zhang et al., 2013). During this process, single endothelial cells move from the DA wall into the sub-aortic space at around 30 hpf and from there into the blood circulation via the PCV. The endothelial cells are derived from the haemogenic endothelium, a specialised population of endothelial cells that have the potential to generate HSCs (Zhang et al., 2013). The haemogenic endothelium can be identified by *runx1* expression, as seen by the dots of staining along the ventral wall of the DA in WT embryos (Fig. 5.5B, left-hand panels). In the *dll4* morphants, *runx1* expression was almost entirely absent in the DA due to a lack of *runx1* positive cells (Fig. 5.5B, left-hand panels). A lack of *runx1* positive HSC progenitors due to *dll4* knockdown has not yet been reported and suggests that Dll4 could be involved in the specification or maintenance of the haemogenic endothelium. The neural expression of *runx1* in the *dll4* morphants was normal (Fig. 5.5B, right-hand panels).

Staining for *runx1* mRNA was reduced in the DA and neural tissue of miR-30b and miR-30c injected embryos when compared to WT or NTC injected embryos (Fig. 5.6A). However, the decreased intensity of staining in the DA was due to reduced expression, not a decreased number of *runx1* positive cells as seen with the *dll4* MO. I would hypothesise that the reduction in Notch signalling in the miR-30 overexpressing embryos was not sufficient to impair HSC emergence. The decrease in *runx1* expression in this scenario could be due to direct targeting of *runx1* by miR-30. In addition to decreased *runx1* expression, the miR-30 overexpressing embryos also displayed aberrant *runx1* neural patterning (Fig. 5.6A, right-hand panels).

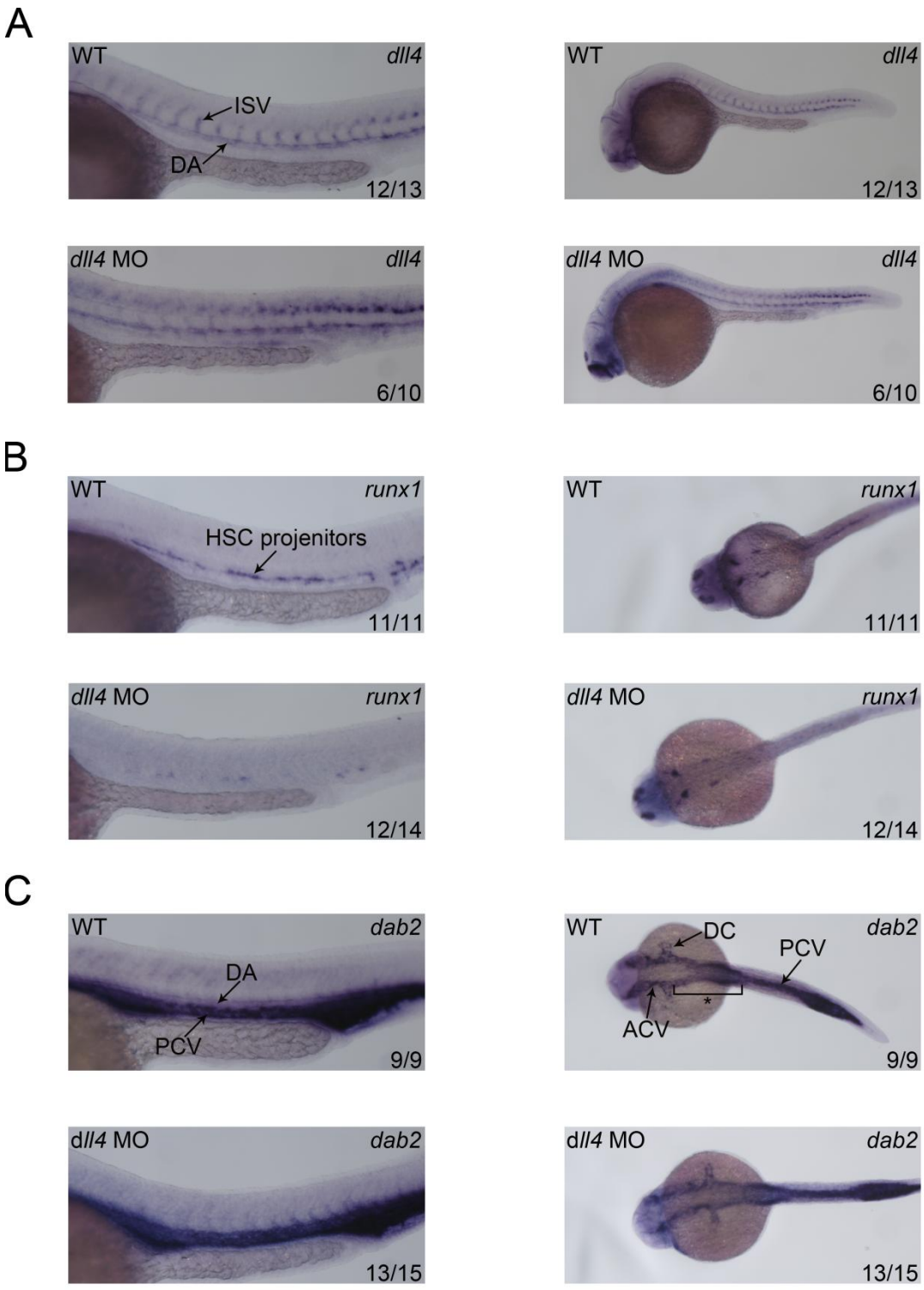

Figure 5.5. Expression of *dll4, runx1* and *dab2* mRNA in *dll4* MO-injected zebrafish embryos.
(A, B and C) Representative *in situ* hybridization showing expression of *dll4* (A), *runx1* (B) and *dab2* (C) mRNA at 27 hpf in the vasculature of wildtype (WT) embryos and embryos injected with 5ng of *dll4* morpholino (*dll4* MO). Values indicate the number of embryos with the predominant, displayed phenotype versus the total number of embryos assayed. Asterisk and brackets denote cardinal vein bifurcation. Dorsal aorta (DA); intersegmental vessels (ISV); haematopoeitic stem cell (HSC); posterior cardinal vein (PCV); anterior cardinal vein (PCV); Duct of Cuvier (DC). Microinjections were performed by Rui Monteiro and Gemma Bridge. *In situ* hybridisations were performed and imaged by Gemma Bridge.

The next gene tested was the venous marker *disabled homolog 2 (dab2)*. DLL4 signalling is known to promote arterial specification, therefore it was hypothesised that *dab2* staining would be increased in miR-30-injected embryos due to increased venous specification upon *dll4* downregulation. The WT embryos had a strong band of staining which denotes the PCV and a very weak line of DA staining just above (Fig. 5.5C, left-hand panels). The cardinal vein was also labelled where it bifurcates just before reaching the head (Fig. 5.5C, right-hand panels). Each cardinal vein empties into a large sinus called the Duct of Cuvier (DC), which fans out across the yolk sac, whilst the remaining anterior cardinal veins (ACV) proceed down into the head of the embryos. *dab2* expression was unaffected in the trunk region of the *dll4* morphants but clearly downregulated in miR-30b and miR-30c injected embryos (Fig. 5.5C and 5.6B, left-hand panels). miR-30 overexpression also caused a wider gap to develop between the bifurcating cardinal veins in the head region (Fig. 5.6B, right-hand panels).

The third VEGFR receptor, *flt4*, is also a venous marker and staining in the WT embryos followed a very similar pattern to *dab2* (Fig. 5.7). The PCV is clearly visible in the trunk (Fig. 5.7, left-hand panels), as is the bifurcation of the cardinal vein in the head (Fig. 5.7, right-hand panels). Unfortunately, due to experimental restrictions, *flt4 in situ* hybridisation was not performed in the *dll4* morphants. The NTC-injected embryos displayed normal, WT expression of *flt4* (Fig. 5.7). However, *flt4* expression was clearly reduced in the trunk of miR-30-injected embryos (Fig. 5.7, left-hand panels). When the embryos were visualised from above, it became apparent that miR-30 overexpression is affecting angioblast migration and/or specification in relation to formation of the PCV. In the majority of miR-30 overexpressing embryos, two parallel lines of venous endothelial cells could be seen in the trunk, rather than the single line that denotes the PCV (Fig. 5.7, right-hand panels). The gap between the two bifurcations of the cardinal vein was also wider and in some embryos the DCs appeared disorganised and spread out (Fig. 5.7, right-hand panels).

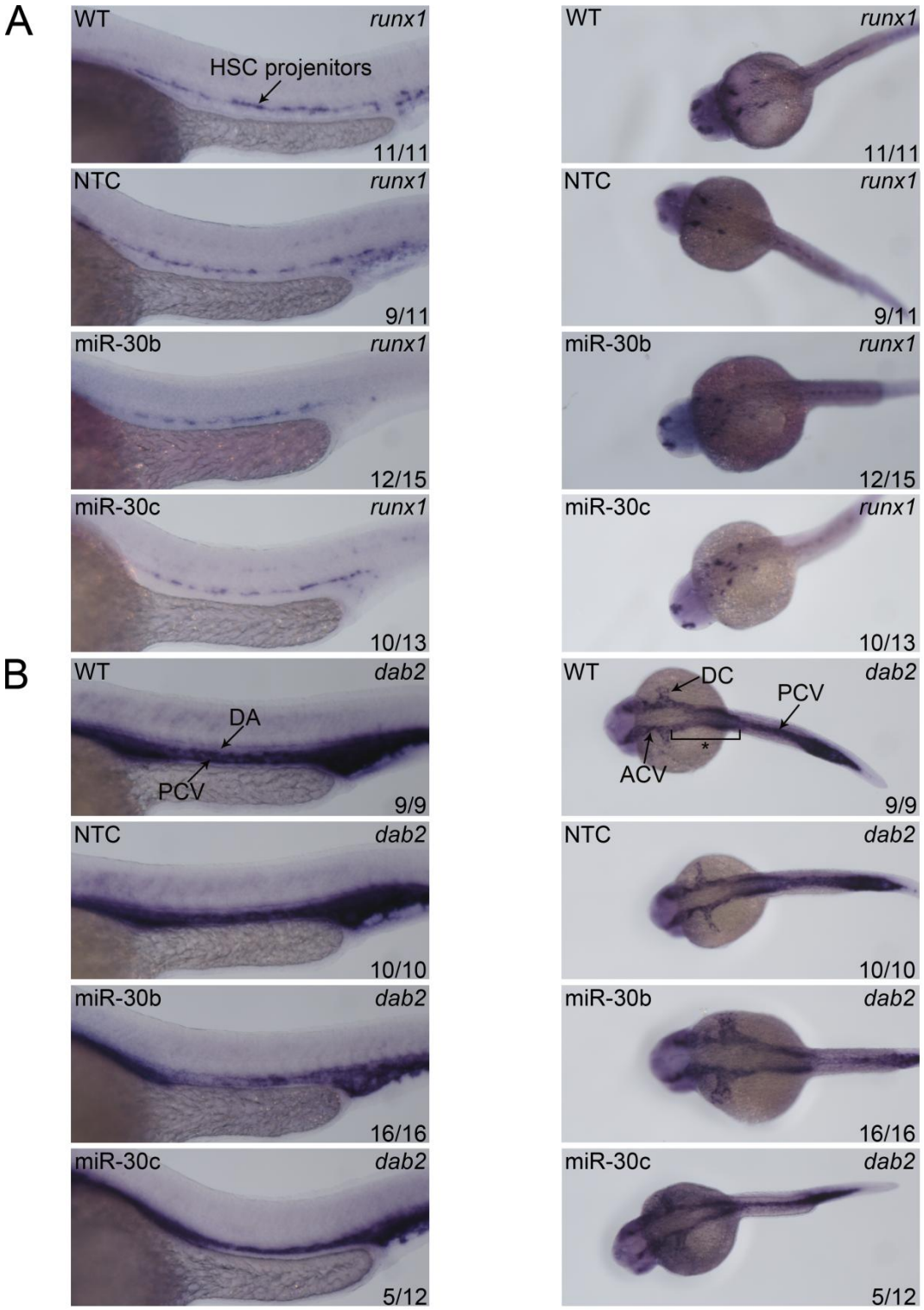

Figure 5.6. Expression of *runx1* and *dab2* mRNA in zebrafish embryos injected with NTC and miR-30 mimics. (A and B) Representative *in situ* hybridization showing expression of *runx1* (A) and *dab2* (B) mRNA at 27 hpf in the vasculature of wildtype (WT) embryos and embryos injected with 0.2ng (NTC), 0.05ng (miR-30b) and 0.1ng (miR-30c) miRNA mimics. Values indicate the number of embryos with the predominant, displayed phenotype versus the total number of embryos assayed. Asterisk and brackets denote cardinal vein bifurcation. Dorsal aorta (DA); intersegmental vessels (ISV); haematopoeitic stem cell (HSC); posterior cardinal vein (PCV); anterior cardinal vein (ACV); Duct of Cuvier (DC). Microinjections were performed by Rui Monteiro. *In situ* hybridisations were performed and imaged by Gemma Bridge.

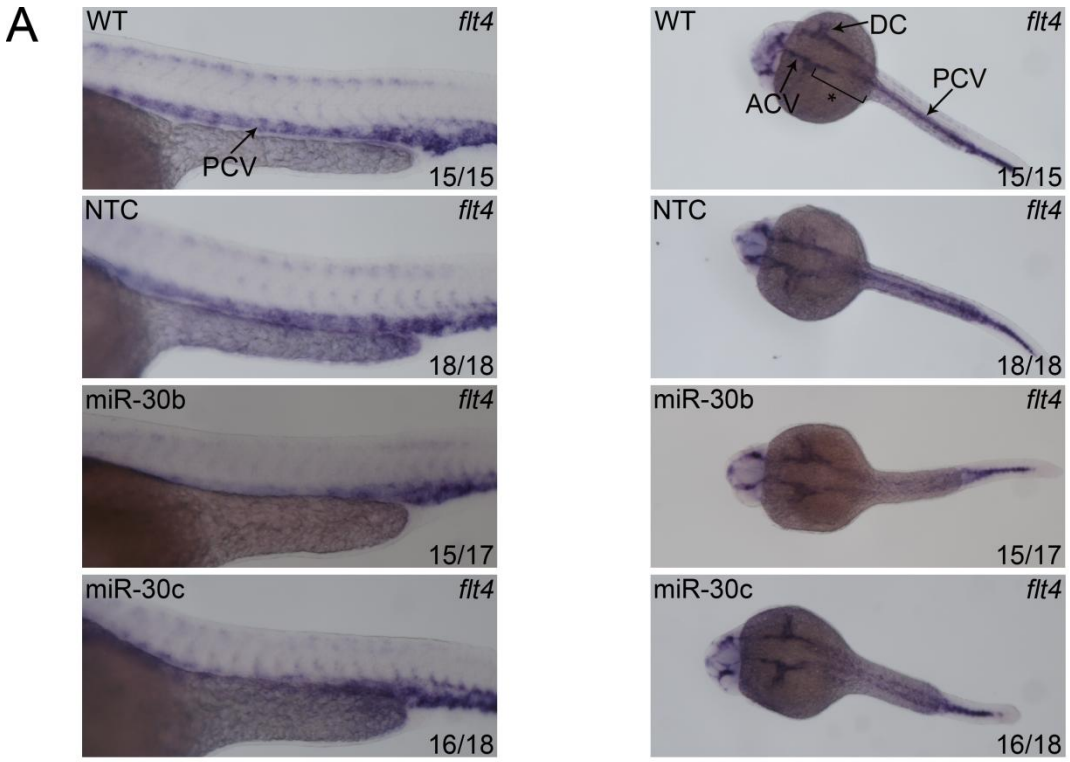

Figure 5.7. Expression of *flt4* mRNA in zebrafish embryos injected with NTC and miR-30 mimics. (A) Representative *in situ* hybridization showing expression of *flt4* mRNA at 26 hpf in the vasculature of wildtype (WT) embryos and embryos injected with 0.2ng (NTC), 0.05ng (miR-30b) and 0.1ng (miR-30c) miRNA mimics. Values indicate the number of embryos with the predominant, displayed phenotype versus the total number of embryos assayed. Asterisk and brackets denote cardinal vein bifurcation. Posterior cardinal vein (PCV); anterior cardinal vein (ACV); Duct of Cuvier (DC). Microinjections were performed by Rui Monteiro and Gemma Bridge. *In situ* hybridisations were performed and imaged by Gemma Bridge.

5.5. Exogenous expression of miR-30 induces aberrant intersegmental vessel development and branching in zebrafish

Having confirmed suitable miR-30 expression and *dll4* downregulation upon microinjection of a viable quantity of miR-30 mimic, experiments were undertaken to investigate the effect of miR-30 overexpression on vascular development. The miR-30 mimics and the chosen *dll4* MO were injected into *Tg(kdrl:EGFP)* embryos and vascular development was examined at 25 and 72 hpf by fluorescent microscopy (Fig. 5.8A).

At 25 hpf, embryos injected with both *dll4* MO and miR-30 mimic possessed ISVs at a more advanced stage of sprouting than the uninjected control (Fig 5.8.A). Some of the endothelial cells from these ISVs displayed a vessel-free hyper-migratory phenotype, whereby they had separated from the sprouting vessel and moved dorsally leading to premature DLAV formation (Fig 5.8.A; yellow arrowheads). At the time of investigation this phenotype had not been reported; however, it was recently also observed by Biyashev *et al*. upon *dll4* knockdown, although at the later time point of 30 hpf (Biyashev et al., 2011). With increasing amounts of miR-30 mimic, a higher percentage of embryos displayed advanced sprouting and a greater proportion of these exhibited premature DLAV formation and hyper-migratory behaviour (severe advanced ISVs) (Fig 5.9A). Upon injection of 0.05ng miR-30b mimic, ~60% of embryos displayed advanced ISVs (21/36), with ~15% of embryos exhibiting the more severe phenotype (5/36) (Fig 5.9A). When miR-30b mimic was increased to 0.2ng, ~90% of embryos displayed some form of abnormal ISVs (71/80) and the incidence of severe hyper-migratory endothelial cells had increased to ~70% (58/80) (Fig 5.9A). Only 10% of embryos injected with the highest amount of NTC mimic possessed abnormal ISVs (3/24) and none of these displayed the hyper-migratory phenotype, confirming that the results reported were not a non-specific effect of miRNA mimic injection (Fig 5.9A).

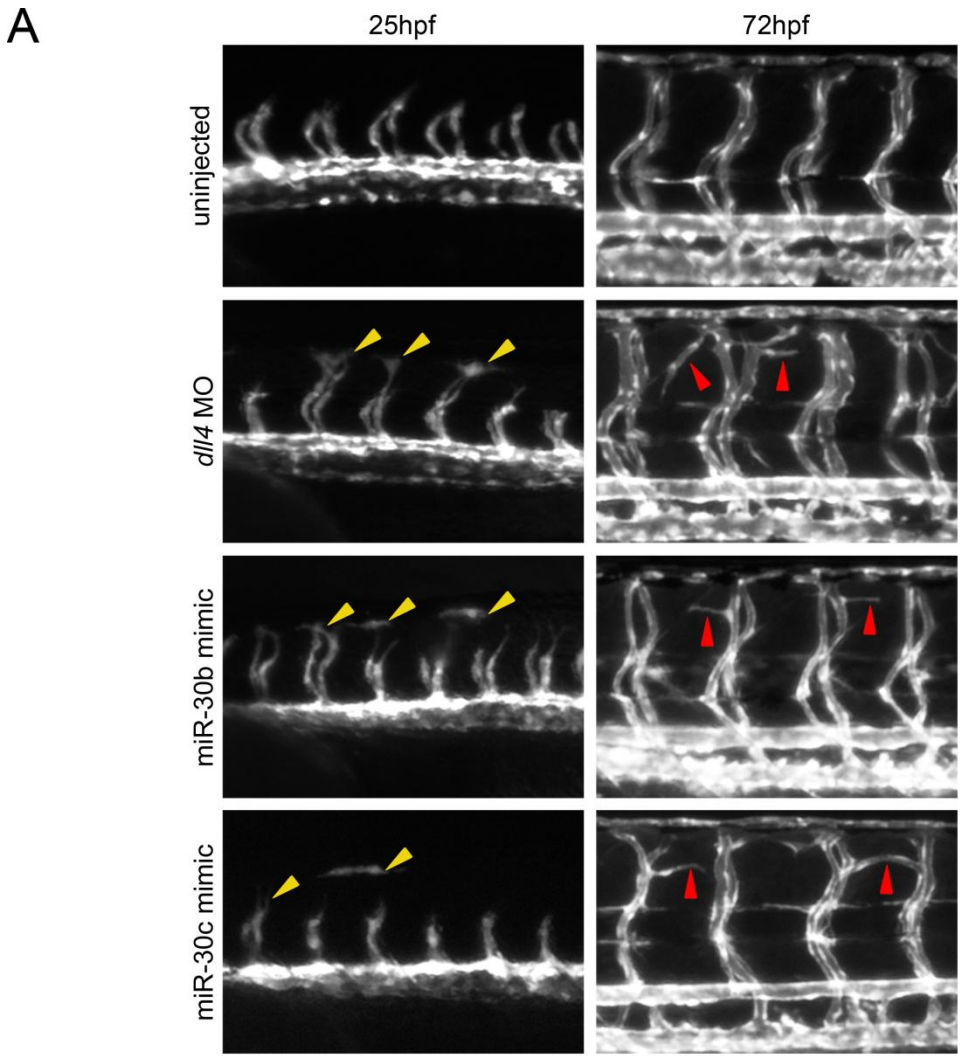

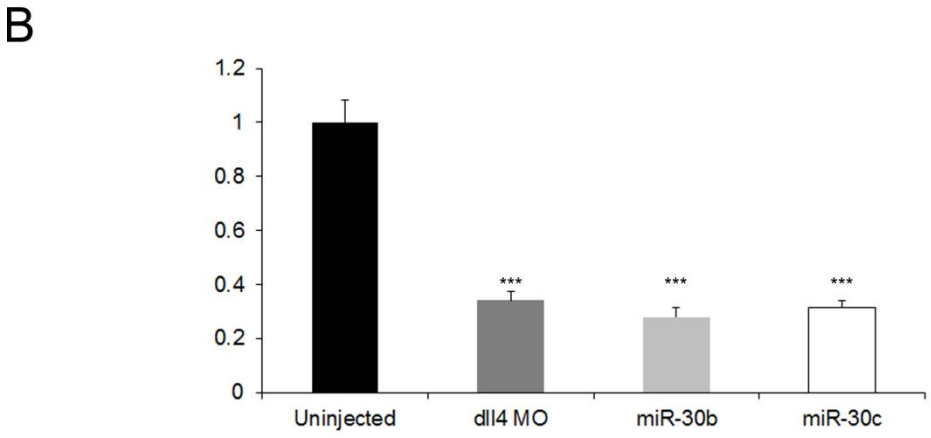

Figure 5.8. Overexpression of miR-30b and miR-30c in zebrafish embryos phenocopies *dll4* knockdown. (A) Trunk vasculature in uninjected *Tg*(*kdrl:EGFP*) embryos or embryos injected with the indicated MO or miRNA mimic. Left panels: advanced sprouting and aberrant endothelial cell migration (yellow arrowheads) at 25 hpf. Right panels: increased branching of the ISVs (red arrowheads) at 72 hpf. (B) DA diameter in embryos injected with *dll4* MO or miR-30 mimic relative to uninjected embryos (means + SEM, n=3). Six DA measurements were made per embryo using Adobe Photoshop CS4. Differences between uninjected embryos and embryos injected with *dll4* MO or miR-30 mimics were significant. ***, $p<0.001$. Microinjections were performed by Rui Monteiro and Gemma Bridge. Images were taken by Rui Monteiro with the assistance of Gemma Bridge. DA measurements were made by Rui Monteiro.

A novel observation at 25 hpf was that the diameter of the DA was significantly reduced in *dll4* morphants and in miR-30–overexpressing embryos compared with WT embryos (Fig. 5.8B). This phenotype has previously been reported following *Dll4* knockdown in mice and the opposite effect has also been observed upon *Dll4* overexpression in mouse embryos (Duarte et al., 2004; Gale et al., 2004). This concurs with studies showing that DLL4 up-regulation in tumours correlates with increased vessel maturation and size (Li et al., 2007; Patel et al., 2006; Trindade et al., 2008).

Excessive ISV branching was observed in embryos expressing miR-30b and miR-30c mimics at 72 hpf (Fig. 5.8A; red arrowheads). This hyperbranching was comparable to that caused by *dll4* MO injection (Fig. 5.8A; red arrowheads) and to the branching induced by *dll4* knockdown in a previous report (Leslie et al., 2007). This phenotype titrated with increasing amounts of miR-30: the higher the amount of mimic injected, the greater the number of branches from the ISVs (Fig. 5.9B). Approximately 50% of embryos injected with 0.05ng of miR-30b mimic presented extra ISV branches at 72 hpf (19/37) (Fig 5.9B). This increased to 85% with 0.2ng of mimic (29/34), with the addition of ~40% of embryos that showed 3-5 extra branches (13/34) (Fig. 5.9B). Again, the NTC mimic had a very mild effect on ISV branching (Fig 5.9B).

Overall this work showed that miR-30 overexpression in the developing zebrafish embryo phenocopies *dll4* knockdown at both 25 and 72 hpf.

A

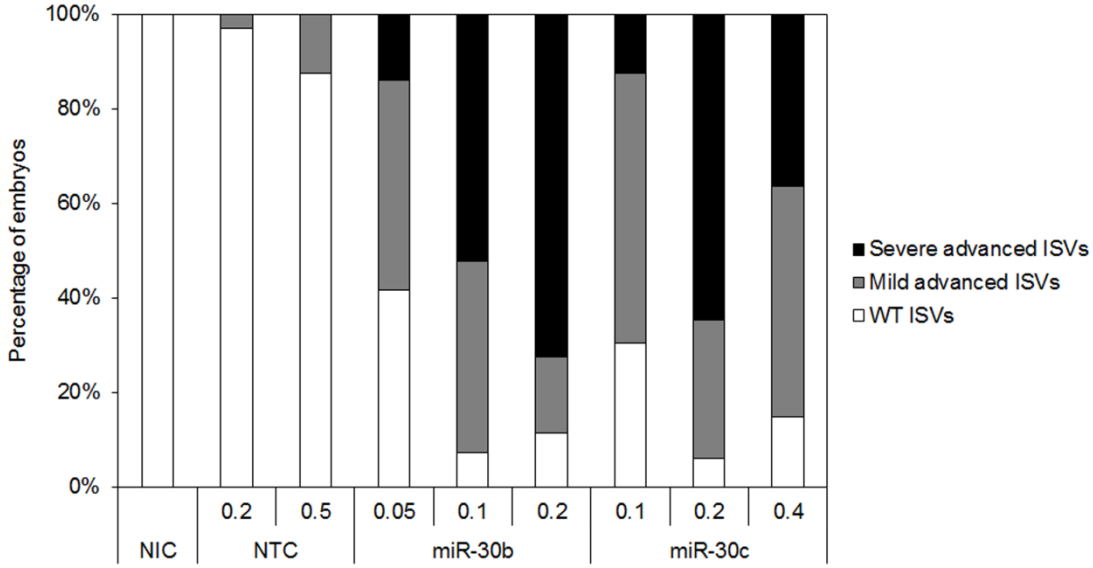

B

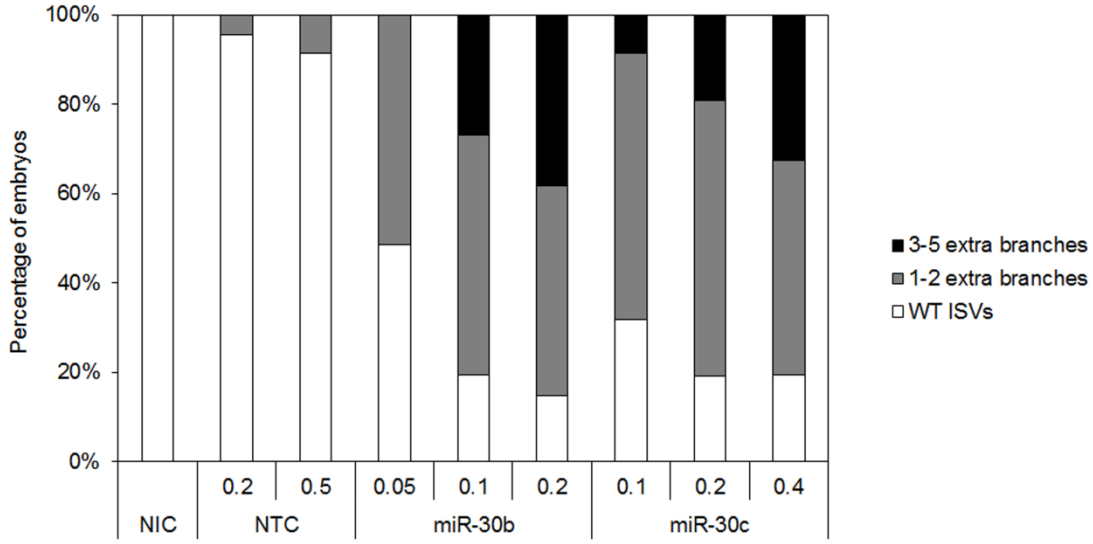

Figure 5.9. Quantification of zebrafish embryo phenotypes following titration of miR-30 mimics. (A and B) Quantification of ISV sprouting defects at 24 hpf (A) and 72 hpf (B) in non-injected control (NIC) *Tg*(*kdrl:EGFP*) embryos or embryos injected with the indicated mimic Values denote the quantity of mimic injected per embryo in ng. Embryos with severe morphological defects which prevented ISV phenotyping were discounted. n values per group ranged from 25-100 and are given in Table 2.10. Mild advanced ISVs: embryos with ISVs that have reached a more dorsal position in the trunk compared to wildtype embryos at the same time point. Severe advanced ISVs: as described for mild advanced ISVs but with the addition of premature DLAV formation and/or vessel-free, hyper-migratory endothelial cells. Microinjections were performed by Rui Monteiro. ISV phenotyping was performed by Gemma Bridge.

5.6. The hyperbranching phenotype induced by miR-30 overexpression occurs due to *dll4* targeting

The work described in Section 5.5 had shown that overexpression of miR-30 in zebrafish embryos induces excessive ISV branching and therefore phenocopies *dll4* knockdown. However, at this stage it could not be concluded that the hyperbranching phenotype was due to miR-30-induced *dll4* suppression, because miRNAs can potentially target hundreds of mRNA transcripts. Downregulation of another, as yet unknown target could be causing the observed vascular phenotype. To dissect the specific role of *dll4* targeting in this setting, a target protector morpholino (TP) was employed.

A TP is a 25nt long morpholino which is designed to bind to a region of mRNA containing a specific miRNA target site. The TP is not only complementary to the miRNA target site, but also to flanking sequences in the 3'UTR, whilst the miRNA is only complementary to the target site and possibly a few downstream nucleotides. Therefore, the TP exhibits preferential binding and sterically blocks the miRNA from accessing the target site. This technique was first devised by Choi *et al*. to investigate the role of miR-430 during zebrafish development (Choi et al., 2007). A TP can be used to disrupt the interaction between a miRNA and one specific target, without affecting any other miRNA-target interactions. A TP was designed with a 3' end that bound to the miR-30 target site within the *dll4* 3'UTR whilst the 5' region bound to the downstream flanking sequence (*dll4*-TP^{miR-30}; Table 2.8). A control TP was also produced which bound to another region of the *dll4* 3'UTR that was not predicted to contain any miRNA target sites (*dll4*-TP^{control}; Table 2.8).

To ascertain the effectiveness of this TP strategy, *dll4*-TP^{miR-30} and *dll4*-TP^{control} were injected into zebrafish embryos at the 1-4 cell stage and *dll4* expression was examined at 28 hpf. Consistent upregulation of *dll4* mRNA in *dll4*-TP^{miR-30} injected embryos was observed by *in situ* hybridisation (Fig. 5.10A) and qRT-PCR (Fig. 5.10B) when compared to embryos injected with *dll4*-TP^{control}. This confirmed that *dll4*-TP^{miR-30} could be used to prevent miR-30 from targeting *dll4 in vivo* and also revealed that miR-30 actively targets *dll4* during zebrafish development.

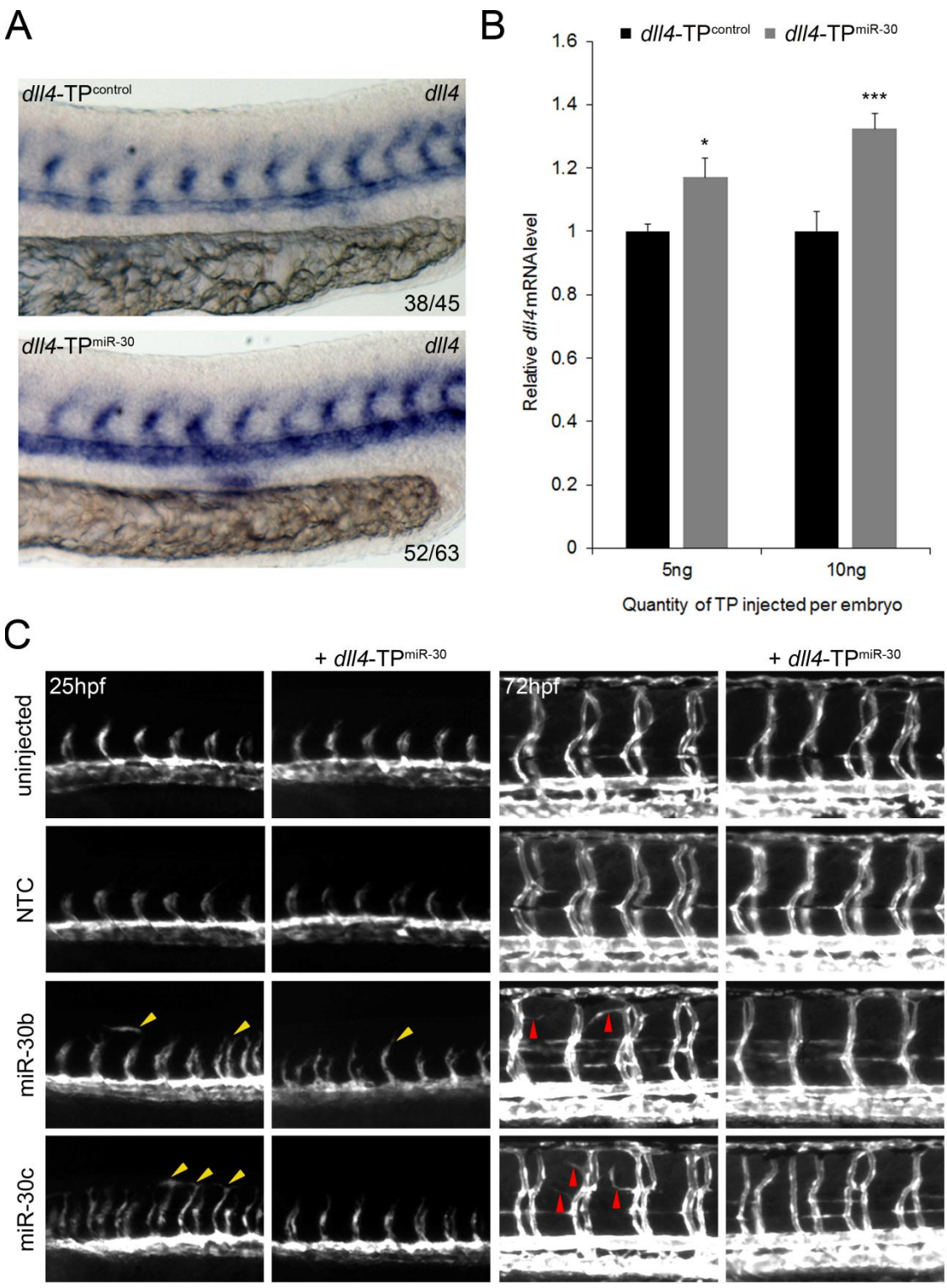

Figure 5.10. Co-injection of *dll4*-TP^{miR-30} partially rescues the aberrant endothelial cell migration and ISV branching caused by miR-30 microinjection. (A) Representative *in situ* hybridization showing expression of *dll4* mRNA in the developing vasculature of zebrafish embryos injected with 10ng of the indicated TP. Values indicated the number of embryos with the predominant, displayed phenotype out of the total number of embryos assayed. (B) Expression of *dll4* mRNA in whole zebrafish embryos following microinjection of *dll4*-TP^{miR-30} measured by qRT-PCR (means + SEM, n=5). Expression is relative to embryos injected with the same quantity of *dll4*-TP^{control}. *, $p<0.05$, ***, $p<0.001$. (C) Trunk vasculature in uninjected Tg(*kdrl*:*EGFP*) embryos or embryos injected with the indicated miRNA mimic and/or TP. Left panels: advanced sprouting and aberrant endothelial cell migration (yellow arrowheads) at 25 hpf. Right panels: increased branching of the ISVs (red arrowheads) at 72 hpf.

To confirm that the hyperbranching phenotype observed upon miR-30 overexpression was due to increased *dll4* suppression, *dll4*-TP^{miR-30} was co-injected with miR-30b or miR-30c mimics into *Tg*(*kdrl*:*EGFP*) embryos. When injected alone, miR-30b and miR-30c caused hyper-migratory endothelial cells and advanced sprouting at 25 hpf (Fig. 5.10C; yellow arrowheads), which later developed into extra branches from the ISVs at 72 hpf (Fig. 5.10C; red arrowheads). These phenotypes were not seen in uninjected or NTC-injected embryos (Fig. 5.10C). Co-injection of *dll4*-TP^{miR-30} led to a partial rescue of aberrant ISV development at both 25 and 72 hpf (Fig. 5.10C). Quantification of the embryos at 24 hpf showed that the advanced sprouting phenotype was reduced by approximately half in co-injected embryos (Fig. 5.11). In this experiment ~65% of embryos injected with miR-30b (24/36) and miR-30c mimics (19/29) displayed advanced sprouting at 24 hpf (Fig. 5.11). This was reduced to 37% (10/27) and 25% (12/47) respectively when the mimics were co-injected with *dll4*-TP^{miR-30}.

The findings described in this section indicated that *dll4* downregulation is a significant contributing factor to the advanced sprouting and excessive branching phenotypes observed upon miR-30 overexpression. These data also suggest that miR-30 can regulate endothelial cell behaviour *in vivo* and that the targeting of *dll4* by miR-30 is functionally relevant during vascular development.

A

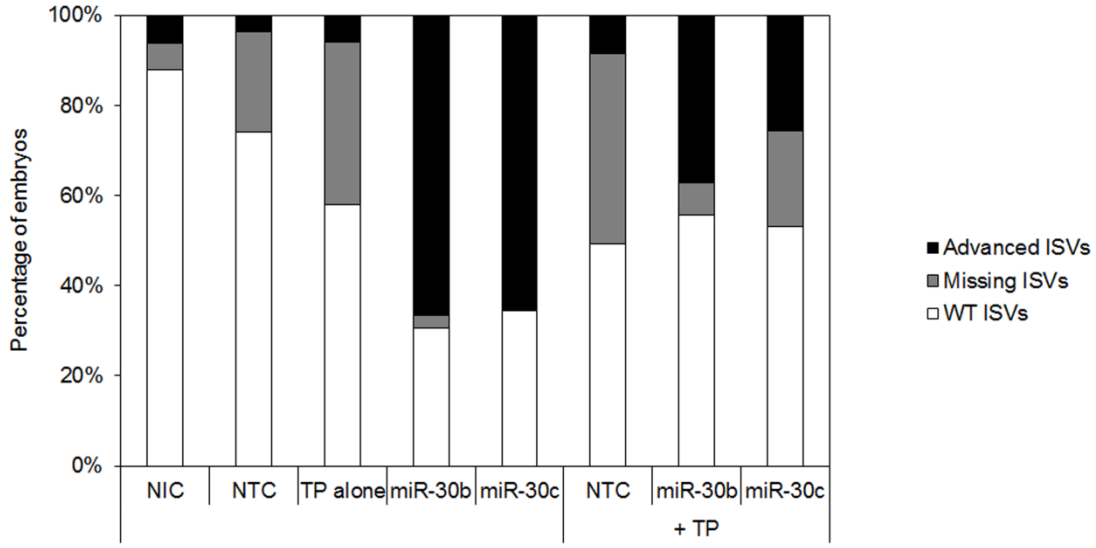

Figure 5.11. Quantification of zebrafish embryo phenotypes following co-injection of *dll4*-TP^{miR-30} with miR-30 mimics. (A) Quantification of ISV sprouting defects at 24 hpf in non-injected control (NIC) *Tg*(*kdrl:EGFP*) embryos or embryos injected with the indicated mimic and/or *dll4*-TP^{miR-30}. Embryos with severe morphological defects which prevented ISV phenotyping were discounted. n values per group ranged from 25-100 and are given in Table 2.10. Missing ISVs: embryos lacking one or more ISVs. Advanced ISVs: embryos with ISVs that have reached a more dorsal position in the trunk compared to wildtype embryos, including those displaying premature DLAV formation and vessel-free, hyper-migratory endothelial cells.

5.7. Increased *dll4* expression synergises with partial loss of Vegfa signalling to inhibit angiogenesis

When *dll4*-TP^{miR-30} was injected alone into zebrafish embryos, 36% were missing one or more ISV sprouts at 24 hpf (18/50), compared to 6% of uninjected embryos (4/66) (Fig. 5.11). Missing ISVs were also observed in 22% of NTC-injected embryos (6/27), suggesting that microinjection could be causing this effect. However, the number of NTC-injected embryos displaying missing ISVs increased to 42% upon co-injection with *dll4*-TP^{miR-30} (25/59). These data suggested that upregulation of *dll4* upon *dll4*-TP^{miR-30} injection inhibits ISV sprouting to a small extent.

To investigate this phenotype further, embryos were injected with either *dll4*-TP^{control} or *dll4*-TP^{miR-30} and *in situ* hybridisations were performed at 27 hpf to examine the expression of various vascular markers (Fig. 5.12). A literature review was conducted to identify genes that are regulated by DLL4 and therefore potentially altered upon *dll4* upregulation in embryos injected with *dll4*-TP^{miR-30} (Table 5.1). From this list *efnb2*, *hey2*, *flt1,* and *kdrl* were chosen for further analysis (Fig. 5.12). Previous experimental evidence would predict an upregulation of *efnb2*, *hey2* and *flt1* and a downregulation of *kdrl* upon *dll4* upregulation in *dll4*-TP^{miR-30} injected embryos (Table 5.1). The expected changes were not observed for *efnb2, hey2 and flt1.* This could be due to insufficient *dll4* upregulation or the differences between the zebrafish model and the *in vitro* or mouse systems in which the studies listed in Table 5.1 were conducted. In fact, changes in expression of these markers have not been observed upon *dll4* knockdown in zebrafish (Hogan et al., 2009b; Leslie et al., 2007). However, *kdrl* mRNA was clearly downregulated in the ISVs and DA of *dll4*-TP^{miR-30} injected embryos (Fig. 5.12).

Human gene ID	Zebrafish gene ID	Upregulated by DLL4/NOTCH	Downregulated by DLL4/NOTCH	Publications
ABL1	*abl1*	X		(Crowner et al., 2003; Le Gall et al., 2008)
BGN	*bgna* *bgnb*	X		(Harrington et al., 2008)
CDH5	*cdh5*	X		(Trindade et al., 2008)
CDH11	*cdh11*	X		(Harrington et al., 2008)
COL1A1	*col1a1a* *col1a1b*	X		(Trindade et al., 2008)
COL3A1	N/A			(Harrington et al., 2008)
COL4A1	*col4a1*	X		(Trindade et al., 2008)
CXCR4	*cxcr4a* *cxcr4b*		X	(Harrington et al., 2008; Williams et al., 2008)
EFNB2	*efnb2a* *efnb2b*	X		(Harrington et al., 2008; Patel et al., 2005; Trindade et al., 2008)
ELN	*elna* *elnb*	X		(Harrington et al., 2008)
EPHB4	*ephb4a* *ephb4b*		X	(Trindade et al., 2008)
FBLN5	*fbln5*	X		(Harrington et al., 2008)
FGF2	*fgf2*	X		(Harrington et al., 2008)
FLT1	*flt1*	X		(Harrington et al., 2008; Suchting et al., 2007; Trindade et al., 2008)
(soluble FLT1)	*(soluble flt1)*	X		(Harrington et al., 2008)
FLT4	*flt4*		X	(Djokovic et al., 2010; Siekmann and Lawson, 2007)
FLT4	*flt4*	X		(Shawber et al., 2007)
FN1	*fn1* *fn1b*	X		(Trindade et al., 2008)
GJA4	*cx39.4*	X		(Trindade et al., 2008)
HES5	*her2*	X		(Trindade et al., 2008)
HEY1	*hey1*	X		(Patel et al., 2005; Trindade et al., 2008)
HEY2	*hey2*	X		(Harrington et al., 2008; Trindade et al., 2008; Williams et al., 2006)
INHBA	*inhbaa* *inhbab*	X		(Harrington et al., 2008)
ITGB3	*itgb3a* *itgb3b*		X	(Harrington et al., 2008)
JAG1	*jag1a* *jag1b*	X		(Harrington et al., 2008)
KDR	*kdr* *kdrl*		X	(Harrington et al., 2008; Henderson et al., 2001; Li et al., 2006; Suchting et al., 2007; Williams et al., 2006)
LAMA1	*lama1*	X		(Trindade et al., 2008)
LAMB1	*lamb1a* *lamb1b*	X		(Trindade et al., 2008)
LAMC1	*lamc1*	X		(Trindade et al., 2008)
MET	*met*		X	(Harrington et al., 2008)
MMP1	N/A		X	(Trindade et al., 2008)
MMP2	N/A		X	(Trindade et al., 2008)
MMP9	*mmp9*		X	(Trindade et al., 2008)
MMP10	N/A	X		(Harrington et al., 2008)

Table 5.1A. Genes regulated by DLL4: A-M. For ease, human and zebrafish gene IDs have been given even if the link between DLL4 and the specified gene was made in another species.

Human gene ID	Zebrafish gene ID	Upregulated by DLL4/NOTCH	Downregulated by DLL4/NOTCH	Publications
NOTCH3	*notch3*	X		(Harrington et al., 2008)
NR2F2	*nr2f2*		X	(Diez et al., 2007)
NRARP	*nrarpa* *nrarpb*		X	(Krebs et al., 2001; Lamar et al., 2001; Pirot et al., 2004)
NRP1	*nrp1a* *nrp1b*		X	(Harrington et al., 2008; Williams et al., 2006)
NRP2	*nrp2a* *nrp2b*		X	(Harrington et al., 2008; Trindade et al., 2008)
PCDH12	N/A		X	(Harrington et al., 2008)
PDGFRB	*pdgfrb*		X	(Djokovic et al., 2010)
PIGF	*pigf*		X	(Harrington et al., 2008)
RASSF2	*rassf2a* *rassf2b*		X	(Harrington et al., 2008)
ROBO4	*robo4*		X	(Trindade et al., 2008)
RND1	*rnd1* *rnd1l*	X		(Harrington et al., 2008)
SEMA5A	*sema5a*	X		(Harrington et al., 2008)
SDC1	N/A	X		(Harrington et al., 2008)
SLIT2	*slit2*	X		(Harrington et al., 2008)
SLIT3	*slit3*	X		(Harrington et al., 2008)
SNAI2	*snai1*	X		(Harrington et al., 2008)
STAT1	*stat1a* *stat1b*	X		(Harrington et al., 2008)
TEK	*tek*	X		(Djokovic et al., 2010)
UNC5B	*unc5b*	X		(Trindade et al., 2008)
VCAM1	*vcam1*	X		(Harrington et al., 2008)
VEGFA	*vegfaa* *vegfab*		X	(Djokovic et al., 2010)
VEGFC	*vegfc*		X	(Djokovic et al., 2010)

Table 5.1B. Genes regulated by DLL4: N-Z. For ease, human and zebrafish gene IDs have been given even if the link between DLL4 and the specified gene was made in another species.

Notch signalling via DLL4 is known to negatively regulate KDR expression (Harrington et al., 2008; Henderson et al., 2001; Li et al., 2006; Suchting et al., 2007; Williams et al., 2006). This regulation is thought to occur through direct binding of HEY1 to the KDR promoter (Henderson et al., 2001; Holderfield et al., 2006). Decreased expression of *kdrl* upon *dll4*-TP$^{miR\text{-}30}$ injection suggested that transcription of *kdrl* is also controlled by Dll4-induced Notch signalling and that endogenous miR-30 could indirectly affect *kdrl* levels by negatively regulating *dll4* expression.

To investigate the functional implications of this potential regulatory network, vascular development was examined in *Tg(fli1a:EGFP)* embryos following microinjection of various MOs and TPs (Fig. 5.13A).

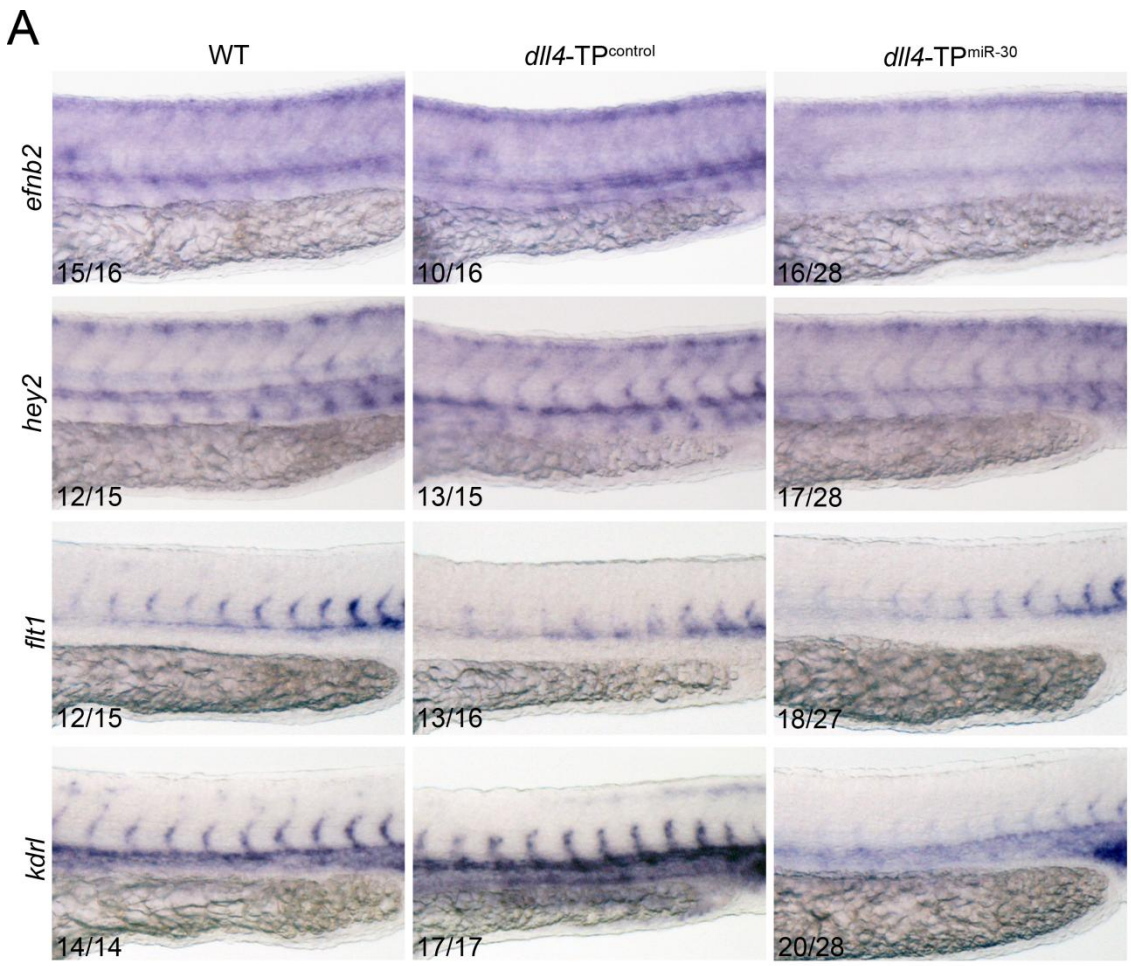

Figure 5.12. Expression of zebrafish vascular markers following microinjection of *dll4*-TP^{miR-30}. (A) Representative *in situ* hybridizations showing expression of *efnb2*, *hey2*, *flt1* and *kdrl* mRNA in the developing vasculature of wildtype (WT) zebrafish embryos or embryos injected with 10ng of the indicated TP. Values denote the number of embryos with the predominant, displayed phenotype out of the total number of embryos assayed. Microinjections and *in situ* hybridisations were performed by Gemma Bridge and Rui Monteiro. Images were taken by Rui Monteiro.

The *Tg(kdrl:EGFP*) line could not be used for these experiments as the intention was to interfere with *kdrl* expression which would subsequently affect *EGFP* expression. *Tg(fli1a:EGFP)* embryos differ slightly from *Tg(kdrl:EGFP)* embryos as both lymphatic and blood endothelial cells fluoresce in *Tg(fli1a:EGFP)* embryos. The *Tg(fli1a:EGFP)* line was chosen, because it had previously been used to characterise the relationship between Kdr and Kdrl with respect to Vegfa signalling and ISV sprouting (Bahary et al., 2007). The *kdr* and *kdrl* MOs used in this study were also adopted and injected in the quantities previously specified (Table 2.8).

When *kdr* MO was injected alone, it had a modest impact on ISV sprouting (Fig. 5.13A ii; B). Approximately half the embryos displayed normal ISV development at 28 hpf compared to uninjected control embryos (19/40) (Fig. 5.13A i and ii; B). The majority of the remaining embryos had moderate impairment of ISV sprouting, lacking at least one ISV, but with a minimum of 6 intact ISVs (19/40) (Fig. 5.13B). The *kdrl* MO had a more significant impact, as the majority of embryos displayed stunted or missing ISVs (29/41) (Fig. 5.13A iii; B). However, this impairment was mainly moderate (21/41), and 20% of embryos had WT ISVs (12/41) (Fig. 5.13B). These findings concur with the work of Bahary and colleagues (Bahary et al., 2007), and confirm that Vegfa signalling can continue to some extent in the absence of one zebrafish VEGFR2 orthologue. If Vegfa signalling was completely abolished, as occurs upon *vegfaa* knockdown, ISV development would be entirely inhibited (Christie et al., 2010; Nasevicius et al., 2000).

Simultaneous knockdown of *kdr* and *kdrl* has previously been shown to cause complete loss of ISVs (Bahary et al., 2007), and this phenotype was successfully recapitulated with MOs (Fig 5.13B iv). When *dll4*-TP$^{miR\text{-}30}$ was injected alone, ~40% of embryos exhibited moderate impairment of ISV sprouting (19/50) (Fig. 5.13B). This concurred with the missing ISVs observed in *Tg(kdrl:EGFP*) embryos injected with *dll4*-TP$^{miR\text{-}30}$ (Fig. 5.11). This effect was not seen in embryos injected with *dll4*-TP^{control} (Fig. 5.13B) and suggested that a decrease in *kdrl* expression in *dll4*-TP$^{miR\text{-}30}$ injected embryos was affecting efficient Vegfa signalling. Co-injection of *dll4*-TP$^{miR\text{-}30}$ with *kdr* MO resulted in a significantly greater loss of ISV sprouting when compared to *dll4*-TP$^{miR\text{-}30}$ alone

(Fig. 5.13A vii and viii; B). Approximately 80% of *dll4*-TP^{miR-30} + *kdr* MO injected embryos had some form of ISV inhibition (30/37) and ~30% had 5 or less intact ISVs (11/37) (Fig. 5.13B). It was concluded that loss of ISV sprouting in *dll4*-TP^{miR-30} + *kdr* MO injected embryos is caused by the combined downregulation of *kdrl* and *kdr,* because this is a partial phenocopy of *kdr* and *kdrl* MO-mediated knockdown (Fig. 5.13A iv) and *kdrl* expression was shown to be reduced upon *dll4*-TP^{miR-30} injection (Fig. 5.12). The reduction in ISV sprouting in TP^{miR-30} + *kdr* MO injected embryos probably occurs because these genes encode the two zebrafish Vegfa receptors (Bahary et al., 2007; Covassin et al., 2006).

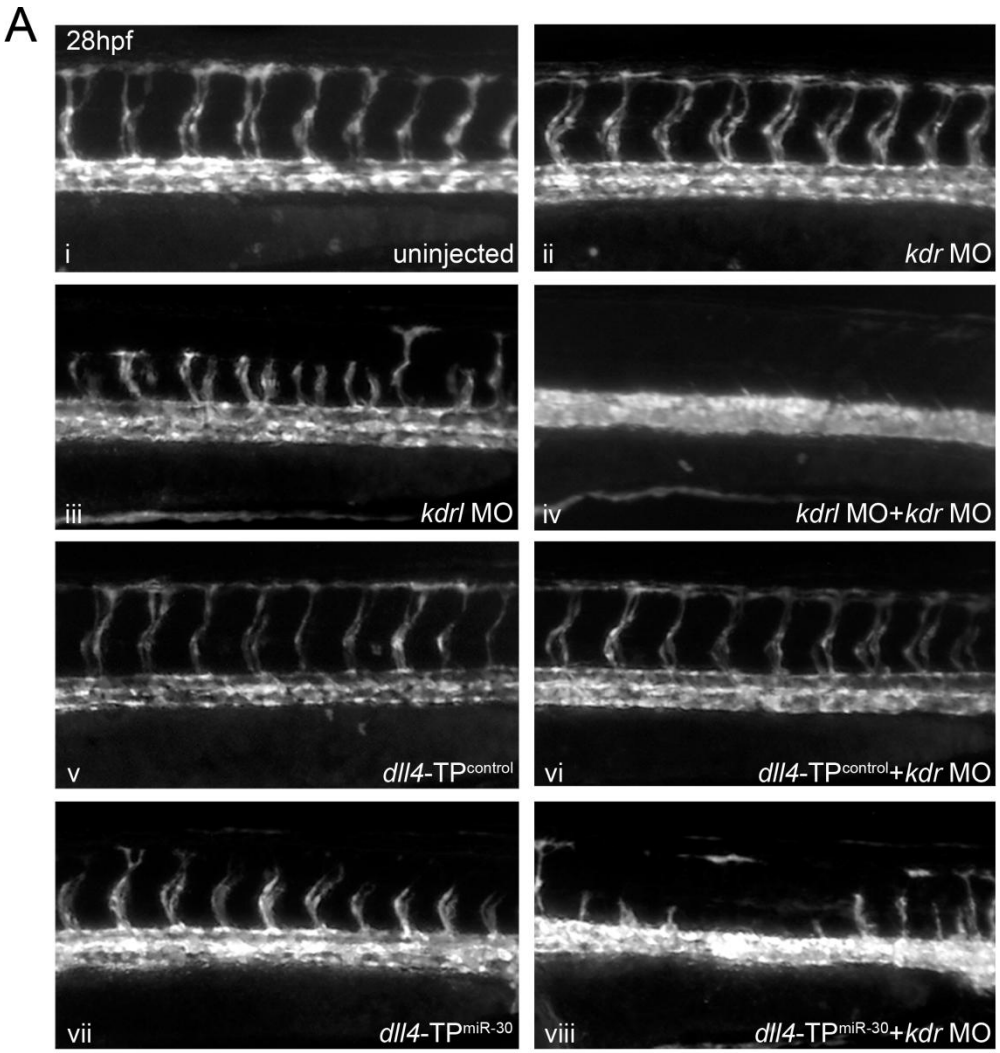

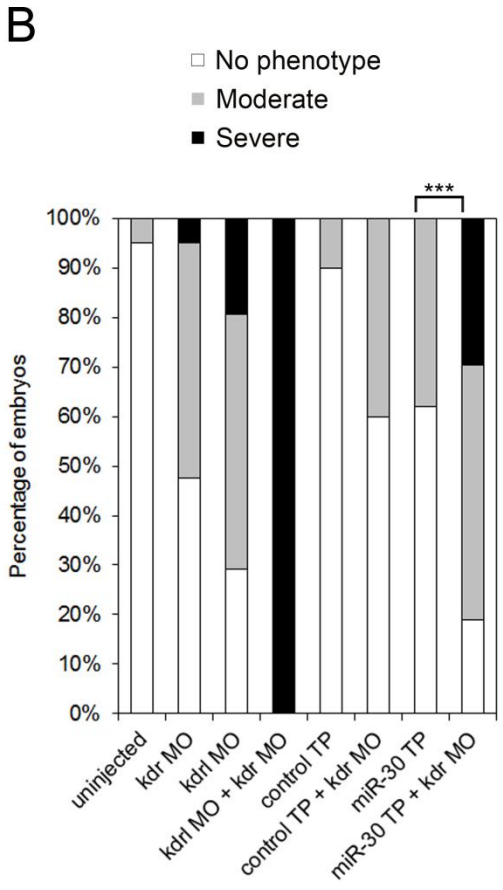

Figure 5.13. Loss of *dll4* regulation by miR-30 synergises with partial Vegfa signalling knockdown to block angiogenesis. (A) Trunk vasculature in uninjected *Tg*(*fli1a:EGFP*) embryos or embryos injected with the indicated MO and/or TP at 28 hpf. (B) Quantification of ISV sprouting defects following injection of the MOs and/or TPs indicated. Columns are the average of two independent experiments with 15-30 embryos counted per sample per experiment. Moderate phenotype: embryos lacking 1 ISV but with a minimum of 6 ISVs. Severe phenotype: embryos with 5 or less ISVs. To determine statistical significance, a Wilcoxon rank-sum test was performed. ***, $p<0.001$. Microinjections were performed by Rui Monteiro. Fluorescent imaging was performed by Rui Monteiro with the assistance of Gemma Bridge. Phenotype quantification was performed by Gemma Bridge.

5.8. Discussion

The work discussed in this chapter confirmed that miR-30 can suppress *dll4 in vivo* and demonstrated that increased targeting of *dll4* through miR-30 overexpression results in aberrant ISV development. Active targeting of *dll4* by endogenous miR-30 was demonstrated through the use of a target protector, and this regulation was shown to provide robustness to Vegfa signalling by indirectly influencing *kdrl* expression.

Analysis of zebrafish RNA from various developmental time points revealed that expression of both *dll4* and miR-30 can be detected from 6 hpf and is strongly induced at 12 hpf. This concurs with previous studies: *dll4* mRNA is first detected by RT-PCR at 8 hpf, but upregulated at 12 hpf (Leslie et al., 2007); zebrafish miRNAs have been detected from 4 hpf by small RNA cloning and from 12 hpf by microarray analysis (Chen et al., 2005; Wienholds et al., 2005). Of particular interest to this study was the inverse correlation between *dll4* and miR-30 expression during the first wave of angiogenic sprouting from the DA (18-24 hpf). These temporally coincident changes in *dll4* and miR-30 are consistent with a functional interaction that may contribute to tight control of Dll4 expression during zebrafish vascular development.

In zebrafish, endothelial cells first begin to sprout from the DA to form SAs at ~22 hpf (Isogai et al., 2003). The initiation of this angiogenic program requires Vegfa signalling via the VEGFR2 functional orthologues, Kdr and Kdrl (Bahary et al., 2007; Habeck et al., 2002). This promotes loosening of cell junctions, cell division and migratory behaviour in endothelial cells of the DA (Ellertsdóttir et al., 2010). DLL4 is known to suppress KDR (VEGFR2) expression (Harrington et al., 2008; Henderson et al., 2001; Li et al., 2006; Suchting et al., 2007; Williams et al., 2006). I therefore hypothesised that the observed downregulation of *dll4* at 18 hpf, continuing until 24 hpf, would permit sufficient Vegfa signalling for successful SA development.

dll4 expression was found to increase again at 30 hpf, which coincides with the end of the first wave of angiogenic sprouting. A secondary wave of angiogenic sprouting begins at 32 hpf from the PCV; these sprouts connect with an existing

SA to form a SV (Isogai et al., 2003). However, Vegfa signalling is not required for SV formation, therefore high Dll4 expression is not an impediment to this process (Covassin et al., 2006; Covassin et al., 2009; Lawson et al., 2003). Venous development in zebrafish is dependent on Vegfc/Flt4 signalling, but in the absence of Dll4, arterial endothelial cells are also stimulated by Vegfc (Covassin et al., 2006; Hogan et al., 2009b). This is because Dll4 acts to suppress the ability of arterial endothelial cells to respond to Vegfc/Flt4 signalling, whereas venous endothelial cells do not express Dll4 and therefore are able to respond to Vegfc (Hogan et al., 2009b). As such, the high levels of *dll4* observed in this study at 30 hpf might be acting to suppress arterial angiogenesis in response to Vegfc during the period of SV formation.

It was concluded from the work shown in Chapter 4 that *DLL4* is a genuine target of miR-30 in human endothelial cells *in vitro* and that this targeting occurs via a specific target site within the *DLL4* 3'UTR. Here, injection of miR-30 mimics into zebrafish embryos proved that *dll4* is also downregulated by exogenous miR-30 *in vivo*. Intriguingly, when injected at high concentrations, miR-30 mimics caused severe morphological abnormalities which could not be attributed solely to *dll4* targeting. Due to the small size of miRNA target sites and the wide range of canonical, marginal and atypical sites, each miRNA has the potential to target hundreds or even thousands of genes (Bartel, 2009). The current version of TargetScanFish predicts 7037 gene targets for the miR-30 family. One potential target for future investigation is the Wnt family member *wingless-type MMTV integration site family member 5b* (*wnt5b)*. This gene is required for tail formation in zebrafish embryos (Rauch et al., 1997), and therefore its downregulation could potentially explain the aberrant tails observed when miR-30 was injected at high concentrations.

Other predicted targets of miR-30 include the Notch ligands deltaC (*dlc)* (*DLL3* orthologue), *jag1a* and *jag2* and the Notch target genes *hairy-related 1* (*her1*) (HES7 orthologue), *her3* (*HES3* orthologue) *her4.3* and *her4.4*. Previous work suggests that downregulation of *dlc* and *her1* could directly interfere with the oscillator mechanism of somite generation (Holley et al., 2002). Therefore, there are multiple possible routes whereby miR-30 could interfere with somitogenesis leading to aberrant embryonic patterning. This could potentially explain the

defects in tail development observed in embryos injected with large quantities of miR-30 mimic.

It is known that Notch signalling plays a fundamental role in zebrafish somitogenesis. Mutations in *notch1a*, *dlc* and *deltaD* (*dld*) (*DLL1* orthologue) all cause defective somitogenesis (Holley et al., 2002; vanEeden et al., 1996). Dll4 predominantly signals through Notch1b rather than Notch1a, as only *notch1b* morphants recapitulated the vascular phenotype of *dll4* morphants, *dll4* mutants and DAPT-treated embryos (Leslie et al., 2007). However, additional signalling through Notch1a could also occur because, although morpholinos against *notch1a* were used by Leslie and colleagues, the phenotypes of these embryos were not described (Leslie et al., 2007). Therefore, Dll4 could play a minor role in somitogenesis. When several other relevant somitogenic regulators are downregulated in the context of miR-30 overexpression, such as *dlc* and *her1*, significant *dll4* suppression could contribute to defective patterning. Mutations in *notch1a*, *dlc* and *dld* are also known to cause defective neurogenesis, therefore the predicted regulation of *dlc* and *her1* by miR-30 could also be of relevance to this process (Gray et al., 2001; Julich et al., 2005). When *runx1* expression was examined in miR-30 overexpressing embryos, abnormal neural patterning was indeed observed.

The expression of *runx1* following miR-30 overexpression was assessed alongside the expression of several other vascular markers. This demonstrated that *runx1*, *dab2* and *flt4* are all downregulated in the trunk of miR-30 injected embryos when compared to WT or NTC-injected embryos. Downregulation of *runx1* was not due to inhibition of haematopoietic endothelium specification, as seen in the *dll4* morphants. *runx1* positive cells could still be identified, but with a reduced level of *runx1* expression. This suggested that *dll4* suppression in miR-30 overexpressing embryos is not sufficient to impair HSC emergence, as seen upon Notch inhibition (Burns et al., 2005; Gering and Patient, 2005). Decreased *runx1* expression in miR-30 injected embryos could be due to direct targeting of *runx1* by miR-30. Exogenous miR-30c has been shown to target the *RUNX1* 3'UTR using a luciferase reporter assay and the miR-30 family is known to regulate human adipogenesis by targeting another RUNX family member, *RUNX2* (Ben-Ami et al., 2009; Zaragosi et al., 2011). When the predicted

targets of the zebrafish homologue of miR-30, dre-miR-30, were examined, *runx2a*, *runx2b* and *runx3* were all found to contain one or more miR-30 target sites within their 3'UTRs. However, it was not possible to assess the likelihood of *runx1* targeting by dre-miR-30 as the 3'UTR of this gene is not currently contained within the TargetScanFish database (Version 6.2). If *runx1* is a functional target of miR-30 *in vivo*, this could implicate the miR-30 family in regulating the emergence and maintenance of HSCs by providing a fine-tuning mechanism to restrict excessive or ill-timed *runx1* expression.

Two venous markers, *dab2* and *flt4*, were downregulated in the trunk region of miR-30 overexpressing embryos and to a lesser extent in the head, a phenotype not seen in *dll4* morphants. *dab2* mRNA suppression could be due to direct targeting of *dab2* by miR-30, as two of the four *dab2* 3'UTRs expressed during zebrafish development contain predicted miR-30 target sites (TargetScanFish). However, *flt4* is not a predicted target of miR-30 therefore *flt4* expression in miR-30 overexpressing embryos is probably altered due to changes in other miR-30 targets.

The pattern of *dab2* and *flt4* staining in the miR-30 overexpressing embryos at 26-27 hpf also revealed that exogenous miR-30 impairs venous positioning. A wider gap was seen between the cardinal veins post-bifurcation, the DCs were larger and disorganised, and in the case of *flt4*, two lines of cells could be seen in a region where only the single path of the PCV should be marked. In addition, *dab2* and *flt4* positive cells had not migrated to the midline correctly at the 14 somite stage (16 hpf) in miR-30 overexpressing embryos (data not shown). These data suggest that one or more miR-30 targets are involved in angioblast migration and/or venous cell specification.

Vasculogenesis of the DA and PCV is initiated in zebrafish when two lateral stripes of angioblasts begin to migrate towards the midline at 14 hpf and coalesce to form a vascular cord. Overexpression of miR-30 appears to prevent complete angioblast migration. This could be due to three predicted targets of dre-miR-30: *semaphorin 3ab* (*sema3ab*) and the genes that encode the Sema3a receptors, *nrp1a* and *nrp1b*. One of the duplicate *sema3a* zebrafish genes, *sema3aa*, has been shown to act as a guidance factor in the migration

of angioblasts by signalling through a receptor complex which contains Nrp1 (Shoji et al., 2003). miR-30 is predicated to target the other sema3a gene, sema3ab, and also both of the *nrp1* genes (*nrp1a* and *nrp1b*). By downregulating a key guidance factor and the receptor through which it signals, exogenous miR-30 may impair angioblast migration in miR-30 injected embryos. The predicted targeting of *sema3a* by miR-30 in zebrafish is supported by the finding that exogenous miR-30b and -30d suppress *SEMA3A* mRNA levels and target the *SEMA3A* 3'UTR *in vitro* (Gaziel-Sovran et al., 2011).

Arterio-venous specification of the primary vascular cord in zebrafish occurs through the differential expression of either *efnb2a* (arterial) or *ephb4a* (venous) and ventral sprouting begins at 21 hpf to form the PCV (Herbert et al., 2009). dre-miR-30 is predicted to target many zebrafish ephrins and ephrin receptors (TargetScanFish). Among these are *efna1a*, *efnb2a*, *epha2*, *ephb2a*, *ephb2b* and *ephb3a,* which have all been linked to endothelial cell migration and angiogenesis (www.genecards.org). Further investigation into the factors regulating cardinal vein bifurcation and DC development is required before potential miR-30 targets can be linked to these processes.

Injection of *dll4* MO was used as a positive control for *dll4* knockdown in this work and successfully recapitulated the hyper-migratory endothelial cells and ISV hyperbranching reported in previous studies (Biyashev et al., 2011; Hogan et al., 2009b; Leslie et al., 2007). Biyashev *et al*. also observed the formation of a single dorsal vessel in *dll4* morphants, rather than the expected DA and PCV (Biyashev et al., 2011), a phenotype which was not seen in this work. They explained that this was consistent with previous observations by Herbert *et al*., where *hey2* MO injection and the Notch inhibitor DAPT promoted the loss of the DA (Herbert et al., 2009). It should be noted that *hey2* knockdown and Notch inhibition will interfere with all Notch signalling and are not specific to Dll4 signalling via Notch1.

Overexpression of miR-30 in zebrafish embryos phenocopied *dll4* knockdown. At 24 hpf, overly advanced ISV sprouts and hyper-migratory endothelial cells were observed leading to premature DLAV formation. Excessive motility of

endothelial cells in *dll4* morphants has been attributed to a lack of tip cell fate restriction (Biyashev et al., 2011). This concurs with the work of Hellström *et al*. in the developing mouse retina, where Dll4-Notch1 signalling between endothelial cells within the angiogenic sprout was shown to maintain the optimal ratio of tip and stalk cells (Hellström et al., 2007). However, the tip cell markers *dll4* and *flt4* are expressed in both tip and stalk cells within the sprouting ISV of zebrafish (Hogan et al., 2009b; Leslie et al., 2007; Siekmann and Lawson, 2007). Additionally, tip and stalk cells proliferate at similar rates in zebrafish ISVs (Blum et al., 2008). Therefore, the model of clearly defined tip and stalk cells is not directly transferable to the zebrafish system. More recent work has shown that tip cell specification in the mouse is actually a dynamic process as endothelial cells within the sprout continually compete for the leading position (Jakobsson et al., 2010). This process is based on differing levels of VEGFR1 and VEGFR2; those cells expressing low VEGFR1 and high VEFR2 obtain the tip cell position, whereas cells with high VEGFR1 and low VEGFR2 temporarily assume the stalk cell position. As receptor levels fluctuate in response to VEGFA signalling and cells continually meet new neighbours the relative ratio of VEGFR1:VEGFR2 is constantly reassessed and cells switch positions (Jakobsson et al., 2010). However, for differential VEGFR levels to impact on tip and stalk specification, DLL4/Notch signalling must be active (Jakobsson et al., 2010). If this dynamic equilibrium also occurs during zebrafish angiogenesis, downregulation of *dll4* upon miR-30 overexpression may abrogate the tip cell advantage of cells with higher Kdr or Kdrl whilst simultaneously increasing Kdrl expression, allowing more cells to respond to Vegfa gradients. Therefore, the hyper-migratory endothelial cells seen upon miR-30 overexpression and *dll4* knockdown may arise due to perturbations in the Flt1:Kdr equilibrium when Notch/Dll4 signalling is repressed.

The excessive ISV branching observed at 72 hpf in both miR-30 and *dll4* MO injected embryos is a later consequence of the aberrant tip cell regulation observed at 24 hpf. However, it is also linked to the role of Dll4 in restricting the exploratory behaviour of endothelial cells once ISV sprouting has finished and the DLAV is formed. In *dll4* morphants, endothelial cells comprising the DLAV and ISVs are not quiescent but continue to extent and retract filopodia and advance into ectopic locations, forming extra ISV branches (Leslie et al., 2007).

A reduction in DA diameter was observed in zebrafish embryos upon *dll4* knockdown by either *dll4* MO or miR-30 mimic. A similar phenotype has been observed in mice following *Dll4* knockdown and DLL4 upregulation is known to promote vessel maturation and increase vessel size in both human cancer and mouse development (Duarte et al., 2004; Gale et al., 2004; Li et al., 2007; Patel et al., 2006; Trindade et al., 2008). However, this is the first report of a decrease in DA width upon *dll4* knockdown in zebrafish.

Co-injection of miR-30 with a TP specific to the dll4/miR-30 target site demonstrated that the excessive vascular sprouting caused by miR-30 overexpression could be explained by *dll4* targeting. The TP was also an elegant tool with which to explore the endogenous role of miR-30 during zebrafish vascular development. It was used to specifically block the interaction of miR-30 with *dll4* mRNA during development, whilst still allowing miR-30 to interact with its other targets. When the normal control of *dll4* by miR-30 was inhibited, *dll4* mRNA was elevated and ISV formation was impaired. This finding suggests that miR-30 actively suppresses *dll4* during normal ISV sprouting, helping to maintain tight control of angiogenesis.

When *dll4* levels were increased using the TP, *kdrl*, a functional orthologue of VEGFR2, was downregulated. Vegfa signalling in zebrafish is mediated through the synergistic action of Kdrl and another Vegfa receptor, Kdr (Bahary et al., 2007; Covassin et al., 2006). ISV sprouting was moderately to severely inhibited in the majority of embryos when *dll4*-TP$^{miR\text{-}30}$ injection was combined with *kdr* knockdown. This partially recapitulated the phenotype seen when the expression of both *kdrl* and *kdr* was blocked using morpholinos and also the phenotype observed upon *vegfaa* knockdown (Bahary et al., 2007; Christie et al., 2010; Nasevicius et al., 2000).

It is proposed that minor increases in *dll4* expression are controlled by miR-30 to ensure appropriate *kdrl* expression and hence ISV development. This model is supported by several studies which show that the majority of miRNAs act to fine-tune the expression of target genes (Baek et al., 2008; Selbach et al., 2008). This work has therefore revealed that the miR-30 family indirectly

regulates Vegfa signalling by controlling *dll4* expression and that this regulatory axis confers robustness to Vegfa-mediated angiogenesis.

Chapter 6. Discussion and future work

6.1 Summary

An investigation into the predicted targets of miRNAs with altered expression in KLEC led to the discovery that the miR-30 family targets the Notch pathway ligand DLL4 and that this interaction is relevant to endothelial biology *in vivo*. The main findings of this work are:

Evaluation of the predicted targets of miRNAs altered upon KSHV infection of LEC (Chapter 3)

- Detailed analysis of *in silico* target prediction results of KSHV-regulated miRNAs and cross-comparison with angiogenic genes.
- Identification of a putative regulatory relationship between miR-30 and DLL4.
- Confirmation of miR-30 upregulation and DLL4 downregulation in human dermal LEC.

miR-30b and miR-30c target DLL4 (Chapter 4)

- DLL4 is an experimentally validated target of miR-30b and miR-30c *in vitro*.
- Overexpression of miR-30 attenuates upregulation of DLL4 in KLEC.
- miR-30b promotes sprouting angiogenesis *in vitro*.

miR-30-mediated regulation of *dll4* affects endothelial cell behaviour during zebrafish development (Chapter 5)

- dll4 is an experimentally validated target of miR-30b and miR-30c *in vivo*.
- Exogenous expression of miR-30 induces aberrant intersegmental vessel development and branching in zebrafish by way of *dll4* targeting.
- Disruption of miR-30/*dll4* targeting causes increased *dll4* expression and hence downregulates *kdrl* and inhibits angiogenesis, particularly in synergy with *kdr* loss.
- miR-30 regulation of *dll4* expression during development confers robustness to Vegfa-mediated angiogenesis.

6.2 Conclusions

The discovery of miRNAs in 1993 has revealed a highly complex additional layer of gene regulation that appears to function in a diverse range of cellular processes. It is therefore not surprising that several miRNAs have been identified as key regulators of endothelial cell behaviour and angiogenesis (Anand et al., 2010; Biyashev et al., 2011; Bonauer et al., 2009; Chen and Gorski, 2008; Fang et al., 2011; Fasanaro et al., 2008; Fish et al., 2008; Lee et al., 2007; Nicoli et al., 2010; Poliseno et al., 2006; Suarez et al., 2008; Urbich et al., 2012; Wang et al., 2008). However, at the onset of this work, the list of angiomiRs was not as extensive and miRNA regulation of key endothelial signalling pathways, such as the Notch pathway, had not been reported. KSHV infection of endothelial cells provided a tractable model with which to study the involvement of miRNAs in vascular biology (Mesri et al., 2010; Wang et al., 2004).

6.2.1 DLL4: a new target of the miR-30 family

This work shows that two members of the miR-30 family, miR-30b and miR-30c, target the Notch ligand *DLL4* and can influence endothelial cell behaviour *in vitro*. Currently validated targets of one or more members of the miR-30 family include B-cell lymphoma 6 (*BCL6*) (Lin et al., 2011), *LIM homeobox 1* (*lhx1*) (Agrawal et al., 2009), lin-28 homolog (*LIN28*) (Zhong et al., 2010), v-myb myeloblastosis viral oncogene homolog (avian)-like 2 (*MYBL2*) (Martinez et al., 2011), *RUNX2* (Zaragosi et al., 2011) and snail family zinc finger 1 (*SNAI1*) (Zhang et al., 2012). Members of the miR-30 family have previously been implicated in adipogenesis (Zaragosi et al., 2011), cancer (Braun et al., 2010; Yu et al., 2010), cellular senescence (Martinez et al., 2011), epithelial-to-mesenchymal transition (EMT) (Braun et al., 2010; Zhang et al., 2012), myocardial matrix remodelling (Duisters et al., 2009), osteoblast differentiation (Wu et al., 2012) and pronephros development (Agrawal et al., 2009). This is the first time that the miR-30 family has been shown to target a member of the Notch signalling pathway and play in role in angiogenesis.

6.2.2 miRNA regulation of the Notch pathway

The work presented in this thesis validates miR-30b and miR-30c as two miRNAs that target the Notch ligand *DLL4*. When this work was begun, miRNA targeting of the Notch ligand *DLL4* had not been described. However, in late 2011, it was reported that miR-27b targets *dll4* in endothelial cells (Biyashev et al., 2011). Knockdown of miR-27b in zebrafish embryos resulted in a severe impairment of ISV and DLAV formation. Interestingly, miR-27b morphants observed in another study did not display as severe a phenotype, perhaps due to differences in morpholino design and injection quantities (Urbich et al., 2012). The phenotype described by Biyashev and colleagues was attributed to *dll4* and *sprouty homolog 2* (*spry2*) targeting, because knockdown of these two genes rescued the defective sprouting, whereas overexpression of *spry2* induced a similar phenotype (Biyashev et al., 2011). However, with each miRNA possibly regulating hundreds of individual genes, it is possible that one or more additional miR-27b targets could be involved. For example, the angiogenesis inhibitor *semaphorin 6A* (*SEMA6A*) has also been identified as a target of miR-27b and silencing of SEMA6A partially reversed the inhibition of endothelial cell sprouting caused by miR-27b inhibition (Urbich et al., 2012). Further studies using target protector morpholinos, as carried out here for miR-30, would allow the delineation of the respective contributions of *dll4* and *spry2* to the phenotype observed upon miR-27b knockdown. From the use of target protectors in this thesis, it can be concluded that *dll4* downregulation is a significant contributing factor to the advanced sprouting and excessive branching phenotypes observed upon miR-30 overexpression.

6.2.3 A novel regulatory axis that confers robustness to Vegfa-mediated angiogenesis

A common reported function of miRNAs in a multitude of biological contexts is that they “confer robustness” to a particular cellular process or signalling pathway (Ebert and Sharp, 2012). Some of these biological processes cannot tolerate fluctuations in mRNA copy number and miRNAs act to suppress any variability, for example during cell fate induction and differentiation (Lüningschrör et al., 2013).

Figure 6.1. A schematic representation of the functional consequences of DLL4 targeting by miR-30. (A) A zebrafish embryo at 72 hpf is depicted. A section of the intersegmental vessels (ISV) has been enlarged. The dorsal aorta (DA) and posterior cardinal vein (PCV) have also been depicted in red and blue respectively. The dorsal longitudinal anastomotic vessel (DLAV) is shown in purple. (B) When miR-30 is overexpressed, *dll4* is downregulated and a deregulated network of intersegmental vessels forms as the tip cell phenotype is not restricted and excessive sprouting occurs. (C) When miR-30 regulation of *dll4* is blocked using a target protector, *dll4* is upregulated and consequently *kdrl* expression is reduced. When combined with *kdr* knockdown, the restriction of tip cell specification and inhibition of Vegfa signalling which ensues prevents normal intersegmental vessel sprouting and the DLAV does not form. (Figure adapted from Figure 6 of Bridge *et al*., 2012).

Other systems require the reinforcement of transcriptional programmes in order to elicit the required outcome, as seen in the response to hypoxia (De Lella Ezcurra et al., 2012). The model that is proposed in this thesis concurs with the former scenario. This work has shown that miR-30 acts to fine tune *dll4* levels during zebrafish vascular development, allowing sprouting angiogenesis to occur to the required extent (Figure 6.1A). When miR-30 is overexpressed, *dll4* is downregulated so tip cell fate is not restricted; this results in excessive branching from the ISVs (Figure 6.1B). If the interaction between miR-30 and *dll4* is inhibited, the latter is up-regulated and consequently there is a reduction in *kdrl* expression (Figure 6C). If *kdr* is also suppressed, the subsequent lack of Vegfa signalling impairs ISV sprouting (Figure 6C). It is suggested that this phenotype is due to impaired Vegfa signalling because Kdr and Kdrl are the two known receptors for Vegfa in zebrafish and co-injection of *dll4*-TP^{miR-30} and the *kdr* MO partially phenocopies knockdown of both *kdr*/*kdrl* and *vegfaa* (Bahary et al., 2007; Christie et al., 2010; Covassin et al., 2006; Habeck et al., 2002; Nasevicius et al., 2000).

6.3 Future work

6.3.1 Target identification for miRNAs altered upon KSHV infection

Confirmation that *DLL4* is a functional target of miR-30 has validated the target prediction strategy adopted in Chapter 3. The identification of miRNA/mRNA pairs that display converse expression changes as a result of an external stimulus is a valuable tool. At the present time, the targets of only two other KSHV-regulated miRNAs have been identified (Lagos et al., 2010; Punj et al., 2010). Punj *et al*. have demonstrated that miR-146a is upregulated by vFLIP in vascular endothelial cells and that enhanced miR-146a expression decreases chemokine receptor 4 (CXCR4) levels (Punj et al., 2010). It is possible that miR-146a mediated CXCR4 suppression promotes the premature release of KSHV-infected endothelial progenitors into the circulation, thereby contributing to KS development (Punj et al., 2010). Upon KSHV infection in LEC, miR-132 is highly upregulated due to CREB-induced transcriptional activation (Lagos et al., 2010). miR-132 facilitates viral replication by inhibiting expression of p300, a

transcriptional co-activator, and this function of miR-132 is also required during herpes simplex virus-1 (HSV-1) and human cytomegalovirus (HCMV) infection (Lagos et al., 2010). Further investigations into the targets of putative KSHV-regulated miRNAs could reveal several other miRNA-mRNA interactions that may be relevant to KSHV biology, the viral immune response, KS pathogenesis or angiogenesis. For example, the pro-angiogenic gene *FGFR2* is upregulated in KLEC and is predicted to be a target of the downregulated miRNAs miR-494 and miR-513. Whereas, a panel of miRNAs that are upregulated in KLEC are predicted to target the putative anti-angiogenic gene *NARG1* which is downregulated in KLEC.

6.3.2 Additional roles of miR-30 during zebrafish development

When miR-30 mimics were injected into zebrafish embryos at high concentrations, severe morphological defects were observed that were not present in the NTC-injected mimics. Additionally, abnormal expression and patterning of *runx1*, *dab2* and *flt4* was observed in miR-30 overexpressing embryos and these changes differed from those seen in *dll4* morphants. This suggests that miR-30 has one or more functional targets in zebrafish that are required for vascular and possibly whole embryo patterning. To investigate this further, TPs could be used to identify which targets are contributing to these phenotypes and exactly what contribution they make to the observed abnormalities. TPs would be designed against predicted miR-30 target sites within in the 3'UTRs of possible candidates. These would include *nrp1*, *sem3aa*, *efna1a*, *efnb2a*, *epha2*, *ephb2a*, *ephb2b*, *wnt4a*, *wnt16*, *wnt6b*, *wnt7a*, *wnt5b*, *wnt10a*, *wnt2bb* and *wnt9a*. Nrp1, Sem3a and the ephrins and EPH receptors are all known to be involved in cell migration and guidance. Wnt signalling is vital for numerous developmental processes including planar cell polarity, neural tube patterning, axon guidance, stem cell differentiation and axis formation. Without the Wnt pathway, cell fate decisions and tissue patterning in both early and late development is severely affected. The fact that exogenous miR-30 is embryonically lethal at concentrations that did not produce whole embryo abnormalities for other miRNA mimics suggests that miR-30 expression may be tightly controlled in the developing zebrafish embryo. Elucidating the other key targets of dre-miR-30 may reveal previously unknown signalling

pathways or regulatory interactions that are vital for zebrafish and vertebrate development.

6.3.3 miR-30/DLL4 regulation during tumour angiogenesis

DLL4 is overexpressed in human tumours, often in association with markers of inflammation, hypoxia and angiogenesis (Jubb et al., 2009; Jubb et al., 2010; Patel et al., 2005; Patel et al., 2006). It appears that DLL4 expression is required for successful tumour angiogenesis as inhibition of DLL4 suppresses experimental tumour growth by inducing non-productive, deregulated angiogenesis (Noguera-Troise et al., 2006; Ridgway et al., 2006). Alongside this, downregulation of the miR-30 family is associated with enhanced tumourigenesis in breast cancer and anaplastic thyroid carcinoma (Braun et al., 2010; Yu et al., 2010). One outcome of this thesis was the discovery that there is a significant negative correlation between one or more miR-30 family members and *DLL4* expression in breast adenocarcinoma, ovarian serous cystadenocarcinoma, and the highly angiogenic renal clear-cell carcinoma. These findings suggest that overexpression of miR-30 during tumour development could suppress tumour progression by downregulating DLL4 expression, thereby promoting inefficient vascular growth. Intratumoural and systemic delivery of the tumour suppressive miRNA miR-34a has been previously achieved using lipid-based delivery reagents (Liu et al., 2011; Wiggins et al., 2010). Therefore, these methods could be used to investigate tumour response to exogenous miR-30 in a colorectal xenograft model.

References

Agrawal, R., Tran, U., and Wessely, O. (2009). The miR-30 miRNA family regulates Xenopus pronephros development and targets the transcription factor Xlim1/Lhx1. Development *136*, 3927-3936.

Alajati, A., Laib, A.M., Weber, H., Boos, A.M., Bartol, A., Ikenberg, K., Korff, T., Zentgraf, H., Obodozie, C., Graeser, R., Christian, S., Finkenzeller, G., Stark, G.B., Héroult, M., Augustin, H.G. (2008). Spheroid-based engineering of a human vasculature in mice. Nat. Methods *5*, 439-445.

Anand, S., Majeti, B.K., Acevedo, L.M., Murphy, E.A., Mukthavaram, R., Scheppke, L., Huang, M., Shields, D.J., Lindquist, J.N., Lapinski, P.E., King, P.D., Weis, S.M., and Cheresh, D.A. (2010). MicroRNA-132-mediated loss of p120RasGAP activates the endothelium to facilitate pathological angiogenesis. Nat. Med. *16*, 909-914.

Augustin, H.G., Young Koh, G., Thurston, G., and Alitalo, K. (2009). Control of vascular morphogenesis and homeostasis through the angiopoietin-Tie system. Nat. Rev. Mol. Cell Biol. *10*, 165-177.

Baek, D., Villen, J., Shin, C., Camargo, F.D., Gygi, S.P., and Bartel, D.P. (2008). The impact of microRNAs on protein output. Nature *455*, 64-71.

Bahary, N., Goishi, K., Stuckenholz, C., Weber, G., LeBlanc, J., Schafer, C.A., Berman, S.S., Klagsbrun, M., and Zon, L.I. (2007). Duplicate VegfA genes and orthologues of the KDR receptor tyrosine kinase family mediate vascular development in the zebrafish. Blood *110*, 3627-3636.

Baltimore, D., Boldin, M.P., O'Connell, R.M., Rao, D.S., and Taganov, K.D. (2008). MicroRNAs: new regulators of immune cell development and function. Nat. Immunol. *9*, 839-845.

Bartel, D.P. (2009). MicroRNAs: target recognition and regulatory functions. Cell *136*, 215-233.

Bauersachs, J., and Thum, T. (2011). Biogenesis and regulation of cardiovascular microRNAs. Circ. Res. *109*, 334-347.

Bechtel, J.T., Liang, Y., Hvidding, J., and Ganem, D. (2003). Host range of Kaposi's Sarcoma-Associated Herpesvirus in cultured cells. J. Virol. *77*, 6474-6481.

Beckstead, J.H., Wood, G.S., and Fletcher, V. (1985). Evidence for the origin of Kaposi's sarcoma from lymphatic endothelium. Am. J. Pathol. *119*, 294-300.

Behm-Ansmant, I., Rehwinkel, J., Doerks, T., Stark, A., Bork, P., and Izaurralde, E. (2006). mRNA degradation by miRNAs and GW182 requires both CCR4:NOT deadenylase and DCP1:DCP2 decapping complexes. Genes Dev. *20*, 1885-1898.

Beis, D., Bartman, T., Jin, S.W., Scott, I.C., D'Amico, L.A., Ober, E.A., Verkade, H., Frantsve, J., Field, H.A., Wehman, A., Baier, H., Tallafuss, A., Bally-Cuif, L., Chen, J.N., Stainier, D.Y.R., and Jungblut, B. (2005). Genetic and cellular analyses of zebrafish atrioventricular cushion and valve development. Development *132*, 4193-4204.

Ben-Ami, O., Pencovich, N., Lotem, J., Levanon, D., and Groner, Y. (2009). A regulatory interplay between miR-27a and Runx1 during megakaryopoiesis. Proc. Natl. Acad. Sci. U.S.A. *106*, 238-243.

Benedito, R., Trindade, A., Hirashima, M., Henrique, D., da Costa, L.L., Rossant, J., Gill, P.S., and Duarte, A. (2008). Loss of Notch signalling induced by Dll4 causes arterial calibre reduction by increasing endothelial cell response to angiogenic stimuli. BMC Dev. Biol. *8*, 117.

Bentley, K., Gerhardt, H., and Bates, P.A. (2008). Agent-based simulation of notch-mediated tip cell selection in angiogenic sprout initialisation. J. Theor. Biol. *250*, 25-36.

Bernstein, E., Caudy, A.A., Hammond, S.M., and Hannon, G.J. (2001). Role for a bidentate ribonuclease in the initiation step of RNA interference. Nature *409*, 363-366.

Bernstein, E., Kim, S.Y., Carmell, M.A., Murchison, E.P., Alcorn, H., Li, M.Z., Mills, A.A., Elledge, S.J., Anderson, K.V., and Hannon, G.J. (2003). Dicer is essential for mouse development. Nat. Genet. *35*, 215-217.

Betel, D., Wilson, M., Gabow, A., Marks, D.S., and Sander, C. (2008). The microRNA.org resource: targets and expression. Nucleic Acids Res. *36*, D149-D153.

Bhagwat, G.P. (1980). Disseminated lymphadenopathic Kaposi's sarcoma in Zambian children. Med. J. Zambia *14*, 61-63.

Biyashev, D., Veliceasa, D., Topczewski, J., Topczewska, J.M., Mizgirev, I., Vinokour, E., Reddi, A.L., Licht, J.D., Revskoy, S.Y., and Volpert, O.V. (2012). MiR-27b controls venous specification and tip cell fate. Blood *119*, 2679-2687.

Blum, Y., Belting, H.G., Ellertsdottir, E., Herwig, L., Lüders, F., and Affolter, M. (2008). Complex cell rearrangements during intersegmental vessel sprouting and vessel fusion in the zebrafish embryo. Dev. Biol. *316*, 312-322.

Bonauer, A., Carmona, G., Iwasaki, M., Mione, M., Koyanagi, M., Fischer, A., Burchfield, J., Fox, H., Doebele, C., Ohtani, K., Chavakis, E., Potente, M., Tjwa, M., Urbich, C., Zeiher, A.M., and Dimmeler, S. (2009). MicroRNA-92a Controls angiogenesis and functional recovery of ischemic tissues in mice. Science *324*, 1710-1713.

Boshoff, C., Endo, Y., Collins, P.D., Takeuchi, Y., Reeves, J.D., Schweickart, V.L., Siani, M.A., Sasaki, T., Williams, T.J., Gray, P.W., Moore, P.S., Chang, Y., and Weiss, R.A. (1997). Angiogenic and HIV-inhibitory functions of KSHV-encoded chemokines. Science *278*, 290-294.

Boshoff, C., Gao, S.J., Healy, L.E., Matthews, S., Thomas, A.J., Coignet, L., Warnke, R.A., Strauchen, J.A., Matutes, E., Kamel, O.W., Moore, P.S., Weiss, R.A., and Chang, Y. (1998). Establishing a KSHV+ cell line (BCP-1) from peripheral blood and characterizing its growth in Nod/SCID mice. Blood *91*, 1671-1679.

Boshoff, C. and Weiss, R. (2002). Aids-related malignancies. Nat. Rev. Cancer *2*, 373-382.

Boshoff, C. (2012). Ephrin receptor: a door to KSHV infection. Nat. Med. *18*, 861-863.

Bourboulia, D., Aldam, D., Lagos, D., Allen, E., Williams, I., Cornforth, D., Copas, A., and Boshoff, C. (2004). Short- and long-term effects of highly active antiretroviral therapy on Kaposi sarcoma-associated herpesvirus immune responses and viraemia. AIDS *18*, 485-493.

Braun, J., Hoang-Vu, C., Dralle, H., and Huttelmaier, S. (2010). Downregulation of microRNAs directs the EMT and invasive potential of anaplastic thyroid carcinomas. Oncogene *29*, 4237-4244.

Brennecke, J., Stark, A., Russell, R.B., and Cohen, S.M. (2005). Principles of microRNA target recognition. PLoS Biol. *3*, e85.

Brou, C., Logeat, F., Gupta, N., Bessia, C., LeBail, O., Doedens, J.R., Cumano, A., Roux, P., Black, R.A., and Israël, A. (2000). A novel proteolytic cleavage involved in Notch signaling: the role of the disintegrin-metalloprotease TACE. Mol. Cell *5*, 207-216.

Burns, C.E., Traver, D., Mayhall, E., Shepard, J.L., and Zon, L.I. (2005). Hematopoietic stem cell fate is established by the Notch-Runx pathway. Genes Dev. *19*, 2331-2342.

Bussmann, J., Lawson, N., Zon, L., Schulte-Merker, S., and Zebrafish Nomenclature Committee (2008). Zebrafish VEGF receptors: a guideline to nomenclature. PLoS Genet. *4*, e1000064.

Cai, X., Hagedorn, C.H., and Cullen, B.R. (2004). Human microRNAs are processed from capped, polyadenylated transcripts that can also function as mRNAs. RNA *10*, 1957-1966.

Carlson, T.R., Yan, Y., Wu, X., Lam, M.T., Tang, G.L., Beverly, L.J., Messina, L.M., Capobianco, A.J., Werb, Z., and Wang, R. (2005). Endothelial expression of constitutively active Notch4 elicits reversible arteriovenous malformations in adult mice. Proc. Natl. Acad. Sci. U.S.A. *102*, 9884-9889.

Carthew, R.W., and Sontheimer, E.J. (2009). Origins and Mechanisms of miRNAs and siRNAs. Cell *136*, 642-655.

Centers for Disease Control (1981). Kaposi's sarcoma and Pneumocystis pneumonia among homosexual men--New York City and California. MMWR Morb. Mortal. Wkly. Rep. *30*, 305-308.

Cesarman, E., Chang, Y., Moore, P.S., Said, J.W., and Knowles, D.M. (1995). Kaposi's Sarcoma-Associated Herpesvirus-like DNA sequences in AIDS-related body-cavity-based lymphomas. N. Engl. J. Med. *332*, 1186-1191.

Chang, Y., Cesarman, E., Pessin, M.S., Lee, F., Culpepper, J., Knowles, D.M., and Moore, P.S. (1994). Identification of herpesvirus-like DNA sequences in AIDS-associated Kaposi's sarcoma. Science *266*, 1865-1869.

Chen, P.Y., Manninga, H., Slanchev, K., Chien, M., Russo, J.J., Ju, J., Sheridan, R., John, B., Marks, D.S., Gaidatzis, D., Sander, C., Zavolan, M., and Tuschl, T. (2005). The developmental miRNA profiles of zebrafish as determined by small RNA cloning. Genes Dev. *19*, 1288-1293.

Chen, Y., and Gorski, D.H. (2008). Regulation of angiogenesis through a microRNA (miR-130a) that down-regulates antiangiogenic homeobox genes GAX and HOXA5. Blood *111*, 1217-1226.

Chen, Z., Lai, T.C., Jan, Y.H., Lin, F.M., Wang, W.C., Xiao, H., Wang, Y.T., Sun, W., Cui, X., Li, Y.S., Fang, T., Zhao, H., Padmanabhan, C., Sun, R., Wang, D.L., Jin, H., Chau, G.Y., Huang, H.D., Hsiao, M., and Shyy, J.Y.J. (2013). Hypoxia-responsive miRNAs target argonaute 1 to promote angiogenesis. J. Clin. Invest. *123*, 1057-1067.

Chendrimada, T.P., Gregory, R.I., Kumaraswamy, E., Norman, J., Cooch, N., Nishikura, K., and Shiekhattar, R. (2005). TRBP recruits the Dicer complex to Ago2 for microRNA processing and gene silencing. Nature *436*, 740-744.

Cheng, F., Pekkonen, P., Laurinavicius, S., Sugiyama, N., Henderson, S., Günther, T., Rantanen, V., Kaivanto, E., Aavikko, M., Sarek, G., Hautaniemi, S., Biberfeld, P., Aaltonen, L., Grundhoff, A., Boshoff, C., Alitalo, K., Lehti, K., and Ojala, P.M. (2011). KSHV-initiated Notch activation leads to membrane-type-1 matrix metalloproteinase-dependent lymphatic endothelial-to-mesenchymal transition. Cell Host Microbe *10*, 577-590.

Choi, W.Y., Giraldez, A.J., and Schier, A.F. (2007). Target protectors reveal dampening and balancing of Nodal agonist and antagonist by miR-430. Science *318*, 271-274.

Christie, T.L., Carter, A., Rollins, E.L., and Childs, S.J. (2010). Syk and Zap-70 function redundantly to promote angioblast migration. Dev. Biol. *340*, 22-29.

Claxton, S. and Fruttiger, M. (2004). Periodic Delta-like 4 expression in developing retinal arteries. Gene Expr. Patterns *5*, 123-127.

Conlon, R.A., Reaume, A.G., and Rossant, J. (1995). Notch 1 is required for the coordinate segmentation of somites. Development *121*, 1533-1545.

Corada, M., Nyqvist, D., Orsenigo, F., Caprini, A., Giampietro, C., Taketo, M.M., Iruela-Arispe, M.L., Adams, R.H., and Dejana, E. (2010). The Wnt/β-catenin pathway modulates vascular remodeling and specification by upregulating Dll4/Notch signaling. Dev. Cell *18*, 938-949.

Covassin, L.D., Villefranc, J.A., Kacergis, M.C., Weinstein, B.M., and Lawson, N.D. (2006). Distinct genetic interactions between multiple Vegf receptors are required for development of different blood vessel types in zebrafish. Proc. Natl. Acad. Sci. U.S.A. *103*, 6554-6559.

Covassin, L.D., Siekmann, A.F., Kacergis, M.C., Laver, E., Moore, J.C., Villefranc, J.A., Weinstein, B.M., and Lawson, N.D. (2009). A genetic screen for vascular mutants in zebrafish reveals dynamic roles for Vegf/Plcg1 signaling during artery development. Dev. Biol. 329, 212-226.

Croce, C.M. (2009). Causes and consequences of microRNA dysregulation in cancer. Nat. Rev. Genet. *10*, 704-714.

Crowner, D., Le Gall, M., Gates, M.A., and Giniger, E. (2003). Notch steers Drosophila ISNb motor axons by regulating the Abl signaling pathway. Curr. Biol. *13*, 967-972.

Davis, R.L., and Turner, D.L. (2001). Vertebrate hairy and Enhancer of split related proteins: transcriptional repressors regulating cellular differentiation and embryonic patterning. Oncogene *20*, 8342-8357.

Davis, B.N., Hilyard, A.C., Nguyen, P.H., Lagna, G., and Hata, A. (2010). Smad proteins bind a conserved RNA sequence to promote microRNA maturation by Drosha. Mol. Cell *39*, 373-384.

Deacon, D.C., Nevis, K.R., Cashman, T.J., Zhou, Y., Zhao, L., Washko, D., Guner-Ataman, B., Burn, C.G., and Burns, C.E. (2010). The miR-143-adducin3 pathway is essential for cardiac chamber morphogenesis. Development *137*, 1887-1896.

De Lella Ezcurra, A.L., Bertolin, A.P., Melani, M., and Wappner, P. (2012). Robustness of the hypoxic response: another job for miRNAs? Dev. Dyn. *241*, 1842-1848.

De Smet, F., Segura, I., De Bock, K., Hohensinner, P.J., and Carmeliet, P. (2009). Mechanisms of vessel branching: filopodia on endothelial tip cells lead the way. Arterioscler. Thromb. Vasc. Biol. *29*, 639-649.

De Strooper, B., Annaert, W., Cupers, P., Saftig, P., Craessaerts, K., Mumm, J.S., Schroeter, E.H., Schrijvers, V., Wolfe, M.S., Ray, W.J., Goate, A., and Kopan, R. (1999). A presenilin-1-dependent γ-secretase-like protease mediates release of Notch intracellular domain. Nature *398*, 518-522.

Detrich, H.W., Kieran, M.W., Chan, F.Y., Barone, L.M., Yee, K., Rundstadler, J.A., Pratt, S., Ransom, D., and Zon, L.I. (1995). Intraembryonic hematopoietic cell migration during vertebrate development. Proc. Natl. Acad. Sci. U.S.A. *92*, 10713-10717.

Dews, M., Homayouni, A., Yu, D., Murphy, D., Sevignani, C., Wentzel, E., Furth, E.E., Lee, W.M., Enders, G.H., Mendell, J.T., and Thomas-Tikhonenko, A. (2006). Augmentation of tumor angiogenesis by a Myc-activated microRNA cluster. Nat. Genet. *38*, 1060-1065.

De Val, S., Chi, N.C., Meadows, S.M., Minovitsky, S., Anderson, J.P., Harris, I.S., Ehlers, M.L., Agarwal, P., Visel, A., Xu, S.M., Pennacchio, L.A., Dubchak, I., Krieg, P.A., Stainier, D.Y.R., and Black, B.L. (2008). Combinatorial regulation of endothelial gene expression by ets and forkhead transcription factors. Cell *135*, 1053-1064.

Diederichs, S. and Haber, D.A. (2007). Dual role for Argonautes in microRNA processing and posttranscriptional regulation of microRNA expression. Cell *131*, 1097-1108.

Diez, H., Fischer, A., Winkler, A., Hu, C.J., Hatzopoulos, A.K., Breier, G., and Gessler, M. (2007). Hypoxia-mediated activation of Dll4-Notch-Hey2 signaling in endothelial progenitor cells and adoption of arterial cell fate. Exp. Cell Res. *313*, 1-9.

Ding, X.C., and Groszhans, H. (2009). Repression of C. elegans microRNA targets at the initiation level of translation requires GW182 proteins. EMBO J. *28*, 213-222.

Dittmer, D., Lagunoff, M., Renne, R., Staskus, K., Haase, A., and Ganem, D. (1998). A cluster of latently expressed genes in Kaposi's sarcoma-associated herpesvirus. J. Virol. *72*, 8309-8315.

Dittmer, D.P. (2003). Transcription profile of Kaposi's sarcoma-associated herpesvirus in primary Kaposi's sarcoma lesions as determined by real-time PCR arrays. Cancer Res. *63*, 2010-2015.

Djokovic, D., Trindade, A., Gigante, J., Badenes, M., Silva, L., Liu, R., Li, X., Gong, M., Krasnoperov, V., Gill, P.S., and Duarte, A. (2010). Combination of Dll4/Notch and Ephrin-B2/EphB4 targeted therapy is highly effective in disrupting tumor angiogenesis. BMC Cancer *23*, 641.

Doebele, C., Bonauer, A., Fischer, A., Scholz, A., Reiss, Y., Urbich, C., Hofmann, W.K., Zeiher, A.M., and Dimmeler, S. (2010). Members of the microRNA-17-92 cluster exhibit a cell-intrinsic antiangiogenic function in endothelial cells. Blood *115*, 4944-4950.

Domenga, V., Fardoux, P., Lacombe, P., Monet, M., Maciazek, J., Krebs, L.T., Klonjkowski, B., Berrou, E., Mericskay, M., Li, Z., Tournier-Lasserve, E., Gridley, T., and Joutel, A. (2004). Notch3 is required for arterial identity and maturation of vascular smooth muscle cells. Genes Dev. *18*, 2730-2735.

Dore, L.C., Amigo, J.D., dos Santos, C.O., Zhang, Z., Gai, X., Tobias, J.W., Yu, D., Klein, A.M., Dorman, C., Wu, W., Hardison, R.C., Paw, B.H., and Weiss, M.J. (2008). A GATA-1-regulated microRNA locus essential for erythropoiesis. Proc. Natl. Acad. Sci. U.S.A. *105*, 3333-3338.

Dou, G.R., Wang, Y.C., Hu, X.B., Hou, L.H., Wang, C.M., Xu, J.F., Wang, Y.S., Liang, Y.M., Yao, L.B., Yang, A.G., and Han, H. (2008). RBP-J, the transcription factor downstream of Notch receptors, is essential for the maintenance of vascular homeostasis in adult mice. FASEB J. *22*, 1606-1617.

Dourmishev, L.A., Dourmishev, A.L., Palmeri, D., Schwartz, R.A., and Lukac, D.M. (2003). Molecular genetics of Kaposi's sarcoma-associated herpesvirus (human herpesvirus 8) epidemiology and pathogenesis. Microbiol. Mol. Biol. Rev. *67*, 175-212.

Du, M.Q., Liu, H., Diss, T.C., Ye, H., Hamoudi, R.A., Dupin, N., Meignin, V., Oksenhendler, E., Boshoff, C., and Isaacson, P.G. (2001). Kaposi sarcoma-associated herpesvirus infects monotypic (IgMλ) but polyclonal naive B cells in Castleman disease and associated lymphoproliferative disorders. Blood *97*, 2130-2136.

Duarte, A.N., Hirashima, M., Benedito, R., Trindade, A., Diniz, P.C., Bekman, E., Costa, L.S., Henrique, D., and Rossant, J. (2004). Dosage-sensitive requirement for mouse Dll4 in artery development. Genes Dev. *18*, 2474-2478.

Duisters, R.F., Tijsen, A.J., Schroen, B., Leenders, J.J., Lentink, V., van der Made, I., Herias, V., van Leeuwen, R.E., Schellings, M.W., Barenbrug, P., Maessen, J.G., Heymans, S., Pinto, Y.M., and Creemers, E.E. (2009). miR-133 and miR-30 regulate connective tissue growth factor: implications for a role of microRNAs in myocardial matrix remodeling. Circ. Res. *104*, 170-178.

Dupin, N., Fisher, C., Kellam, P., Ariad, S., Tulliez, M., Franck, N., van Marck, E., Salmon, D., Gorin, I., Escande, J.P., Weiss, R.A., Alitalo, K., and Boshoff, C. (1999). Distribution of human herpesvirus-8 latently infected cells in Kaposi's sarcoma, multicentric Castleman's disease, and primary effusion lymphoma. Proc. Natl. Acad. Sci. U.S.A. *96*, 4546-4551.

Dupin, N., Diss, T.L., Kellam, P., Tulliez, M., Du, M.Q., Sicard, D., Weiss, R.A., Isaacson, P.G., and Boshoff, C. (2000). HHV-8 is associated with a plasmablastic variant of Castleman disease that is linked to HHV-8-positive plasmablastic lymphoma. Blood *95*, 1406-1412.

Duursma, A.M., Kedde, M., Schrier, M., le Sage, C., and Agami, R. (2008). miR-148 targets human DNMT3b protein coding region. RNA *14*, 872-877.

Ebert, M.S., and Sharp, P.A. (2012). Roles for microRNAs in conferring robustness to biological processes. Cell *149*, 515-524.

Eble, J.A. and Niland, S. (2009). The extracellular matrix of blood vessels. Curr. Pharm. Des. *15*, 1385-1400.

Ellertsdóttir, E., Lenard, A., Blum, Y., Krudewig, A., Herwig, L., Affolter, M., and Belting, H.G. (2010). Vascular morphogenesis in the zebrafish embryo. Dev. Biol. *341*, 56-65.

Emuss, V., Lagos, D., Pizzey, A., Gratrix, F., Henderson, S.R., and Boshoff, C. (2009). KSHV manipulates Notch signaling by DLL4 and JAG1 to alter cell cycle genes in lymphatic endothelia. PLoS Pathog. *5*, e1000616.

Ensoli, B., Nakamura, S.Z., Salahuddin, P., Biberfeld, P., Larsson, L., Beaver, B., Wong-Staal, F., and Gallo, R.C. (1989). AIDS-Kaposi's sarcoma-derived cells express cytokines with autocrine and paracrine growth effects. Science *243*, 223-226.

Ensoli, B., and Stürzl, M. (1998). Kaposi's sarcoma: a result of the interplay among inflammatory cytokines, angiogenic factors and viral agents. Cytokine Growth Factor Rev. *9*, 63-83.

Eriksson, J. and Löfberg, J. (2000). Development of the hypochord and dorsal aorta in the zebrafish embryo (Danio rerio). J. Morphol. *244*, 167-176.

Eulalio, A., Huntzinger, E., and Izaurralde, E. (2008). GW182 interaction with Argonaute is essential for miRNA-mediated translational repression and mRNA decay. Nat. Struct. Mol. Biol. *15*, 346-353.

Fang, L., Deng, Z., Shatseva, T., Yang, J., Peng, C., Du, W.W., Yee, A.J., Ang, L.C., He, C., Shan, S.W., and Yang, B.B. (2011). MicroRNA miR-93 promotes tumor growth and angiogenesis by targeting integrin-β8. Oncogene *30*, 806-821.

Fantin, A., Vieira, J.M., Gestri, G., Denti, L., Schwarz, Q., Prykhozhij, S., Peri, F., Wilson, S.W., and Ruhrberg, C. (2010). Tissue macrophages act as cellular chaperones for vascular anastomosis downstream of VEGF-mediated endothelial tip cell induction. Blood *116*, 829-840.

Fantin, A., Schwarz, Q., Davidson, K., Normando, E.M., Denti, L., and Ruhrberg, C. (2011). The cytoplasmic domain of neuropilin 1 is dispensable for angiogenesis, but promotes the spatial separation of retinal arteries and veins. Development *138*, 4185-4191.

Fantin, A., Vieira, J.M., Plein, A., Denti, L., Fruttiger, M., Pollard, J.W., and Ruhrberg, C. (2013). NRP1 acts cell autonomously in endothelium to promote tip cell function during sprouting angiogenesis. Blood *121*, 2352-2362.

Fasanaro, P., D'Alessandra, Y., Di Stefano, V., Melchionna, R., Romani, S., Pompilio, G., Capogrossi, M.C., and Martelli, F. (2008). MicroRNA-210 modulates endothelial cell response to hypoxia and inhibits the receptor tyrosine kinase ligand Ephrin-A3. J. Biol. Chem. *283*, 15878-15883.

Favre, C.J., Mancuso, M., Maas, K., McLean, J.W., Baluk, P., and McDonald, D.M. (2003). Expression of genes involved in vascular development and angiogenesis in endothelial cells of adult lung. Am. J. Physiol. Heart Circ. Physiol. *285*, H1917-H1938.

Fischer, A., Schumacher, N., Maier, M., Sendtner, M., and Gessler, M. (2004). The Notch target genes Hey1 and Hey2 are required for embryonic vascular development. Genes Dev.*18*, 901-911.

Fischer, A., and Gessler, M. (2007). Delta Notch and then? Protein interactions and proposed modes of repression by Hes and Hey bHLH factors. Nucleic Acids Res. *35*, 4583-4596.

Fischer, M., Yen, W.C., Kapoun, A.M., Wang, M., O'Young, G., Lewicki, J., Gurney, A., and Hoey, T. (2011). Anti-DLL4 inhibits growth and reduces tumor-initiating cell frequency in colorectal tumors with oncogenic KRAS mutations. Cancer Res. *71*, 1520-1525.

Fish, J.E., Santoro, M.M., Morton, S.U., Yu, S., Yeh, R.F., Wythe, J.D., Ivey, K.N., Bruneau, B.G., Stainier, D.Y.R., and Srivastava, D. (2008). miR-126 regulates angiogenic signaling and vascular integrity. Dev. Cell *15*, 272-284.

Friedman, R.C., Farh, K.K., Burge, C.B., and Bartel, D.P. (2009). Most mammalian mRNAs are conserved targets of microRNAs. Genome Res. *19*, 92-105.

Fujita, S., and Iba, H. (2008). Putative promoter regions of miRNA genes involved in evolutionarily conserved regulatory systems among vertebrates. Bioinformatics *24*, 303-308.

Funes, J.M., Quintero, M., Henderson, S., Martinez, D., Qureshi, U., Westwood, C., Clements, M.O., Bourboulia, D., Pedley, R.B., Moncada, S., and Boshoff, C. (2007). Transformation of human mesenchymal stem cells increases their dependency on oxidative phosphorylation for energy production. Proc. Natl. Acad. Sci. U.S.A. *104*, 6223-6228.

Gaengel, K., Genové, G., Armulik, A., and Betsholtz, C. (2009). Endothelial-mural cell signaling in vascular development and angiogenesis. Arterioscler. Thromb. Vasc. Biol. *29*, 630-638.

Gale, N.W., Dominguez, M.G., Noguera, I., Pan, L., Hughes, V., Valenzuela, D.M., Murphy, A.J., Adams, N.C., Lin, H.C., Holash, J., Thurston, G., and Yancopoulos, G.D. (2004). Haploinsufficiency of delta-like 4 ligand results in embryonic lethality due to major defects in arterial and vascular development. Proc. Natl. Acad. Sci. U.S.A. *101*, 15949-15954.

Ganem, D. (2010). KSHV and the pathogenesis of Kaposi sarcoma: listening to human biology and medicine. J. Clin. Invest. *120*, 939-949.

Gates, M.A., Kim, L., Egan, E.S., Cardozo, T., Sirotkin, H.I., Dougan, S.T., Lashkari, D., Abagyan, R., Schier, A.F., and Talbot, W.S. (1999). A genetic linkage map for zebrafish: comparative analysis and localization of genes and expressed sequences. Genome Res. *9*, 334-347.

Gaziel-Sovran, A., Segura, M.F., Di Micco, R., Collins, M.K., Hanniford, D., Vega-Saenz de Miera, E., Rakus, J.F., Dankert, J.F., Shang, S., Kerbel, R.S., Bhardwaj, N., Shao, Y., Darvishian, F., Zavadil, J., Erlebacher, A., Mahal, L.K., Osman, I., and Hernando, E. (2011). miR-30b/30d regulation of GalNAc transferases enhances invasion and immunosuppression during metastasis. Cancer Cell *20*, 104-118.

Gendron, R.L., Good, W.V., Adams, L.C., and Paradis, H. (2001). Suppressed expression of tubedown-1 in retinal neovascularization of proliferative diabetic retinopathy. Invest. Ophthalmol. Vis. Sci. *42*, 3000-3007.

Gendron, R.L., Good, W.V., Miskiewicz, E., Tucker, S., Phelps, D.L., and Paradis, H. (2006). Tubedown-1 (Tbdn-1) suppression in oxygen-induced retinopathy and in retinopathy of prematurity. Mol. Vis. *12*, 108-116.

Gentleman, R.C., Carey, V.J., Bates, D.M., Bolstad, B., Dettling, M., Dudoit, S., Ellis, B., Gautier, L., Ge, Y., Gentry, J., Hornik, K., Hothorn, T., Huber, W., Iacus, S., Irizarry, R., Leisch, F., Cheng, L., Maechler, M., Rossini, A.J., Sawitzki, G., Smith, C., Smyth, G., Tierney, L., Yang, J.YH., and Zhang, J. (2004). Bioconductor: open software development for computational biology and bioinformatics. Genome Biol. *5*, R80.

Gerhardt, H., Golding, M., Fruttiger, M., Ruhrberg, C., Lundkvist, A., Abramsson, A., Jeltsch, M., Mitchell, C., Alitalo, K., Shima, D., and Betsholtz, C. (2003). VEGF guides angiogenic sprouting utilizing endothelial tip cell filopodia. J. Cell Biol. *161*, 1163-1177.

Gerhardt, H., Ruhrberg, C., Abramsson, A., Fujisawa, H., Shima, D., and Betsholtz, C. (2004). Neuropilin-1 is required for endothelial tip cell guidance in the developing central nervous system. Dev. Dyn. *231*, 503-509.

Gering, M., Rodaway, A.R.F., Gottgens, B., Patient, R.K., and Green, A.R. (1998). The SCL gene specifies haemangioblast development from early mesoderm. EMBO J. *17*, 4029-4045.

Gering, M., and Patient, R. (2005). Hedgehog signaling is required for adult blood stem cell formation in zebrafish embryos. Dev. Cell *8*, 389-400.

Ghildiyal, M., Xu, J., Seitz, H., Weng, Z., and Zamore, P.D. (2010). Sorting of Drosophila small silencing RNAs partitions microRNA* strands into the RNA interference pathway. RNA *16*, 43-56.

Giraldez, A.J., Cinalli, R.M., Glasner, M.E., Enright, A.J., Thomson, J.M., Baskerville, S., Hammond, S.M., Bartel, D.P., and Schier, A.F. (2005). MicroRNAs regulate brain morphogenesis in zebrafish. Science *308*, 833-838.

Giraldez, A.J., Mishima, Y., Rihel, J., Grocock, R.J., van Dongen, S., Inoue, K., Enright, A.J., and Schier, A.F. (2006). Zebrafish miR-430 promotes deadenylation and clearance of maternal mRNAs. Science *312*, 75-79.

Godfrey, A., Anderson, J., Papanastasiou, A., Takeuchi, Y., and Boshoff, C. (2005). Inhibiting primary effusion lymphoma by lentiviral vectors encoding short hairpin RNA. Blood *105*, 2510-2518.

Gottlieb, G.J., Ragaz, A., Vogel, J.V., Friedman-Kien, A., Rywlin, A.M., Weiner, E.A., and Ackerman, A.B. (1981). A preliminary communication on extensively disseminated Kaposi's sarcoma in young homosexual men. Am. J. Dermatopathol. *3*, 111-114.

Gray, M., Moens, C.B., Amacher, S.L., Eisen, J.S., and Beattie, C.E. (2001). Zebrafish deadly seven functions in neurogenesis. Dev. Biol. *237*, 306-323.

Grego-Bessa, J., Luna-Zurita, L., del Monte, G., Bolós, V., Melgar, P., Arandilla, A., Garratt, A.N., Zang, H., Mukouyama, Y.S., Chen, H., Shou, W., Ballestar, E., Esteller, M., Rojas, A., Pqrez-Pomares, J.M., and de la Pompa, J.L. (2007). Notch signaling is essential for ventricular chamber development. Dev. Cell *12*, 415-429.

Gregory, R.I., Yan, K.p., Amuthan, G., Chendrimada, T., Doratotaj, B., Cooch, N., and Shiekhattar, R. (2004). The Microprocessor complex mediates the genesis of microRNAs. Nature *432*, 235-240.

Griffiths-Jones, S., Saini, H.K., van Dongen, S., and Enright, A.J. (2008). miRBase: tools for microRNA genomics. Nucleic Acids Res. *36*, D154-D158.

Grimson, A., Farh, K.K., Johnston, W.K., Garrett-Engele, P., Lim, L.P., and Bartel, D.P. (2007). MicroRNA targeting specificity in mammals: determinants beyond seed pairing. Mol. Cell *27*, 91-105.

Grossmann, C., Podgrabinska, S., Skobe, M., and Ganem, D. (2006). Activation of NFκB by the latent vFLIP gene of Kaposi's sarcoma-associated herpesvirus is required for the spindle shape of virus-infected endothelial cells and contributes to their proinflammatory phenotype. J. Virol. *80*, 7179-7185.

Gu, S., Jin, L., Zhang, F., Sarnow, P., and Kay, M.A. (2009). Biological basis for restriction of microRNA targets to the 3’ untranslated region in mammalian mRNAs. Nat. Struct. Mol. Biol. *16*, 144-150.

Guo, H., Ingolia, N.T., Weissman, J.S., and Bartel, D.P. (2010). Mammalian microRNAs predominantly act to decrease target mRNA levels. Nature *466*, 835-840.

Haase, A.D., Jaskiewicz, L., Zhang, H., Laine, S., Sack, R., Gatignol, A., and Filipowicz, W. (2005). TRBP, a regulator of cellular PKR and HIV-1 virus expression, interacts with Dicer and functions in RNA silencing. EMBO Rep. *6*, 961-967.

Habeck, H., Odenthal, J., Walderich, B., Maischein, H., Schulte-Merker, S., and Tübingen 2000 screen consortium. (2002). Analysis of a zebrafish VEGF receptor mutant reveals specific disruption of angiogenesis. Curr. Biol. *2*, 1405-1412.

Hahn, A.S., Kaufmann, J.K., Wies, E., Naschberger, E., Panteleev-Ivlev, J., Schmidt, K., Holzer, A., Schmidt, M., Chen, J., Konig, S., Ensser, A., Myoung, J., Brockmeyer, N.H., Sturzl, M., Fleckenstein, B., and Neipel, F. (2012). The ephrin receptor tyrosine kinase A2 is a cellular receptor for Kaposi's sarcoma-associated herpesvirus. Nat. Med. *18*, 961-966.

Haller, B.K., Brave, A., Wallgard, E., Roswall, P., Sunkari, V.G., Mattson, U., Hallengard, D., Catrina, S.B., Hellstrom, M., and Pietras, K. (2010). Therapeutic efficacy of a DNA vaccine targeting the endothelial tip cell antigen delta-like ligand 4 in mammary carcinoma. Oncogene *29*, 4276-4286.

Hamada, Y., Kadokawa, Y., Okabe, M., Ikawa, M., Coleman, J.R., and Tsujimoto, Y. (1999). Mutation in ankyrin repeats of the mouse Notch2 gene induces early embryonic lethality. Development *126*, 3415-3424.

Han, J., Lee, Y., Yeom, K.H., Nam, J.W., Heo, I., Rhee, J.K., Sohn, S.Y., Cho, Y., Zhang, B.T., and Kim, V.N. (2006). Molecular basis for the recognition of primary microRNAs by the Drosha-DGCR8 complex. Cell *125*, 887-901.

Hansen, A., Henderson, S., Lagos, D., Nikitenko, L., Coulter, E., Roberts, S., Gratrix, F., Plaisance, K., Renne, R., Bower, M., Kellam, P., and Boshoff,C. (2010). KSHV-encoded miRNAs target MAF to induce endothelial cell reprogramming. Genes Dev. *24*, 195-205.

Harrington, L.S., Sainson, R.C.A., Williams, C.K., Taylor, J.M., Shi, W., Li, J.L., and Harris, A.L. (2008). Regulation of multiple angiogenic pathways by Dll4 and Notch in human umbilical vein endothelial cells. Microvasc. Res. *75*, 144-154.

Hassel, D., Cheng, P., White, M.P., Ivey, K.N., Kroll, J., Augustin, H.G., Katus, H.A., Stainier, D.Y.R., and Srivastava, D. (2012). MicroRNA-10 regulates the angiogenic behavior of zebrafish and human endothelial cells by promoting vascular endothelial growth factor signaling. Circ. Res. *111*, 1421-1433.

He, J., Jing, Y., Li, W., Qian, X., Xu, Q., Li, F.S., Liu, L.Z., Jiang, B.H., and Jiang, Y. (2013). Roles and mechanism of miR-199a and miR-125b in tumor angiogenesis. PLoS ONE *8*, e56647.

Hellström, M., Phng, L.K., Hofmann, J.J., Wallgard, E., Coultas, L., Lindblom, P., Alva, J., Nilsson, A.K., Karlsson, L., Gaiano, N., Yoon, K., Rossant, J., Iruela-Arispe, M.L., Kalén, M., Gerhardt, H., and Betsholtz, C. (2007). Dll4 signalling through Notch1 regulates formation of tip cells during angiogenesis. Nature *445*, 776-780.

Henderson, A., Wang, S.J., Taylor, A., Aitkenhead, M., and Hughes, C.C.W. (2001). The basic helix-loop-helix transcription factor HESR1 regulates endothelial cell tube formation. J. Biol. Chem. *276*, 6169-6176.

Herbert, C., Norris, K., Scheper, M., Nikitakis, N., and Sauk, J. (2007). High mobility group A2 is a target for miRNA-98 in head and neck squamous cell carcinoma. Mol. Cancer *6*, 5.

Herbert, S.P., Huisken, J., Kim, T.N., Feldman, M.E., Houseman, B.T., Wang, R.A., Shokat, K.M., and Stainier, D.Y.R. (2009). Arterial-venous segregation by selective cell sprouting: an alternative mode of blood vessel formation. Science *326*, 294-298.

Hodkinson, P.S., Elliott, P., Lad, Y., McHugh, B.J., MacKinnon, A.C., Haslett, C., and Sethi, T. (2007). Mammalian NOTCH-1 activates β1 integrins via the small GTPase R-Ras. J. Biol. Chem. *282*, 28991-29001.

Hoey, T., Yen, W.C., Axelrod, F., Basi, J., Donigian, L., Dylla, S., Fitch-Bruhns, M., Lazetic, S., Park, I.K., Sato, A., Satyal, S., Wang, X., Clarke, M.F., Lewicki, J., and Gurney, A. (2009). DLL4 blockade inhibits tumor growth and reduces tumor-initiating cell frequency. Cell Stem Cell *5*, 168-177.

Hogan, B.M., Bos, F.L., Bussmann, J., Witte, M., Chi, N.C., Duckers, H.J., and Schulte-Merker, S. (2009a). ccbe1 is required for embryonic lymphangiogenesis and venous sprouting. Nat. Genet. *41*, 396-398.

Hogan, B.M., Herpers, R., Witte, M., Heloterä, H., Alitalo, K., Duckers, H.J., and Schulte-Merker, S. (2009b). Vegfc/Flt4 signalling is suppressed by Dll4 in developing zebrafish intersegmental arteries. Development *136*, 4001-4009.

Holderfield, M.T., Henderson Anderson, A.M., Kokubo, H., Chin, M.T., Johnson, R.L., and Hughes, C.C.W. (2006). HESR1/CHF2 suppresses VEGFR2 transcription independent of binding to E-boxes. Biochem. Biophys. Res. Commun. *346*, 637-648.

Holley, S.A., Julich, D., Rauch, G.J., Geisler, R., and Nusslein-Volhard, C. (2002). her1 and the notch pathway function within the oscillator mechanism that regulates zebrafish somitogenesis. Development *129*, 1175-1183.

Hong, Y.K., Foreman, K., Shin, J.W., Hirakawa, S., Curry, C.L., Sage, D.R., Libermann, T., Dezube, B.J., Fingeroth, J.D., and Detmar, M. (2004). Lymphatic reprogramming of blood vascular endothelium by Kaposi sarcoma-associated herpesvirus. Nat. Genet. *36*, 683-685.

Hong, C.C., Peterson, Q.P., Hong, J.Y., and Peterson, R.T. (2006). Artery/Vein Specification Is Governed by Opposing Phosphatidylinositol-3 Kinase and MAP Kinase/ERK Signaling. Curr. Biol. *16*, 1366-1372.

Hua, Z., Qing, L., Wenbin, Y., Chung-Kwun, A.W., Guoping, C., Dayong, G., Yanhong, J., Chen, Z., Jifeng, W., Burton, B.Y., and Yaou, Z. (2006). MiRNA-directed regulation of VEGF and other angiogenic factors under hypoxia. PLoS ONE *1*, e116.

Huse, J.T., Brennan, C., Hambardzumyan, D., Wee, B., Pena, J., Rouhanifard, S.H., Sohn-Lee, C., le Sage, C., Agami, R., Tuschl, T., and Holland, E.C. (2009). The PTEN-regulating microRNA miR-26a is amplified in high-grade glioma and facilitates gliomagenesis in vivo. Genes Dev. *23*, 1327-1337.

Hutvágner, G., and Zamore, P.D. (2002). A microRNA in a multiple-turnover RNAi enzyme complex. Science *297*, 2056-2060.

Hutvágner, G., Simard, M.J., Mello, C.C., and Zamore, P.D. (2004). Sequence-specific inhibition of small RNA function. PLoS Biol. *2*, e98.

Irizarry, R.A., Hobbs, B., Collin, F., Beazer-Barclay, Y.D., Antonellis, K.J., Scherf, U., and Speed, T.P. (2003). Exploration, normalization, and summaries of high density oligonucleotide array probe level data. Biostatistics *4*, 249-264.

Iruela-Arispe, M.L., and Davis, G.E. (2009). Cellular and molecular mechanisms of vascular lumen formation. Dev. Cell *16*, 222-231.

Ishitani, T., Matsumoto, K., Chitnis, A.B., and Itoh, M. (2005). Nrarp functions to modulate neural-crest-cell differentiation by regulating LEF1 protein stability. Nat. Cell Biol. *7*, 1106-1112.

Isogai, S., Lawson, N.D., Torrealday, S., Horiguchi, M., and Weinstein, B.M. (2003). Angiogenic network formation in the developing vertebrate trunk. Development *130*, 5281-5290.

Itoh, M., Kim, C.H., Palardy, G., Oda, T., Jiang, Y.J., Maust, D., Yeo, S.Y., Lorick, K., Wright, G.J., Ariza-McNaughton, L., Weissman, A.M., Lewis, J., Chandrasekharappa, S.C., and Chitnis, A.B. (2003). Mind bomb Is a ubiquitin ligase that Is essential for efficient activation of Notch signaling by Delta. Dev. Cell *4*, 67-82. 1

Jakobsson, L., Franco, C.A., Bentley, K., Collins, R.T., Ponsioen, B., Aspalter, I.M., Rosewell, I., Busse, M., Thurston, G., Medvinsky, A., Schulte-Merker, S., and Gerhardt, H. (2010). Endothelial cells dynamically compete for the tip cell position during angiogenic sprouting. Nat. Cell Biol. *12*, 943-953.

Jakymiw, A., Lian, S., Eystathioy, T., Li, S., Satoh, M., Hamel, J.C., Fritzler, M.J., and Chan, E.K.L. (2005). Disruption of GW bodies impairs mammalian RNA interference. Nat Cell Biol. *7*, 1267-1274.

Jarriault, S., Brou, C., Logeat, F., Schroeter, E.H., Kopan, R., and Israel, A. (1995). Signalling downstream of activated mammalian Notch. Nature *377*, 355-358.

Jenner, R.G. and Boshoff, C. (2002). The molecular pathology of Kaposi's sarcoma-associated herpesvirus. Biochim. Biophys. Acta. *1602*, 1-22.

Jenner, R.G., Maillard, K., Cattini, N., Weiss, R.A., Boshoff, C., Wooster, R., and Kellam, P. (2003). Kaposi's sarcoma-associated herpesvirus-infected primary effusion lymphoma has a plasma cell gene expression profile. Proc. Natl. Acad. Sci. U.S.A. *100*, 10399-10404.

Jeong, J.W., Bae, M.K., Ahn, M.Y., Kim, S.H., Sohn, T.K., Bae, M.H., Yoo, M.A., Song, E.J., Lee, K.J., and Kim, K.W. (2002). Regulation and destabilization of HIF-1α by ARD1-mediated acetylation. Cell *111*, 709-720.

Jiang, B., and Liu, L. (2009). Chapter 2 - PI3K/PTEN signaling in angiogenesis and tumorigenesis. In Advances in Cancer Research. 5th ed., George: Academic Press.

Jin, S.W., Beis, D., Mitchell, T., Chen, J.N., and Stainier, D.Y.R. (2005). Cellular and molecular analyses of vascular tube and lumen formation in zebrafish. Development *132*, 5199-5209.

John, B., Enright, A.J., Aravin, A., Tuschl, T., Sander, C., and Marks, D.S. (2004). Human microRNA targets. PLoS Biol. *2*, e363.

Jones, E.A.V., Yuan, L., Breant, C., Watts, R.J., and Eichmann, A. (2008). Separating genetic and hemodynamic defects in neuropilin 1 knockout embryos. Development *135*, 2479-2488.

Jones-Rhoades, M.W., Bartel, D.P., and Bartel, B. (2006). MicroRNAs and their roles in plants. Annu. Rev. Plant Biol. *57*, 19-53.

Joutel, A., Andreux, F., Gaulis, S., Domenga, V., Cecillon, M., Battail, N., Piga, N., Chapon, F., Godfrain, C., and Tournier-Lasserve, E. (2000). The ectodomain of the Notch3 receptor accumulates within the cerebrovasculature of CADASIL patients. J. Clin. Invest. *105*, 597-605.

Jubb, A.M., Turley, H., Moeller, H.C., Steers, G., Han, C., Li, J.L., Leek, R., Tan, E.Y., Singh, B., Mortensen, N.J., Noguera-Troise, I., Pezzella, F., Gatter, K.C., Thurston, G., Fox, S.B., and Harris, A.L. (2009). Expression of delta-like ligand 4 (Dll4) and markers of hypoxia in colon cancer. Br. J. Cancer *101*, 1749-1757.

Jubb, A.M., Soilleux, E.J., Turley, H., Steers, G., Parker, A., Low, I., Blades, J., Li, J.L., Allen, P., Leek, R., Noguera-Troise, I., Gatter, K.C., Thurston, G., and Harris, A.L. (2010). Expression of vascular Notch ligand Delta-like 4 and inflammatory markers in breast cancer. Am. J. Pathol. *176*, 2019-2028.

Julich, D., Lim, C.H., Round, J., Nicolaije, C., Schroeder, J., Davies, A., Geisler, R., Lewis, J., Jiang, Y.J., and Holley, S.A. (2005). beamter/deltaC and the role of Notch ligands in the zebrafish somite segmentation, hindbrain neurogenesis and hypochord differentiation. Dev. Biol. *286*, 391-404.

Jussila, L., Valtola, R., Partanen, T.A., Salven, P., Heikkilä, P., Matikainen,M.T., Renkonen, R., Kaipainen, A., Detmar, M., Tschachler, E., Alitalo, R., and Alitalo, K. (1998). Lymphatic endothelium and Kaposi's sarcoma spindle cells detected by antibodies against the Vascular endothelial growth factor receptor-3. Cancer Res. *58*, 1599-1604.

Kamei, M., Brian Saunders, W., Bayless, K.J., Dye, L., Davis, G.E., and Weinstein, B.M. (2006). Endothelial tubes assemble from intracellular vacuoles *in vivo*. Nature *442*, 453-456.

Kandachar, V., and Roegiers, F. (2012). Endocytosis and control of Notch signaling. Curr. Opin. Cell Biol. *24*, 534-540.

Kane, D.A. and Kimmel, C.B. (1993). The zebrafish midblastula transition. Development *119*, 447-456.

Kao, H.Y., Ordentlich, P., Koyano-Nakagawa, N., Tang, Z., Downes, M., Kintner, C.R., Evans, R.M., and Kadesch, T. (1998). A histone deacetylase corepressor complex regulates the Notch signal transduction pathway. Genes Dev. *12*, 2269-2277.

Kaposi, M. (1872). Idiopathisches multiples Pigmentsarkom der Haut. Archive fur Dermatologie und Syphilis *4*, 265-273.

Keniry, M., and Parson, R. (2008). The role of PTEN signaling perturbations in cancer and in targeted therapy. Oncogene *27*, 5477-5485.

Kertesz, M., Iovino, N., Unnerstall, U., Gaul, U., and Segal, E. (2007). The role of site accessibility in microRNA target recognition. Nat. Genet. *39*, 1278-1284.

Khan, A.A., Betel, D., Miller, M.L., Sander, C., Leslie, C.S., and Marks, D.S. (2009). Transfection of small RNAs globally perturbs gene regulation by endogenous microRNAs. Nat. Biotechnol. *27*, 549-555.

Khvorova, A., Reynolds, A., and Jayasena, S.D. (2003). Functional siRNAs and miRNAs exhibit strand bias. Cell *115*, 209-216.

Kim, V.N., Han, J., and Siomi, M.C. (2009). Biogenesis of small RNAs in animals. Nat. Rev. Mol. Cell Biol. *10*, 126-139

Kim, Y.H., Hu, H., Guevara-Gallardo, S., Lam, M.T.Y., Fong, S.Y., and Wang, R.A. (2008). Artery and vein size is balanced by Notch and ephrin B2/EphB4 during angiogenesis. Development *135*, 3755-3764.

Kimmel, C.B., Ballard, W.W., Kimmel, S.R., Ullmann, B., and Schilling, T.F. (1995). Stages of embryonic development of the zebrafish. Dev. Dyn. *203*, 253-310.

Kong, W., He, L., Richards, E.J., Challa, S., Xu, C.X., Permuth-Wey, J., Lancaster, J.M., Coppola, D., Sellers, T.A., Djeu, J.Y., and Cheng, J.Q. (2013). Upregulation of miRNA-155 promotes tumour angiogenesis by targeting VHL and is associated with poor prognosis and triple-negative breast cancer. Oncogene Epub ahead of print.

Kopan, R., and Ilagan, M. (2009). The canonical Notch signaling pathway: unfolding the activation mechanism. Cell *137*, 216-233.

Kota, J., Chivukula, R.R., O'Donnell, K.A., Wentzel, E.A., Montgomery, C.L., Hwang, H.W., Chang, T.C., Vivekanandan, P., Torbenson, M., Clark, K.R., Mendell, J.R., and Mendell, J.T. (2009). Therapeutic microRNA delivery suppresses tumorigenesis in a murine liver cancer model. Cell *137*, 1005-1017.

Kozomara, A., and Griffiths-Jones, S. (2011). miRBase: integrating microRNA annotation and deep-sequencing data. Nucleic Acids Res. *39*, D152-D157.

Krebs, L.T., Xue, Y., Norton, C.R., Shutter, J.R., Maguire, M., Sundberg, J.P., Gallahan, D., Closson, V., Kitajewski, J., Callahan, R., Smith, G.H., Stark, K.L., and Gridley, T. (2000). Notch signaling is essential for vascular morphogenesis in mice. Genes Dev. *14*, 1343-1352.

Krebs, L.T., Deftos, M.L., Bevan, M.J., and Gridley, T. (2001). The Nrarp gene encodes an ankyrin-repeat protein that is transcriptionally regulated by the Notch signaling pathway. Dev. Biol. *238*, 110-119.

Krebs, L.T., Shutter, J.R., Tanigaki, K., Honjo, T., Stark, K.L., and Gridley, T. (2004). Haploinsufficient lethality and formation of arteriovenous malformations in Notch pathway mutants. Genes Dev. *18*, 2469-2473.

Krek, A. (2005). Combinatorial microRNA target predictions. Nat. Genet. *37*, 495-500.

Krol, J., and Loedige, I. (2010). The widespread regulation of microRNA biogenesis, function and decay. Nat. Rev. Genet. *11*, 597-610.

Krown, S.E., Testa, M.A., and Huang, J. (1997). AIDS-related Kaposi's sarcoma: prospective validation of the AIDS Clinical Trials Group staging classification. AIDS Clinical Trials Group Oncology Committee. J. Clin. Oncol. *15*, 3085-3092.

Kuehbacher, A., Urbich, C., Zeiher, A.M., and Dimmeler, S. (2007). Role of Dicer and Drosha for endothelial microRNA expression and angiogenesis. Circ. Res. *101*, 59-68.

Kuhnert, F., Mancuso, M.R., Hampton, J., Stankunas, K., Asano, T., Chen, C.Z., and Kuo, C.J. (2008). Attribution of vascular phenotypes of the murine Egfl7 locus to the microRNA miR-126. Development *135*, 3989-3993.

Kulshreshtha, R., Ferracin, M., Wojcik, S.E., Garzon, R., Alder, H., Agosto-Perez, F.J., Davuluri, R., Liu, C.G., Croce, C.M., Negrini, M., Calin, G.A., and Ivan, M. (2007). A microRNA signature of hypoxia. Mol. Cell. Biol. *27*, 1859-1867.

Lagos, D., Trotter, M.W., Vart, R.J., Wang, H.W., Matthews, N.C., Hansen, A., Flore, O., Gotch, F., and Boshoff, C. (2007). Kaposi sarcoma herpesvirus-encoded vFLIP and vIRF1 regulate antigen presentation in lymphatic endothelial cells. Blood *109*, 1550-1558.

Lagos, D., Pollara, G., Henderson, S., Gratrix, F., Fabani, M., Milne, R.S.B., Gotch, F., and Boshoff, C. (2010). miR-132 regulates antiviral innate immunity through suppression of the p300 transcriptional co-activator. Nat. Cell Biol. *12*, 513-519.

Lagos-Quintana, M., Rauhut, R., Lendeckel, W., and Tuschl, T. (2001). Identification of novel genes coding for small expressed RNAs. Science *294*, 853-858.

Lai, E.C. (2004). Notch signaling: control of cell communication and cell fate. Development *131*, 965-973.

Lal, A., Navarro, F., Maher, C.A., Maliszewski, L.E., Yan, N., O'Day, E., Chowdhury, D., Dykxhoorn, D.M., Tsai, P., Hofmann, O., Becker, K.G., Gorospe, M., Hide, W., and Lieberman, J. (2009). miR-24 inhibits cell proliferation by targeting E2F2, MYC, and other cell-cycle genes via binding to seedless 3'UTR microRNA recognition elements. Mol. Cell *35*, 610-625.

Lall, S., Grün, D., Krek, A., Chen, K., Wang, Y.L., Dewey, C.N., Sood, P., Colombo, T., Bray, N., MacMenamin, P., Kao, H.L., Gunsalus, K.C., Pachter, L., Piano, F., and Rajewsky, N. (2006). A genome-wide map of conserved microRNA targets in C. elegans. Curr. Biol. *16*, 460-471.

Lam, L.T. and Bresnick, E.H. (1998). Identity of the β-globin locus control region binding protein HS2NF5 as the mammalian homolog of the notch-regulated transcription factor suppressor of hairless. J. Biol. Chem. *273*, 24223-24231.

Lamar, E., Deblandre, G.l., Wettstein, D., Gawantka, V., Pollet, N., Niehrs, C., and Kintner, C. (2001). Nrarp is a novel intracellular component of the Notch signaling pathway. Genes Dev.*15*, 1885-1899.

Lanahan, A., Zhang, X., Fantin, A., Zhuang, Z., Rivera-Molina, F., Speichinger, K., Prahst, C., Zhang, J., Wang, Y., Davis, G., Toomre, D., Ruhrberg, C., and Simons, M. (2013). The neuropilin 1 cytoplasmic domain is required for VEGF-A-dependent arteriogenesis. Dev. Cell *25*, 156-168.

Lardelli, M., Dahlstrand, J., and Lendahl, U. (1994). The novel Notch homologue mouse Notch 3 lacks specific epidermal growth factor-repeats and is expressed in proliferating neuroepithelium. Mech. Dev. *46*, 123-136.

Lau, N.C., Lim, L.P., Weinstein, E.G., and Bartel, D.P. (2001). An abundant class of tiny RNAs with probable regulatory roles in Caenorhabditis elegans. Science *294*, 858-862.

Lawson, N.D., Scheer, N., Pham, V.N., Kim, C.H., Chitnis, A.B., Campos-Ortega, J.A., and Weinstein, B.M. (2001). Notch signaling is required for arterial-venous differentiation during embryonic vascular development. Development *128*, 3675-3683.

Lawson, N.D., and Weinstein, B.M. (2002). *In vivo* imaging of embryonic vascular development using transgenic zebrafish. Dev. Biol. *248*, 307-318.

Lawson, N.D., Vogel, A.M., and Weinstein, B.M. (2002). sonic hedgehog and vascular endothelial growth factor act upstream of the Notch pathway during arterial endothelial differentiation. Dev. Cell *3*, 127-136.

Lawson, N.D., Mugford, J.W., Diamond, B.A., and Weinstein,B.M. (2003). phospholipase C gamma-1 is required downstream of vascular endothelial growth factor during arterial development. Genes Dev. *17*, 1346-1351.

Le Gall, M., De Mattei, C., and Giniger, E. (2008). Molecular separation of two signaling pathways for the receptor Notch. Dev. Biol. *313*, 556-567.

Lee, R.C., Feinbaum, R.L., and Ambros, V. (1993). The C. elegans heterochronic gene lin-4 encodes small RNAs with antisense complementarity to lin-14. Cell *75*, 843-854.

Lee, R.C., and Ambros, V. (2001). An extensive class of small RNAs in Caenorhabditis elegans. Science *294*, 862-864.

Lee, Y., Jeon K., Lee, J.T., Kim, S., and Kim, V.N. (2002). MicroRNA maturation: stepwise processing and subcellular localization. EMBO J. *21*, 4663-4670.

Lee, Y., Ahn, C., Han, J., Choi, H., Kim, J., Yim, J., Lee, J., Provost, P., Radmark, O., Kim, S., and Kim, V.N. (2003). The nuclear RNase III Drosha initiates microRNA processing. Nature *425*, 415-419.

Lee, Y., Kim, M., Han, J., Yeom, K.H., Lee, S., Baek, S.H., and Kim, V.N. (2004). MicroRNA genes are transcribed by RNA polymerase II. EMBO J. *23*, 4051-4060.

Lee, Y., Hur, I., Park, S.Y., Kim, Y.K., Suh, M.R., and Kim, V.N. (2006). The role of PACT in the RNA silencing pathway. EMBO J. *25*, 522-532.

Lee, D.Y., Deng, Z., Wang, C.H., and Yang, B.B. (2007). MicroRNA-378 promotes cell survival, tumor growth, and angiogenesis by targeting SuFu and Fus-1 expression. Proc. Natl. Acad. Sci. U.S.A. *104*, 20350-20355.

Lehmann, R., Jimenez, F., Dietrich, U., and Campos-Ortega, J. (1983). On the phenotype and development of mutants of early neurogenesis in Drosophila melanogaster. Roux's Arch. Dev. Biol. *192*, 62-74.

Leong, K.G., Hu, X., Li, L., Noseda, M., Larrivée, B., Hull, C., Hood, L., Wong, F., and Karsan, A. (2002). Activated Notch4 inhibits angiogenesis: role of β1-Integrin activation. Mol. Cell. Biol. *22*, 2830-2841.

Leslie, J.D., Ariza-McNaughton, L., Bermange, A.L., McAdow, R., Johnson, S.L., and Lewis, J. (2007). Endothelial signalling by the Notch ligand Delta-like 4 restricts angiogenesis. Development *134*, 839-844.

Leung, A.K.L., and Sharp, P.A. (2010). MicroRNA functions in stress responses. Mol. Cell *40*, 205-215.

Lewis, B.P., Shih, I.H., Jones-Rhoades, M.W., Bartel, D.P., and Burge, C.B. (2003). Prediction of mammalian microRNA targets. Cell *115*, 787-798.

Lewis, B.P., Burge, C.B., and Bartel, D.P. (2005). Conserved seed pairing, often flanked by adenosines, indicates that thousands of human genes are microRNA targets. Cell *120*, 15-20.

Li, B., Tang, S.b., Hu, J., Gao, Y., Zhang, G., Lin, S.F., Chen, J.H., and Li, B.J. (2006). Protective effects of transcription factor HESR1 on retinal vasculature. Microvasc. Res.*72*, 146-152.

Li, J.L., Sainson, R.C.A., Shi, W., Leek, R., Harrington, L.S., Preusser, M., Biswas, S., Turley, H., Heikamp, E., Hainfellner, J.A., and Harris, A.L. (2007). Delta-like 4 Notch ligand regulates tumor angiogenesis, improves tumor vascular function, and promotes tumor growth *in vivo*. Cancer Res. *67*, 11244-11253.

Lim, L.P., Lau, N.C., Garrett-Engele, P., Grimson, A., Schelter, J.M., Castle, J., Bartel, D.P., Linsley, P.S., and Johnson, J.M. (2005). Microarray analysis shows that some microRNAs downregulate large numbers of target mRNAs. Nature *433*, 769-773.

Limbourg, A., Ploom, M., Elligsen, D., Sörensen, I., Ziegelhoeffer, T., Gossler, A., Drexler, H., and Limbourg, F.P. (2007). Notch ligand Delta-like 1 is essential for postnatal arteriogenesis. Circ. Res. *100*, 363-371.

Lin, J., Lwin, T., Zhao, J.J., Tam, W., Choi, Y.S., Moscinski, L.C., Dalton, W.S., Sotomayor, E.M., Wright, K.L., and Tao, J. (2011). Follicular dendritic cell-induced microRNA-mediated upregulation of PRDM1 and downregulation of BCL-6 in non-Hodgkin's B-cell lymphomas. Leukemia *25*, 145-152.

Liu, Z.J., Shirakawa, T., Li, Y., Soma, A., Oka, M., Dotto, G.P., Fairman, R.M., Velazquez, O.C., and Herlyn, M. (2003). Regulation of Notch1 and Dll4 by vascular endothelial growth factor in arterial endothelial cells: implications for modulating arteriogenesis and angiogenesis. Mol. Cell. Biol. *23*, 14-25.

Liu, J., Carmell, M.A., Rivas, F.V., Marsden, C.G., Thomson, J.M., Hammond, S.M., Joshua-Tor, L., and Hannon, G.J. (2004). Argonaute 2 is the catalytic engine of mammalian RNAi. Science *305*, 1437-1441.

Liu, J., Valencia-Sanchez, M.A., Hannon, G.J., and Parker, R. (2005). MicroRNA-dependent localization of targeted mRNAs to mammalian P-bodies. Nat. Cell Biol. *7*, 719-723.

Liu, Z.J., Xiao, M., Balint, K., Soma, A., Pinnix, C.C., Capobianco, A.J., Velazquez, O.C., and Herlyn, M. (2006). Inhibition of endothelial cell proliferation by Notch1 signaling is mediated by repressing MAPK and PI3K/Akt pathways and requires MAML1. FASEB J. *20*, 1009-1011.

Liu, F., and Patient, R. (2008). Genome-wide analysis of the zebrafish ETS family identifies three genes required for hemangioblast differentiation or angiogenesis. Circ. Res. *103*, 1147-1154.

Liu, C., Kelnar, K., Liu, B., Chen, X., Calhoun-Davis, T., Li, H., Patrawala, L., Yan, H., Jeter, C., Honorio, S., Wiggins, J.F., Bader, A.G., Fagin, R., Brown, D., and Tang, D.G. (2011). The microRNA miR-34a inhibits prostate cancer stem cells and metastasis by directly repressing CD44. Nat. Med. *17*, 211-215.

Lobov, I.B., Renard, R.A., Papadopoulos, N., Gale, N.W., Thurston, G., Yancopoulos, G.D., and Wiegand, S.J. (2007). Delta-like ligand 4 (Dll4) is induced by VEGF as a negative regulator of angiogenic sprouting. Proc. Natl. Acad. Sci. U.S.A. *104*, 3219-3224.

Loeb, G.B., Khan, A.A., Canner, D., Hiatt, J.B., Shendure, J., Darnell, R.B., Leslie, C.S., and Rudensky, A.Y. (2012). Transcriptome-wide miR-155 binding map reveals widespread noncanonical microRNA targeting. Mol. Cell *48*, 760-770.

Longnecker, R. and Neipel, F. (2007). Introduction to the human gamma-herpesvirus. In Human Herpesviruses: Biology, Therapy and Immunoprophylaxis, Arvin, A., Campadelli-Fiume, G., Mocarski, E., Moore, P.S., Roizman, B., Whitley, R., and Koichi Y., eds. (Cambridge: Cambridge University Press), pp. 341-359.

Lucitti, J.L., Jones, E.A.V., Huang, C., Chen, J., Fraser, S.E., and Dickinson, M.E. (2007). Vascular remodeling of the mouse yolk sac requires hemodynamic force. Development *134*, 3317-3326.

Lüningschrör, P., Hauser, S., Kaltschmidt, B., and Kaltschmidt, C. (2013). MicroRNAs in pluripotency, reprogramming and cell fate induction. Biochim. Biophys. Acta *1833*, 1894-1903.

Luzi, E., Marini, F., Sala,S.C., Tognarini, I., Galli, G., and Brandi, M.L. (2008). Osteogenic differentiation of human adipose tissue-derived stem cells is modulated by the miR-26a targeting of the SMAD1 transcription factor. J. Bone Miner. Res. *23*, 287-295.

Mailhos,C., Modlich,U., Lewis,J., Harris,A., Bicknell,R., and Ish-Horowicz,D. (2001). Delta4, an endothelial specific Notch ligand expressed at sites of physiological and tumor angiogenesis. Differentiation 69, 135-144.

Marinescu, V.D., Kohane, I.S., and Riva, A. (2005). The MAPPER database: a multi-genome catalog of putative transcription factor binding sites. Nucleic. Acids Res. *33*, D91-D97.

Martinez, I., Cazalla, D., Almstead, L.L., Steitz, J.A., and DiMaio, D. (2011). miR-29 and miR-30 regulate B-Myb expression during cellular senescence. Proc. Natl. Acad. Sci. U.S.A. *108*, 522-527.

McCright, B., Gao, X., Shen, L., Lozier, J., Lan, Y., Maguire, M., Herzlinger, D., Weinmaster, G., Jiang, R., and Gridley, T. (2001). Defects in development of the kidney, heart and eye vasculature in mice homozygous for a hypomorphic Notch2 mutation. Development *128*, 491-502.

Meehan, R.R., Dunican, D.S., Ruzov, A., and Pennings, S. (2005). Epigenetic silencing in embryogenesis. Exp. Cell Res. *309*, 241-249.

Meijer, H., Kong, Y., Lu, W., Wilczynska, A., Spriggs, R., Robinson, S., Godfrey, J., Willis, A., and Bushell, M. (2013). Translational repression and eIF4A2 activity are critical for microRNA-mediated gene regulation. Science *340*, 82-85.

Meister,G., Landthaler,M., Dorsett,Y., and Tuschl,T. (2004). Sequence-specific inhibition of microRNA- and siRNA-induced RNA silencing. RNA *10*, 544-550.

Mesri, E.A., Cesarman, E., and Boshoff, C. (2010). Kaposi's sarcoma and its associated herpesvirus. Nat. Rev. Cancer *10*, 707-719.

Moore, P., and Chang, Y. (2003). Kaposi's sarcoma-associated herpesvirus immunoevasion and tumorigenesis: two sides of the same coin? Annu. Rev. Microbiol. *57*, 609-639.

Morgan, T.H. (1917). The theory of the gene. Am. Nat. *51*, 513-544.

Morton, S.U., Scherz, P.J., Cordes, K.R., Ivey, K.N., Stainier, D.Y.R., and Srivastava, D. (2008). microRNA-138 modulates cardiac patterning during embryonic development. Proc. Natl. Acad. Sci. U.S.A.*105*, 17830-17835.

Mukherji, S., Ebert, M.S., Zheng, G.X.Y., Tsang, J.S., Sharp, P.A., and van Oudenaarden, A. (2011). MicroRNAs can generate thresholds in target gene expression. Nat. Genet. *43*, 854-859.

Nakagawa, O., McFadden, D.G., Nakagawa, M., Yanagisawa, H., Hu, T., Srivastava, D., and Olson, E.N. (2000). Members of the HRT family of basic helix-loop-helix proteins act as transcriptional repressors downstream of Notch signaling. Proc. Natl. Acad. Sci. U.S.A. *97*, 13655-13660.

Nasevicius, A., and Ekker, S.C. (2000). Effective targeted gene 'knockdown' in zebrafish. Nat. Genet. *26*, 216-220.

Nasevicius, A., Larson, J., and Ekker, S.C. (2000). Distinct requirements for zebrafish angiogenesis revealed by a VEGF-A morphant. Yeast *17*, 294-301.

Newman, M.A., Thomson, J.M., and Hammond, S.M. (2008). Lin-28 interaction with the Let-7 precursor loop mediates regulated microRNA processing. RNA *14*, 1539-1549.

Nicoli, S., Standley, C., Walker, P., Hurlstone, A., Fogarty, K.E., and Lawson, N.D. (2010). MicroRNA-mediated integration of haemodynamics and Vegf signalling during angiogenesis. Nature *464*, 1196-1200.

Nicoli, S., Knyphausen, C.P., Zhu, L.J., Lakshmanan, A., and Lawson, N.D. (2012). miR-221 is required for endothelial tip cell behaviors during vascular development. Dev. Cell *22*, 418-429.

Noguera-Troise, I., Daly, C., Papadopoulos, N.J., Coetzee, S., Boland, P., Gale, N.W., Lin, H.C., Yancopoulos, G.D., and Thurston, G. (2006). Blockade of Dll4 inhibits tumour growth by promoting non-productive angiogenesis. Nature *444*, 1032-1037.

Noseda, M., Chang, L., McLean, G., Grim, J.E., Clurman, B.E., Smith, L.L., and Karsan, A. (2004). Notch activation induces endothelial cell cycle arrest and participates in contact inhibition: role of p21Cip1 repression. Mol. Cell. Biol. *24*, 8813-8822.

Ny, A., Autiero, M., and Carmeliet, P. (2006). Zebrafish and Xenopus tadpoles: small animal models to study angiogenesis and lymphangiogenesis. Exp. Cell Res. *312*, 684-693.

Oettle, A.G. (1962). Geographical and racial differences in the frequency of Kaposi's sarcoma as evidence of environmental or genetic causes. Acta Unio Int. Contra Cancrum *18*, 330-363.

Oishi, H., Sunamura, M., Egawa, S., Motoi, F., Unno, M., Furukawa, T., Habib, N.A., and Yagita, H. (2010). Blockade of Delta-like ligand 4 signaling inhibits both growth and angiogenesis of pancreatic cancer. Pancreas *39*, 897-903.

Okamura, K., Hagen, J.W., Duan, H., Tyler, D.M., and Lai, E.C. (2007). The mirtron pathway generates microRNA-Class regulatory RNAs in Drosophila. Cell *130*, 89-100.

Otsuka, M., Zheng, M., Hayashi, M., Lee, J.D., Yoshino, O., Lin, S., and Han, J. (2008). Impaired microRNA processing causes corpus luteum insufficiency and infertility in mice. J. Clin. Invest. *118*, 1944-1954.

Pan, Q., Chanthery, Y., Liang, W.C., Stawicki, S., Mak, J., Rathore, N., Tong, R.K., Kowalski, J., Yee, S.F., Pacheco, G., Ross, S., Cheng, Z., Le Couter, J., Plowman, G., Peale, F., Koch, A.W., Wu, Y., Bagri, A., Tessier-Lavigne, M., and Watts, R.J. (2007). Blocking Neuropilin-1 function has an additive effect with anti-VEGF to inhibit tumor growth. Cancer Cell *11*, 53-67.

Pardali, E., Goumans, M.J., and ten Dijke, P. Signaling by members of the TGF-β family in vascular morphogenesis and disease. Trends Cell Biol. *20*, 556-567.

Pasquinelli, A.E., Reinhart, B.J., Slack, F., Martindale, M.Q., Kuroda, M.I., Maller, B., Hayward, D.C., Ball, E.E., Degnan, B., Muller, P., Spring, J., Srinivasan, A., Fishman, M., Finnerty, J., Corbo, J., Levine, M., Leahy, P., Davidson, E., and Ruvkun, G. (2000). Conservation of the sequence and temporal expression of let-7 heterochronic regulatory RNA. Nature *408*, 86-89.

Patel,N.S., Li,J.L., Generali,D., Poulsom,R., Cranston,D.W., and Harris,A.L. (2005). Up-regulation of Delta-like 4 Ligand in human tumor vasculature and the role of basal expression in endothelial cell function. Cancer Res. *65*, 8690-8697.

Patel, N.S., Dobbie, M.S., Rochester, M., Steers, G., Poulsom, R., Le Monnier, K., Cranston, D.W., Li, J.L., and Harris, A.L. (2006). Up-regulation of endothelial Delta-like 4 expression correlates with vessel maturation in bladder cancer. Clin. Cancer Res. *12*, 4836-4844.

Phng, L.K., and Gerhardt, H. (2009). Angiogenesis: a team effort coordinated by Notch. Dev Cell *16*, 196-208.

Phng, L.K., Potente, M., Leslie, J.D., Babbage, J., Nyqvist, D., Lobov, I., Ondr, J.K., Rao, S., Lang, R.A., Thurston, G., and Gerhardt, H. (2009). Nrarp coordinates endothelial Notch and Wnt signaling to control vessel density in angiogenesis. Dev. Cell *16*, 70-82.

Pin, A.L., Houle, F., Guillonneau, M., Paquet, E.R., Simard, M.J., and Huot, J. (2012). miR-20a represses endothelial cell migration by targeting MKK3 and inhibiting p38 MAP kinase activation in response to VEGF. Angiogenesis *14*, 593-608.

Pirot, P., Grunsven, L.A., Marine, J.C., Huylebroeck, D., and Bellefroid, E.J. (2004). Direct regulation of the Nrarp gene promoter by the Notch signaling pathway. Biochem. Biophys. Res. Commun. *322*, 526-534.

Poliseno, L., Tuccoli, A., Mariani, L., Evangelista, M., Citti, L., Woods, K., Mercatanti, A., Hammond, S., and Rainaldi, G. (2006). MicroRNAs modulate the angiogenic properties of HUVECs. Blood *108*, 3068-3071.

Poole, T.J., and Coffin, J.D. (1989). Vasculogenesis and angiogenesis: two distinct morphogenetic mechanisms establish embryonic vascular pattern. J. Exp. Zool. *251*, 224-231.

Potente, M., Gerhardt, H., and Carmeliet, P. (2011). Basic and therapeutic aspects of angiogenesis. Cell *146*, 873-887.

Poulson, D. (1945). Chromosomal control of embryogenesis in Drosophila. Am. Nat. *79*, 340-363.

Pulkkinen, K., Malm, T., Turunen, M., Koistinaho, J., and Ylä-Herttuala, S. (2008). Hypoxia induces microRNA miR-210 in vitro and in vivo: Ephrin-A3 and neuronal pentraxin 1 are potentially regulated by miR-210. FEBS Lett. *582*, 2397-2401.

Punj, V., Matta, H., Schamus, S., Tamewitz, A., Anyang, B., and Chaudhary, P.M. (2010). Kaposi's sarcoma-associated herpesvirus-encoded viral FLICE inhibitory protein (vFLIP) K13 suppresses CXCR4 expression by upregulating miR-146a. Oncogene *29*, 1835-1844.

Rauch, G.J., Hammerschmidt, M., Blader, P., Schauerte, H.E., Strähle, U., Ingham, P.W., McMahon, A.P., and Haffter, P. (1997). WNT5 is required for tail formation in the zebrafish embryo. Cold Spring Harb. Symp. Quant. Biol. *62*, 227-234.

Rebay, I., Fleming, R.J., Fehon, R.G., Cherbas, L., Cherbas, P., and Artavanis-Tsakonas, S. (1991). Specific EGF repeats of Notch mediate interactions with Delta and serrate: Implications for notch as a multifunctional receptor. Cell *67,* 687-699.

Reinhart, B.J., Slack, F.J., Basson, M., Pasquinelli, A.E., Bettinger, J.C., Rougvie, A.E., Horvitz, H.R., and Ruvkun, G. (2000). The 21-nucleotide let-7 RNA regulates developmental timing in Caenorhabditis elegans. Nature *403*, 901-906.

Renne, R., Zhong, W., Herndier, B., McGrath, M., Abbey, N., Kedes, D., and Ganem, D. (1996). Lytic growth of Kaposi's sarcoma-associated herpesvirus (human herpesvirus 8) in culture. Nat. Med. *2*, 342-346.

Ridgway, J., Zhang, G., Wu, Y., Stawicki, S., Liang, W.C., Chanthery, Y., Kowalski, J., Watts, R.J., Callahan, C., Kasman, I., Singh, M., Chien, M., Tan, C., Hongo, J.A., de Sauvage, F., Plowman, G., and Yan, M. (2006). Inhibition of Dll4 signalling inhibits tumour growth by deregulating angiogenesis. Nature *444*, 1083-1087.

Risau, W., Sariola, H., Zerwes, H.G., Sasse, J., Ekblom, P., Kemler, R., and Doetschman, T. (1988). Vasculogenesis and angiogenesis in embryonic-stem-cell-derived embryoid bodies. Development *102*, 471-478.

Roehl, H., Bosenberg, M., Blelloch, R., and Kimble, J. (1996). Roles of the RAM and ANK domains in signaling by the C. elegans GLP-1 receptor. EMBO J. *15*, 7002-7012.

Roman, B.L., Pham, V.N., Lawson, N.D., Kulik, M., Childs, S., Lekven, A.C., Garrity, D.M., Moon, R.T., Fishman, M.C., Lechleider, R.J., and Weinstein, B.M. (2002). Disruption of acvrl1 increases endothelial cell number in zebrafish cranial vessels. Development *129*, 3009-3019.

Ruby, J.G., Jan, C.H., and Bartel, D.P. (2007). Intronic microRNA precursors that bypass Drosha processing. Nature *448*, 83-86.

Ruhrberg, C., Gerhardt, H., Golding, M., Watson, R., Ioannidou, S., Fujisawa, H., Betsholtz, C., and Shima, D.T. (2002). Spatially restricted patterning cues provided by heparin-binding VEGF-A control blood vessel branching morphogenesis. Genes Dev. *16*, 2684-2698.

Sainson, R.C.A., Aoto, J., Nakatsu, M.N., Holderfield, M., Conn, E., Koller, E., and Hughes, C.C.W. (2005). Cell-autonomous notch signaling regulates endothelial cell branching and proliferation during vascular tubulogenesis. FASEB J. *19*, 1027-1029.

Selbach, M., Schwanhausser, B., Thierfelder, N., Fang, Z., Khanin, R., and Rajewsky, N. (2008). Widespread changes in protein synthesis induced by microRNAs. Nature *455*, 58-63.

Shawber, C.J., Funahashi, Y., Francisco, E., Vorontchikhina, M., Kitamura, Y., Stowell, S.A., Borisenko, V., Feirt, N., Podgrabinska, S., Shiraishi, K., Chawengsaksophak, K., Rossant, J., Accili, D., Skobe, M., and Kitajewski, J. (2007). Notch alters VEGF responsiveness in human and murine endothelial cells by direct regulation of VEGFR-3 expression. J. Clin. Invest. *117*, 3369-3382.

Shin, C., Nam, J.W., Farh, K.K., Chiang, H.R., Shkumatava, A., and Bartel, D.P. (2010). Expanding the microRNA targeting code: functional sites with centered pairing. Mol. Cell *38*, 789-802.

Shoji, W., Isogai, S., Sato-Maeda, M., Obinata, M., and Kuwada, J.Y. (2003). Semaphorin3a1 regulates angioblast migration and vascular development in zebrafish embryos. Development *130*, 3227-3236.

Siegel, J.H., Janis, R., Alper, J.C., Schutte, H., Robbins, L., and Blaufox, M.D. (1969). Disseminated visceral Kaposi's sarcoma: appearance after human renal homograft operation. JAMA *207*, 1493-1496.

Siekmann, A.F. and Lawson, N.D. (2007). Notch signalling limits angiogenic cell behaviour in developing zebrafish arteries. Nature *445*, 781-784.

Slack, F.J., Basson, M., Liu, Z., Ambros, V., Horvitz, H.R., and Ruvkun, G. (2000). The lin-41 RBCC Gene Acts in the C. elegans heterochronic pathway between the let-7 regulatory RNA and the LIN-29 Transcription Factor. Mol. Cell *5*, 659-669.

Slavin, G. (1970). Kaposi's sarcoma in East African children: a report of 51 cases. J. Pathol. *100*, 187-199.

Small, E.M., Sutherland, L.B., Rajagopalan, K.N., Wang, S., and Olson, E.N. (2010). MicroRNA-218 regulates vascular patterning by modulation of Slit-Robo signaling. Circ. Res. *107*, 1336-1344.

Smyth, G.K. (2012). Linear models and empirical bayes methods for assessing differential expression in microarray experiments. Stat. Appl. Genet. Mol. Biol. *3*, Article 3.

Soares, A.R., Reverendo, M., Pereira, P.M., Nivelles, O., Pendeville, H., Bezerra, A.R., Moura, G.R., Struman, I., and Santos, M.A.S. (2012). Dre-miR-2188 targets Nrp2a and mediates proper intersegmental vessel development in zebrafish embryos. PLoS ONE *7*, e39417.

Soulier, J., Grollet, L., Oksenhendler, E., Cacoub, P., Cazals-Hatem, D., Babinet, P., d'Agay, M.F., Clauvel, J.P., Raphael, M., Degos, L., and Sigaux, F. (1995). Kaposi's sarcoma-associated herpesvirus-like DNA sequences in multicentric Castleman's disease. Blood *86*, 1276-1280.

Stahlhut, C., Suárez, Y., Lu, J., Mishima, Y., and Giraldez, A.J. (2012). miR-1 and miR-206 regulate angiogenesis by modulating VegfA expression in zebrafish. Development *139*, 4356-4365.

Stainier, D.Y., Weinstein, B.M., Detrich, H.W., Zon, L.I., and Fishman, M.C. (1995). Cloche, an early acting zebrafish gene, is required by both the endothelial and hematopoietic lineages. Development *121*, 3141-3150.

Staton, A.A., Knaut, H., and Giraldez, A.J. (2011). miRNA regulation of Sdf1 chemokine signaling provides genetic robustness to germ cell migration. Nat. Genet. *43*, 204-211.

Strilić, B., Kucera, T., Eglinger, J., Hughes, M.R., McNagny, K.M., Tsukita, S., Dejana, E., Ferrara, N., and Lammert, E. (2009). The Molecular Basis of Vascular Lumen Formation in the Developing Mouse Aorta. Dev. Cell *17*, 505-515.

Suárez, Y., Fernández-Hernando, C., Pober, J.S., and Sessa, W.C. (2007). Dicer dependent microRNAs regulate gene expression and functions in human endothelial cells. Circ. Res. *100*, 1164-1173.

Suárez, Y., Fernández-Hernando, C., Yu, J., Gerber, S.A., Harrison, K.D., Pober, J.S., Iruela-Arispe, M.L., Merkenschlager, M., and Sessa, W.C. (2008). Dicer-dependent endothelial microRNAs are necessary for postnatal angiogenesis. Proc. Natl. Acad. Sci. U.S.A. *105*, 14082-14087.

Suchting, S., Freitas, C., Ferdinand, l.N., Benedito, R., Bréant, C., Duarte, A., and Eichmann, A. (2007). The Notch ligand Delta-like 4 negatively regulates endothelial tip cell formation and vessel branching. Proc. Natl. Acad. Sci. U.S.A. *104*, 3225-3230.

Sun, C.Y., She, X.M., Qin, Y., Chu, Z.B., Chen, L., Ai, L.S., Zhang, L., and Hu, Y. (2013). miR-15a and miR-16 affect the angiogenesis of multiple myeloma by targeting VEGF. Carcinogenesis *34*, 426-435.

Suzuki, H.I., Yamagata, K., Sugimoto, K., Iwamoto, T., Kato, S., and Miyazono, K. (2009). Modulation of microRNA processing by p53. Nature *460*, 529-533.

Swiatek, P.J., Lindsell, C.E., Del Amo, F.F., Weinmaster, G., and Gridley, T. (1994). Notch1 is essential for postimplantation development in mice. Genes Dev. *8*, 707-719.

Tammela, T., Zarkada, G., Wallgard, E., Murtomaki, A., Suchting, S., Wirzenius, M., Waltari, M., Hellstrom, M., Schomber, T., Peltonen, R., Freitas, C., Duarte, A., Isoniemi, H., Laakkonen, P., Christofori, G., Yla-Herttuala, S., Shibuya, M., Pytowski, B., Eichmann, A., Betsholtz, C., and Alitalo, K. (2008). Blocking VEGFR-3 suppresses angiogenic sprouting and vascular network formation. Nature *454*, 656-660.

Thomas, M., Lieberman, J., and Lal, A. (2010). Desperately seeking microRNA targets. Nat. Struct. Mol. Biol. *17*, 1169-1174.

Thompson, M.A., Ransom, D.G., Pratt, S.J., MacLennan, H., Kieran, M.W., Dietrich, H.W. 3rd, Vail, B., Huber, T.L., Paw, B., Brownlie, A.J., Oates, A.C., Fritz, A., Gates, M.A., Amores, A., Bahary, N., Talbot, W.S., Her, H., Beier, D.R., Postlethwait, J.H., and Zon, L.I. (1998). The cloche and spadetail genes differentially affect hematopoiesis and vasculogenesis. Dev. Biol. *197*, 248-269.

Trabucchi, M., Briata, P., Garcia-Mayoral, M., Haase, A.D., Filipowicz, W., Ramos, A., Gherzi, R., and Rosenfeld, M.G. (2009). The RNA-binding protein KSRP promotes the biogenesis of a subset of microRNAs. Nature *459*, 1010-1014.

Trindade, A., Kumar, S.R., Scehnet, J.S., Lopes-da-Costa, L., Becker, J., Jiang, W., Liu, R., Gill, P.S., and Duarte, A. (2008). Overexpression of delta-like 4 induces arterialization and attenuates vessel formation in developing mouse embryos. Blood *112*, 1720-1729.

Urbich, C., Kaluza, D., Frömel, T., Knau, A., Bennewitz, K., Boon, R.A., Bonauer, A., Doebele, C., Boeckel, J.N., Hergenreider, E., Zeiher, A.M., Kroll, J., Fleming, I., and Dimmeler, S. (2012). MicroRNA-27a/b controls endothelial cell repulsion and angiogenesis by targeting semaphorin 6A. Blood *119*, 1607-1616.

Uyttendaele, H., Marazzi, G., Wu, G., Yan, Q., Sassoon, D., and Kitajewski, J. (1996). Notch4/int-3, a mammary proto-oncogene, is an endothelial cell-specific mammalian Notch gene. Development *122*, 2251-2259.

van Eeden, F.J., Granato, M., Schach, U., Brand, M., Furutani-Seiki, M., Haffter, P., Hammerschmidt, M., Heisenberg, C.P., Jiang, Y.J., Kane, D.A., Kelsh, R.N., Mullins, M.C., Odenthal, J., Warga, R.M., Allende, M.L., Weinberg, E.S., and Nüsslein-Volhard,C. (1996). Mutations affecting somite formation and patterning in the zebrafish, Danio rerio. Development *123*, 153-164.

Vart, R.J., Nikitenko, L.L., Lagos, D., Trotter, M.W.B., Cannon, M., Bourboulia, D., Gratrix, F., Takeuchi, Y., and Boshoff, C. (2007). Kaposi's sarcoma-associated herpesvirus-encoded interleukin-6 and G-protein-coupled receptor regulate angiopoietin-2 expression in lymphatic endothelial cells. Cancer Res. *67*, 4042-4051.

Vieira, J., O'Hearn, P., Kimball, L., Chandran, B., and Corey, L. (2001). Activation of Kaposi's sarcoma-associated herpesvirus (human herpesvirus 8) lytic replication by human cytomegalovirus. J. Virol. *75*, 1378-1386.

Villa, N., Walker, L., Lindsell, C.E., Gasson, J., Iruela-Arispe, M.L., and Weinmaster, G. (2001). Vascular expression of Notch pathway receptors and ligands is restricted to arterial vessels. Mech. Dev. *108*, 161-164.

Viswanathan, S.R., and Daley, G.Q. (2010). Lin28: a microRNA regulator with a macro role. Cell *140*, 445-449.

Vogel, J., Hinrichs, S.H., Reynolds, R.K., Luciw, P.A., and Jay, G. (1988). The HIV tat gene induces dermal lesions resembling Kaposi's sarcoma in transgenic mice. Nature *335*, 606-611.

Wang, L., Zeng, H., Wang, P., Soker, S., and Mukhopadhya, D. (2003). Neuropilin-1-mediated vascular permeability factor/vascular endothelial growth factor-dependent endothelial cell migration. J. Biol. Chem. *278*, 48848-48860.

Wang, H.W., Trotter, M.W.B., Lagos, D., Bourboulia, D., Henderson, S., Makinen, T., Elliman, S., Flanagan, A.M., Alitalo, K., and Boshoff, C. (2004). Kaposi sarcoma herpesvirus-induced cellular reprogramming contributes to the lymphatic endothelial gene expression in Kaposi sarcoma. Nat. Genet. *36*, 687-693.

Wang, S., Aurora, A.B., Johnson, B.A., Qi, X., McAnally, J., Hill, J.A., Richardson, J.A., Bassel-Duby, R., and Olson, E.N. (2008). The endothelial-specific microRNA miR-126 governs vascular integrity and angiogenesis. Dev. Cell *15*, 261-271.

Wang, S., and Olson, E.N. (2009). AngiomiRs--key regulators of angiogenesis. Curr. Opin. Genet. Dev. *19*, 205-211.

Wang, Z., Li, Y., Kong, D., Ahmad, A., Banerjee, S., and Sarkar, F.H. (2010). Cross-talk between miRNA and Notch signaling pathways in tumor development and progression. Cancer Lett. *292*, 141-148.

Wang, J., Wang, Y., Wang, Y., Ma, Y., Lan, Y., and Yang, X. (2013a). Transforming Growth Factor β-regulated microRNA-29a promotes angiogenesis through targeting the phosphatase and tensin homolog in endothelium. J. Biol. Chem. *288*, 10418-10426.

Wang, X.H., Qian, R.Z., Zhang, W., Chen, S.F., Jin, H.M., and Hu, R.M. (2013b). MicroRNA-320 expression in myocardial microvascular endothelial cells and its relationship with insulin-like growth factor-1 in type 2 diabetic rats. Clin. Exp. Pharmacol. Physiol. *36*, 181-188.

Westerfield, M. (2000). Chapter 3 - Embryonic and larval culture. In The Zebrafish Book: A guide for laboratory use of zebrafish (Brachydanio rerio). 4th ed., Eugene: Univ. of Oregon Press.

Wienholds, E., Koudijs, M.J., van Eeden, F.J.M., Cuppen, E., and Plasterk, R.H.A. (2003). The microRNA-producing enzyme Dicer1 is essential for zebrafish development. Nat. Genet. *35*, 217-218.

Wienholds, E., Kloosterman, W.P., Miska, E., Alvarez-Saavedra, E., Berezikov, E., de Bruijn, E., Horvitz, H.R., Sakari, K., and Plasterk, R.H.A. (2005). MicroRNA expression in zebrafish embryonic development. Science *309*, 310-311.

Wiggins, J.F., Ruffino, L., Kelnar, K., Omotola, M., Patrawala, L., Brown, D., and Bader, A.G. (2010). Development of a lung cancer therapeutic based on the tumor suppressor microRNA-34. Cancer Res. *70*, 5923-5930.

Wightman, B., Ha, I., and Ruvkun, G. (1993). Posttranscriptional regulation of the heterochronic gene lin-14 by lin-4 mediates temporal pattern formation in C. elegans. Cell *75*, 855-862.

Williams, C.K., Li, J.L., Murga, M., Harris, A.L., and Tosato, G. (2006). Up-regulation of the Notch ligand Delta-like 4 inhibits VEGF-induced endothelial cell function. Blood *107*, 931-939.

Williams, C.K., Segarra, M., De La Luz Sierra, M., Sainson, R.C.A., Tosato, G., and Harris, A.L. (2008). Regulation of CXCR4 by the Notch ligand Delta-like 4 in endothelial cells. Cancer Res. *68*, 1889-1895.

Wong, C.F., and Tellam, R.L. (2008). MicroRNA-26a targets the histone methyltransferase Enhancer of Zeste homolog 2 during myogenesis. J. Biol. Chem. *283*, 9836-9843.

Wu, L., Fan, J., and Belasco, J.G. (2006). MicroRNAs direct rapid deadenylation of mRNA. Proc. Natl. Acad. Sci. U.S.A. *103*, 4034-4039.

Wu, J., and Bresnick, E.H. (2007). Bare rudiments of notch signaling: how receptor levels are regulated. Trends Biochem. Sci. *32*, 477-485.

Wu, T., Zhou, H., Hong, Y., Li, J., Jiang, X., and Huang, H. (2012). miR-30 family members negatively regulate osteoblast differentiation. J. Biol. Chem. *287*, 7503-7511.

Würdinger, T., Tannous, B.A., Saydam, O., Skog, J., Grau, S., Soutschek, J., Weissleder, R., Breakefield, X.O., and Krichevsky, A.M. (2008). miR-296 regulates growth factor receptor overexpression in angiogenic endothelial cells. Cancer Cell *14*, 382-393.

Wythe, J.D., Dang, L.T., Devine, W.P., Boudreau, E., Artap, S.T., He, D., Schachterle, W., Stainier, D.Y., Oettgen, P., Black, B.L., Bruneau, B.G., and Fish, J.E. (2013). ETS factors regulate Vegf-dependent arterial specification. Dev. Cell *26*, 45-58.

Xu, A., Haines, N., Dlugosz, M., Rana, N.A., Takeuchi, H., Haltiwanger, R.S., and Irvine, K.D. (2007). *In vitro* reconstitution of the modulation of Drosophila Notch-ligand binding by Fringe. J. Biol. Chem. *282*, 35153-35162.

Yan, M., Callahan, C.A., Beyer, J.C., Allamneni, K.P., Zhang, G., Ridgway, J.B., Niessen, K., and Plowman, G.D. (2010). Chronic DLL4 blockade induces vascular neoplasms. Nature *463*, E6-E7.

Yang, W.J., Yang, D.D., Na, S., Sandusky, G.E., Zhang, Q., and Zhao, G. (2005). Dicer is required for embryonic angiogenesis during mouse development. J. Biol. Chem. *280*, 9330-9335.

Yang, Z., Wu, L., Zhu, X., Xu, J., Jin, R., Li, G., and Wu, F. (2013). MiR-29a modulates the angiogenic properties of human endothelial cells. Biochem. Biophys. Res. Commun. *434*, 143-149.

Yaniv, K., Isogai, S., Castranova, D., Dye, L., Hitomi, J., and Weinstein, B.M. (2006). Live imaging of lymphatic development in the zebrafish. Nat. Med. *12*, 711-716.

Ye, J., Wu, X., Wu, D., Wu, P., Ni, C., Zhang, Z., Chen, Z., Qiu, F., Xu, J., and Huang, J. (2013). miRNA-27b targets vascular endothelial growth factor C to inhibit tumor progression and angiogenesis in colorectal cancer. PLoS ONE *8*, e60687.

Yi, R., Qin, Y., Macara, I.G., and Cullen, B.R. (2003). Exportin-5 mediates the nuclear export of pre-microRNAs and short hairpin RNAs. Genes Dev. *17*, 3011-3016.

Yin, R., Wang, R., Guo, L., Zhang, W., and Lu, Y. (2013). MiR-17-3p inhibits angiogenesis by downregulating Flk-1 in the cell growth signal pathway. J. Vasc. Res. *50*, 157-166.

Yochem, J., Weston, K., and Greenwald, I. (1988). The Caenorhabditis elegans lin-12 gene encodes a transmembrane protein with overall similarity to Drosophila Notch. Nature *335*, 547-550.

You, L.R., Lin, F.J., Lee, C.T., DeMayo, F.J., Tsai, M.J., and Tsai, S.Y. (2005). Suppression of Notch signalling by the COUP-TFII transcription factor regulates vein identity. Nature *435*, 98-104.

Yu, F., Deng, H., Yao, H., Liu, Q., Su, F., and Song, E. (2010). Mir-30 reduction maintains self-renewal and inhibits apoptosis in breast tumor-initiating cells. Oncogene *29*, 4194-4204.

Zaragosi, L.E., Wdziekonski, B., Le Brigand, K., Villageois, P., Mari, B., Waldmann, R., Dani, C., and Barbry, P. (2011). Small RNA sequencing reveals miR-642a-3p as a novel adipocyte-specific microRNA and miR-30 as a key regulator of human adipogenesis. Genome Biol. *12*, R64.

Zeeb, M., Strilić, B., and Lammert, E. (2010). Resolving cell-cell junctions: lumen formation in blood vessels. Curr. Opin. Cell Biol. *22*, 626-632.

Zeng, L., Carter, A.D., and Childs, S.J. (2009). miR-145 directs intestinal maturation in zebrafish. Proc. Natl. Acad. Sci. U.S.A. *106*, 17793-17798.

Zhang, X., Wan, G., Berger, F.G., He, X., and Lu, X. (2011). The ATM kinase induces microRNA biogenesis in the DNA damage response. Mol. Cell *41*, 371-383.

Zhang, J., Zhang, H., Liu, J., Tu, X., Zang, Y., Zhu, J., Chen, J., Dong, L., and Zhang, J. (2012). miR-30 inhibits TGF-β1-induced epithelial-to-mesenchymal transition in hepatocyte by targeting Snail1. Biochem. Biophys. Res. Commun. *417*, 1100-1105.

Zhang, C., Patient, R., and Liu, F. (2013). Hematopoietic stem cell development and regulatory signaling in zebrafish. Biochim. Biophys. Acta *1830*, 2370-2374.

Zhong, W., Wang, H., Herndier, B., and Ganem, D. (1996). Restricted expression of Kaposi sarcoma-associated herpesvirus (human herpesvirus 8) genes in Kaposi sarcoma. Proc. Natl. Acad. Sci. U.S.A. *93*, 6641-6646.

Zhong, T.P., Childs, S., Leu, J.P., and Fishman, M.C. (2001). Gridlock signalling pathway fashions the first embryonic artery. Nature *414*, 216-220.

Zhong, X., Li, N., Liang, S., Huang, Q., Coukos, G., and Zhang, L. (2010). Identification of microRNAs regulating reprogramming factor LIN28 in embryonic stem cells and cancer cells. J. Biol. Chem. *285*, 41961-41971.

Zhou, R., Hu, G., Liu, J., Gong, A.Y., Drescher, K.M., and Chen, X.M. (2009). NF-κB p65-dependent transactivation of miRNA genes following *Cryptosporidium parvum* infection stimulates epithelial cell immune responses. PLoS Pathog. *5*, e1000681.

Zhou, R., Hu, G., Gong, A.Y., and Chen, X.M. (2010). Binding of NF-κB p65 subunit to the promoter elements is involved in LPS-induced transactivation of miRNA genes in human biliary epithelial cells. Nucleic Acids Res. *38*, 3222-3232.

Zhou, B., Ma, R., Si, W., Li, S., Xu, Y., Tu, X., and Wang, Q. (2013). MicroRNA-503 targets FGF2 and VEGFA and inhibits tumor angiogenesis and growth. Cancer Lett. *333*, 159-169.

Zou, C., Xu, Q., Mao, F., Li, D., Bian, C., Liu, L.Z., Jiang, Y., Chen, X., Qi, Y., Zhang, X., Wang, X., Sun, Q., Kung, H.F., Lin, M.C., Dress, A., Wardle, F., Jiang, B.H., and Lai, L. (2012). MiR-145 inhibits tumor angiogenesis and growth by N-RAS and VEGF. Cell Cycle *11*, 2137-2145.

Appendix

Please refer to the CD which is included with this thesis.